The role of TREM2 in neurodegeneration

By

Christina Elizabeth Murray

Thesis submitted for the degree of Doctor of Philosophy at University College London

Acknowledgements

Writing this thesis has been a challenging experience for me and I would therefore like to thank the people that have helped me to succeed.

Firstly, none of this research would have been possible without the generous funding from Alzheimer's Research UK and the donation of precious brain tissue from those who donated their brains, so I would like to say thank you for your wonderful gifts.

To my primary supervisor, Dr Tammaryn Lashley, you have been such a support for me throughout the entirety of my PhD. No matter how busy you were, you always made time to give me the guidance that I needed and fitted me in. We have been through this journey together and I very much look forward to the work we will continue to do together in the next steps of my career. I look up to you and if I am as successful as you are, I will be very happy.

I also give thanks to my secondary supervisors, Dr Kevin Mills, Prof V. Hugh Perry and Prof John Hardy for overseeing my project and giving me their thoughts and guidance along the way.

Thank you to Dr Yasmine Asi, Dr Abi Li and April Murray for their tireless time spent proof-reading my thesis for me. Your insights were needed and very much appreciated. I hope to repay this favour one day.

QSBB has been a welcome home for me to produce my research and I am grateful for the team environment I am able to work in here. Prof Janice Holton and Prof Tom Warner, to you both I give thanks for giving me the opportunity to gain extra income as this helped with the financial stress during this period. Thank you to Bridget Benson for providing technical help for the analysis of the pathology studied in Chapters 3 and 4. I am indebted to you for your help. I would also like to give a special mention to Dr Sandrine Foti, Dr Aoife Kiely, Karen Davey, Melissa Wren, Nanet Willumsen, Lauren Gittings, Phoebe Walsh and everybody at QSBB for your open ears and general support when I had problems to solve or needed to talk.

Parts of this thesis could not have been done without the help of my collaborators. Dr Kevin Mills and Dr Wendy Heywood, thank you for your guidance on all proteomic work and for making your lab facilities open to me. Dr Angela Hodges and Yau Lim, thank you for allowing me to use the macro you created in order to complete the pathological analysis. Prof Henrik Zetterberg and colleagues, thank you for the collaboration enabling us to look at the Aβ peptides in the presubiculum. I look forward to continuing my work with you.

Those who have completed a PhD will know how it becomes your world but this can be difficult to understand if you are not part of the academic world. I would therefore like to thank all my wonderful friends and family for understanding when I was too busy to come to one function or the other. I am really looking forward to making up for this.

My family mean the world to me and I can not thank my Mum, Dad and sisters enough for the pillar of love and support they have been for me throughout this time. Thank you for the hugs, the laughter and for cheering me up when things felt tough. I love you all very much.

Lastly but definitely not least I would like to thank my supporting fiancé, John Toomey. It cannot have been easy living with me the past three years but you have dealt with my many ups and downs so well and have really been my rock. I could not have got through it without you. Thank you from the bottom of my heart and I promise to do more housework from now on!

I, Christina Elizabeth Murray, confirm that the work presented in this thesis is my own. Where information has been derived from other sources, I confirm that this has been indicated in the thesis.

_____

Christina Elizabeth Murray

Abstract

Introduction: Alzheimer's disease (AD) is the most common neurodegenerative disease and has a high prevalence worldwide. Neuroinflammation has long been known to play a role in AD. However, the findings that several genes associated with inflammation were identified as hits in AD GWAS studies brought closer attention to neuroinflammatory mechanisms in AD. *TREM2* was identified as a genetic risk factor for late onset AD with a similar odds ratio to that of *APOE4*. TREM2 is expressed on microglia, and has been shown to be upregulated on the microglia surrounding amyloid plaques both in human post mortem tissue and AD mouse models. In this thesis, the AD pathology, microglial phenotype, genetic inflammatory profile and proteomic profile of six *TREM2* variant cases (5 *R47H* and 1 *D87N* variant) were investigated and compared to sporadic AD (SAD), familial AD (FAD) and neurologically normal control cases with the hypothesis that the *TREM2* variant cases will differ from both SAD and FAD cases.

Materials and Methods: Immunohistochemistry was performed on the frontal cortex, temporal cortex, hippocampus, putamen and cerebellum of SAD (n=19), FAD (n=11), *TREM2* variant SAD (n=3), *TREM2* variant controls (no AD pathology, n=2) and neurologically normal controls (n=6) using antibodies against Aβ, tau (AT8) and microglia (Iba1, CD68, CR3-43 and P2RY12). Microglial load/area, circularity and perimeter scores were calculated for all microglial markers. The frontal cortex was homogenised from a subset of each group and RNA and protein extracted. Nanostring's Human Inflammation panel with their nCounter Technology was used to determine the genetic profile. The proteomic profile was assessed using label-free quantitative mass spectrometry. The pathological and proteomic profile of the presubiculum was investigated using immunohistochemistry, matrix-assisted laser desorption ionisation mass spectrometry, laser-capture microdissection and further label free quantitative mass spectrometry and compared to the neighbouring area, the entorhinal cortex to assess whether it has protective properties against neurodegeneration.

Results: *TREM2* variant AD cases differed from other SAD and FAD cases with a significantly increased CD68 load, more circular Iba1, CR3-43 and CD68 microglial positivity suggesting the microglia were in a phenotype more consistent with phagocytosis. Furthermore, these cases showed an increased upregulation of neuroinflammatory processes and neurodegenerative processes at the genetic and proteomic level than SAD cases. *TREM2* variant controls however, showed large levels of downregulation in these processes compared to all groups. APOE genotyping identified the *TREM2* variant cases correlated with the presence of the ApoE4 isoform. Investigation of the presubiculum area identified a large non-fibrillar Aβ deposit that contained significantly less NFT's, activated microglia and N-terminally truncated Aβ peptides than in the entorhinal cortex and had an altered proteomic profile more comparable to the *TREM2* variant controls than any other AD cases.

Conclusions: Overall, this thesis has shown that *TREM2* variant cases posess differences in microglial phenotype, genetic and proteomic expression compared to either sporadic or familial AD cases. *TREM2* variant controls show altered pathology and genetic profiles compared to *TREM2* variant SAD cases and it can be hypothesised that these cases may use similar mechanisms to the neuroprotection observed in the presubiuclum of AD cases. TREM2's link to APOE and the fact that the *APOE* genotype lacks an *ApoE4* allele in *TREM2* variant controls, indicates that APOE may be exerting this change between *TREM2* variants, leading us to question whether the *TREM2 R47H* variant is acting independently. Further investigations into these pathways and the differences between *TREM2* variants that develop disease and those that don't may lead us to the mechanisms that can be targeted for treatments.

Table of contents

Table of tables

Table of figures

Glossary of terms

ABCA1	ATP-binding cassette sub-family A member 1
ABCA7	ATP-binding cassette sub-family A member 7
ACN	Acetonitrile
AD	Alzheimer's disease
AGPS	Alkyldihydroxyacetonephosphate synthase, peroxisomal
AHSG	Alpha-2-HS-glycoprotein
ALS	Amyotrophic lateral sclerosis
ANOVA	Analysis of variance
ANXA1	Annexin A1
ANXA2	Annexin A2
APH-1	Gamma-secretase subunit APH-1
APOE	Apolipoprotein E
APP	Amyloid precursor protein
AQP4	Aquaporin-4
ASAP3	Arf-GAP with SH3 domain, ANK repeat and PH domain-containing protein 3
ASB-14	Amidosulfobetaine-14
ATP	Adenosine triphosphate
Aβ	Amyloid-beta
BACE1	Beta-secretase 1
BGN	Biglycan
BIN1	Myc box-dependent-interacting protein 1
BRI2	Integral membrane protein 2B
C1q	Complement C1q
C3	Complement C3
C4A	Complement C4-A
C4B	Complement C4-B
CAA	Cerebral Amyloid Angiopathy
CBM	Cerebellum
CBD	Corticobasal degeneration
CCNG1	Cyclin-G1
CD11b	Integrin alpha-M
CD200	OX-2 membrane glycoprotein
CD33	Myeloid cell surface antigen CD33
CD45	Receptor-type tyrosine-protein phosphatase C
CD68	Macrosialin
CDH8	Cadherin-8
cDNA	Complementary deoxyribonucleic acid
CERAD	Consortium to Establish a Registry for Alzheimer's Disease
CFH	Complement factor H
CHCA	Alpha-cyano-4-hydroxycinnamic acid
CLU	Clusterin
CNS	Central Nervous System
COL25A1	Collagen alpha-1(XXV) chain

COL4A1	Collagen alpha-1(IV) chain
CR1	Complement receptor type 1
CRABP1	Cellular retinoic acid-binding protein 1
CRK	Adapter molecule crk
CRTC1	CREB-regulated transcription coactivator 1
CRYZL1	Quinone oxidoreductase-like protein 1
CSF	Cerebrospinal fluid
CSF-1	Macrophage colony-stimulating factor 1
CTGF	Connective tissue growth factor
CX3CR1	CX3C chemokine receptor 1
CXCR4	C-X-C chemokine receptor type 4
CYP46A1	Cholesterol 24-hydroxylase
DAB	3,3′-di-aminobenzidine
DAM	Disease associated microglia
DAP12	TYRO protein tyrosine kinase-binding protein
DAPI	4',6-diamidino-2-phenylindole
DAVID	Database for Annotation, Visualization and Integrated Discovery
DG	Dentate gyrus
DNA	Deoxyribonucleic acid
dNTP	Deoxyribonucleotide triphosphate
DOCK2	Dedicator of cytokinesis protein 2
DSC1	Desmocollin-1
EC	Entorhinal cortex
EDTA	Ethylenediaminetetraacetic acid
EIF2	Eukaryotic Initiation Factor 2
EPC2	Enhancer of polycomb homolog 2
ERK	Extracellular signal–regulated kinases
ERK5	Mitogen-activated protein kinase 7
FA	Formic acid
FAD	Familial Alzheimer's disease
FBD	Familial British Dementia
FCTX	Frontal cortex
FDD	Familial Danish Dementia
FDR	False Discovery Rate
FFPE	Fomalin-fixed paraffin embedded
FTD	Frontotemporal dementia
GAP43	Neuromodulin
GFAP	Glial fibrillary acidic protein
GO	Gene ontology
GOLGA8R	Golgin subfamily A member 8R
GRB2	Growth factor receptor-bound protein 2
GRIA2	Glutamate receptor 2
GTP	Guanosine-5'-triphosphate
GWAS	Genome wide association study
H_2O	Water
H_2O_2	Hydrogen peroxide

HBG2	Hemoglobin subunit gamma-2
HIPPO	Hippocampus
HLA-DR	HLA class II histocompatibility antigen, DR alpha chain
HSPA9	Stress-70 protein, mitochondrial
HSPG	Heparan sulfate proteoglycan
HTRA1	Serine protease HTRA1
IAA	Iodoacetamide
Iba1	Ionized calcium-binding adapter molecule 1
IFN	Interferon
IFN-γ	Interferon-gamma
IGF-1	Insulin-like growth factor 1
IL-1	Interleukin 1
IL-10	Interleukin 10
IL-1β	Interleukin 1 beta
IL-6	Interleukin 6
IL6R	Interleukin 6 receptor
INPP5D	Phosphatidylinositol 3,4,5-trisphosphate 5-phosphatase 1
IPA	Ingenuity Pathway Analysis
IPAD	Intramural periarterial drainage
ITAM	Immunoreceptor tyrosine-based activation motifs
ITIM	Immunoreceptor tyrosine-based inhibition motifs
KCNIP4	Kv channel-interacting protein 4
kDa	Kilodalton
KPNA6	Importin subunit alpha-7
KRT6A	Keratin, type II cytoskeletal 6A
LAMP	Lysosome-associated membrane family
LCM	Laser-capture microdissection
LDHA	Lactate dehydrogenase A
LDL	Low-density lipoprotein
LOAD	Late onset Alzheimer's disease
LPS	Lipopolysaccharide
LRP1	LDL-receptor related protein 1
LXR/RXR	Liver X receptor/ retinoid X receptor
mAb	Monoclonal antibody
MALDI	Matrix Assisted Laser Desorption Ionization
MAP1B	Microtubule Associated Protein 1B
MAPK	Mitogen-activated protein kinase
MAPT	Microtubule-associated protein tau
MCI	Mild cognitive impairment
MEF2C	Myocyte-specific enhancer factor 2C
$MgCl_2$	Magnesium Chloride
MGnD	Microglia in neurodegenerative state
MHC	Major histocompatability complex
MHC II	Major histocompatability complex class II
MHC III	Major histocompatability complex class III
MRC1	Macrophage mannose receptor 1

mRNA	Messenger ribonucleic acid
MS	Mass spectrometry
NaAC	Sodium acetate
NaCl	Sodium chloride
NADPH	Nicotinamide adenine dinucleotide phosphate
NFKB1	Nuclear factor NF-kappa-B p105 subunit
NFT	Neurofibrillary tangle
NT	Neuritic thread
NSG1	Neuronal vesicle trafficking-associated protein 1
OTUB1	Ubiquitin thioesterase OTUB1
P2RY12	P2Y purinoceptor 12
pAb	Polyclonal antibody
PARP1	Poly [ADP-ribose] polymerase 1
PC	Pressure cook
PCR	Polymerase Chain Reaction
PD	Parkinson's disease
pE	Pyroglutamate
PEN	Polyethylene naphthalate
PEN2	Gamma-secretase subunit PEN-2
PFA	Paraformaldehyde
PGE2	Prostaglandin E2
pGlu	Pyroglutamate
PiB	Pittsburgh compound B
PICALM	Phosphatidylinositol-binding clathrin assembly protein
PIK3C2G	Phosphatidylinositol 4-phosphate 3-kinase C2 domain-containing subunit gamma
PPIL2	Peptidyl-prolyl cis-trans isomerase-like 2
PRIM1	DNA primase small subunit
PRMT5	Protein arginine N-methyltransferase 5
PRPH	Peripherin
PrS	Presubiculum
PSAP	Prosaposin
PSEN1	Presenilin 1
PSEN2	Presenilin 2
PSMB7	Proteasome subunit beta type-7
PSP	Progressive Supranuclear Palsy
PURA	Transcriptional activator protein Pur-alpha
PUT	Putamen
PXN	Paxillin
qPCR	Quantitative polymerase chain reaction
QToF	Quadrupole time of flight
RAB21	Ras-related protein Rab-21
RB1CC1	RB1-inducible coiled-coil protein 1
RhoA	Ras homolog gene family, member A
RNA	Ribonucleic acid
ROS	Reactive oxygen species
RT-PCR	Real-time Polymerase Chain Reaction

SAD	Sporadic Alzheimer's disease
SCFD1	Sec1 family domain-containing protein 1
SEM	Standard error of mean
SERPINA3	Alpha-1-antichymotrypsin
SFTPC	Pulmonary surfactant-associated protein C
SNCA	Alpha-synuclein
SNP	Single nucleotide polymorphism
SNX6	Sorting nexin-6
SORL1	Sortilin-related receptor
SQSTM1	Sequestosome-1
sTREM2	Soluble triggering receptor expressed on myeloid cells 2
Sub	Subiculum
SYNPO	Synaptopodin
TBS	Tris buffered saline
TCTX	Temporal cortex
TE	Tris-EDTA
TFA	TriFluroacetic Acid
TGFB1	Transforming growth factor beta-1
TGFB2	Transforming growth factor beta-2
TLR	Toll-like receptor
TNF	Tumour necrosis factor
TNFα	Tumour necrosis factor alpha
TREM2	Triggering receptor expressed on myeloid cells 2
TSA	Tyramide signal amplification
TUSC5	Tumor suppressor candidate 5
TYROBP	TYRO protein tyrosine kinase-binding protein
VGF	Neurosecretory protein VGF
WM	White matter
XPO1	Exportin-1
XRCC5	X-ray repair cross-complementing protein 5

Publications

Manuscripts published

1. **Murray CE**, Gami-Patel P, Gkanatsiou E , Brinkmalm G, Portelius E, Blennow K, Ghiso J, Holton JL, Zetterberg H, Revesz T, Lashley T, Is the presubiculum preserved from neurodegenerative changes? A pathological and biochemical investigation, Acta Neuopathologica Communications, 2018

2. **Murray CE**, King A, Troakes C, Hodges A, Lashley T, *APOE ε4* is also required in *TREM2 R47H* variant carriers for Alzheimer's disease to develop, Neuropathology and Applied Neurobiology, 2018

3. **Murray CE**, Gami-Patel P, Kiely AP, Holton JL, Heywood WE, Mills K, Lashley T, Genetic and proteomic profiling of sporadic and familial Alzheimer's disease post-mortem brains. Neurodegener Dis 2017;17(suppl 1):8-590 – Page 241

4. **Murray CE,** Lim YM, Hodges A, Lashley T, Investigation of amyloid and microglial pathology in sporadic, familial and TREM2 variant Alzheimer's disease cases, Neuropathology and Applied Neurobiology, 2017 Feb 43: 47-48

5. **Murray CE**, Gami P, Kiely AP, Salih D, Holton J, Lashley T, Inflammatory gene expression profiles in sporadic, familial and TREM2 variant Alzheimer's disease, Neuropathology and Applied Neurobiology, 2016 Mar 42:15

6. **Murray CE**, Gami P, Portelius E, Holton JL, Zetterberg H, Revesz T, Lashley T, Could the parvopyramidal layer hold clues to protecting neurons from degeneration? Neuropathology and Applied Neurobiology, 2015 Mar 41:33

7. Cummings DM, Benway TA, Ho H, Tedoldi A, Fernandes Freitas MM, Shahab L, **Murray CE**, Richard-Londt A, Brandner S, Lashley TA, Salih DA, Edwards FA,

Neuronal and Peripheral pentraxins modify glutamate release and may interact in blood-brain barrier failure. Cerebral Cortex. 2017 Feb 23:1-12

8. Wauters SC, **Murray CE**, Heywood WE, Mills K, Lashley T, Proteomic profiling of frontotemporal lobar degeneration in post-mortem brains, Neuropathology and Applied Neurobiology, 2017 Feb 43: 41

9. Kvartsberg H, Lashley T, **Murray CE**, Zetterberg H, Blennow K, Portelius E, Characterization of the postsynaptic protein neurogranin in different brain regions from patients with familial Alzheimer's disease, sporadic Alzheimer's disease, pathological aging and healthy controls, Alzheimer's & Dementia 12 (Suppl 7S) 2016

10. Lim Y, Dumas A, King A, Troakes C, **Murray CE,** Lin K, Al-Sarraj S, Sivakumar L, Lashley T, Hodges A, AD-associated TREM2 variants lead to some subpopulations of microglia to be less abundant but more activated, Alzheimer's & Dementia 12 (Suppl 7S) 2016

11. Kiely AP, **Murray C**E, Asi YT, Ahmed Z, Lashley T, Revesz T, Holton JL, NanoString analysis of neuroinflammation in multiple system atrophy, Neuropathology and Applied Neurobiology. 2016 Mar 42:36-37

12. Gami P, **Murray CE**, Schottlaender L, Bettencourt C, De Pablo Fernandez E, Mudanohwo E, Mizielinska S, Polke JM, Holton JL, Isaacs AM, Houlden H, Revesz T, Lashley T, A 30-unit hexanucleotide repeat expansion in C9orf72 induces pathological lesions with dipeptide-repeat proteins and RNA foci, but not TDP-43 inclusions and clinical disease, Acta Neuropathol. 2015 Oct;130(4):599-601

13. **Murray CE,** Pressey SN, Heywood WE, Hargreaves IP, Neergheen V, Wauters S, Palkovits M, Gelpi E, Troakes C, Gentleman SM, Mills K, Holton JL, Revesz T,

Gandhi S, Mitochondrial dysfunction in Parkinson's disease: Is it the earliest feature? Neuropathology and Applied Neurobiology, 2015 Mar 41:11

14. Gami P, **Murray CE,** Schottlaender L, Bettencourt C, Mudanohwo E, Polke J, Revesz T, Houlden H, Lashley T, Comparative clinical, genetic and pathological study of C9orf72 expansion repeat cases, Neuropathology and Applied Neurobiology, 2015 Mar 41:25-26

15. **Murray CE,** Pressey SN, Gentleman SM, Holton JL, Gandhi S, Revesz T, Alpha-synuclein expression in early stage post-mortem Parkinson's disease brain, Neuropathology and Applied Neurobiology, 2014 Mar 40:12-13

16. Pressey SN, **Murray CE,** Heywood W, Gentleman SM, Mills K, Holton JL, Gandhi S, Revesz T, Uncovering early markers of Parkinson's disease pathological progression using proteomics, Movement Disorders, 2013 Jun 28:S369

Manuscripts in preparation

1. **Murray CE**, Lim YM, Hodges A, Lashley T, Distribution of pathology in *TREM2* variant cases compared to SAD and FAD

2. **Murray CE**, Gami-Patel P, Kiely AP, Salih D, Holton JL, Heywood WE, Mills K, Lashley T, Genetic and proteomic profiling of *TREM2* variant post-mortem brains compared to sporadic and familial Alzheimer’s disease cases

Chapter 1

Introduction

1 Introduction

1.1 Alzheimer's disease

Alzheimer's disease (AD) is the most common neurodegenerative disease and has a high prevalence worldwide. Over 50 million people have dementia worldwide and as life expectancy increases, this number is predicted to rise to 152 million by 2050 (World Health Organisation, Dementia fact sheet, 2017). With such large numbers, the cost to the economy will be huge and there is therefore a need for research to establish what causes the disease.

Symptoms vary between individuals, however, common symptoms include; memory loss, confusion, decreased visual perception and spatial awareness, changes in mood and problems finding the correct words.

A number of risk factors have been identified for sporadic AD, the largest of these being age with a significantly increased risk after the age 65 (Lane et al., 2017). Others include; smoking, alcohol, obesity, high cholesterol and blood pressure and those with Down syndrome are more at risk (Yaghmoor et al., 2014). In addition, having variants in the allelic ε4 expression in the *APOE* gene or variants in the *TREM2* gene can lead to an increased risk of late onset AD (Guerreiro et al., 2013a; Strittmatter et al., 1993a).

1.1.1 Pathology

Alzheimer's disease is characterized by its pathological hallmarks, Aβ plaques, neurofibrillary tau tangles (NFTs), and severe neuronal loss. A three-tiered grading system has been set out by the National Institute of Aging, Alzheimer Association guidelines to classify and confirm AD in post-mortem human brain. Firstly, the distribution of Aβ plaques are given an 0-5 score, as Thal staging, where the presence of Aβ deposits are assessed in the neocortex, allocortex and basal ganglia before later affecting the brain stem and cerebellum (Thal et al., 2002). Secondly, a Braak and Braak score of 0-6 is given for the distribution of tau pathology, where the NFT pathology is assessed according to the spread throughout the

brain reported by Braak and Braak, (1991). Lastly the frequency of neuritic plaques are staged with a score of none to frequent, called the CERAD score. The three different scores are then used to determine how severe the AD is as illustrated in Figure 1.1 (Montine et al., 2011).

"A"	Thal Phase for Aβ plaques [57]
0	0
1	1 or 2
2	3
3	4 or 5

"B"	Braak and Braak NFT stage [14,15]
0	None
1	I or II
2	III or IV
3	V or VI

"C"	CERAD neuritic plaque score [41]
0	None
1	Sparse
2	Moderate
3	Frequent

AD neuropathologic change		B[a]		
A[b]	C[c]	0 or 1	2	3
0	0	Not[d]	Not[d]	Not[d]
1	0 or 1	Low	Low	Low[e]
	2 or 3[f]	Low	Intermediate	Intermediate[e]
2	Any C	Low[g]	Intermediate	Intermediate[e]
3	0 or 1	Low[g]	Intermediate	Intermediate[e]
	2 or 3	Low[g]	Intermediate	High

Figure 1.1: Table outlining criteria for National Institute of Aging, Alzheimer Association classification system to diagnose stage of AD in any particular case (modified from Montine et. al 2011)

The underlying disease pathogenesis is still not fully understood. The amyloid cascade hypothesis suggests that Aβ is the causative seed of disease while others suggest it is tau (Hardy and Higgins, 1992). Some believe that it is the Aβ that initiates the tau pathology and that once seeded, neurodegeneration occurs. Recent evidence in which human pathological tau was injected into an AD mouse model and tau pathology indicative of AD such as NFT's, neuritic threads (NT) and dystrophic neurites surrounding the amyloid plaques accumulated, supports this hypothesis as the amyloid pathology already present seems to have induced the tau aggregation (He et al., 2018). Several pathogenic mutations for familial AD (FAD) are in genes involved with Aβ processing, giving strength to the argument of Aβ involvement in disease pathogenesis. Aβ can be detected in the CSF up to 10 years before dementia is observed in mild cognitive impairment (MCI) cases indicating that the protein accumulates over a long period of time (Buchhave et al., 2012; Zetterberg and Mattsson, 2014). Aβ pathology is also observed in cerebral amyloid angiopathy (CAA), in which the peptide

accumulates along the vessel walls. CAA is observed in 80-90% of AD cases. (Bergeron et al., 1987; Ellis et al., 1996; Nicoll et al., 2004; Yamada, 2000, 2002; Yamada et al., 1987). These findings provide evidence that Aβ accumulation has a detrimental effect in AD. However, another view is that the oligomeric, more soluble species of Aβ are more detrimental to the brain and the Aβ plaques accumulate as a protective mechanism (Glabe, 2006; Paranjape et al., 2012; Sengupta et al., 2016).

Tau forms aggregates in a number of neurodegenerative diseases named tauopathies. As tau pathology is present in several dementias such as progressive supranuclear palsy (PSP) and corticobasal degeneration (CBD), others believe that tau is the causative pathology in AD. Some believe tau to propagate in a prion-like manner and this has been the subject of investigation recently. Ahmed et al., (2014), created a model in P301S transgenic tau mice that shows spread of tau via synaptic connections. Furthermore, Vasconcelos et al., (2016) demonstrated that aggregated Aβ seeded tau pathology and aggregation using a tau aggregation assay. NFTs consist of hyperphosphorylated tau and have a different pattern of progression throughout the brain compared to Aβ plaques suggesting that the two proteins act through different mechanisms (Zetterberg and Mattsson, 2014). However, as the distribution of NFT's can be shown to relate to the clinical stages of the disease, first appearing in the entorhinal cortex, tau could be the protein that is closely linked to disease progression (Gentier and van Leeuwen, 2015; Zetterberg and Mattsson, 2014). Moreover, as tau can accumulate many years before AD symptoms are observed, tau could potentially be protective. However, as both Aβ and Tau accumulate in different areas of the brain before the onset of symptoms, this could indicate that a third mechanism is needed to start the cognitive decline, for cells to begin to die and that the presence of just Aβ and tau are not enough alone. Some argue that this third mechanism is linked to inflammation (Zetterberg and Mattsson, 2014). The presence of both Aβ and tau in pathological aging cases in which no clinical signs of dementia are seen suggests that this could be true (Murray and Dickson, 2014).

1.1.2 Amyloid processing

The Amyloid Precursor Protein (APP) is expressed in the brain and is a transmembrane protein that plays a role in functions such as brain development and plasticity (Zetterberg and Mattsson, 2014). The protein is sequentially cleaved with multiple secretases, creating different length peptide fragments as a result (Figure 1.2). It can be processed with alpha-secretase cleaving the Aβ domain nearest the N-terminus before a gamma-secretase complex consisting of presenilin-1 and 2, nicastrin and anterior pharynx defective 1 (APH-1), then cleaves the C-terminal part of the domain (Camargo et al., 2015; Zhang et al., 2014b). The segment of the protein is therefore released out of the cell and creates a non-amyloidogenic peptide. Secondly, the first cleavage at the N-terminal end is carried out by beta-secretase (BACE1) and produces a number of different length amyloidogenic peptides (Aβ) instead. These amyloidogenic Aβ peptides have normal roles in synaptic plasticity, alongside the presenilins that cleave them (Abramov et al., 2009; Zhang et al., 2009). However, during AD, the ratio of non-amyloidogenic peptides to amyloidogenic peptides is altered resulting in greater numbers of Aβ peptides which are more prone to aggregation than the non-amyloidogenic forms and they start to form amyloid plaques in the extracellular space. Gamma secretase cleaves in both the non-amyloidogenic pathway and the amyloidogenic pathway but helps to create different lengths of amyloid peptide. It can cleave after 40 amino acids or 42 amino acids. The $A\beta_{42}$ peptide is more prone to aggregation and higher levels of the $A\beta_{42}$ can be seen in AD (Masters and Selkoe, 2012).

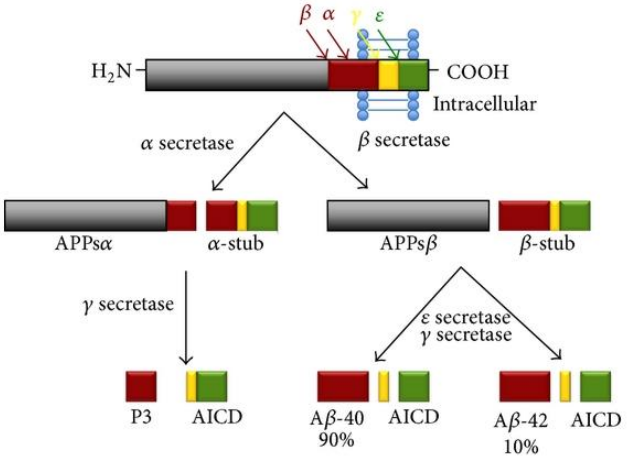

Figure 1.2: Proteolytic cleavage of Amyloid Precursor Protein. Sequential cleavage by α or β-secretase followed by γ- secretase at amino acid 40 or 42 (adapted from Mohktar et. al, 2013)

The amyloid cascade hypothesis formulated in 1992 suggested that other pathology all results from Aβ peptide aggregation (Hardy and Higgins, 1992). This led to the hypothesis that the formation of NFTs and cell loss occurs because of an imbalance between Aβ production and its clearance (Hardy and Selkoe, 2002).

1.1.3 Aβ clearance pathways

A number of mechanisms are involved in the clearance of Aβ. Examples include phagocytosis, enzymatic degradation and receptor-mediated efflux out of the brain, highlighted in Figure 1.3 (Tanzi et al., 2004). Intracellular Aβ is degraded via the Ubiquitin-proteosome system (UPS) or by the autophagy/ lysosomal system (ALS), whereas extracellular Aβ is cleared from the brain via different mechanisms (Xin et al., 2018). Aβ can be degraded by particular enzymes, such as neprilysin and insulin-degrading enzyme (Bohm et al., 2015; Hickman et al., 2008). Alternatively Aβ can be removed via phagocytosis by microglial cells. Microglia are known to accumulate around amyloid plaques and are thought to contribute to clearance mechanisms in this way (Hickman et al., 2008). However, the fastest route of Aβ efflux from the brain is thought to occur via the perivascular drainage pathway. In this pathway, Aβ is transported across the BBB into the vascular basement membrane and travels from the interstitial fluid into the blood away from the brain (Bohm et al., 2015; Xin et al., 2018). More recently, the concept of glyphatic drainage in addition to perivascular drainage has come to attention as an alternative route in which Aβ is drained into the CSF (Xin et al., 2018).

Many of these clearance systems have been shown to have reduced efficiency during AD pathogenesis. Inhibitors of Aβ clearance include antibodies against LDL- receptor related protein 1 (LRP1) and α_2-macroglobulin (Shibata et al., 2000). Clearance is thought to be inhibited if the triggering receptor expressed on myeloid cells 2 (TREM2) is impaired (Zhao and Lukiw, 2015). There have been a number of drug trials that have tried to increase the amount of Aβ clearance; however these have been largely unsuccessful (Karran and Hardy, 2014).

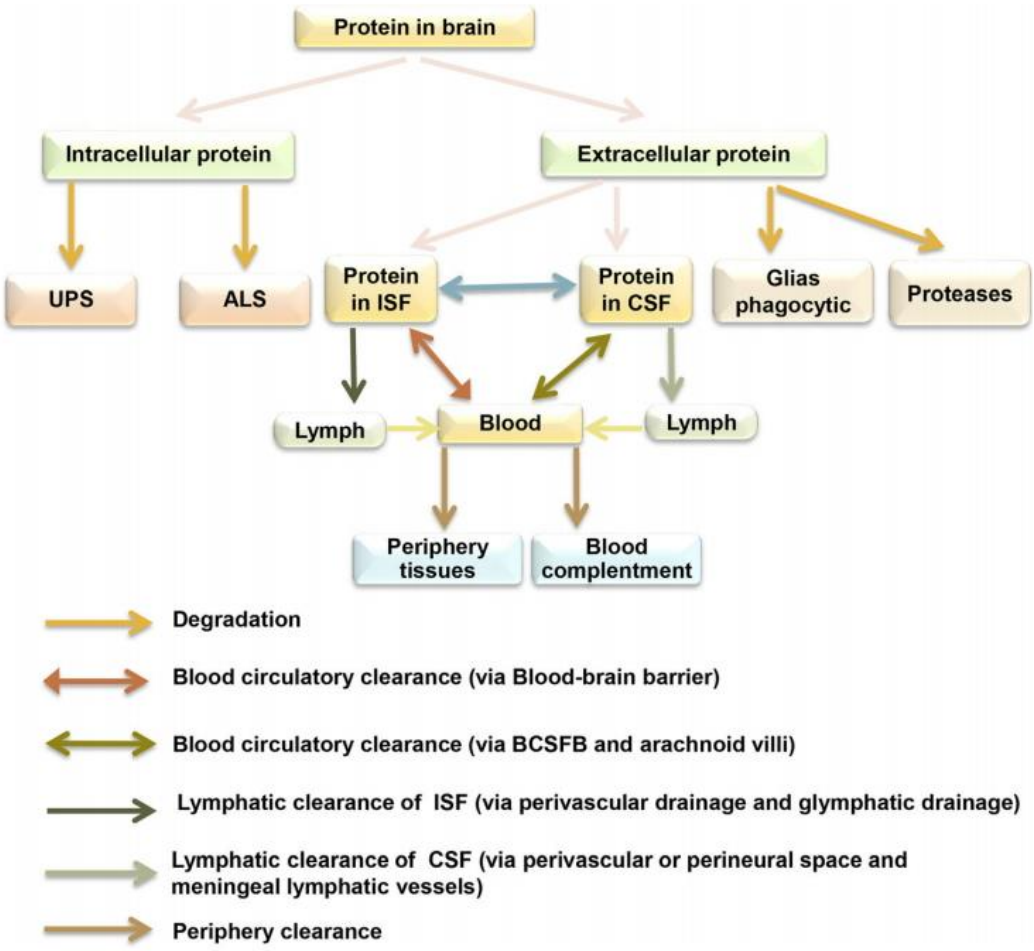

Figure 1.3: Clearance pathways present within the brain. UPS, Ubiquitin proteasome system; ALS, Autophagic/lysosomal system; ISF, Institial fluid; CSF, Cerebrospinal fluid; BCSFB, Blood-CSF- Barrier (adapted from Xin et. al, 2018)

1.1.4 Genetics

Familial forms of AD have been found to have mutations in the *APP* gene, presenilin 1 (*PSEN1*) and presenilin 2 (*PSEN2*) genes (Bertram and Tanzi, 2012; Bohm et al., 2015). Mutations in the *APP* gene affect the cleavage sites for the different secretases. For example, the Swedish mutation, K670N + M671L, changes the conformation of the protein so that a beta-secretase (BACE1) can bind more easily, therefore meaning a higher ratio of amyloidogenic peptides (Mullan et al., 1992; Zetterberg and Mattsson, 2014). However, it has been found that mutation A673T, has the opposite effect, decreasing the binding affinity

of BACE1 therefore producing less amyloidogenic peptides and having a decreased risk of AD (Jonsson et al., 2012a; Zetterberg and Mattsson, 2014).

The presenilin complex is involved in regulating the cleavage of a number of proteins. As it is part of the gamma-secretase complex, it is involved in *APP* processing. Mutations in the *PSEN1* gene are the most common form of familial AD (Russo et al., 2000). Missense, splice site and duplication mutations have been found in the presenilin genes and this also has an effect on the production of Aβ (Bohm et al., 2015). The increased production of Aβ in these familial forms of the disease cause early onset and a greater severity of symptoms. miRNA's have been shown to have a role in regulating APP processing by providing post-transcriptional regulation of the secretases. For example miR-339-5p downregulates BACE1 expression (Long et al., 2014). Alterations in the expression of these genes may highlight how sporadic AD can work along the same mechanisms as familial forms.

A variety of genome wide association studies have been performed in different populations of AD. The first large hit discovered was the *APOE* gene. It was discovered that having two *ApoE4* alleles in this gene increases susceptibility to late onset AD with a high odds ratio (Strittmatter et al., 1993a). Multiple lines of evidence in studies since this result have shown that ApoE has roles in Aβ clearance, metabolism and aggregation and can affect synaptogenesis (Huang and Mahley; Puglielli et al., 2003; Zetterberg and Mattsson, 2014).

More recently, GWAS studies have identified over 20 loci of common variants with small risk (Humphries and Kohli, 2014; Rosenthal and Kamboh, 2014). The majority of these hits identified genes involved in one of three different functions: inflammatory response (*TREM2, CR1 and CFH*) (Tanzi et al., 2004); endosome vesicle recycling (*BIN1, PICALM, and SORL1*); and cholesterol management (*ABCA7, ABCA1, CLU and CYP46A1*), (Camargo et al., 2015; Rosenthal and Kamboh, 2014; Zetterberg and Mattsson, 2014). Interestingly, some of these genes are also linked to *APP* processing and Aβ clearance showing that the mechanisms of AD may include defects in a number of different pathways (Camargo et al., 2015).

TREM2 was the largest of these hits and variants in this gene were found to be a risk factor for late onset AD with a similar odds ratio to *APOE* (Guerreiro et al., 2013a). Variants were found to be a risk factor for AD, Frontotemporal dementia (FTD), Amyotrophic lateral sclerosis (ALS) and Parkinson's disease (PD) (Jiao et al., 2014; Jin et al., 2015; Jonsson et al., 2012b; Kober et al., 2014; Lu et al., 2015).

1.2 TREM2

1.2.1 Genetic variants

A number of GWAS studies have reported variants in *TREM2* as a significant hit in the risk for neurodegenerative diseases (Jiao et al., 2014; Jin et al., 2015; Jonsson et al., 2012b; Kober et al., 2014; Lu et al., 2015). A number of different variants in the gene were discovered with only a few of these inferring risks of disease. The most common finding is the *R47H* variant which infers a risk for late onset AD in European populations with studies also showing significant association in Icelandic and African American populations, (Abduljaleel et al., 2014; Hooli et al., 2014; Korvatska O et al., 2015; Malkki, 2015; Ortega-Cubero et al., 2015; Rosenthal et al., 2015; Slattery et al., 2014). However, the variant did not reach significance in Iranian, Chinese or East Asian populations. Some also reported associations of risk for FTD with this variant but others found no association (Borroni et al., 2014; Thelen et al., 2014). Thelen et al., (2014) proposes that an FTD association is seen when underlying AD pathology is observed. Slattery et al., (2014) reported that people with the *R47H* variant often have earlier symptom onset but otherwise they are reported to have a similar disease course to those that have sporadic AD without a variant. Luis et al., (2014) also show the *R47H* variant carriers have a greater degree of grey matter loss, as measured by MRI volumetric analysis, suggesting that although they follow the same disease course clinically as the sporadic cases without a variant, they may get the disease earlier.

Twelve other *TREM2* variants were identified as outlined in Table 1.1 from Guerreiro et al., (2013a). Twenty-two variant alleles were found in 1092 AD cases and 5 variant alleles were found in 1107 control cases. They have been associated mainly with FTD and late onset AD with different odds ratios that do not associate as strongly as *R47H*.

1.2.2 Nasu-Hakola

Homozygous mutations in the *TREM2* gene result in a disease called Nasu-Hakola disease (Neumann and Daly, 2013). The *TREM2* variants Q33X, Y38C and T66M are responsible for the inherited form of this disease (Guerreiro et al., 2013a; Neumann and Daly, 2013). However, variants in the *TYROBP/DAP12* gene can also be responsible (Neumann and Daly, 2013; Solje et al., 2014). TYROBP/DAP12 is an adaptor molecule that binds to TREM2 and signals a downstream cascade of events (Dempsey, 2015; Jones et al., 2014; Lue et al., 2015; Neumann and Daly, 2013). This pathway is clearly indicated in the pathogenesis of this disease and the fact that some of these variants have been associated with risk for LOAD suggests that both diseases could share some common mechanisms (Neumann and Daly, 2013).

Nasu-Hakola, also known as polycystic lipomembranous osteodysplasia with sclerosing leukoencephalopathy, is a rare disease in which patients have a frontal-like dementia and multiple bone cysts at an early age (Neumann and Daly, 2013; Sasaki et al., 2015). These patients have a loss of myelin and white matter gliosis occurring in both the frontal and temporal lobes (Satoh et al., 2014). The glycosylation status of TREM2 is disrupted with some of these variants, impairing the ability for the cell to traffic TREM2 to the plasma membrane for further cleaving/shedding (Park et al., 2015a). A study using immunohistochemistry look at the microglia in this disease alongside protein analysis to correlate with DAP12 expression show that Nasu-Hakola patients have variable microglial expression of DAP12 (Sasaki et al., 2015). Satoh et al., (2011) report that whilst

Variant	SNP Number	Position†	Minor Alleles	Patients with Alzheimer's Disease		Controls		Reference Allele	P Value‡	Odds Ratio (95% CI)	PolyPhen-2§
				No. of Nonreference Alleles	No. of Cases	No. of Nonreference Alleles	No. of Controls				
All variants				60		38			0.02¶		
L211P	rs2234256	41126655	G	0	281	3	503	A	0.56	0	Benign (0.001)
H157Y	rs2234255	41127543	A	1	281	0	504	G	0.36	NA	Possibly damaging (0.7)
R136Q	rs149622783	41127605	T	1	281	1	501	C	1.00	1.8 (0.1–28.6)	Benign (0.0)
R98W	rs147564421	41129100	A	1	1091	0	1107	G	0.50	NA	Probably damaging (1.0)
T96K	rs2234253	41129105	T	4	1091	3	1105	G	0.72	1.4 (0.3–6.0)	Probably damaging (1.0)
D87N	rs142232675	41129133	T	6	1091	0	1105	C	0.02	NA	Probably damaging (1.0)
N68K	NA	41129188	C	0	1090	1	1105	G	1.00	0	Benign (0.05)
T66M	rs201258663	41129195	A	1	1091	0	1107	G	0.50	NA	Probably damaging (1.0)
R62H	rs143332484	41129207	T	25	1090	31	1104	C	0.50	0.8 (0.5–1.4)	Benign (0.02)
R47H	rs75932628	41129252	T	22	1091	5	1105	C	<0.001	4.5 (1.7–11.9)	Probably damaging (1.0)
Y38C	NA	41129279	G	3	1091	0	1107	A	0.12	NA	Probably damaging (1.0)
Q33X	rs104894002	41129295	A	2	1084	0	1103	G	0.25	NA	NA
Nasu–Hakola mutations	Q33X, Y38C, T66M			6		0			0.01	NA	Known damaging

Table 1.1: Coding Variants Found in *TREM2* through DNA Sequencing in Patients with Alzheimer's (adapted from Guerriero et. al, 2013a)

DAP12 can be detected on ramified microglia in controls, there is an absence of DAP12 expressing microglia in Nasu-Hakola patients. The microglia in the demyelinated lesions do however express CD33 (Satoh et al., 2015). CD33 has also been indicated to play a role in AD, thus adding further to the evidence that these two diseases share some common mechanisms (Rosenthal and Kamboh, 2014).

1.2.3 TREM2 structure and function

TREM2 (triggering receptor expressed on myeloid cells 2) is a 40kD, 230 amino acid transmembrane protein belonging to the immunoglobulin family that is expressed on the plasma membrane of a number of different dendritic cells, including microglia (Jones et al., 2014; Kober et al., 2014; Neumann and Daly, 2013; Paradowska-Gorycka and Jurkowska, 2013). TREM2 is mapped on human chromosome 6p21 and consists of an extracellular domain, a transmembrane domain and a cytoplasmic tail as shown in Figure 1.4 (Allcock et al., 2003; Paradowska-Gorycka and Jurkowska, 2013). The extracellular domain has three N-glycosylation sites (Paradowska-Gorycka and Jurkowska, 2013). It is part of a cluster of genes also including TREM1, TREM4, TREM5, TREML1, and TREML2. TREM3 is also found in mice (Klesney-Tait et al., 2006; Whittaker et al., 2010). It is a highly conserved

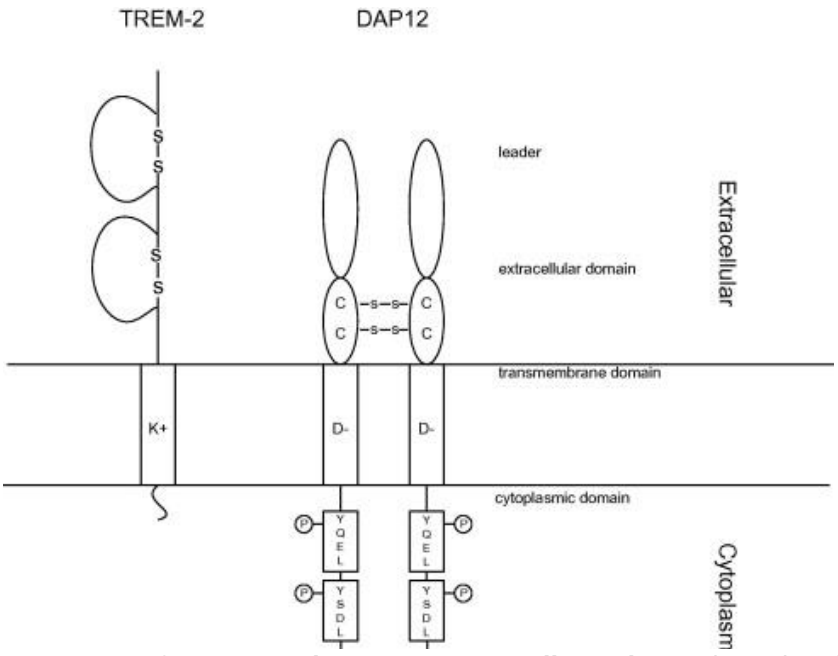

Figure 1.4: Structure of TREM2 and DAP12 across cell membrane (Paradowska-Gorycka et. al, 2013)

protein and is thought to be a hub or highly connected gene for microglia in a number of different brain regions, including regions that are affected in AD such as the hippocampus where the gene is highly connected (Forabosco et al., 2013; Matarin et al., 2015).

TREM2 is thought to function through two different pathways, one that suppresses inflammation and one that aids phagocytosis of any debris in or around the neurons (Frank et al., 2008; Guerreiro et al., 2013a; Park et al., 2015b; Rohn, 2013). It has been shown that TREM2 induces phagocytosis of apoptotic/injured neurons, Aβ plaques, damaged myelin and any cell debris (Jiang et al., 2013). Multiple studies have shown that when *TREM2* is downregulated there is less microglial activation, impaired phagocytosis of injured neurons/Aβ plaques and an increase in levels of Tumor Necrosis Factor (TNF) and nitric oxygen species whereas when *TREM2* is overexpressed there is increased phagocytosis and a decrease in pro-inflammatory signals (Jones et al., 2014; Takahashi et al., 2005). TREM2 is thought to suppress the inflammatory response through reducing any by-standing damage from inflammation, specifically inhibiting release and secretion of microglial cytokines and releasing TNF to promote survival (Jiang et al., 2013).

Multiple studies suggest that TREM2 plays an important role in AD through the clearance of Aβ plaques (Guerreiro et al., 2013a; Jones et al., 2014; Lue et al., 2015). In those with *TREM2* variants, microglia are less able to phagocytose the plaques and are therefore more at risk of disease (Jones et al., 2014). For example, *TREM2* expression correlates with β-secretase expression and the level of cortical Aβ (Guerreiro et al., 2013a; Martiskainen et al., 2015). TREM2 induces phagocytosis of Aβ peptides in culture and has been shown to be localized and upregulated in microglia that surround plaques in mice models. However, this is not the case when the mice are *TREM2* deficient (Lue et al., 2015). It is also reported that as AD progresses TREM2 is downregulated, Aβ42 is less efficiently cleared and the pro-inflammatory response increases (Hickman and El Khoury, 2014; Jones et al., 2014; Zhao et al., 2013).

One way that TREM2 performs these functions is by being able to recognise and bind to anionic lipids, lipopolysaccharides and zwitterions such as dextran sulphate, phosphatidylserine, sulfatides and sphingomyelin, both exposed in damaged neurons and in

bacteria (Dempsey, 2015; Neumann and Daly, 2013; Poliani et al., 2015; Wang et al., 2015). When fibrillar Aβ accumulates, it is thought to associate with lipids in lipid membranes and some bacteria (Grösgen et al., 2010; Zinser et al., 2007). When TREM2 recognises this, phagocytosis starts and plaques are cleared. It has been shown that when the *R47H TREM2* variant causes a change in the structure of the protein, it makes it more tightly folded and less able to bind to lipids (Abduljaleel et al., 2014; Wang et al., 2015). Therefore, it is hypothesized that this is the reason people with the *TREM2 R47H* variant are less able to clear plaques and are therefore at a higher risk of developing AD later in life.

TREM2 undergoes proteolytic processing at the plasma membrane in which γ-secretase cleaves the ectodomain creating both a C-terminal fragment and a secreted/soluble fragment that is released extracellularly called sTREM2, with sTREM2 binding to other nearby cells (Kleinberger et al., 2014; Wunderlich et al., 2013). Once cleaved, the Srk kinases are triggered to start their signalling cascade and when the tyrosine residues in the DAP12 protein (also known as TYROBP) are phosphorylated, the two bind and start the signal cascade that promotes phagocytosis and suppresses pro-inflammatory cytokine release from microglia (Colonna, 2003; Lue et al., 2015; Neumann and Daly, 2013). Several ligands for TREM2 have been identified, such as lipid ions and heat shock 60 protein that are reported to initiate the signalling cascade (Lue et al., 2015). Interestingly, both Bailey et al., (2015) and Atagi et al., (2015) provide evidence that APOE can bind to TREM2, suggesting that the two AD mechanisms are linked.

DAP12 is a transmembrane adaptor protein that contains ITAMS (immunoreceptor tyrosine-based activation motifs) and can also couple with Killer cell activating receptors on the surface of Natural Killer cells for antigen presentation (Aoki et al., 2003; Ma et al., 2014; Satoh et al., 2011). It is reported that DAP12 can also bind to the C-terminal fragment that is cleaved from the full-length protein therefore providing competition to the binding of DAP12 to full-length TREM2 and initiating the downstream signalling cascade (Ma et al., 2014; Wunderlich et al., 2013; Zhong et al., 2015). Over-expression of either the full-length protein or the C-terminal fragment show a decrease in inflammatory response so Zhong et al., (2015) suggest that DAP12 stabilises the concentration of TREM2 providing protection

against increased inflammatory responses. Satoh et al., (2015) also report that this type of ITAM signalling is controlled by ITIM (immunoreceptor tyrosine-based inhibitory motif) signalling.

1.3 Microglia

Microglia are immune cells of the central nervous system and derived from the myeloid lineage (Town et al., 2005). Originally it was thought that microglia had three different forms; amoeboid, ramified and intermediates and that when not in these forms they were resting microglia (Lynch, 2009). However, they are constantly scanning their environment looking for potential damage or debris, even when they are not activated. These resting microglia were thought to have a ramified appearance and cover all areas between neurons without any contact with one another (Altman, 1994). It was then believed that once they became activated they would become more amoeboid and migrate to the area affected (Altman, 1994).

Some believed that microglia had different phenotypes and activation states that determine what function and morphology they take on. Different markers were used to determine each of these phenotypes. It was thought that there were M1 (classical activation) and M2 (alternate activation) types of activated microglia with the M1 phenotype being pro-inflammatory and the M2 type being anti-inflammatory. The M2 subtypes were further classified into M2a and M2b phenotypes (Boche et al., 2013; Tang and Le, 2015). Although markers can be seen for the different functions of the microglia, either pro-inflammatory or anti-inflammatory, this classification of microglia being a certain phenotype was tentative.

There is now a consensus that microglia are actually in a state of continuum in which they can change phenotype/morphology depending on the environment around them, meaning a microglial cell can become any one of the phenotypes previously discussed (Lynch, 2009; Town et al., 2005). Microglia from the choroid plexus or perivascular microglia have a different origin so are thought to be in a more constantly activated state whereas the microglia from the parenchyma are found in a wider number of states (Altman, 1994). Environmental cues give signals to the microglia to determine what state they take. A

number of molecules found on microglia, such as TREM2, CD200 and CX3CR1, regulate the transition of microglia from one type to the next (Kierdorf and Prinz, 2013). This change can be seen within a few hours of any change in environment with the cells becoming more antigen presenting, more amoeboid, and starting to surround neurons (Altman, 1994).

Microglia become activated when there is a change in the environment surrounding it. For example, if there are foreign bodies in the space, if a neuron is dying or if the tissue is damaged, ATP can be released which also activates the microglia (Altman, 1994). A number of receptors are expressed on the cells once activated. IFN stimulates the microglia to present MHC antigens whereas Fc receptors are expressed when TNF/IL-1 are detected (Altman, 1994). When microglia are activated they release a number of molecules. One branch of these molecules are the complement proteins (Thameem Dheen et al., 2007). Other molecules released include CSF-1, IL-1, reactive oxygen species, nitric oxide, TNFα, PGE2 (Jones et al., 2014).

Wu et al., (2014) report that in mice the microglia can be transformed into a more protective phenotype when neural stem cells are in the environment. The presence of neural stem cells increases protective markers such as CX3CR1, IGF-1 and TREM2 and they are thought to activate the TLR9/ERK1/2 pathway. TGF and IL10 are also released by this type of microglia and are responsible for regulating tissue repair and suppressing reactive oxygen species (Chakrabarty et al., 2015).

Microglial priming is thought to increase the inflammatory response in aging individuals (Norden and Godbout, 2013; Perry and Holmes, 2014). By primed, it is meant that the microglia increase the amount of pro-inflammatory cytokines released and the number of receptors expressed on their surfaces meaning that when the immune system is challenged, the microglia are in a hyper-active state intensifying the inflammatory reaction (Perry and Holmes, 2014).

When microglia are in a pro-inflammatory phenotype, their actions can also be detrimental to the local environment as the molecules that they release can be cytotoxic (McGeer and McGeer, 1995). For example, cytokines, complement proteins and reactive oxygen species

(Shih et al., 2006; Thameem Dheen et al., 2007). When this occurs in neurodegenerative diseases such as AD, this can worsen the symptoms of the disease. As the majority of these diseases occur in the older population, brains are already primed due to aging, meaning the inflammatory aspect of the disease will have a larger effect.

Inflammation in AD therefore plays two roles in the disease. The pro-inflammatory reaction causes more neuronal damage, meaning that symptoms worsen (Wang et al., 2015). However, the anti-inflammatory reaction may help to clear the amyloid plaques and neurofibrillary tangles in the brain. The role that is most prominent in AD pathogenesis and neurodegeneration is still unclear.

There is a great deal of evidence showing that microglia are responsible for clearing amyloid plaques from the extracellular space (Lee et al., 2013; Rogers and Lue, 2001; Rogers et al., 2002). Dense plaques are surrounded by microglia that have thick cell processes and cytoplasmic swelling whereas more diffuse plaques have a more ramified microglial phenotype (Mattiace et al., 1990a). It is believed that after surrounding the plaques, the microglia phagocytose them by internalizing microaggregates of Aβ peptides (Paresce et al., 1997). Tuppo and Arias, (2005) reports that Aβ is pro-inflammatory itself as it can activate other inflammatory components. The anti-inflammatory microglia also try and suppress the pro-inflammation occurring by releasing CSF-1 which has been shown by Gomez-Nicola et al., (2013) to slow neuronal damage and progression. Increased amounts of MHC II molecules have also been observed in patients with AD and a number of different complement proteins are found to be in the plaques (Eikelenboom and Gool, 2004; Emmerling et al., 2000; Ishii and Haga, 1984; Kolev et al., 2009; Veerhuis et al., 1995).

1.4 Aims

This thesis aims to further elucidate the role that TREM2 is playing in AD and what this infers for other neurodegenerative diseases. By looking at human post-mortem brain tissue carrying *TREM2* variants and comparing these to sporadic AD cases (SAD), familial AD cases (FAD) and neurologically normal controls, it is hoped the impact that *TREM2* variants

have can be determined. This can be then used to evaluate what role the TREM2 protein plays normally and will potentially help us to further understand the pathogenesis of Alzheimer's disease and other neurodegenerative diseases.

To achieve this cases will be used to:

1. Investigate the pathological hallmarks of Aβ plaques and NFT's by performing immunohistochemistry to assess load of both pathologies and type of amyloid plaque across Thal phases

2. Investigate the microglial phenotype that is present by performing immunohistochemistry with multiple microglial markers and assessing the load, shape and perimeter of the cells stained with each marker

3. Investigate the human inflammatory genetic profile using nanostring

4. Investigate the proteomic profile using label-free quantitative mass spectrometry techniques and comparing to genetic profile data

5. Investigate the presubiculum, an area protected from AD pathology, using immunohistochemistry and biochemical techniques.

1.5 Hypothesis

The *TREM2* variant cases will differ in their pathological, genetic and proteomic profiles when compared to SAD and FAD. *TREM2* variant AD cases will have increased Aβ loads and a different composition of amyloid plaques determined by immunohistochemistry. In addition, they will have an altered tau load. Microglia will not surround the amyloid plaques in the *TREM2* variant cases to the same extent as other AD cases and will therefore be less activated and in a more ramified, homeostatic phenotype. As *TREM2* is an inflammatory marker, the *TREM2* variant cases will have an altered inflammatory profile both genetically and proteomically. The presubiculum will be an area that is protected from neurodegeneration and will have an altered proteomic profile to the neighbouring entorhinal cortex region.

Chapter 2

Materials and Methods

2 Materials and Methods

2.1 Case demographics and ethics

2.1.1 Case selection

All cases were provided by the collection at Queen Square Brain Bank for Neurological Disorders, London, United Kingdom. Cases were fully consented and have full ethical approval for use in this study. The six cases that have previously been identified as having a *TREM2* variant by Guerreiro et al., (2013a) using exome or full genome sequencing were used in this study . Two of these are pathologically diagnosed as healthy controls with three having a neuropathologically confirmed diagnosis of sporadic Alzheimer's disease (SAD) and one having a diagnosis of familial Alzheimer's disease (FAD) due to a *PSEN1* mutation. Five of the cases have the *R47H* variant with one AD case having the *D87N* variant (Table 2.3). Nineteen SAD cases (Table 2.3) were selected to match the *TREM2* variant cases in sex, age, post-mortem delay and disease stage (Table 2.2). A third group of eleven FAD cases were selected (Table 2.3); eight *PSEN1* variants and three *APP* variants. However, due to the early onset of FAD cases these did not match the other cases in age of onset or death but do match for post-mortem delay and disease duration (Table 2.2). A control group of pathological aging cases were used to determine if any differences seen were due to AD or pathological aging (Table 2.3). Other GWAS hits related to AD were not investigated in these cases.

2.1.2 Staging of cases

A neuropathological diagnosis was determined by neuropathologists at Queen Square Brain Bank. Cases were assessed using the three-tiered grading system set out by the National Institute of Aging, Alzheimer's Association guidelines. Firstly, the distribution of Aβ plaques were given a Thal phase 0-5 score, where the presence of Aβ deposits are assessed in the neocortex, allocortex and basal ganglia before later affecting the brain stem and cerebellum (Thal et al., 2002). Secondly, a Braak and Braak score of 0-6 was given for the distribution of

tau pathology, where the NFT pathology is assessed according to its suggested spread throughout the brain (Braak and Braak, 1991). Lastly the frequencies of neuritic plaques were staged with a score of none to frequent, called the CERAD score. The three different scores are then used to determine how severe the AD is using the criteria shown in Table 2.1 (Montine et al., 2011). The detailed pathological staging of the cases is outlined in Table 2.3.

A	Thal phase for Aβ plaques	B	Braak and Braak NFT stage	C	CERAD neuritic plaque score
0	0	0	none	0	none
1	1 or 2	1	I or II	1	sparse
2	3	2	III or IV	2	moderate
3	4 or 5	3	V or VI	3	frequent

Table 2.1: National Institute of Aging, Alzheimer's Association staging criteria for determining severity of Alzheimer's disease. Table modified from (Montine et al., 2011).

Age at onset	**p=0.0016**	****
SAD vs. FAD	p=0.0011	**
SAD vs. TREM2	p=0.6769	ns
FAD vs. TREM2	p=0.7215	ns
Age at death	**p=0.0002**	*******
SAD vs. FAD	p=0.0199	*
SAD vs. TREM2	p>0.9999	ns
SAD vs. Control	p=0.1448	ns
FAD vs. TREM2	p=0.4102	ns
FAD vs. Control	p=0.0001	***
TREM2 vs. Control	p=0.1873	ns
Disease duration	**p=0.9971**	**ns**
SAD vs. FAD	p>0.9999	ns
SAD vs. TREM2	p>0.9999	ns
FAD vs. TREM2	p>0.9999	ns
Post-mortem delay	**p=0.2705**	**ns**
SAD vs. FAD	p>0.9999	ns
SAD vs. TREM2	p>0.9999	ns
SAD vs. Control	p=0.4607	ns
FAD vs. TREM2	p>0.9999	ns
FAD vs. Control	p>0.9999	ns
TREM2 vs. Control	p>0.9999	ns

Table 2.2: Statistics comparing disease groups. Kruskal-Wallis one way ANOVA with Dunn's multiple comparisons was performed on age of onset, age at death, disease duration and post-mortem delay. * for p<0.05, ** for p<0.005, *** for p<0.0005, ****p<0.0001, ns for non-significant.

Case	Sex	Age of onset	Age at death	Disease duration	Post-mortem delay	Mutations	ApoE status	Clinical diagnosis	Pathological diagnosis	Braak and Braak	Thal	CERAD	ABC
TREM2 Variant cases													
1	M	55	64	9	35:40:00	R47H	E3/E4	CBS	SAD	6	5	Frequent	A3B3C3
2	F	56	66	15	51:20:00	R47H	E4/E4	SAD	SAD	6	5	Frequent	A3B3C3
3	M	-	76	-	60:35:00	R47H	E2/E2	Control	Control	0	0	None	A0B0C0
4	M	-	82	-	25:30:00	R47H	E3/E3	Control	Control	0	0	None	A0B0C0
5	M	60	71	11	52:30:00	D87N	E3/E4	FTD	SAD	6	5	Frequent	A3B3C3
6	F	36	41	5	64:15:00	R47H Pre 200 PS1	E3/E3	SAD	FAD	6	5	Frequent	A3B3C3
Sporadic Alzheimer's disease cases (SAD)													
7	M	63	73	10	31:10:00	-	-	SAD	SAD	6	5	Frequent	A3B3C3
8	F	51	63	12	16:00:00	-	E3/E4	SAD	SAD	6	5	Frequent	A3B3C3
9	F	51	62	11	62:55:00	-	E3/E4	SAD	SAD	6	5	Frequent	A3B3C3
10	F	65	70	5	46:58:00	-	E3/E3	SAD	SAD	5	5	Moderate	A3B3C3
11	M	64	77	13	90:05:00	-	E4/E4	SAD	SAD	6	5	Frequent	A3B3C3
12	F	49	62	13	76:40:00	-	E3/E3	SAD	SAD	6	5	Frequent	A3B3C3
13	M	72	88	16	85:35:00	-	E3/E4	SAD	SAD	6	5	Frequent	A3B3C3
14	M	52	69	17	35:04:00	-	E3/E3	SAD	SAD	6	5	Frequent	A3B3C3
15	M	65	72	7	38:55:00	-	E3/E4	SAD	SAD	5	5	Moderate	A3B3C3
16	F	76	85	9	90:20:00	-	E3/E4	SAD	SAD	6	5	Frequent	A3B3C3
17	M	55	64	9	76:45:00	-	E3/E4	SAD	SAD	6	5	Frequent	A3B3C3
18	F	69	74	5	93:40:00	-	-	SAD	SAD	6	5	Frequent	A3B3C3
19	M	80	85	5	129:15:00	-	-	SAD	SAD	5	5	Moderate	A3B3C3
20	F	46	52	6	51:55:00	-	-	LBD	SAD	6	5	Frequent	A3B3C3
21	F	49	55	6	47:50:00	-	E3/E3	SAD	SAD	6	5	Frequent	A3B3C3

Case	Sex	Age of onset	Age at death	Disease duration	Post-mortem delay	Mutations	ApoE status	Clinical diagnosis	Pathological diagnosis	Braak and Braak	Thal	CERAD	ABC
22	M	67	72	5	91:10:00	-	E2/E4	bvFTD	SAD	6	5	Frequent	A3B3C3
23	F	65	79	14	22:30:00	-	E3/E4	SAD	SAD	6	5	Frequent	A3B3C3
24	M	52	68	16	35:20:00	-	E3/E4	FTD/Picks	SAD	6	5	Frequent	A3B3C3
25	M	58	68	10	52:05:00	-	E3/E4	SAD	SAD	6	5	Frequent	A3B3C3
Familial Alzheimer's disease cases (FAD)													
26	F	48	59	11	26:15:00	PSEN1 202F	E4/E4	FAD	FAD	6	5	Frequent	A3B3C3
27	F	35	52	17	32:30:00	PSEN1 Intron 4	E4/E4	FAD	FAD	6	5	Frequent	A3B3C3
28	M	61	70	9	161:15:00	PSEN1 S132A	E3/E4	FAD	FAD	5	5	Frequent	A3B3C3
29	M	42	51	9	43:10:00	PSEN1 mutation	E3/E3	FAD	FAD	6	5	Frequent	A3B3C3
30	F	48	59	11	89:42:00	V717L APP	E3/E3	FAD	FAD	6	5	Frequent	A3B3C3
31	M	60	66	6	68:05:00	V717L APP	E3/E3	FAD	FAD	6	5	Frequent	A3B3C3
32	M	42	47	5	43:50:00	PSEN1 A434T & T291A	E3/E3	MSA	FAD	5	5	Frequent	A3B3C3
33	F	46	66	20	31:55:00	R278I	E3/E4	FAD	FAD	6	5	Frequent	A3B3C3
34	F	33	37	4	24:15:00	E120K exon 5 PSEN1	E3/E3	FAD	FAD	6	5	Frequent	A3B3C3
35	F	44	56	12	16:25:00	APP V717I	E3/E3	FAD	FAD	6	5	Frequent	A3B3C3
36	F	39	47	8	-	PSEN1 Intron 4	E3/E3	FAD	FAD	6	5	Frequent	A3B3C3
Control cases													
37	M	-	87	-	57:00:00	-	E3/E3	Normal	Normal/ pathological aging	2	3	Moderate	A2B1C2

Case	Sex	Age of onset	Age at death	Disease duration	Post-mortem delay	Mutations	ApoE status	Clinical diagnosis	Pathological diagnosis	Braak and Braak	Thal	CERAD	ABC
38	M	-	81	-	50:55:00	-	E2/E2	Normal	Normal/ pathological aging	2	1	Sparse	A1B1C0
39	F	-	73	-	24:00:00	-	E3/E4	Normal	Pathological aging	2	2	Sparse	A1B1C2
40	M	-	88	-	16:15:00	-	E3/E3	Normal	Pathological aging	2	2	Moderate	A1B1C2
41	F	-	80	-	49:10:00	-	E3/E3	Normal	Normal/ pathological aging	0	2	None	A0B1C0
42	F	-	93	-	29:40:00	-	E3/E3	Normal	Normal/ pathological aging	3	1	Moderate	A1B2C2
Averages													
TREM2	2F:4M	52	67	10	50:35:00	-	-	-	-	4	3	-	A2B2C2
SAD	9F:10M	60	70	10	61:48:00	-	-	-	-	6	5	-	A3B3C3
FAD	7F:4M	45	55	10	53:44:12	-	-	-	-	6	5	-	A3B3C3
Control	3F:3M	-	84	-	37:50:00	-	-	-	-	2	2	-	A1B1C1

Table 2.3: Case demographics

2.2 APOE status

2.2.1 DNA extraction

100mg of frozen cerebellum was chipped from a selection of cases (cases 1-5, 8-17, 21-25, 37-42) where ApoE status was not already determined (cases 6, 26-36) and where frozen tissue was available (cases 7, 18-20). Tissue was homogenised in extraction buffer (0.1M NaCl, 20mM Trizma base, 25mM EDTA disodium, 0.5% SDS), proteinase-K solution (10mg/ml) added, the samples inverted and incubated at 55°C for three days to digest the tissue. A 1:1:1 mix of phenol, chloroform and IAA (Invitrogen) was added, samples vortexed and centrifuged for five minutes at 12,000rpm. The top aqueous layer was removed into a clean Eppendorf tube and 3M NaAC pH5.3 added to it. Samples were vortexed and 100% ethanol was added to enable the DNA to precipitate. Samples were kept at -20°C for twenty-four hours to allow further precipitation to occur before being spun for twenty minutes at 12,000rpm at 4°C. The aqueous supernatant was removed by aspiration and 70% ethanol was used to wash the pellets containing the DNA. Samples were kept at 4°C for twenty minutes before being spun again for five minutes at 12,000rpm. Ethanol wash was removed by aspiration. The pellet was left to dry at room temperature before being resuspended in TE (Tris-EDTA) solution and stored at 4°C.

2.2.2 Genotyping

The Qiagen PCR Mix–GC Rich kit was used to create a PCR master mix including Q solution, dNTPs, Taq, a forward primer, a reverse primer and a buffer containing 15mM $MgCl_2$ and H_2O. The primers used to determine the ApoE status were previously reported and detailed in Table 2.4 (Emi et al., 1988). The master mix was added to DNA from each sample and a PCR run with the following settings: 94°C for five minutes, 30x (94°C for thirty seconds, 60°C for thirty seconds, 72°C for thirty seconds), 72°C for five minutes before being left at 4°C. The PCR end products were digested using the *Hha*I kit (Promega). The buffer with HhaI was added to samples, vortexed and spun before being incubated at 37°C for two hours. A metaphor agarose gel was prepared with 3% metaphor agarose and 2% normal agarose with GelRed dye added. Thermo Scientific O'Range Ruller 10bp DNA ladder was

added to one well and the digested PCR end product for each sample added to the other wells. The gel was run for one hour thirty minutes at 80V before being visualised in a DNR Bio-Imaging Systems MiniBIS Pro.

F4 primer:	ACAGAATTCGCCCCGGCCTGGTACAC
F6 primer:	TAAGCTTGGCACGGCTGTCCAAGGA

Table 2.4: Primers used for *APOE* genotyping. Reported in (Emi et al. 1988).

2.3 Tissue processing

Post-mortem brain tissue donated to Queen Square Brain Bank arrives fresh and is hemi-dissected. The right half is coronally sectioned and is flash frozen at -80°C. The left half is immersed in 10% buffered formalin solution for three weeks before being examined and cut into five mm coronal slices. Small blocks are then taken and are processed to ensure preservation of the material. They are processed on a six-day cycle through graded alcohols and chloroform as outlined in Table 2.5. They are then embedded into paraffin wax and eight µm sections are taken for immunohistochemistry.

Step	Reagent	Time spent (6 day cycle)
1	70% Alcohol	12.00hrs
2	90% Alcohol	12.00hrs
3	90% Alcohol	12.00hrs
4	Absolute alcohol	12.00hrs
5	Absolute alcohol	12.00hrs
6	Absolute alcohol	12.00hrs
7	Absolute alcohol	12.00hrs
8	Chloroform	12.00hrs
9	Chloroform	12.00hrs
10	Wax	12.00hrs
11	Wax	12.00hrs
12	Wax	12.00hrs

Table 2.5: Steps of 6 day tissue processing cycle

2.4 Immunohistochemistry

2.4.1 Formalin fixed paraffin embedded (FFPE) sections

Eight µm thick sections were cut from formalin-fixed, paraffin-embedded tissue from frontal cortex, temporal cortex, hippocampus, putamen and cerebellum of all cases. Slides were dried overnight at 37°C before being adhered at 60°C. The paraffin was removed using xylene and slides were rehydrated with absolute alcohol. Endogenous peroxide activity was blocked using a methanol/H_20_2 (0.3%) solution. Sections were pre-treated according to subsequent antibody use shown in Table 2.6. Additionally, some sections were treated with 98% formic acid for ten minutes at room temperature before being washed in H_2O. All slides were placed in citrate buffer (0.45g citric acid, 5.8g tri-sodium citrate, 2 litres deionised H_2O, pH6) and heated in a pressure cooker for ten minutes. Slides were incubated in 10% non-fat milk solution/ TBS for thirty minutes at room temperature, to block unspecific antibody binding. Primary antibodies were applied for one hour at room temperature, the concentration of each antibody used is shown in Table 2.6. Antibodies are commercially available and the majority are used in routine practice for neuropathological diagnosis. Those antibodies that are not used routinely in diagnostic practice underwent a round of quality control, incubating with a range of dilutions to see if the signal was specific. The slides were washed in TBS-Tween solution (Thermo Scientific) before being placed in the respective biotinylated secondary antibodies (rabbit anti-mouse, 1:200, Dako, swine anti-rabbit, 1:200, Dako) for thirty minutes. After a second round of washing in TBS-Tween, Avidin-Biotin Complex solution (Vector) was applied for thirty minutes. Slides were washed before 3,3′-di-aminobenzidine-TBS-H_20_2 solution (1ml 5% DAB in 100ml TBS-Tween, 32µl H_2O_2) was used as the chromogen and slides were counterstained in Mayer's haematoxylin (1g haematoxylin, 50g potassium or aluminium alum, 0.2g sodium iodate, 50g chloral hydrate). Slides were dehydrated through 70% alcohol, 90% alcohol, absolute alcohol and xylene, then mounted using DPX mounting medium (Thermo Scientific). Slides were then viewed under the Nikon Eclipse Ni microscope and photographs were taken for illustrative purposes at several magnifications. For quantitative analysis slides were scanned at 40x magnification using a Leica SCN400F slide scanner.

2.4.2 Frozen sections

Frozen sections from SAD cases and control cases were cut at 10µm on a cryostat (Bright, OTF5000) and mounted onto superfrost slides (Solmedia), then stored at -80^{0}C until required. Sections were air dried for ten minutes before either being fixed in 4% PFA or ice-cold acetone for thirty minutes depending on the downstream immunohistochemical analysis. Slides were washed for five minutes, three times in TBS-Tween before being incubated in 10% non-fat milk for thirty minutes. The rest of the immunohistochemical protocol followed the methods in section 2.4.1.

2.4.3 Immunoflourescence

Double immunohistochemistry was performed with several antibodies to check if staining was specific to certain cell types. Frozen sections were used and treated with the same protocol detailed in section 2.4.2. After the avidin-biotin complex was applied, TSA red (Perkin Elmer) was applied for fifteen minutes at room temperature before the second primary antibody was added onto the sections and left to incubate overnight at 4°C. The sections were washed in TBS-Tween for five minutes, three times, the relevant secondary antibody and avidin-biotin complex applied as previously described before the sections were incubated in TSA green (Perkin Elmer). Slides were washed in TBS-Tween before the sections were mounted using mounting medium with DAPI (Vector Labs). These slides were then observed on Leica DM5500B microscope and fluorescent images taken from z stacks with both stains and overlaid to investigate co-localisation.

Antibody	Catalogue number	Species	Clonality	Dilution	Pretreaments	Secondary antibody used
TREM2	Abcam (ab117645)	goat	pAb	1:50/1:100	PC tested	rabbit anti goat biotinylated
TREM2	Abgent (AP5469a)	rabbit	pAb	1:50/1:200	PC tested	swine anti rabbit biotinylated
TREM2	SantaCruz (sc-373828)	mouse	mAb	1:150	PC tested	rabbit anti mouse biotinylated
TREM2	Sigma (HPA010917)	rabbit	pAb	1:100	PC tested	swine anti rabbit biotinylated
TREM2	Sigma (HPA012571)	rabbit	pAb	1:100	PC + FA tested	swine anti rabbit biotinylated
TREM2	R&D (AF1828)	goat	pAb	1:;40	PC + FA tested	rabbit anti goat biotinylated
TREM2	Proteintech (13483-1-AP)	rabbit	pAb	1:100/1:200	PC + FA tested	swine anti rabbit biotinylated
Aβ	Dako (M0872)	mouse	mAb	1:100	PC + FA	rabbit anti mouse biotinylated
AT8	Thermo (MN1020)	mouse	mAb	1:600	PC	rabbit anti mouse biotinylated
Iba1 (microglial motility marker)	Wako (019-19741)	rabbit	pAb	1:1000	PC	swine anti rabbit biotinylated
CD68 (microglial phagocytic marker)	Dako (M0876)	mouse	mAb	1:100	PC	rabbit anti mouse biotinylated
CR3-43 (microglial antigen-presenting marker)	Dako (M0775)	mouse	mAb	1:150	PC	rabbit anti mouse biotinylated
P2RY12 (microglial homeostatic marker, unique to microglia)	Sigma (HPA014518)	rabbit	pAb	1:100	PC	swine anti rabbit biotinylated
1-57 (N-terminal $A\beta_{pE3)}$	Synaptic systems (#218311)	mouse	mAb	1:1000	PC + FA	rabbit anti mouse biotinylated
2-48 (N-terminal $A\beta_{pE3}$)	Synaptic systems (#218011)	mouse	mAb	1:100	PC + FA	rabbit anti mouse biotinylated
pE-Aβ	Synaptic Systems (#218011)	rabbit	pAb	1:200	PC + FA	swine anti rabbit biotinylated

Table 2.6: Details of primary antibodies used

2.4.4 Thioflavin S staining

Thioflavin-S staining was performed to visualise Aβ in an amyloid conformational state. Immunofluorescence with an Aβ antibody was performed with methods outlined in section 2.4.3 in the red channel. Sections were then incubated in 0.1% aqueous Thioflavin-S solution (Sigma) for seven minutes at room temperature. 70% ethanol was used to dehydrate the sections and wash the excess Thioflavin-S off the sections. Sections were then mounted with Vector mounting medium with DAPI and coverslipped. These slides were then observed on Leica DM5500B microscope and fluorescent images taken from z stacks with both stains.

2.5 Pathology analysis

2.5.1 Regions analysed

To analyse the amount of Aβ plaques, tau and microglial loads throughout the AD brains, the Thal staging regions were analysed, as these regions are an indicator of pathology progression throughout the brain. This included the frontal cortex, temporal cortex, hippocampus, putamen and cerebellum regions (Thal et al., 2000). The substantia nigra is also a Thal staging region. However, as the neuromelanin in the dopaminergic neurons is also brown they were sometimes hard to distinguish from the DAB staining meaning it was difficult to decipher the pathology being invesigated (Aβ plaques, NFT's or microglia). Therefore, this area was not used in final analysis. P2RY12 microglial analysis was undertaken later than other microglial analysis, as it was only recently discovered to be a marker of homeostatic microglia (Hickman and El Khoury, 2014). Therefore, due to time constraints only the frontal cortex, temporal cortex and hippocampal areas were analysed with this antibody.

2.5.2 Region selection

All sections were scanned using a Leica slide scanner at 40x magnification and a digital image was then stored. Aperio Imagescope (v12.3.0.5056) was used to view the images and

extract the area of interest decreasing the file size. The extracted images were loaded into ImageJ (https://imagej.nih.gov/ij/) and a macro used, developed by a collaborator (Yau Lim, Kings College London), to analyse the areal fraction of the immunohistochemistry, the number of microglia and the circularity of the microglial staining. The macro allowed a region of interest to be selected on the image. Image J measured the coordinates of the region of interest. The coordinates were added to a Python script which generated coordinates of random squares. The random squares from the region of interest were then analysed (Figure 2.1). Random squares were selected at 1000x1000 pixels square which represented 500µm^2. Bland-Altman plots with linear regression were utilised to determine the number of squares needed for reproducibility of results (Appendix Figure 1).

2.5.3 Manual counting

The macro could not be used to distinguish the type of plaque or the number of NFT's alone due to all DAB staining being counted in the analysis. The analysis would therefore count all plaque types together and pathological tau including NFTs, neurites and dystrophic neurites. Therefore, a manual counting method was utilised for this type of analysis. After random squares had been generated using the Python script for each area in each case, NFT's and different plaque types (diffuse or dense-core) were manually counted to determine how many NFTs or plaques were in the representative sample. Whole NFTs were systematically counted with any partial NFT's on the edge of images excluded. NFTs were identified as large, globose masses in the neuron cytoplasm (Probst et al., 1991a). Dense core plaques were only counted when a dense core could be seen (Figure 2.2a), otherwise they were counted as diffuse plaques (Figure 2.2b). Only whole plaques were counted as to not exclude any dense cores. The number for each random square was taken before a mean was calculated for each case in each region and Wilcoxon-paired rank tests were performed to determine any significant differences between each region at a level of $p<0.05$.

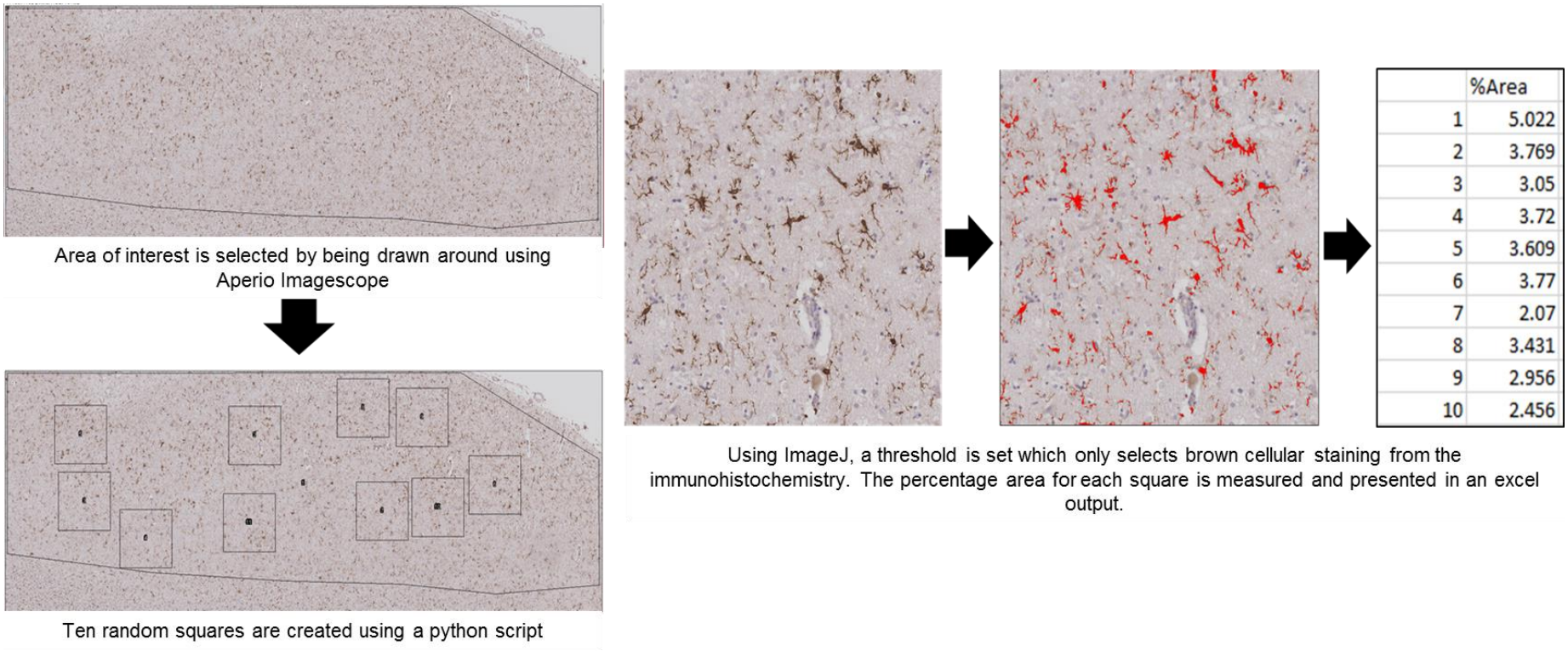

	%Area
1	5.022
2	3.769
3	3.05
4	3.72
5	3.609
6	3.77
7	2.07
8	3.431
9	2.956
10	2.456

Figure 2.1: A flow diagram showing process of analysing the immunohistochemical staining using Imagescope, Python and ImageJ software

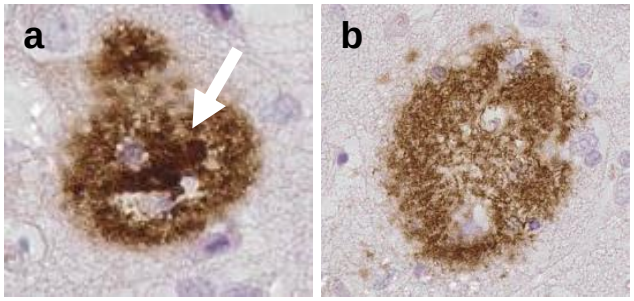

Figure 2.2: Distinguishing between dense-core (a) and diffuse (b) Aβ plaques. Dense core highlighted by white arrow

2.5.4 Density/Areal fraction

After random squares were generated using a Python script as detailed above, the macro developed by Yau Lim (unpublished method) was used to determine the area of the square that was immunohistochemically stained with 3,3′-di-aminobenzidine by each antibody. A threshold was set between sixty-eighty saturation to select all the brown chromogen (Figure 2.1). Areal fractions were calculated for each square and means were then taken for each case, each region and each antibody. Kruskal-Wallis one way ANOVA tests with Dunn's multiple comparisons were performed to determine any significant differences at a level of $p<0.05$.

2.5.5 Circularity and size

For all microglial antibodies, the shape and size of the microglia were assessed using the same macro. Each single microglia was given a measure on how round it was using the hull and circle function in ImageJ, with 1 being a perfect circle and 0 being an imperfect shape. A rounder score closer to one indicates the microglia more amoeboid in shape whereas a score closer to zero indicates the microglia were more ramified. This was done to assess the phenotype within the microglia observed. The perimeter of each microglia was also measured to determine the size of the microglia. An average perimeter and circularity value was taken for each square and a mean of the squares were taken for each case, region and stain. Kruskal-Wallis one way ANOVA tests with Dunn's multiple comparisons were performed to determine any significant differences at a level of $p<0.05$.

2.6 Genetic expression

2.6.1 RNA extraction

RNA extraction was performed using the Qiagen RNeasy kit and protocol. 100mg of frozen frontal cortex tissue from each case was sampled and placed into Qiazol lysis buffer. A Qiagen TissueRuptor was used to homogenise the tissue. Chloroform was added and the samples were vortexed before being spun at 12,000g at 4℃ for fifteen minutes. The samples separated into three layers, with the top layer being aqueous RNA. The top layer was removed and one and a half times 100% ethanol was added. The solution was put into a Qiagen RNeasy Mini Spin Column and spun at 10,000 rpm for one minute. The flow-through was discarded and buffer RW1 was added. Samples were spun again at 10,000rpm for fifteen seconds and flow through discarded. Qiagen DNase I incubation mix was added to the samples and left to degrade any genomic DNA for fifteen minutes. Buffer RW1 was added subsequently and columns were spun at 10,000 rpm for fifteen seconds. Samples were washed three times with Buffer RPE being spun twice at 10,000rpm for one minute and lastly for two minutes to dry out the columns. RNase free water was added, left to stand for a couple of minutes and then eluted into a new tube by being spun at 10,000rpm for three minutes. The eluent was then re-added to the column and the same was repeated to get maximum RNA elution.

2.6.2 Nanostring

The RNA concentration and purity was measured using an Eppendorf spectrophotometer. The concentration, the A260/A280 ratio and the A260/A230 ratio were measured (Appendix Table 1). All samples were diluted to 50ng/ul and were analysed at NanoString Technologies Seattle. The samples were analysed on the Human Inflammation panel containing two hundred and fifty-six genes and thirty extra genes were also added that were relevant to AD (Appendix Table 2). As shown in Figure 2.3, the probes for each gene consist of a reporter probes are hybridised into solution. Excess probes are removed and probe/target complexes aligned and immobilised in the nCounter cartridges. The digital analyser then read and quantitated all the individual barcodes. This technique allowed for direct analysis of gene

expression within a sample without the need for conversion to cDNA and additional rounds of amplification. The nSolver software was used to analyse the raw data (Geiss et al., 2008). Negative controls that did not contain probes were used to detect any background and averages of these were subtracted from the counts. The results were then normalised using positive controls and five housekeeping genes (*CLTC, GAPDH, GUSB, PGK1, TUBB*). All pairwise ratios between groups were made from the normalised data and two-tailed t-tests were performed to establish any significance at $p<0.05$. In order to correct for false discovery rate (FDR) the Benjamini-Yekutieli method was used to exclude any false positive results.

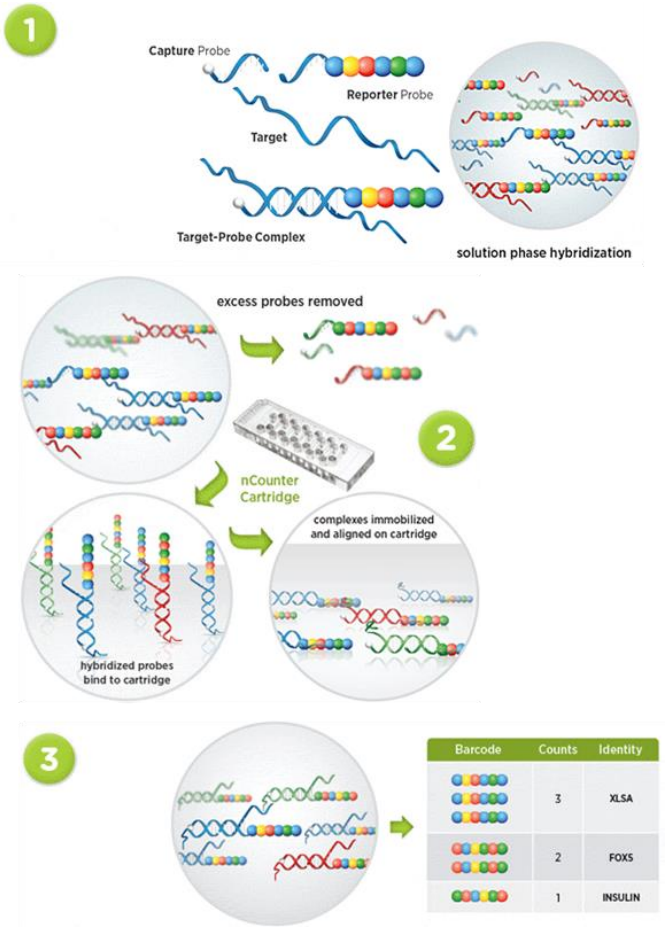

Figure 2.3: Diagram showing the nanostring method. Hybridising probes to the targets within the sample, purifying and immobilising the sample by washing away excess probes and aligning them to the cartridge before a digital analyser counts how many of each barcode. (diagram adapted from www.nanostring.com)

2.7 Proteomics

2.7.1 LCM

Frozen hippocampal sections were cut at 10µm thick as above for the cases selected. Sections were mounted onto PEN-membrane slides that are coated with polyethylene naphthalate (Leica). Slides were treated with the normal immunohistochemistry protocol above and left to dry overnight. Using the Leica DM6000B laser capture microdissection microscope the individual cells of a certain type /area of interest were drawn around, cut out with a laser and collected in the lids of separate 0.2ml Eppendorf tubes. Samples were then kept at -20°C until needed.

2.7.2 Protein extraction

Frozen frontal cortex or LCM samples as prepared above were homogenised in 50mM Ambic buffer with 2% ASB-14 using the Precellys 24 homogenizer (Bertin Instruments) in the CK-14 tubes with a cycle of speed 6500 for two x twenty seconds with a five second gap in between. An Eppendorf spectrophotometer was then used to determine the protein concentration of each sample and the amount needed to reach the optimal protein concentration was calculated. Due to time and money limitations a pool of each disease group was created that had equal protein concentration from each case in order to get the maximum depth possible. Samples were spun at maximum speed for ten minutes at 4°C and the supernatant was removed and kept in a different tube. The remaining pellet was resuspended in ice cold acetone, vortexed and left at -20°C for at least an hour. They were then vortexed again, spun at 14000rpm for ten minutes at 4°C and the supernatant containing the metabolites was removed and kept for future analysis. The pellets were allowed to air-dry before being suspended in 70% formic acid and vortexed. They were then left shaking overnight before being dried in a speed-vac. The original supernatants had ice-cold acetone added and left at -20°C overnight. The next day they were vortexed and spun at 14000rpm for ten minutes at 4°C. The supernatant containing the metabolites was removed and added to the metabolites from the pellet for future analysis. The remaining pellet was dried in the freeze dryer.

2.7.3 Protein digestion

Dried supernatants and pellets were reconstituted in 100mM Tris 8M Urea 2% ASB-14 pH7.79, vortexed and left shaking for one hour to resolubilise the proteins. Dithioerythritol (Sigma) was then added, vortexed and left shaking for a further hour as a reducing agent. To stop the peptides forming disulphide bonds Iodoacetamide (Sigma) was added to alkylate the proteins and act as a peptidase inhibitor. The samples were vortexed and left for thirty minutes. Trypsin-LysC enzyme (Promega Trypsin/Lys-C Mix, Mass Spec Grade cat no. V5073) was added to digest the proteins and was left for three-four hours at 37°C before H_2O was added and the samples were left overnight at 37°C.

2.7.4 C18 peptide clean up

The digested samples were diluted 1:1 in 0.2% TriFluroacetic Acid (TFA) and 5pmol of Waters MassPREP enolase digestion standard (part no. 186002325) was added to the digest. The Agilent C18 Bond Elut 96 well plates (Part no. A496011C) were used to clean the peptides. The wells were primed with 50% acetonitrile (ACN) 0.1%TFA and then washed twice with 0.1% TFA. The diluted digest samples were added to the wells and allowed to drip through. The flow-through was collected and re-applied. The residual salts were washed away by adding 2 x 3% ACN 0.1% TFA and the peptides were eluted using 2 x 50% ACN 0.1% TFA into a new 96-well plate. Samples were transferred to eppendorfs and dried using a speed vac.

2.7.5 Quantitative label free mass spectrometry

The digested cleaned peptides were reconstituted in 3% ACN 0.1% TFA and transferred to a QToF Trueview vial. A pool of all samples was created to be a quality control. Label-free mass spectrometry was performed with a SYNAPT G2-Si High Definition machine with 2D fractionation. There were four fractions run for each sample and 0.5µg of protein were injected per fraction per run. The order of samples was randomised to avoid technical bias. The raw data was loaded into Progenesis for proteomics software and automatically processed with the following settings: low energy threshold set to two hundred and fifity counts; elevated energy threshold set to seventy-five counts; intensity threshold set to seven

hundred and fifty counts; elution start at ten minutes and elution end at fifty minutes. The alignment was reviewed and if less than 80%, the alignment was manually corrected. The results were filtered to exclude any charges above ten. Healthy controls were compared to diseased groups. Peptides were identified with an MSe search with the following parameters: missed cleavages, max one; max protein mass, 800000 kDa; modifications of carbamidomethyl C, oxidation M, deamidation N and Q. The ion matching requirements were set as follows: three fragments/peptide, five fragments/protein, one peptide/protein. The identifications were refined by deleting any with a sequence length less than five. The fold change for each protein was then exported before further downstream analysis was performed on it. Proteins that had been identified with only one unique peptide were excluded from the analysis.

2.7.6 Matrix-assisted laser desorption ionisation time-of-flight mass spectrometry

Collected whole presubiculum and amyloid plaques from the entorhinal cortex samples were sent off for mass spectrometry analysis in Prof Henrik Zetterberg's lab in Sweden. The samples were aspirated with 70% formic acid ten times, centrifuged and aspirated again. Samples were vortexed and dried before being resuspended in 5 µl 0.1% FA 20 % ACN. To prepare the matrix, 0.5µl of the seed-layer (20 g/L α cyano (CHCA) in 90% acetone, 10 % methanol with 0.005 % TFA) was added to the probe and 1ul of sample, 1µl sample matrix (15 g/L α cyano (CHCA) in ACN (CH3CN) and 0.1 % TFA (1:1)) were mixed before being placed on the probe. Aβ was extracted using this method. The number of Aβ peptides in each sample was determined using matrix-assisted laser desorption ionization time-of-flight mass spectrometry as outlined in (Portelius et al., 2015).

2.8 Bioinformatics

As a label-free approach was taken, all genes or proteins that met the threshold set ($p<0.05$ for nanostring, >2-fold change in expression for proteomics) were put into publicly available databases to assess the relationships between them and the biological processes, molecular functions and cell components that were enriched in the different disease groups. To assess

the enriched gene ontology terms Webgestalt (Zhang et al., 2005) was used. GOview was used to compare terms that were over-represented between regions or disease group.

Ingenuity Pathway Analysis software was used to perform in depth canonical pathway analysis and determine any bio functions altered in the datasets. Ingenuity Pathway Analysis is a tool that uses the database, Ingenuity Knowledge base to identify canonical pathways that are represented within the data. The Ingenuity Knowledge base is created by manually curating the literature as well as combining other publically available resources, listed in Figure 2.4. The pathways that are represented are each given a z-score, which is a predictor of whether the pathway is activated or inhibited in the dataset being analysed. This prediction is based upon the upregulation or downregulation of the individual genes/proteins that are represented from each pathway. Understanding which pathways are the most altered, highlights which disease mechanisms are changing the most.

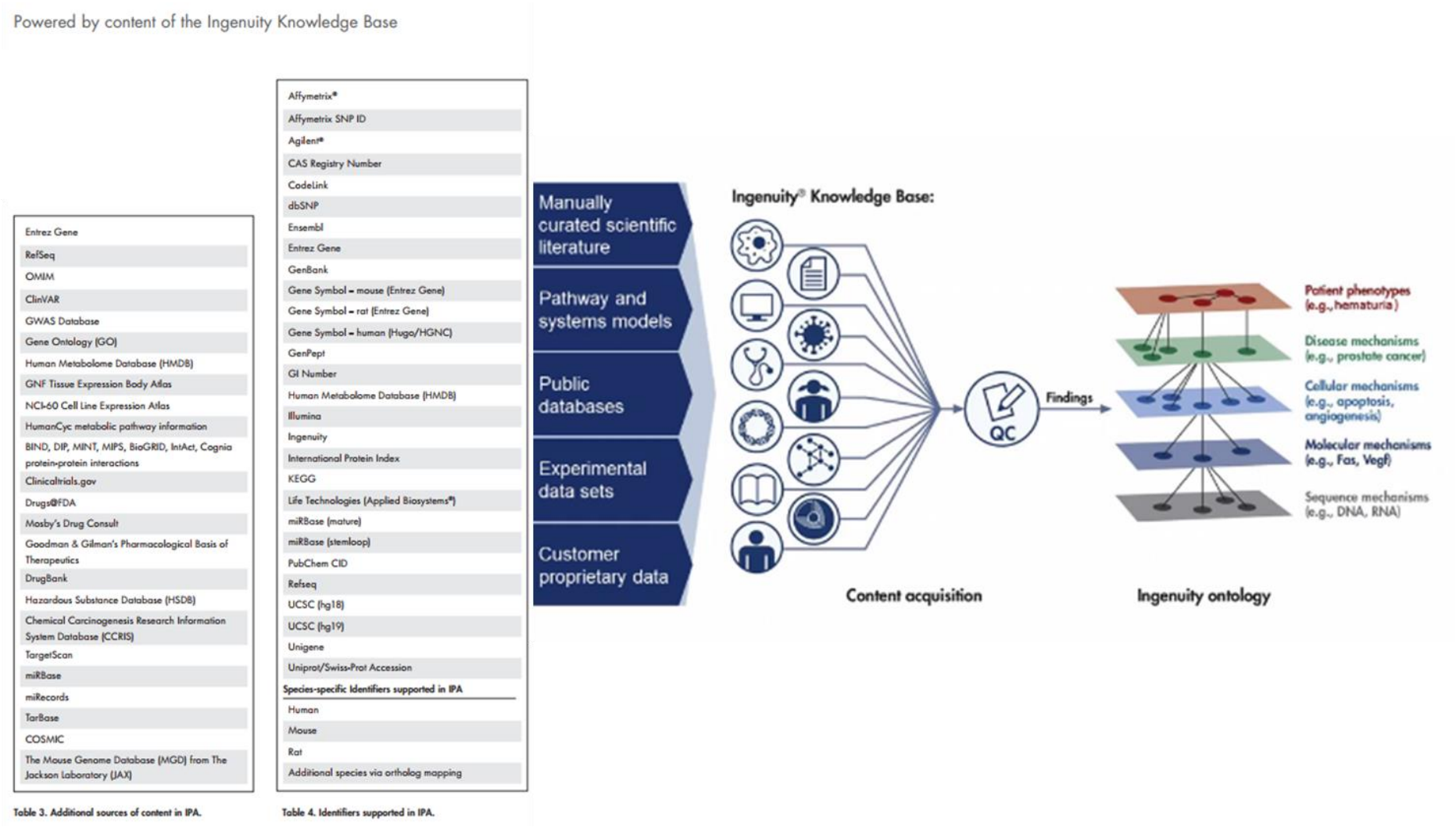

Figure 2.4: Diagram to show design of Ingenuity Knowledge Base. Adapted from www.qiagenbioinfomatics.com.

Chapter 3

Neurodegenerative pathology in *TREM2* variant cases

3 Neurodegenerative pathology in *TREM2* variant cases

3.1 Abstract

Introduction: *TREM2* was identified as a genetic risk factor for late onset AD with a similar odds ratio to that of *APOE4*. Numerous studies have looked at different models to identify what role *TREM2* variants have on the underlying pathomechanisms of AD and whether this influences the pathological hallmarks; Aβ plaques and neurofibrillary tangles. In this study, the AD pathology of six *TREM2* variant cases (5 R47H and 1 D87N variant) were assessed and compared to sporadic and familial AD cases.

Methods and materials: All cases (*TREM2* n=6; SAD n=19; FAD n=11) underwent a pathological assessment using the current diagnostic criteria (Montine et al., 2011). A detailed pathological analysis was undertaken to assess the pathological hallmarks including; Aβ load, plaque type (diffuse or dense-cored) and tau load. Load was assessed in the Thal phase regions: frontal cortex, temporal cortex, hippocampus, putamen and cerebellum. Random areas were taken for analysis using Python and ImageJ analysis software. *APOE* genotypes were determined in all cases and the affect of each genotype on load was assessed.

Results: *TREM2* variant AD cases were identified to have varying levels of cortical and hippocampal atrophy. They had amyloid and tau pathology as well as additional alpha-synuclein pathology present in some cases. All but one *TREM2* variant case had additional CAA and *APOE* genotypes identified no *ApoE2* isoforms within the *TREM2* variant AD cases. There were significantly different loads of Aβ and AT8 between brain regions and FAD cases had significant differences to SAD and *TREM2* variants in both pathologies. The frontal cortex, temporal cortex and putamen regions had significantly greater diffuse plaques

than dense-core plaques in both SAD and FAD cases. However, there were no significant differences in the hippocampus.

Conclusions: *TREM2* variant cases that had an *ApoE4* allele have similar pathology to those of sporadic AD cases whereas TREM2 variant cases without an *ApoE4* allele were diagnosed as normal controls and do not have Aβ plaques or NFT's. *APOE* risk and *TREM2* risk may be linked as they could share similar mechanisms through being binding partners. *TREM2* variants may be involved in reduced elimination of Aβ and therefore result in increased risk of AD. However, these results do not indicate any change in pathology between SAD and *TREM2* variants. Further investigation into what other mechanisms TREM2 utilises is needed to understand its role in more depth.

3.2 Introduction

3.2.1 *TREM2* as a genetic risk factor

As previously discussed in 1.2.1, *TREM2* was discovered in 2012 as a genetic risk factor for late onset AD with a similar odds ratio to that of *APOE4* (Guerreiro et al., 2013a; Jonsson et al., 2012b). Subsequently, a number of *TREM2* variants were found to have links to not only AD but also Frontotemporal dementia (FTD), Amyotrophic lateral sclerosis (ALS) and Parkinson's disease (PD) (Borroni et al., 2014; Cady et al., 2014; Ghani et al., 2016; Giraldo et al., 2013; Guerreiro et al., 2013b; Lill et al., 2015; Rayaprolu et al., 2013; Thelen et al., 2014). The variants that were identified to be risk variants for AD were *R47H, Q33X, Y38C, T66M, D87D, R98W, H157Y, R62H, T96K, L211P, W191X* and *D87N*. However, the variant with the highest frequency and the one that has been validated by many groups is *R47H*.

The *R47H* variant has been reported to be a risk variant in several cohorts with the range of 1.6-fold to 3.4-fold effect size being described between groups (Guerreiro et al., 2013a; Hooli et al., 2014; Rosenthal et al., 2015; Slattery et al., 2014). Several groups have investigated the *R47H TREM2* variant using imaging, pathology and structural studies to try and establish what effect this mutation has on the biological function of TREM2. Many believe that the *R47H* mutation leads to a loss-of-function of TREM2 due to the protein's secondary structure

becoming distorted and therefore no longer being able to bind anionic lipids or alternative ligands (Abduljaleel et al., 2014; Wang et al., 2015).

Additionally, it has been suggested that the *R47H* variant leads to a more severe form of AD than those without a *TREM2* variant. Notably, *R47H* carriers have been observed to have either earlier age of onset or shorter disease duration (Korvatska O et al., 2015; Slattery et al., 2014). Imaging studies have shown *R47H* carriers (n=16 and n=12 respectively) to have increased frontal atrophy, particularly in the orbitofrontal cortex, increased temporal atrophy and relative sparing of the hippocampus (Luis et al., 2014; Slattery et al., 2014). Pathological observations from a series of cases show that *R47H* variants have a greater amount of AD pathology such as amyloid plaques and neurofibrillary tangles as well as some reports of greater alpha-synuclein pathology being present (Korvatska O et al., 2015; Roussos et al., 2015). In addition to this, the *R47H* variant has been associated with increased levels of both sTREM2 levels, tau and hyper-phosphorylated tau in CSF (Cruchaga et al., 2013; Piccio et al., 2016).

The *D87N* variant has not been as widely reported and is not as frequent as the *R47H*

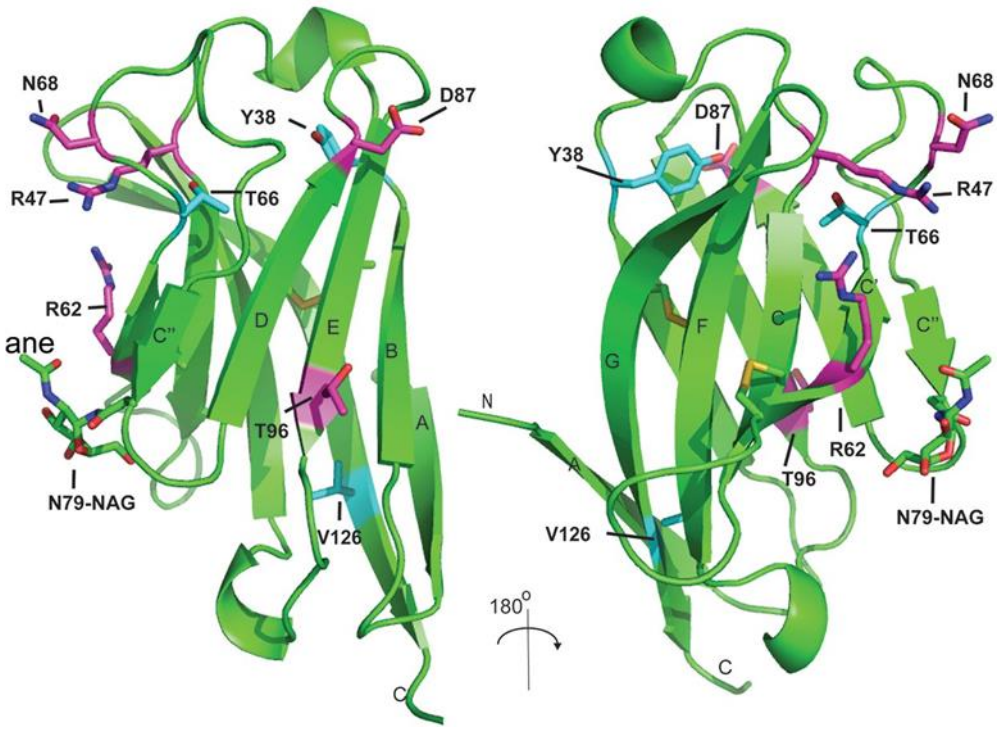

Figure 3.1: TREM2 ectodomain structure. Disease-associated residues are highlighted with sticks. Adapted from Kober et. al 2016.

variant as it is more frequently associated with Nasu-Hakola disease than AD (Ghani et al., 2016; Guerreiro et al., 2013a). Both *R47H* and *D87N* variants are located on the extracellular domain of the TREM2 protein, however the position of the mutations have been reported to have different effects on TREM2 function (Ghani et al., 2016). Soluble TREM2 levels in the CSF of *D87N* carriers is reduced whereas in *R47H* carriers it was increased (Ghani et al., 2016; Piccio et al., 2016). The *D87N* variant is situated on the inside of the protein whereas the *R47H* variant is located on the outside and is therefore accessible to ligand binding as illustrated in Figure 3.1 (Kober et al., 2016). The *R47H* variant has been shown to have less maturation, secretion and phagocytosis than wildtype *TREM2* in HEK293 cells indicating that the variant impairs the normal processing of the protein (Kleinberger et al., 2014).

3.2.2 Pathological observations for *TREM2* variants

As *TREM2* was identified as a risk factor for AD, it led to the hypothesis that the TREM2 protein may have a role in the pathogenesis of AD. The role of TREM2 in AD was investigated in several animal models known to have typical amyloid or tau pathology. TREM2 was found to be upregulated or positively correlated in the presence of amyloid plaques and phosphorylated tau or tau deposition (Chan et al., 2015; Frank et al., 2008; Guerreiro et al., 2013a; Jiang et al., 2015; Lue et al., 2014; Martiskainen et al., 2015; Matarin et al., 2015; Melchior et al., 2010; Varvel et al., 2015). However, Lue et al., (2014) showed no correlation between TREM2 levels and amyloid plaque burden but did confirm the correlation with tau pathology in human post-mortem temporal cortices from AD cases. TREM2 is not thought to directly increase the load of AD pathology. However, when TREM2 is upregulated it has been hypothesised that the number of microglia surrounding plaques increases or the activation of inflammatory pathways is triggered via activation of tau kinases, leading to greater levels of phosphorylated tau. (Jay et al., 2017; Jiang et al., 2016a; Melchior et al., 2010; Yuan et al., 2016). Jiang et al., (2014) indicate that the TREM2 upregulation could be down to compensating for increased $A\beta_{1\text{-}42}$ levels.

Numerous studies demonstrate that TREM2 is responsible for the phagocytosis of Aβ by causing activation or proliferation of microglia around the amyloid plaques. However, Yuan et al., (2016) propose that it is in fact a microglia barrier expressing TREM2 that helps to keep

amyloid plaques compact and protected from neuritic damage in neurons. They have shown that the amyloid plaques in *TREM2* deficient mice are more diffuse and less compact than those of wildtype mice.

1.5.1 Effects of TREM2 expression on pathology in experimental models

To establish what effect a variant in *TREM2* may have, *TREM2* deficient and *TREM2* overexpression models were studied with varying results. Jay et al., (2015) demonstrated that in an *APPPS1-21*;*TREM2*$^{-/-}$ model at 4 months of age there was reduced Aβ in the hippocampus but no change in the cortical load compared to *APPPS1-21; TREM2*$^{+/+}$ mice and at 8 months of age there was no difference in amyloid load measured in the hippocampus (Jay et al., 2017). On the other hand, 4 months of age *5xFAD; TREM*$^{-/-}$ mice showed no change in the hippocampal Aβ deposition but 8.5 month old mice showed no effect on the Aβ cortical load, but had an increase in hippocampal Aβ deposition (Wang et al., 2015, 2016). This indicates that TREM2 function changes during disease progression.

Further evidence for this can be seen in *TREM2* overexpression models. *TREM2* overexpression in *APPPS1* mice at 7 months shows a reduction in the number of amyloid plaques and increased Aβ phagocytosis, therefore, rescuing the neurons from injury, whereas the same strain at 18 months did not rescue neuronal or synaptic loss (Jiang et al., 2014, 2016b). In addition, when *TREM2* was overexpressed in primary microglia from the same mice at 7 months and 18 months, there was increased Aβ phagocytosis or no response from the microglia, respectively (Jiang et al., 2016b). However, the 18-month-old microglia were less able to phagocytose Aβ than the 7-month-old microglia in normal conditions. More importantly, *TREM2* haploinsufficiency has no effect on amyloid plaque burden in 3 or 7 month *APPPS1* mice which correlates with the heterozygous variants in *TREM2* that cause the risk of AD (Ulrich et al., 2014).

While this is the case with TREM2 and its effect on amyloid function, a similar instance can be observed for tau deposition. Increased tau pathology and phosphorylation is observed when *TREM2* is silenced in P301S mice whereas overexpression of *TREM2* at 7 months

rescued this effect by decreased phosphorylation and reduced neuronal and synaptic loss in the hippocampus (Jiang et al., 2015, 2016a).

3.2.3 TREM2 and APOE

APOE was identified as a genetic risk factor for AD, with different allelic compositions determining the level of risk (Allen D. Roses, 1996). The *ApoE4* allele confers the greatest risk, followed by ApoE3 and then ApoE2. ApoE2 has been shown to have protective properties in AD (Corder et al., 1993).

The main function of APOE is to transport lipids across different cells and tissues although it plays a role in other functions too, such as APP processing, tissue repair, immunoregulation and remodelling (Herz and Bock, 2002; Huang and Mahley, 2014; Mahley, 1988; Mahley and Huang, 1999; Mahley and Ji, 1999; Weisgraber et al., 1994). The mechanism by which APOE transports lipids across different cells and tissues is by binding to lipoproteins and heparan sulphate proteoglycans (HSPG's). The different *APOE* isoforms have different affinities for lipoproteins due to their different structural conformations so have different effects on this function (Huang and Mahley; Weisgraber et al., 1994).

APOE appears to be required for amyloid plaque production in mice and there have been several studies that have reported APOE to be associated with amyloid plaque pathology (Bales et al., 1999; Namba et al., 1991; Strittmatter et al., 1993b; Wisniewski and Frangione, 1992). Further to this Cho et al., (2001) reported that APOE is responsible for amyloid plaques increasing in size. It is thought that APOE effects Aβ metabolism through interaction with several other molecules such as lipoproteins and HSPGs and suggests that this allows for the plaques to increase in size (Verghese et al., 2013).

The *ApoE4* isoform has been shown to increase the amount of amyloid pathology compared to other isoforms by forming complexes with Aβ more rapidly and effectively (Bogdanovic et al., 2002; Cho et al., 2001; Strittmatter et al., 1993a). On the other hand, *ApoE4* has been shown to decrease Aβ clearance in mice compared to *ApoE3* and causes neuronal and behavioural deficits even in mice that have no Aβ deposition (Castellano et al., 2011; Huang and Mahley, 2014). These findings indicate that increased amyloid production and

decreased clearance in carriers of the *ApoE4* isoform leads to the increased susceptibility identified for AD.

Furthermore, *ApoE4* has been identified to be more susceptible to proteolytic cleavage than *ApoE3* and therefore produces carboxyl terminal truncated fragments at a greater rate. These fragments have been linked to amyloid plaques and neurofibrillary tangles in AD brains and they are thought to disrupt the cytoskeletal structure of both tau and neurofilament (Brecht et al., 2004; Harris et al., 2003; Huang, 2011; Huang et al., 2001; Jones et al., 2011). In addition, *ApoE4* transgenic mice were demonstrated to have increased levels of phosphorylated tau and *APOE* was identified as being genetically associated with CSF tau and phosphorylated tau (Brecht et al., 2004; Cruchaga et al., 2013; Harris et al., 2003).

As both *APOE* and *TREM2* have been identified as genetic risk factors for AD, and TREM2 has been shown to also bind anionic lipids, it has been hypothesised that TREM2 may function along similar mechanisms as APOE (Daws et al., 2003; Wang et al., 2015). Subsequently, APOE was identified to be an agonist to TREM2 (Atagi et al., 2015; Bailey et al., 2015; Jendresen et al., 2017). Nevertheless, no difference was observed in the binding affinities for the different *APOE* isoforms to TREM2 (Atagi et al., 2015; Yeh et al., 2016).

APOE has previously been identified to have two binding sites; a receptor binding site and a lipid binding site (Cho et al., 2001; Jendresen et al., 2017). Jendresen et al., (2017) identified that TREM2 binds to the receptor binding site on APOE. Heparan sulphate and Aβ have both been shown to bind to both or either of the binding sites and both heparan sulphate and APOE have been reported within amyloid plaques (Jendresen et al., 2017; Strittmatter et al., 1993b; Winkler et al., 1999). Therefore, if Aβ is associated with lipoproteins via APOE, using its lipid binding region, then TREM2 could scavenge Aβ attached to lipoproteins and stimulate a TREM2/APOE signalling pathway that leads to increased Aβ clearance (LaDu et al., 2012; Liao et al., 2014; Verghese et al., 2013).

Interestingly, *TREM2* variants associated with AD have been revealed to have less activation by lipids or partial loss of binding of lipids when compared to wildtype *TREM2*, in

particular to lipoproteins including APOE (Atagi et al., 2015; Bailey et al., 2015; Wang et al., 2015; Yeh et al., 2016). Conversely, *APOE* genotype has not been shown to influence TREM2 binding. *ApoE4* carriers do have less TREM2 expression than *ApoE3* carriers but there is no significant difference in *ApoE4* carriers to non-carriers in sTREM2 CSF levels (Gispert et al., 2016; Heslegrave et al., 2016; Li et al., 2015; Suarez-Calvet et al., 2016).

3.2.4 Aims

At Queen Square Brain Bank, *TREM2* variants have been identified in six cases. These include *R47H* variants with (n=3) and without AD (n=2) at time of death and a *D87N* variant with AD (n=1). Here, the pathological features of these brains were compared to sporadic AD, familial AD and controls.

In addition to this, a detailed quantitative pathological analysis of plaque burden and plaque type together with tau load was undertaken to look at the pathological loads in these cases by determining the load in Thal phase regions of the brain.

The *APOE* genotype was determined on these cases and the effects of these genotypes on all pathological analysis were explored.

3.3 Materials and Methods

3.3.1 Case demographics

All cases from Table 2.3 were used for pathological analysis of Aβ and hyperphosphorylated tau load (see table for detailed case demographics). The macroscopic observations reported in the coronal slices were available from all six *TREM2* cases using detailed reports from Queen Square Brain Bank. A summary of these findings is listed in Table 3.2. Macroscopic images were only available for the *D87N TREM2* variant case (case 5, Table 3.1).

3.3.2 *APOE* genotyping

APOE genotyping was performed for cases where frozen tissue was available (*TREM2* (n=5), SAD (n=15)) as described in the methods in 2.2. This included all cases excluding

cases 1, 12, 13 and 14 from Table 2.3. *APOE* genotype for other cases were already known from a previous study.

3.3.3 Pathology analysis

Immunohistochemistry with Aβ or AT8 antibodies was performed as described in 2.4 on sections from each of the cases (SAD (n=19), FAD (n=11), TREM2 SAD (n=3)) in the Thal phase regions (frontal cortex, temporal cortex, hippocampus, putamen and cerebellum). Antibody supplier, concentrations and species are listed in Table 2.6.

Analysis for Aβ or Tau load was calculated using methods described in 2.5. The type of plaque was determined by manual counting as described in 2.5.3.

3.3.4 Statistics

Kruskal-Wallis one way ANOVA with Dunn's multiple comparisons was performed on load analysis. Wilcoxon paired ranks test was performed on plaque type analysis. Significance is shown as * for $p<0.05$, ** for $p<0.005$, *** for $p<0.0005$, ****$p<0.0001$. GraphPad Prism v7 was used to complete this analysis.

3.4 Results

3.4.1 Pathological observations

All cases with a *TREM2* variant underwent routine macroscopic and microscopic inspection by a neuropathologist to confirm diagnosis. Table 3.1 outlines the primary and differential diagnoses for each of the *TREM2* variant cases. Four of the cases had a confirmed diagnosis of AD and two cases were confirmed to be neurologically normal controls. Macroscopic images were only available for the *D87N* variant case (case 5, Table 3.1) as illustrated in Figure 3.2. External appearances showed there was a degree of atrophy in the frontal and temporal cortices, whereas the parietal, occipital and cerebellum showed no macroscopic abnormalities (Figure 3.2a). Examination of the coronal slices confirmed the reduction in height of the frontal cortex with an enlargement of the lateral ventricle (Figure 3.2b), whilst the hippocampus was a relatively normal size (Figure 3.2c and Figure 3.2d).

Case	Brain Weight	Primary diagnosis and additional pathology	Braak and Braak Tau Staging	Thal phase
1	1252g	Alzheimer's disease (NIA Reagan high likelihood of dementia) ·Amygdala predominant Lewy body pathology ·Cerebral amyloid angiopathy (mild)	6	5
2	811g	Alzheimer's disease (NIA Reagan high likelihood of dementia) ·Moderate/severe cerebral amyloid angiopathy ·TDP-43 pathology in the amygdala and Entorhinal cortex	6	5
3	1327g	Cerebral amyloid angiopathy (moderate)	0	0
4	1350g	Cerebrovascular disease ·White matter infarcts	0	0
5	1029g	Alzheimer's disease (NIA Reagan high likelihood of dementia) ·Cerebral amyloid angiopathy (moderate) ·Neocortical Lewy body disease (intermediate likelihood of DLB as cause of dementia)	6	5
6	1108g	Alzheimer's disease (NIA Reagan high likelihood of dementia) ·Moderate cerebral amyloid angiopathy	6	5

Table 3.1 Neuropathologically confirmed primary and differential diagnoses for TREM2 variant cases. Details tabulated from histology reports at Queen Square Brain Bank.

Case	1	2	3	4	5	6
Ventricles	Moderate dilatation	Severe dilatation	Normal	Normal	Severe dilatation	Mild dilatation
Frontal	Moderate atrophy	Severe atrophy	Normal	Normal	Severe atrophy	Moderate atrophy
Temporal	Mild reduction	Severe atrophy	Normal	Normal	Moderate atrophy	Mild atrophy
Occipital	Normal	Severe atrophy	Normal	Normal	Normal	Normal
Parietal	Mild atrophy	Severe atrophy	Normal	Normal	Normal	Mild atrophy
Deep white matter	Reduced	Reduced	Normal	Normal	Reduced	Reduced
Hippocampus	Mild atrophy	Severe atrophy	Normal	Normal	Normal	Mild atrophy
Amygdala	Normal	Severe atrophy	Normal	Normal	Mildly reduced	Normal
Thalamus	Moderate atrophy	Mild atrophy	Normal	Normal	Normal	Normal
Sub-Thalamic	Normal	Normal	Normal	Normal	Normal	Normal
Caudate	Mild atrophy/ convex	Reduced / flattened	Normal	Normal	Reduced/ flattened	Normal
Putamen	Normal	Mild reduction	Normal	Normal	Normal	Normal
Globus pallidus	Normal	Mild reduction	Normal	Normal	Normal	Normal
Substania Nigra	Mild Pallor	Mild Pallor	Normal	Normal	Mild Pallor	Marked pallor
Locus Coeruleus	Mild Pallor	Mild Pallor	Normal	Normal	Mild Pallor	Marked pallor
Medulla	Normal	Normal	Normal	Normal	Normal	Normal
Pons	Normal	Normal	Normal	Normal	Normal	Normal
Cerebellum WM	Normal	Normal	Normal	Normal	Normal	Normal
Dentate nucleus	Normal	Normal	Normal	Normal	Normal	Normal

Table 3.2 Macroscopic observations for all TREM2 variant cases. These observations were made by an experienced neuropathologist at Queen Square Brain Bank.

The caudate nucleus showed slight flattening whilst the bulk of the putamen was normal. The subthalamic nucleus was unremarkable, whilst the thalamus was significantly reduced in bulk. All macroscopic observations for all six *TREM2* variant cases are outlined in Table 3.2. *TREM2* variant AD cases had varying patterns of atrophy in different brain regions whereas both *TREM2* variant controls showed no macroscopic abnormalities.

Routine immunohistochemistry was performed on each case to determine the final diagnosis. Microscopic observations showed similar patterns for all four AD confirmed *TREM2* variant cases (Table 2.2, cases 1, 2, 5, 6). There were frequent neuritic amyloid plaques throughout the cortical layers in the frontal cortex (Figure 3.3a) made up of diffuse amyloid plaques and mature dense core amyloid plaques (Figure 3.3b). These four cases fulfilled level 5 of Thal phase for amyloid pathology where Aβ deposition was seen in the cortex (Figure 3.3a and Figure 3.3b), the CA1 region of the hippocampus (Figure 3.3d), the striatum (Figure 3.3e), the substantia nigra (Figure 3.3f) and the cerebellum (Figure 3.3g). Braak and Braak stage 6 was fulfilled as the cases showed tau pathology in the presence of neurofibrillary tangles (NFT's) in the cortex (Figure 3.3h) and occipital cortex (Figure 3.3i). Two cases (case 1 and case 5) also had additional alpha-synuclein pathology with Lewy bodies being observed in the amygdala (Figure 3.3j) and substantia nigra (Figure 3.3k). The two controls (Table 3.1, case 3 and 4) had a Thal phase of zero for Aβ pathology, therefore no Aβ plaque pathology was found in any brain region examined and both cases had a Braak and Braak score of zero (Figure 3.3l, case 3) indicating no tau pathology.

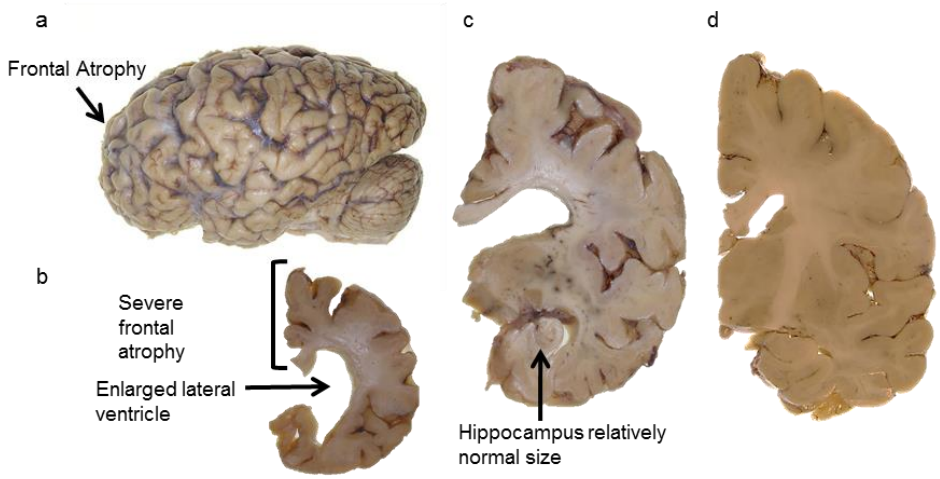

Figure 3.2 Macroscopic photographs of Case 5 from Table 2.1. (a) External appearances, (b) Coronal section of frontal cortex, (c), Coronal section displaying the hippocampus (d) Coronal section from a neurologically confirmed healthy control case displaying the hippocampus.

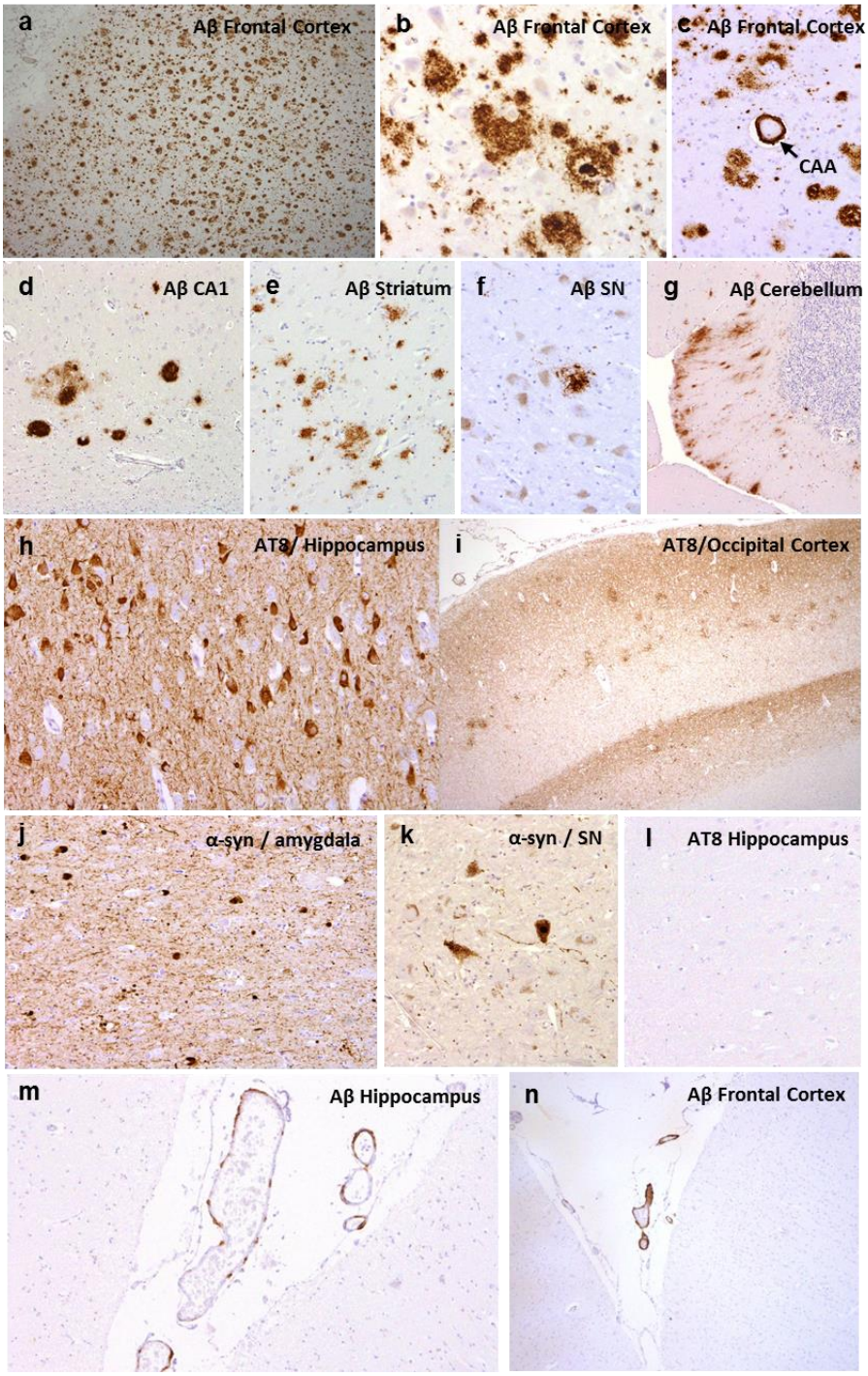

Figure 3.3 Microscopic observations of TREM2 variant cases. Case 1 with *R47H TREM2* variant diagnosed with AD (a-k). (a) Aβ pathology in frontal cortex showing the density of the plaques; (b) Aβ pathology in frontal cortex showing both diffuse and dense-core plaques; (c) Aβ in parenchymal blood vessel of frontal cortex demonstrating CAA as highlighted with arrow; (d) Aβ staining in CA1 region of hippocampus; (e) Aβ staining in striatum; (f) Aβ staining in substantia nigra surrounding the dopaminergic neurons; (g) Aβ staining in cerebellum; (h) AT8 staining in the CA1 subregion of the hippocampus; (i) AT8 staining in the occipital cortex; (j) alpha-synuclein staining in the amygdala; (k) alpha-synuclein staining in substantia nigra. Case 3 (l-n) with *R47H TREM2* variant with neurologically normal diagnosis. (l) AT8 staining in the hippocampus (m) Aβ staining in blood vessels of hippocampus; (n) Aβ staining in blood vessels of frontal cortex. (a-k)

3.4.2 CAA in *TREM2* variant cases

Five out of six of the *TREM2* variant cases were observed to have cerebral amyloid angiopathy (CAA) in the neuropathogist reports (Table 3.1). This includes one of the cases that was diagnosed to be a neurologically normal control as CAA is not included in the diagnostic criteria for AD. Case one had occasional leptomingeal vessels showing patchy Aβ deposition so mild CAA, case two had moderate leptomingeal CAA with patchy and circumferential Aβ deposition along with a small number of cortical vessels having Aβ deposition. Case three had a moderate number of leptomingeal and superficial cortical vessels with patchy or circumferential Aβ deposition (Figure 3.3c, Figure 3.3m and Figure 3.3n). Case five had occasional leptomingeal arterioles with circumferential Aβ deposition leading to moderate CAA. Case 4 did not have CAA and was a neurologically normal control and was reported to have cerebrovascular disease as white matter infarcts were found (Table 3.1). A new criteria for scoring CAA cases was determined in 2016 (Skrobot et. al, 2016). However as these cases were achived cases the new criteria has not been used to score these cases.

To observe whether there were any differences in the amyloid plaque pathology between SAD, FAD and *TREM2* variant AD cases, the Aβ load was determined for each case in each disease group across the Thal staging regions (Figure 3.5a). There was a significant difference in Aβ load between regions (*p=0.0028*) but not disease groups (*p=0.6667*). The frontal cortex had the bulk of Aβ load whereas the hippocampus and putamen had markedly less Aβ. The FAD cases in both the hippocampus and putamen were an exception to this having significantly more Aβ than both SAD (hippocampus *p=0.0411*, putamen *p=0.0330*) and *TREM2* variant AD cases (putamen *p=0.0283*). The *TREM2* variant AD cases followed a close pattern to the SAD cases across all regions except for a decrease in Aβ in the temporal cortex but this was not significant.

Using software analysis to assess the Aβ load does not allow the different plaque morphologies to be distinguished. To investigate whether different plaque types were more prominent in the *TREM2* cases, a semi-quantitative assessment was undertaken in all brain regions studied for Aβ load. Dense-core amyloid plaques (Figure 3.4a) and diffuse amyloid

plaques (Figure 3.4b) were manually counted as described in 2.5.3. There was no significant difference in plaque types between the disease groups (*TREM2*, SAD and FAD) for all regions: frontal cortex (Figure 3.6a, *p=0.8*); temporal cortex (Figure 3.6b, *p=0.9333*); hippocampus (Figure 3.6c, *p=0.6667*); and putamen (Figure 3.6d, *p=0.6667)*.

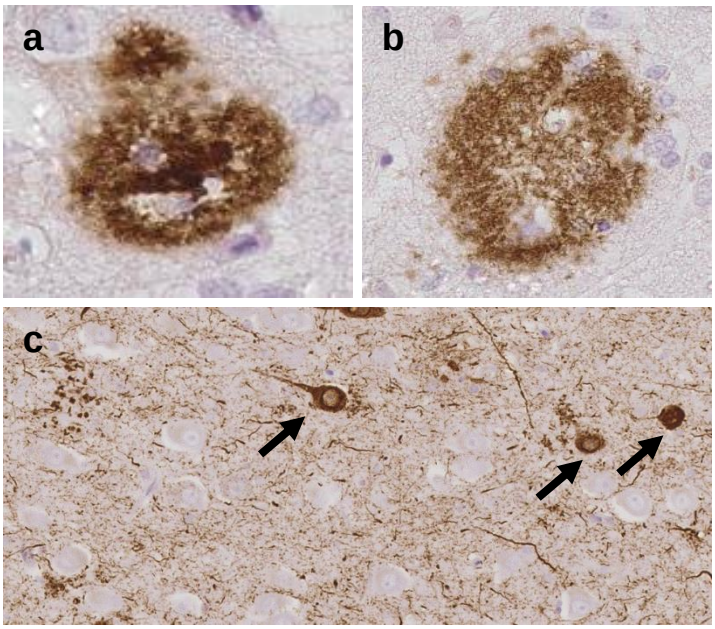

Figure 3.4 Example of amyloid plaque and neurofibrillary tangle pathology. (a) a mature dense core amyloid plaque; (b) diffuse amyloid plaques; (c) AT8 staining with NFT's indicated by black arrows.

Dunn's multiple comparisons post-hoc analysis also showed that in the frontal cortex, temporal cortex and putamen both SAD and FAD cases had significantly more diffuse plaques than dense-core plaques (frontal cortex, SAD *p=0.002*, FAD *p=0.0156*, *TREM2* variant AD *p=0.125*; temporal cortex, SAD *p=0.001*, FAD *p=0.0156*, *TREM2* variant AD *p=0.25*; putamen, SAD *p=0.002*, FAD *p=0.0156*, *TREM2* variant AD *p=0.125*). *TREM2* variant AD cases did not reach significance but this could be due to the small number of cases in this group as the trend followed suit. In the hippocampus, no significant differences were observed between plaque types (SAD, *p=0.0938*; FAD, *p=0.125*; *TREM2* variant AD, *p=0.25*).

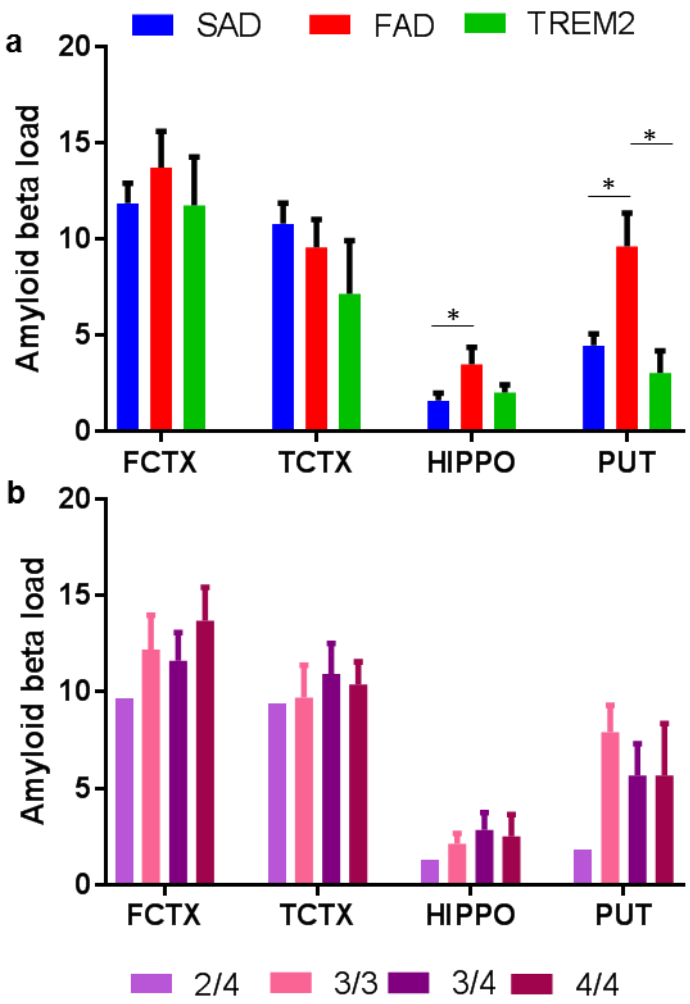

Figure 3.5: Quantitative analysis of Aβ load. In frontal cortex (FCTX), temporal cortex (TCTX), hippocampus (HIPPO) and putamen (PUT) brain regions. (a) Aβ load of SAD, FAD and *TREM2* variant cases. SAD in blue; FAD in red; *TREM2* variant cases in green. (b) Aβ load of different *APOE* genotypes: 2/4 in light purple; 3/3 in light pink; 3/4 in dark purple; and 4/4 in dark pink. (a-b) Load measured as mean % area stained. Kruskal-Wallis one way ANOVA was performed for each region or *APOE* genotype with Dunn's multiple comparisons. Significance is shown as * for $p<0.05$, ** for $p<0.005$, *** for $p<0.0005$, ****$p<0.0001$. Error bars represent SEM.

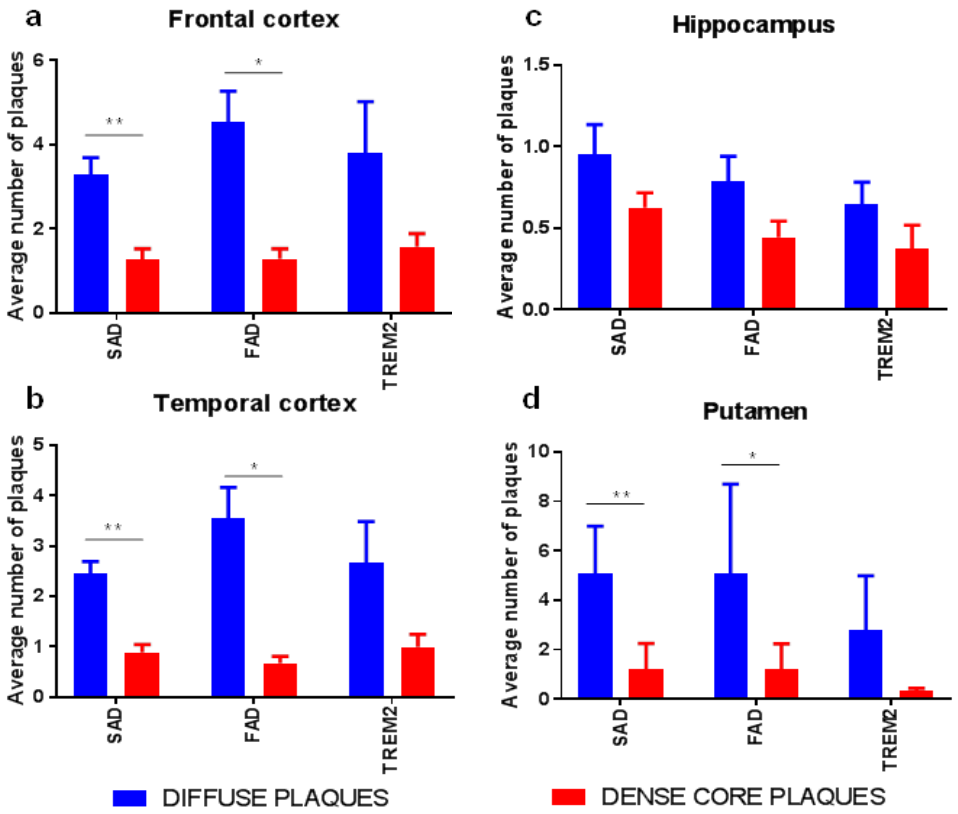

Figure 3.6: Semi-quantitative analysis of plaque type; diffuse or dense-core plaques in SAD, FAD, and TREM2 variant cases. Measured across (a) frontal cortex, (b) temporal cortex, (c) hippocampus, and (d) putamen brain regions. Diffuse plaques in blue; dense core plaques in red. Kruskal-Wallis one way ANOVA was performed to determine statistical differences between disease groups. Wilcoxon-paired ranks test was performed to determine statistical differences between types of plaques for each disease group in each region. Significance is shown as * for p<0.05, ** for p<0.005, *** for p<0.0005, ****p<0.0001. Error bars represent SEM.

3.4.3 Neurofibrillary tangles in *TREM2* variant cases

To assess the level of tau that had accumulated in the *TREM2* variant AD cases compared to SAD and FAD cases, the AT8 load was quantified (Figure 3.7) in the frontal and temporal cortices, hippocampus, putamen and cerebellum. An example of tau pathology is shown in Figure 3.4c. There was a significant difference of AT8 load between brain regions (*p<0.0003)* but not between disease groups (*p=0.8068*). There is a significant increase in AT8 load in the frontal cortex of FAD cases to *TREM2* variant AD cases (*p=0.0248*) and

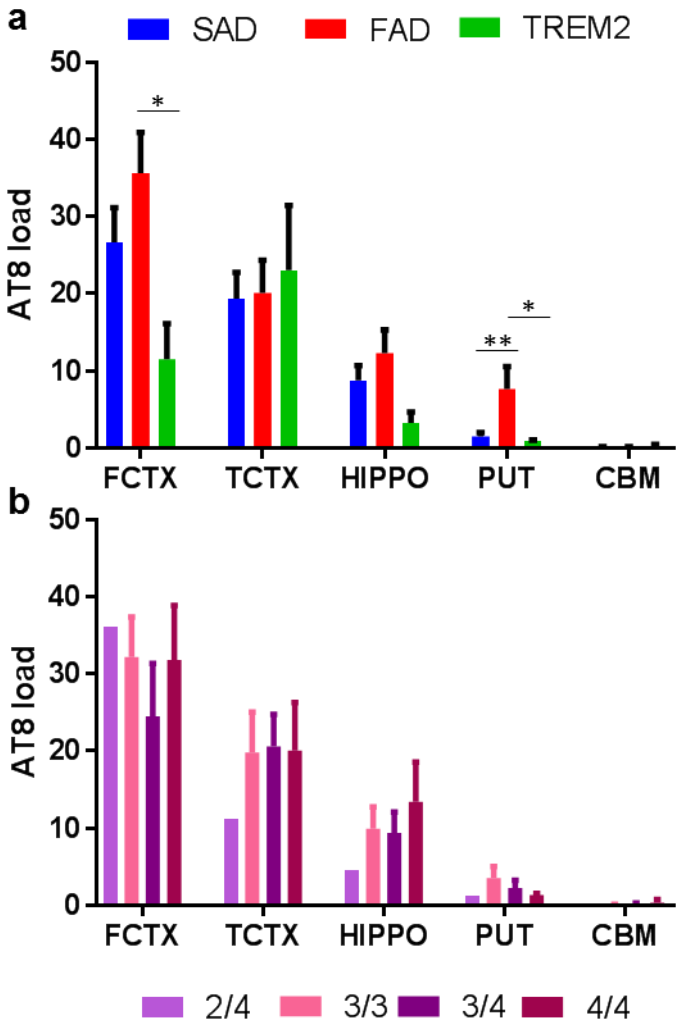

Figure 3.7: Quantitative analysis of tau load using AT8 staining. In frontal cortex (FCTX), temporal cortex (TCTX), hippocampus (HIPPO), putamen (PUT) and cerebellum (CBM) brain regions. (a) AT8 load of SAD, FAD and *TREM2* variant cases. SAD in blue; FAD in red; *TREM2* variant cases in green. (b) AT8 load of different *APOE* genotypes: 2/4 in light purple; 3/3 in light pink; 3/4 in dark purple; and 4/4 in dark pink. (a-b) Load measured as mean % area stained. Kruskal-Wallis one way ANOVA was performed for each region or *APOE* genotype with Dunn's multiple comparisons. Significance is shown as * for $p<0.05$, ** for $p<0.005$, *** for $p<0.0005$, ****$p<0.0001$. Error bars represent SEM.

similarly this was observed in the putamen (p=0.0476). Additionally, the FAD cases had a significantly higher AT8 load compared to SAD cases (p=0.0016). All other comparisons were non-significant (Figure 3.7). The *TREM2* variant AD cases differ from region to region and appear to have a different pattern of AT8 load compared to SAD and FAD cases. Extra power with additional *TREM2* variant cases would identify if these differences were worth investigating further.

3.4.4 *APOE* genotypes in *TREM2* variant cases

As *APOE* genotypes have been identified as a strong genetic risk factor with an increased risk of up to 10-fold, the *APOE* genotypes of cases used in this study were identified where possible as shown in Table 2.3. Each cases' *APOE* genotype was identified by bands on a metaphor agarose gel (Figure 3.8). There are six combinations of *APOE* genotype possible with the ε2 allele reported to be protective against AD and the ε4 allele reported to be detrimental to the risk of AD. Table 3.3 shows the distribution of *APOE* alleles for all types of disease group studied. As expected there were predominantly more ε3 and ε4 alleles present throughout the cases. When looking at the *TREM2* variant cases in detail, the cases that were pathologically confirmed as controls did not include any ε4 alleles. However, those *TREM2* variant cases that were confirmed to have AD, all had at least one ε4 allele.

APOE genotype had no influence on Aβ load between the different disease groups (*p=0.5867*) but was significantly different between regions (*p=0.0001*, Figure 3.5b). However, this may just be an effect seen across all cases as the pathology spreads throughout the brain in agreement with the Thal phases.

The same was true of APOE genotype effect on AT8 load (Figure 3.7b). There was a significant difference between regions (*p=0.0012*) but no significant difference between disease groups (*p=0.9794*).

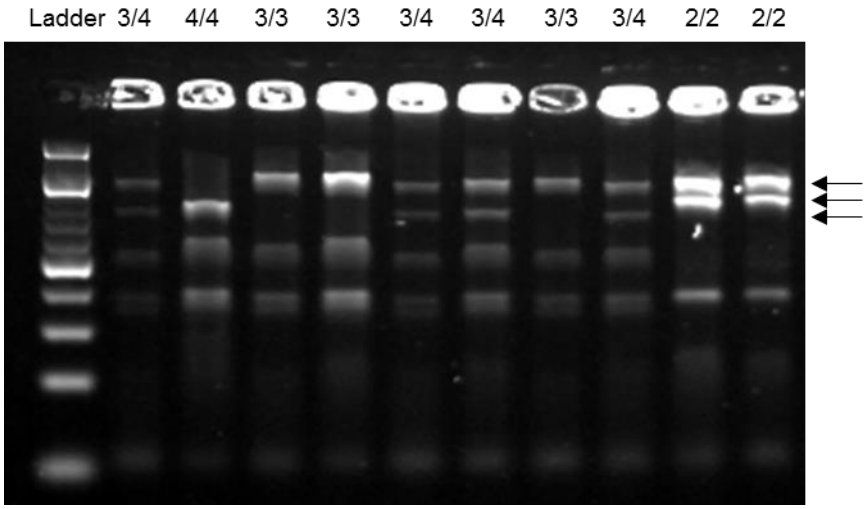

Figure 3.8: Representative image of gel indicating *APOE* genotypes in different cases. The three arrows point to the bands we are interested in to determine the genotype. The labels at the top state what *APOE* genotype is shown in each corresponding lane.

	APOE genotype					
Disease group	**2/2**	**2/3**	**2/4**	**3/3**	**3/4**	**4/4**
Control	Y			Y	Y	
SAD			Y	Y	Y	Y
FAD				Y	Y	Y
TREM2 control	Y			Y		
TREM2 SAD					Y	Y
TREM2 FAD				Y		

Table 3.3 *APOE* genotypes found within each disease group

3.5 Discussion

In this study, each *TREM2* variant case has been assessed for the classic AD pathology and the amount of amyloid and tau pathology in each of these cases has been identified and compared to sporadic and familial forms of the disease.

As described previously by Guerreiro et al., (2013a) all of the cases that were pathologically confirmed to have AD, fulfilled the criteria of Braak stage 6 and Thal phase 5. Further to this, two of the cases had additional alpha-synuclein Lewy-body pathology, some of which was identified in the substantia nigra, which is a pathological hallmark of Parkinson's disease. *TREM2* variants have been previously suggested to be a susceptibility factor in Parkinson's

disease, however, there has been some debate on how true this association is (Lill et al., 2015; Mengel et al., 2016; Rayaprolu et al., 2013; Tan et al., 2016). If true, having PD pathology may not be a surprise and Korvatska O et al., (2015) showed that *R47H* carriers are more likely to have additional alpha-synuclein pathologies than non-carriers. Luis et al., (2014) also showed that *R47H* carriers with AD, present with significantly more parkinsonian signs than AD cases that are non-*R47H* carriers. As both an *R47H* variant case (case1) and a *D87N* variant case (case 5) showed alpha-synuclein pathology, it suggests that alpha-synuclein pathology is not specific to a certain *TREM2* variant.

Imaging studies have shown *R47H* variants to have increased frontal and temporal atrophy and minimal change in the hippocampus (Luis et al., 2014; Slattery et al., 2014). Here, we observe moderate to severe frontal atrophy, mild to severe temporal atrophy and normal to severe hippocampal atrophy in the pathologically confirmed AD *TREM2* cases. Although certain changes have been observed in imaging studies, pathological observations of *TREM2* variant cases with AD do not show the same differences from case to case as they range from mild to severe atrophy in different brain regions. A comparison with more *TREM2* variant AD cases together would indicate whether a pattern does emerge.

Interestingly, five out of the six *TREM2* variant cases had CAA including one of the cases that was clinically normal and pathologically confirmed as a neurologically normal control. This presence of CAA is not an uncommon finding as 80-90% of AD cases have a form of CAA and up to 35% of elderly patients without AD are reported to have CAA although not as severe as in AD cases. However, only three of the SAD cases and two of the FAD cases in this cohort had CAA (Ellis et al., 1996; Nicoll et al., 2004; Yamada, 2000, 2002; Yamada et al., 1987). Further investigation should be done to determine the incidence of *TREM2* variant cases having CAA. Having a *TREM2* variant may lead to a higher incidence of CAA may hinder the clearance of Aβ along the intramural periarterial drainage pathway. This may lead to an increase in the levels of soluble Aβ in the parenchyma, increase amyloid pathology and lead to an increased risk of AD. Evidence for this is shown by the fact that many CAA cases have increased neuritic plaques and NFT's present to those without CAA (Brenowitz et al., 2015; Pfeifer et al., 2002).

APOE genotypes have been shown to have increased risk on the severity of CAA that occurs in a similar manner to AD (Alonzo et al., 1998; Pfeifer et al., 2002). *ApoE4* giving the greatest risk, followed by *ApoE3* but unlike in AD where *ApoE2* confers a protection rather than a risk, *ApoE2* instead is known to cause vascular changes that may lead to vessel rupture within the brain (Yu et al., 2015). As APOE has been reported to be a ligand for TREM2, it is therefore interesting that the *APOE* genotypes of the *TREM2* variant cases that have been confirmed to have SAD all lack an *ApoE2* allele and contain an *ApoE4* allele. This was also the case in three other studies, amounting to twenty-six cases in total (Korvatska O et al., 2015; Krasemann et al., 2017; Yuan et al., 2016). This indicates that the risk that *TREM2* variants confer (*R47H* in particular) may be linked to the risk that the *APOE* genotype confers either by acting through similar mechanisms or by having similar effects (Murray et al. 2018). As they bind to each other however, it is more likely to be the former.

TREM2 variants have been shown to have a reduced affinity to bind lipids and lipoproteins such as APOE so perhaps TREM2 normally binds to an APOE-Aβ complex and stops it from crossing over the vessel wall but instead when TREM2 is impaired, APOE is free to complex with Aβ and cross the blood vessel wall (Abduljaleel et al., 2014; Wang et al., 2015). This may result in the IPAD pathway being utilised to clear Aβ from the brain but the increased load in Aβ in the vessels may cause modifications in HSPG's and therefore greater CAA. LRP1, a low-density lipoprotein receptor is known to bind to APOE and Aβ and can be found in both senile plaques and in amyloid deposits in vessel walls (Bu, 2009; Kim et al., 2009; Rebeck et al., 1995). It has been reported that *ApoE4* blocks the receptor mediated endocytosis employed by LRP1 which is part of a lipid transport pathway and therefore reduces the elimination of Aβ and causes increased Aβ in the vessel walls (Deane et al., 2008; Huynh et al., 2017). LRP1 can also bind to HSPG's and similarly these are found in senile plaques and CAA as well as also binding to APOE and Aβ (Cooper, 1997; Cotman et al., 2000; van Horssen et al., 2001; Mahley and Ji, 1999; Van Gool et al., 1993; Zhang et al., 2014a). CAA is reported to worsen as the basement membrane of the vessels thickens and one cause for this is increased levels of HSPG's in the basement membrane (Hawkes et al., 2013; Qi and Ma, 2017).

It has been hypothesised that *TREM2* variants cause a loss in ability of the microglia to phagocytose Aβ (Boche et al., 2013; Guerreiro et al., 2013a; Jonsson et al., 2012b). As APOE is a ligand for TREM2, it has been suggested that through binding to APOE sequestered in amyloid plaques, it triggers the phagocytic mechanism (Atagi et al., 2015; Jendresen et al., 2017). As *TREM2* variants are less able to bind APOE this phagocytosis is not triggered and greater accumulation of Aβ ensues. As having an *ApoE4* genotype causes increased Aβ deposition and decreased Aβ clearance, *TREM2* variant cases that additionally have an *ApoE4* variant, as most commonly do, would be at increased risk for Aβ accumulation and therefore increased risk of AD (Castellano et al., 2011). Although the results here show that Aβ load does not significantly differ between SAD and *TREM2* variant cases, the mechanism in which the Aβ plaques accumulate may differ. TREM2's link to APOE may highlight the mechanism that confers cases with a *TREM2* variant to be at a higher risk of accumulating AD pathology.

Conversely, Yuan et al., (2016) suggest that the microglia that surround amyloid plaques form a barrier and that TREM2 helps to form this barrier keeping the plaques compact. They have shown that this barrier is reduced in *TREM2 R47H* carriers and that in this instance the plaques are more diffuse and less neuritic in nature. However, here it is observed that all AD cases have significantly more diffuse plaques than dense-core plaques (compact plaques) in all regions tested but there is no significant difference in the levels of diffuse plaques between disease groups. A limitation to this study was that the diffuse or dense-core plaques were counted manually which may be a less reliable method due to capacity for human error and a reason for inconsistent results with Yuan et al. On the other hand, neither the microglia surrounding the amyloid plaques nor the size of the amyloid plaques were assessed, so further assessment of the microglia surrounding the plaques in these *TREM2* variant cases may determine why these discrepancies between results exist. Then again, Yuan et al. only quantified amyloid plaques within the middle frontal gyrus whereas here multiple regions have been shown to have varying results. Neither this study nor Yuan et al's study determined what cortical layer the plaques analysed were from. Further investigations into whether cortical layers have different pathological characteristics may give further insight into the discrepancies observed within the two sets of results.

The affect that TREM2 has on Aβ load has been debated in the literature. *TREM2* deficiency mouse models showed differences between the cortical load and hippocampal load depending on the age of mice tested (Jay et al., 2015, 2017, Wang et al., 2015, 2016). Additionally, this was observed in *TREM2* overexpression models (Jiang et al., 2014, 2016b). Nevertheless, *TREM2* haploinsufficient models showed no difference in Aβ load compared to wildtypes (Ulrich et al., 2014). Here we see significant differences between regions with a marked increase in Aβ load in the cortical areas compared to the hippocampus and we see this across all three AD subtypes. There is also a significant difference in Aβ load between disease groups but this is mainly due to the FAD cases having significantly more Aβ in the later Thal stages than SAD or *TREM2* variant cases. Thus, the results here show the most similarity to the haploinsufficient models, indicating a modest effect if any. That aside, *TREM2* variant cases follow the levels of Aβ in SAD cases more closely than FAD levels indicating that the *TREM2* variants may cause risk through mechanisms operating in sporadic cases. There was no significant difference in Aβ load according to *APOE* genotype which differs from the literature in which *ApoE4* is reported to cause greater Aβ deposition (Bogdanovic et al., 2002; Cho et al., 2001; Strittmatter et al., 1993a). Therefore, the way that Aβ is deposited between cortical layers may be more important here rather than how much of the protein is present.

In comparison, tau pathology is described to increase in *TREM2* deficient models and decrease in *TREM2* overexpression models (Jiang et al., 2015, 2016a). Here we identify that although there are significant differences in the amount of tau across the Thal phase regions, these are seen in all three AD subgroups. Again, the FAD cases have significantly more hyperphosphorylated tau in the frontal cortex and putamen than the *TREM2* variant cases and this trend follows in the hippocampus. However, no differences can be observed in the comparison between *TREM2* variant and SAD cases indicating again that *TREM2* variant cases could act in the same manner as SAD cases or have mechanisms that reach the same conclusion. It is likely that as *TREM2* variants are heterozygous, that the effect seen by *TREM2* deficient mice is more extreme than the one we see here when comparing to SAD cases as the wildtype.

3.5.1 Conclusions

To summarise, *TREM2* variant cases with AD display all the pathological characteristics of sporadic AD and although the amount of Aβ or hyperphosphorylated tau does not differ significantly from the sporadic form of AD, CAA was present in all but one *TREM2* variant case. Both SAD and *TREM2* variant cases may differ from FAD cases though, indicating that further elucidation of the different mechanisms involved throughout sporadic and familial disease should be investigated to understand the full pathogenesis of this disease.

The *TREM2* cases investigated in this study that had a pathological diagnosis of AD all had an *ApoE4* genotype whereas the *TREM2* variant cases that were diagnosed as normal controls did not carry an *ApoE4* allele. This brings into question the known link between TREM2 and APOE and whether the risk associated with TREM2 is independent of *ApoE4*. They both are thought to have a role in the processing of amyloid deposits and through interaction with APOE, TREM2 may play a role in Aβ elimination either through Aβ phagocytosis or by other mechanisms that still need exploring. In this case, *TREM2* variants have reduced APOE binding, and therefore reduced Aβ elimination from the brain. Perhaps this is why increased risk of AD is observed in these cases. However, the lack of difference between Aβ load in SAD and TREM2 variant AD cases suggest that TREM2 may be playing an alternative role than that of Aβ elimination.

TREM2 variants were identified to have other pathologies such as alpha-synuclein pathology which is indicative of it having an effect in other neurodegenerative disease such as Parkinson's disease. If TREM2 influences Aβ elimination, it may also influence clearance of other insoluble deposits that form within the brain such as Lewy bodies in Parkinson's disease, TDP-43 inclusions in frontotemporal dementias and more. Investigating this clearance mechanism further will help us to elucidate the role that TREM2 is playing and identify whether this is how *TREM2* variants are at greater risk of these diseases.

Chapter 4

Microglial phenotype of *TREM2* variant cases

4 Microglial phenotype of *TREM2* variant cases

4.1 Abstract

Introduction: It is now accepted that microglia have a continuum of activation states and that any one microglia can be in any given state at any one time. Amoeboid shaped microglia are linked to an activated, phagocytic phenotype whereas ramified shaped microglia are more indicative of a homeostatic or surveillant phenotype. Activated microglia have been shown to surround neuritic plaques, but not diffuse plaques, and are thought to play a role in Aβ deposition as well as Aβ clearance. *TREM2* was identified as a genetic risk factor for late onset AD with similar odds ratio to *APOE*. TREM2 is expressed on microglia, and has been shown to be upregulated on the microglia surrounding amyloid plaques both in human post mortem tissue and in AD mouse models. *TREM2* deficient animal models show a decrease in phagocytosis and increased AD pathology compared to wildtype. Therefore, the microglial phenotype of *TREM2* variant cases were investigated in post-mortem human brains and compared to the microglial phenotypes in SAD, FAD and controls.

Materials and methods: Immunohistochemistry was performed with the following microglial markers; Iba1, CD68, CR3-43 (HLA-DR) and P2RY12 on a variety of disease groups; SAD (n=19), FAD (n=11), *TREM2* variant AD cases (n=4), *TREM2* variant controls (n=2) and controls (n=6) in the following areas; frontal cortex, temporal cortex, hippocampus, putamen and cerebellum. Random squares were selected and microglial load, circularity and perimeter were assessed using ImageJ software and Python scripts. Seven commercially available TREM2 antibodies were used to investigate whether TREM2 could be identified in post-mortem human brain tissue.

Results: Microglia in *TREM2* variant AD cases have an increased CD68 load, more circular Iba1, CR3-43 and CD68 positivity. They also exhibit smaller size Iba1 and CR3-43 microglia indicating that these cases have a more amoeboid microglial phenotype than all other disease groups including *TREM2* variant controls, which suggests that more phagocytosis

occurs in these cases. *ApoE2/2* has a ramified microglial phenotype whereas *ApoE4/4* cases have an amoeboid microglial phenotype, matching that of *TREM2* variant AD cases.

Conclusions: *TREM2* variant AD cases have a more morphologically activated microglial phenotype compared to SAD and FAD cases. This data therefore shows that the different disease groups have altered microglial phenotypes with a microglial phenotype less consistent with activation seen in other AD subgroups. This could indicate that different microglial responses occur in different AD subgroups. *APOE* could influence the effects of these responses. Further understanding of these responses and the different mechanisms that are needed to make them occur will allow us to understand why *TREM2* variant AD cases are at an increased risk of AD.

4.2 Introduction

4.2.1 Microglia in AD

It has long been thought that inflammation, and in particular, microglia, play a role in the pathogenesis of AD. However, exactly what that role is, is still being debated and the evidence from previous studies points to them having multiple functions within the progression of AD. Some reports point to microglia being neuroprotective while others suggest they further exacerbate the disease.

Microglia have been shown to be in close proximity to amyloid plaques with studies indicating that microglia appear to be activated when early amyloid plaques appear although these studies do have their limitations due to limited antibodies being available at the time to detect microglial morphology (Arends et al., 2000; Frautschy et al., 1998; Gahtan and Overmier, 1999; Gentleman, 2013; Mann et al., 1995; Martin et al., 1994; Rogers et al., 1988; Wegiel and Wisniewski, 1990; Wegiel et al., 2000). Further studies by Wegiel's group show that microglia form an amyloid star morphology, consisting of five or six microglial cells surrounding an amyloid core (Wegiel and Wisniewski, 1990; Wegiel et al., 2000). This hypothesis was confirmed by Yuan and colleagues, (2016) who show a microglial barrier forming around amyloid plaques. However in transgenic mice models of AD, the plaques are formed by recruiting new microglia to the plaque (Wegiel et al., 2000). Aβ is thought to be

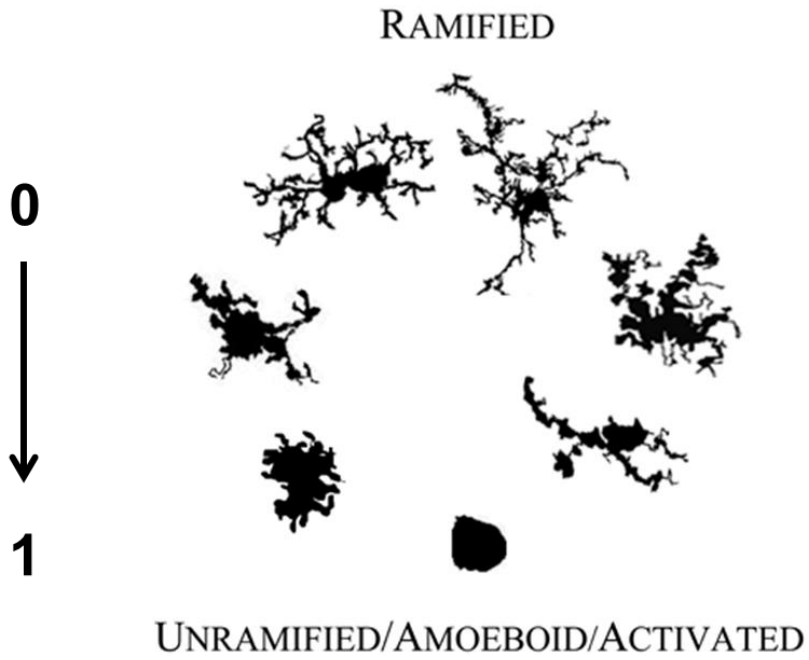

Figure 4.1: Different morphologies and activation states of microglial cells. The spectrum from ramified homeostatic microglia to activated and amoeboid microglia. The circularity score is indicated by the number between 0 and 1 as shown.

produced mainly by neurons but has also been shown to be produced by microglia since they also express APP (Banati et al., 1993; Frackowiak et al., 1992; Lassmann et al., 1993; Pappolla et al., 1991; Probst et al., 1991b; Wegiel and Wisniewski, 1990; Wegiel et al., 2000; Wisniewski et al., 1989, 1996, 1998). Whilst it has been demonstrated that microglia could contribute to the formation of amyloid plaques, studies show that removing the microglia does not affect plaque load, suggesting that the microglia cannot be solely responsible (Grathwohl et al., 2009). Bolmont et al., (2008) suggest that instead the microglia are rapidly recruited to the amyloid plaque and that they have a role in maintaining the amyloid plaque.

There are two types of plaques in the AD brain, with different compositions, morphology and toxicity. Neuritic plaques are amyloid plaques that are also surrounded by dystrophic neurites and are thought to be more toxic than diffuse amyloid plaques that do not contain the dystrophic neurites (Serrano-Pozo et al., 2011). Microglial density has been shown to be correlated with the levels of neuritic plaque but not diffuse plaques (Arends et al., 2000; Giulian, 1999; Mattiace et al., 1990a; Paresce et al., 1997; Rogers et al., 1988; Wegiel and Wisniewski, 1990; Wisniewski et al., 1989). Microglia display an amoeboid morphology in the presence of dense core or neuritic plaques, whereas a more ramified morphology when in

the vicinity of diffuse plaques (Figure 4.1). Bisht et al., (2016) even suggest that the microglia that surround amyloid plaques have a different underlying structure that becomes apparent during disease or under chronic stress and identified them as dark microglia. Greater numbers of microglia have been shown to co-localise to Aβ40 than to Aβ42 and it has been suggested that the areas of an amyloid plaque that are uncovered by microglia contain the Aβ42 fibrils (Mann et al., 1995). These uncovered Aβ42 fibrils become toxic to nearby neurons and recruit phagocytic activated microglia by initiating an inflammatory response (Wegiel et al., 2000). This inflammatory response, a combination of TNFα, IL-1β and IFN-γ, can be toxic to neurons and stimulate an increase in Aβ production in neurons, thereby creating a vicious circle (Blasko et al., 2004; Goldgaber et al., 1989).

Microglia are also thought to be responsible for Aβ clearance via phagocytic mechanisms. Aβ has been shown to cause activation of microglia and induce a chemotactic and phagocytic response, partly due to release of IL-1β and complement proteins (Barger and Harmon, 1997; Boche et al., 2013; Gahtan and Overmier, 1999; Gentleman, 2013; Giulian et al., 1996; Griffin et al., 1989, 1995; Itagaki et al., 1989; Meda et al., 1995, 1995; Rogers and Lue, 2001; Rogers et al., 1992a, 1992b; Sheng et al., 1998; Yin et al., 2017). Both Aβ in plaques and dystrophic neurites become targets for phagocytosis (Gahtan and Overmier, 1999). Microglia have been shown to be capable of phagocytosing Aβ in several studies but there are also reports that the Aβ resides in microglial phagosomes for long periods of time making this a non-efficient mechanism of clearance (Frackowiak et al., 1992; Gahtan and Overmier, 1999; Paresce et al., 1997; Shaffer et al., 1995; Weldon et al., 1998). However, at end stage disease activated microglial number no longer correlates with disease progression and there is a reduction of dense-core plaques and greater numbers of diffuse plaques suggesting that mechanisms of Aβ clearance start to outweigh mechanisms of Aβ deposition as the disease progresses (Hyman et al., 1993; Thal et al., 1998; Wegiel et al., 2000).

Although the number of amyloid plaques decreases at the end stage of disease, the levels of NFT's continue to increase and microglia have been shown to correlate strongly with NFT levels throughout all stages of disease (DiPatre and Gelman, 1997; Kitazawa et al., 2004). Sanchez-Mejias et al., (2016) showed that there were reduced levels of microglia in the

hippocampus compared to cortical areas and that this was due to soluble phosphorylated tau being toxic towards the microglia and making them apoptotic. They suggest that this then causes a decreased inflammatory response which leads to exacerbated disease. Alternatively, microglia may drive tau pathology via the fratalkine receptor as demonstrated in a hTau mouse model deficient for CX3CR1 in which these mice exhibited increased levels of phosphorylation and aggregation at an earlier age compared to wildtypes (Bhaskar et al., 2010; Maphis et al., 2015).

4.2.2 Microglial markers

As discussed previously in 1.3, there are conflicting views in the literature reporting microglial phenotypes correlating with different functions they undertake. It is now viewed that there are many different functional phenotypic states of microglia (Figure 4.1) and that one microglia may be transitioning between states at any one given time (Boche et al., 2013; Korzhevskii and Kirik, 2016). This makes it difficult to determine the role microglia are playing in different diseases. To investigate microglial activation in post-mortem human brain tissue multiple markers (Iba1, CD68, CR3/43 and P2RY12) were used that identify different aspects of the activation states in microglia (Table 4.1).

Microglial marker	Type of marker	Activation state	Morphology
Iba1	motility	homeostatic and activated microglia	Mostly ramified
CD68	lysosomal	activated	amoeboid
CR3-43	antigen presenting	activated	ramified with shorter processes
P2RY12	motility	homeostatic	ramified

Table 4.1: Range of microglial markers and different properties of each. Markers used to reflect the range of microglial pathology present from resting to activated in different phenotypic states.

4.2.2.1 Iba1

Ionized calcium binding adapter molecule 1 (Iba1), was identified to be a pan microglial marker that detects ramified and amoeboid forms of microglia (Boche et al., 2013; Streit et al., 2009). It is a member of the calcium binding group of proteins and is thought to play a role in reorganising the cytoskeleton in the microglial processes through binding to actin (Sasaki et al., 2001). It is a 17kDa protein consisting of 147 amino acids and is encoded in the major histocompatibility complex class (MHC) III region (Boche et al., 2013; Imai et al., 1996; Yamada et al., 2006). Some groups have reported Iba1 to be present in both microglia and macrophages whereas others have only found it exclusively in microglia (Boche et al., 2013; Imai et al., 1996; Ito et al., 1998). Regardless of the differing reports on which microglia are stained, Iba1 is used widely as a standard marker as it is found in both the cytoplasm and ramified processes of microglia (Korzhevskii and Kirik, 2016).

4.2.2.2 CD68

CD68 is used as a phagocytic marker for microglia as it is a lysosomal protein found within microglia, monocytes and macrophages (Boche et al., 2013; Fadini et al., 2013; Holness and Simmons, 1993; Korzhevskii and Kirik, 2016; Shikuma et al., 2014; Smith et al., 2013; Zotova et al., 2011). It is a transmembrane protein that belongs to the lysosome-associated membrane family (LAMP) and is involved in the process of microglia binding to low density lipoproteins (Song et al., 2011). It detects activated microglia, with amoeboid microglia being detected more readily than microglial processes on ramified forms although this could be due to CD68 around the nucleus being detected more readily than CD68+ve lysosomes in the processes (Albright et al., 2000; Andjelkovic et al., 1998; de Groot et al., 2001; Hulette et al., 1992; Korzhevskii and Kirik, 2016; Lue et al., 1996; Nagai et al., 2001; Roggendorf et al., 1996; Ulvestad et al., 1994).

4.2.2.3 HLA-DR (CR3-43)

HLA-DR is a marker that is used to identify reactive/activated microglia. It is a glycoprotein that is part of the major histocompatibility complex class II (MHC II) subgroup (Dandrea et

al., 2001; Esiri et al., 1991; Guillemin and Brew, 2004; Hassan et al., 1991; Korzhevskii and Kirik, 2016; Lee et al., 2002; Mattiace et al., 1990b; McGeer et al., 1988; Nagai et al., 2001; Rogers et al., 1988; Sasaki and Nakazato, 1992; Streit et al., 2004; Styren et al., 1990; Zotova et al., 2011). It stains the plasma membrane of microglia cells or brain macrophages but does not stain other cells such as astrocytes, oligodendrocytes or neurons (McGeer et al., 1988; Styren et al., 1990). It has been shown to be upregulated in several neurodegenerative diseases, including AD, PD, Pick's disease and ALS (Carpenter et al., 1993; DiPatre and Gelman, 1997; Itagaki et al., 1989; McGeer et al., 1988, 1993).

4.2.2.4 P2RY12

All markers described so far stain both microglia and macrophages. Hickman et al., (2013) and Butovsky et al., (2013) identified a set of genes that are specific to microglia, which would allow the differentiation between microglia and macrophages in the brain tissue. P2RY12 has been shown to be involved in the early microglial response to injury and is involved in the motility of the processes and a chemotactic response to ATP released from injured neurons or astrocytes (Sipe et al., 2016; Swiatkowski et al., 2016). P2RY12 stains predominantly ramified microglia. As this receptor is expressed as part of the microglia's homeostatic signature, the signal is lost as the cells become activated and move away from their homeostatic state.

4.2.3 TREM2 and microglia

Since *TREM2* was discovered as a genetic risk factor for late onset AD, research into the role of TREM2 has greatly increased. However, as it stands, much of the literature is conflicting, especially in terms of the precise role TREM2 has on Aβ clearance and whether its activation is linked to pro- or anti-inflammatory mechanisms.

4.2.3.1 TREM2 cellular location and aged studies

TREM2 was identified as a receptor on myeloid cells before it was identified to be a risk factor for late-onset AD and its role in microglia has therefore been extensively studied. TREM2 has been shown to be expressed by myeloid cells throughout the CNS.

Immunofluorescence was used to identify that TREM2 is variably expressed in multiple brain regions such as the cortex, hippocampus, putamen and spinal cord (Hsieh et al., 2009). However, the quality of TREM2 antibodies is questionable, making the expression of TREM2 complex to determine. Further to this variability between regions, microglia expressing TREM2 were counted using the number of silver grains exposed to a TREM2 riboprobe and revealed that TREM2 expression also varies within regions as not all microglia in any one region express TREM2 (Schmid et al., 2002).

There has been some debate on whether TREM2 is specifically expressed on microglia or whether TREM2 is also expressed on peripheral macrophages and circulating monocytes (Chertoff et al., 2013; Jay et al., 2015). Poor reagents that are not well characterised have led to confusion over the reliability of TREM2 antibodies in human tissue. Some believe they are only staining the circulating monocytes and not microglia, however, this could be an antibody sensitivity or specificity issue (Fahrenhold et al., 2017; Satoh et al., 2013). Jay et al suggested that it was in fact TREM2-expressing peripheral macrophages that were surrounding amyloid plaques and not microglia due to the fact they were CD45+ve and P2RY12-ve, with CD45 being believed to be a marker of macrophages and P2RY12 of resident microglia. Other studies also reported that there was no change in TREM2 expression between microglia and peripheral macrophages (Frank et al., 2008; Jay et al., 2015; Prokop et al., 2015; Ulrich et al., 2014). However, since that discovery, it has become clear that the P2RY12 marker of resident microglia marks a more ramified homeostatic form of microglia and not an activated amoeboid form that is typical of phagocytosis. Different markers can be up or down regulated in different activation states. This may be where the discrepancy lies. Subsequently, it was found that *TREM2* is a gene that is highly enriched in microglia compared to macrophages in using direct RNA- sequencing and qPCR (Hickman et al., 2013).

Long-term aging studies have shown that the amount of microglia in wild type mice does not differ significantly from mice that are *TREM2* knockouts until they are 2 years of age (Poliani et al., 2015). However, in primary microglia *in vitro* models the number of microglia decrease when TREM2 levels decrease and *TREM2* knockout primary microglia showed reduced

proliferation suggesting that TREM2 may play a role in microglial proliferation in certain conditions (Cantoni et al., 2015; Zheng et al., 2016, 2017).

4.2.3.2 TREM2 and inflammation

TREM2 is thought to have a role in determining homeostatic control within microglia with high levels promoting phagocytosis and low levels promoting a pro-inflammatory state (Boche et al., 2013; Guerreiro et al., 2013a; Jonsson et al., 2012b; Wu et al., 2014). Increases in TREM2 expression leads to increased phagocytosis and decreased TREM2 expression leads to decreased phagocytosis. TREM2 is thought to induce phagocytosis through NF-κB independent mechanisms. However, NF-κB sensitive miRNA-34a has been shown to affect TREM2 expression levels, indicating that NF-κB may still have an indirect effect on TREM2 activity (Bouchon et al., 2001; Jones et al., 2014; Takahashi et al., 2005). Alternative activation of phagocytosis works through toll-like receptors and activates NF-κB and inflammatory cytokine levels (Blander and Medzhitov, 2004; Frank et al., 2008; Guerreiro et al., 2013a; Jonsson et al., 2012b; Takahashi et al., 2005). TREM2 expression is also affected by other pro-inflammatory molecules such as TNFα, IFNγ and LPS (Hickman et al., 2013; Satoh et al., 2013; Zhao and Lukiw, 2013; Zheng et al., 2016). When TREM2 is knocked down in primary microglia, an increase in inflammatory responses through toll-like receptors is observed, suggesting that when TREM2 is deficient, an alternative method of inflammation and phagocytosis is triggered (Takahashi et al., 2005). However, this method causes higher levels of cytokines, such as TNFα, nitric oxide synthase-2 and IL-1β, and therefore has a more detrimental effect on the brain (Frank et al., 2008; Guerreiro et al., 2013a; Jonsson et al., 2012b; Piccio et al., 2007; Takahashi et al., 2005). This is validated by *TREM2* knockout models which display increased levels of age-related neuroinflammation compared to wildtypes (Jiang et al., 2014). Further to this, TREM2 ablation causes reduced motility of microglia towards chemo-attractants and gene expression levels in these models show a signature that is more closely associated with homeostatic microglia (Mazaheri et al., 2017).

TREM2 is not expressed by neurons and is not known to be expressed by other cell types but TREM2 ligands are thought to be expressed on apoptotic neurons, providing signals to

microglia for phagocytosis (Hsieh et al., 2009). Further evidence for this is that TREM2 expression increases when there is injury induced cell death and *TREM2* deficient models show impaired clearance of apoptotic neurons (Frank et al., 2008; Hsieh et al., 2009; Satoh et al., 2013; Sieber et al., 2013; Takahashi et al., 2005). This leads to increased levels of necrotic debris and neuroinflammation which can exacerbate disease (Hsieh et al., 2009; Thrash et al., 2009).

4.2.3.3 Evidence of factors that can influence TREM2 expression

Levels of TREM2 expression have been shown to differ between brain regions in post-mortem human brain. However, regardless of region they are increased in microglia that surround amyloid plaques in both human brain and AD mice models (APP23, 5xFAD) (Frank et al., 2008; Jay et al., 2015; Perez et al., 2017; Satoh et al., 2013). They are not detected on P2RY12+ve parenchymal microglia (Jay et al., 2015). Oligomeric Aβ is thought to have the same effect on TREM2 expression as lipopolysaccharide (LPS), causing a decrease in expression (Zheng et al., 2016). LPS is found in the outer membrane of Gram-negative bacteria and it is commonly used in experiments to stimulate an inflammatory response.

This decreased expression of TREM2 is thought to reduce the levels of phagocytosis and exacerbate the disease. There is a reduced ability for the microglia to respond to Aβ and phagocytose Aβ42 peptides in *TREM2* deficient models compared to wildtypes, with additional reduction of phagocytosis of apoptotic neurons in these models (Jay et al., 2015; Jones et al., 2014; Kleinberger et al., 2014; Satoh et al., 2013; Ulrich and Holtzman, 2016; Wang et al., 2015; Zhao and Lukiw, 2013). Overall, *TREM2* deficient models have reduced inflammation and increased amyloid and tau pathology (Colonna and Wang, 2016; Jay et al., 2015; Painter et al., 2015; Ulrich and Holtzman, 2016). *TREM2* deficiency in a 5xFAD mouse model showed reduced microgliosis with the microglia around amyloid plaques not fully enclosing them (Wang et al., 2015, 2016; Yuan et al., 2016). In a *TREM2* haploinsufficient mouse model (*TREM2*$^{+/-}$*/APPPS1-21*) there were also less microglia found around the amyloid plaques (Ulrich and Holtzman, 2016; Ulrich et al., 2014).

TREM2 is able to bind to APOE and *APOE* has been reported to be upregulated in microglia that surround amyloid plaques. The microglia that surround the neuritic plaques in AD were found to have a distinct phenotype to other microglial cells and have been termed 'dark microglia', disease-associated microglia (DAM) or microglia of neurodegeneration (MGnD) by different groups using both electron microscopy and transcriptomic profiling techniques (Bisht et al., 2016; Keren-Shaul et al., 2017; Krasemann et al., 2017). These microglia have been found to act differently to other activated microglia and this is thought to occur through the upregulation of several genes that stimulate the TREM2 pathway, including *APOE* (Keren-Shaul et al., 2017). Recently, Krasemann et al., (2017) have identified that APOE triggers the differentiation of microglia from a homeostatic state to that of this new disease-associated phenotype found in AD via activation of TREM2 (Keren-Shaul et al., 2017).

4.2.4 Aims

In this chapter, the microglial phenotype in the brains identified with a *TREM2* variant were investigated and compared to sporadic AD cases, familial AD cases and controls. Differences between the *TREM2* variants that had pathologically confirmed AD and those that were pathologically confirmed as neurologically normal controls at time of death were also compared.

To identify the microglial phenotype in these cases three factors were measured: 1), microglial load; to assess the abundance of microglia; 2) the circularity; to assess whether the microglia were in an amoeboid, more phagocytic shape or whether they were ramified; and 3) the perimeter; to assess the size of the microglia. These factors were measured in the frontal cortex, temporal cortex, hippocampus, putamen and cerebellum. Four different microglial markers were investigated; Iba1, CD68, CR3-43 and P2RY12.

To assess whether *APOE* genotype influenced the microglial phenotype in these cases, an analysis based on *APOE* genotype for all measures was undertaken.

As TREM2 antibodies have been unreliable and unspecific in the past, seven commercially available TREM2 antibodies were optimised using several conditions to try and determine a good antibody to measure TREM2 distribution within AD post-mortem brain tissue.

4.3 Materials and Methods

4.3.1 Case demographics and selection

All case demographics are detailed in Table 2.3. All cases were used for pathological analysis of microglia using the antibodies, Iba1, CD68 and CR3-43, whereas only cases 1-9, 12, 14-15, 17, 26-27, 29-35, 37-42 were used for P2RY12 analysis. Case 25 was used for TREM2 antibody optimisation.

4.3.2 Immunohistochemistry

Immunohistochemistry with Iba1, CD68, CR3-43 and P2RY12 antibodies was performed as described in 2.4 (SAD (n=19), FAD (n=11), *TREM2* AD (n=4), *TREM2* controls (n=2), controls (n=6). Representative brain regions from the five Thal phases were investigated (frontal cortex, temporal cortex, hippocampus, putamen and cerebellum). Only frontal cortex, temporal cortex and hippocampus were assessed with the P2RY12 antibody. Details of the antibodies used in this study are listed in Table 2.6.

Seven TREM2 antibodies listed in Table 2.6 were tested with different conditions using the methods of immunohistochemistry on formalin fixed paraffin embedded sections and frozen sections from flash frozen tissue, which are both outlined in 2.4.1 and 2.4.2. Each antibody was tested with different pre-treatments which included pressure cooking in citrate buffer (0.45g citric acid, 5.8g tri-sodium citrate, two litres deionised H_2O, pH6) for ten minutes with or without prior immersion in 100% formic acid for ten minutes. Frozen cryostat sections were subjected to 4% paraformaldehyde solution for thirty minutes or ice-cold acetone for thirty minutes. Sections were visualised under a microscope (Nikon Eclipse Ni) and pictures taken for each condition at 40x magnification.

4.3.3 Pathology analysis

Analysis for Iba1, CD68, CR3-43 and P2RY12 load was calculated using methods described in 2.5. The circularity and perimeter were calculated using the hull and circle macro described in 2.5.5.

4.3.4 Statistics

Kruskal-Wallis one way ANOVA tests with Dunn's multiple comparison analysis were performed on each region for each antibody and each microglial analysis (load, circularity, and perimeter) with a 0.05 significance level. Significance is shown as * for $p<0.05$, ** for $p<0.005$, *** for $p<0.0005$, ****$p<0.0001$. GraphPad Prism v7 was used to complete this analysis.

4.4 Results

4.4.1 Microglial load in *TREM2* variant cases compared to Alzheimer's disease

To assess the percentage of the grey matter, across all six cortical layers, that was occupied by microglia, the microglial load was assessed and compared between SAD, FAD, *TREM2* variant AD cases, *TREM2* variant controls and controls across brain regions that represent the five Thal phases. Load was expressed as a percentage of the area stained by the antibody. The highest microglial load was observed with the P2RY12 marker (Figure 4.2d and l), followed by Iba1 (Figure 4.2a and i) then CD68 (Figure 4.2b and k) and CR3-43 (Figure 4.2c and j).

TREM2 variant AD cases had a significantly higher CD68 load in the frontal cortex compared to the FAD cases (*p=0.0127*) and the TREM2 variant controls (*p=0.0147,* Figure 4.2k). Representative CD68 images from SAD, FAD, TREM2 variant AD and TREM2 variant control cases can be seen to show these differences (Figure 4.2e-h). There was also a significant increase in the *TREM2* variant AD cases compared to the controls in the cerebellum (*p=0.0444*). This trend follows suit throughout all regions whereas all other disease groups appear to be at similar levels throughout all regions.

There were no significant differences that could be seen when assessing Iba1 load. However, *TREM2* variant AD cases appeared to have a markedly increased Iba1 load in the frontal cortex compared to other groups but was markedly decreased in the temporal cortex, putamen and cerebellum (Figure 4.2i). *TREM2* variant controls followed an opposite pattern

to the *TREM2* variant AD cases in the frontal cortex, temporal cortex and putamen. SAD and FAD cases had consistent loads across regions.

No significant differences were seen between disease groups when assessing CR3-43 load (Figure 4.2j). The levels of CR3-43 load were observed across all regions in each disease group with the highest levels being observed in the frontal cortex. TREM2 variant AD cases appear to follow the same trend as SAD cases when comparing to other disease groups.

SAD, FAD, *TREM2* variant controls and controls had similar levels of P2RY12 load in both the frontal and temporal cortices with a greater level of variation between disease groups observed in the hippocampus (Figure 4.2l).

The microglial load with each marker was correlated to both the Aβ load and the tau load and linear regression analysis performed to determine if the line significantly deviated from zero (Figure 4.3 and Figure 4.4). There was a significant correlation between Iba1 and Aβ in the *TREM2* variant cases frontal cortex (p=0.0003), FAD hippocampus (p=0.0071), SAD putamen (p=0.0383) and FAD putamen (p=0.0046). However, the TREM2 variant cases were negatively correlated whereas the SAD and FAD cases were positively correlated. CD68 and Aβ were also significantly correlated in SAD putamen (p=0.0497).

CR3-43 and tau are significantly correlated in SAD temporal cortex (p=0.0365), TREM2 variant temporal cortex (p=0.0310) and SAD putamen (p=0.0424) with the TREM2 variant cases showing negative correlation and the others positive as with the Aβ. CD68 and tau are also significantly correlated in TREM2 variant temporal cortex in the same direction (p=0.0382)

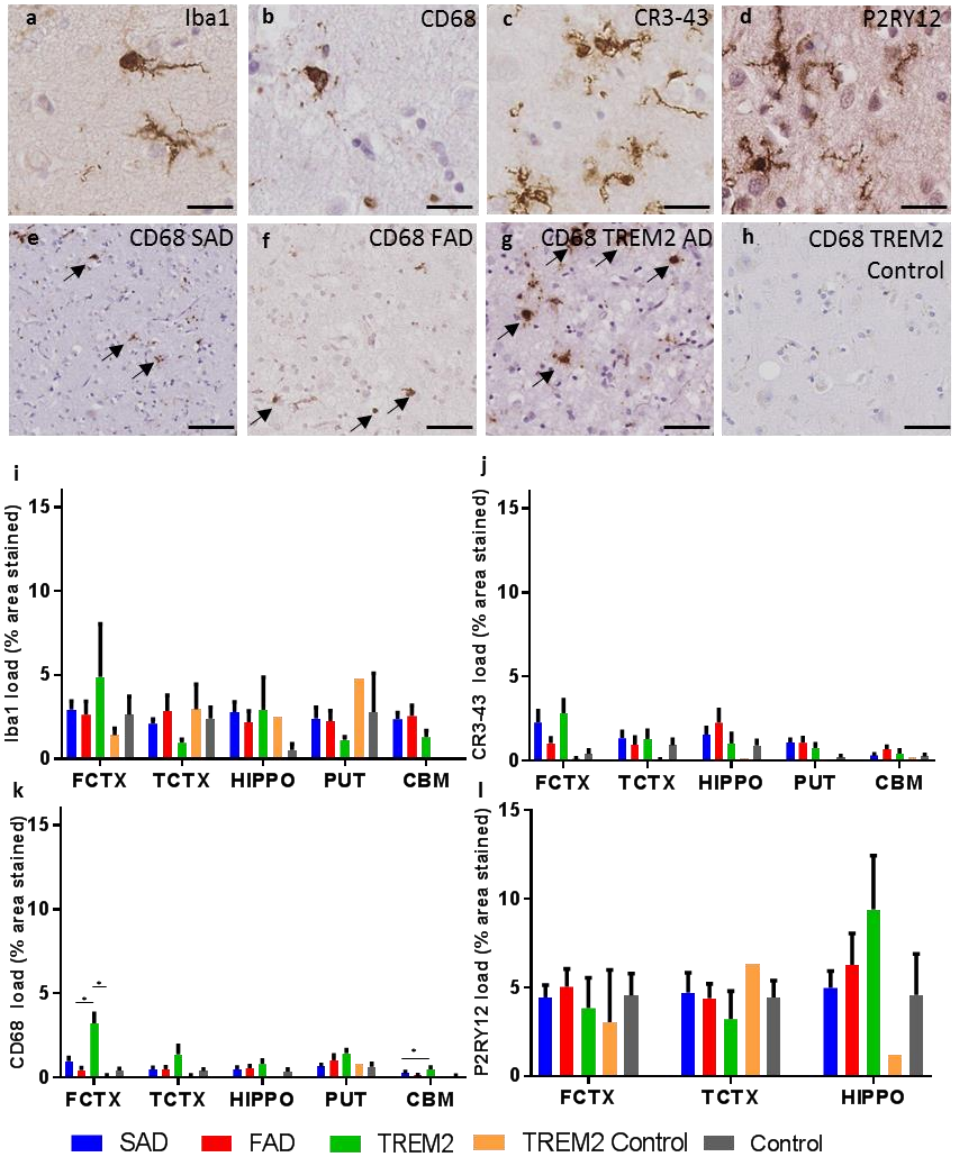

Figure 4.2: Microglial load in *TREM2* variant cases compared to AD and controls. Measured using different microglial markers in frontal cortex (FCTX), temporal cortex (TCTX), hippocampus (HIPPO), putamen (PUT) and cerebellum (CBM) and compared in disease groups; SAD, FAD, *TREM2* AD, *TREM2* Control and Control. Load measured as mean percentage of squares stained. Representative images of microglial immunohistochemistry for Iba1 (a), CD68 (b), CR3-43 (c) and P2RY12 (d) on case 7. Representative images of CD68 staining in the frontal cortex of SAD (e, case 13), FAD (f, case 27), *TREM2* AD (g, case 2) and *TREM2* control (h, case 3). Iba1 load (i), CD68 load (k), CR3-43 load (j), and P2RY12 load (l). Key is shown to show colour for each disease group. Black arrows highlight CD68+ve microglia. Scale bar represents 50µm. Kruskal-Wallis one way ANOVA was performed with Dunn's multiple comparison to assess significance. Significance is shown as * for $p<0.05$, ** for $p<0.005$, *** for $p<0.0005$, ****$p<0.0001$. Error bars represent SEM.

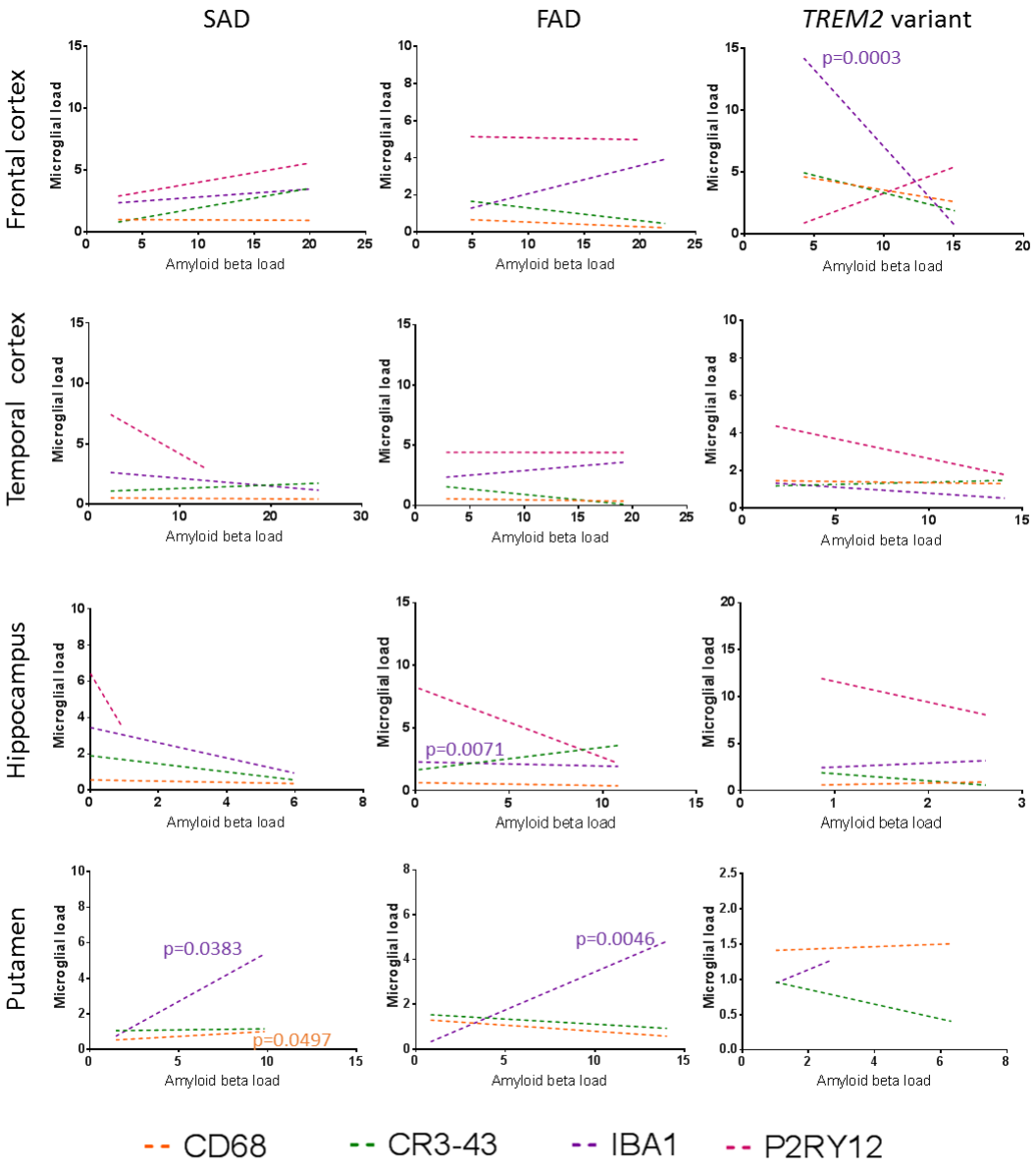

Figure 4.3: Correlations between Aβ load and microglial load. Each graph highlights the correlations between Aβ load and each microglial marker as indicated by colour in the key shown. Each graph is individual for disease group and region. Linear regression analysis was performed and any significant deviations of the line from zero are indicated with their p value with significance $p<0.05$.

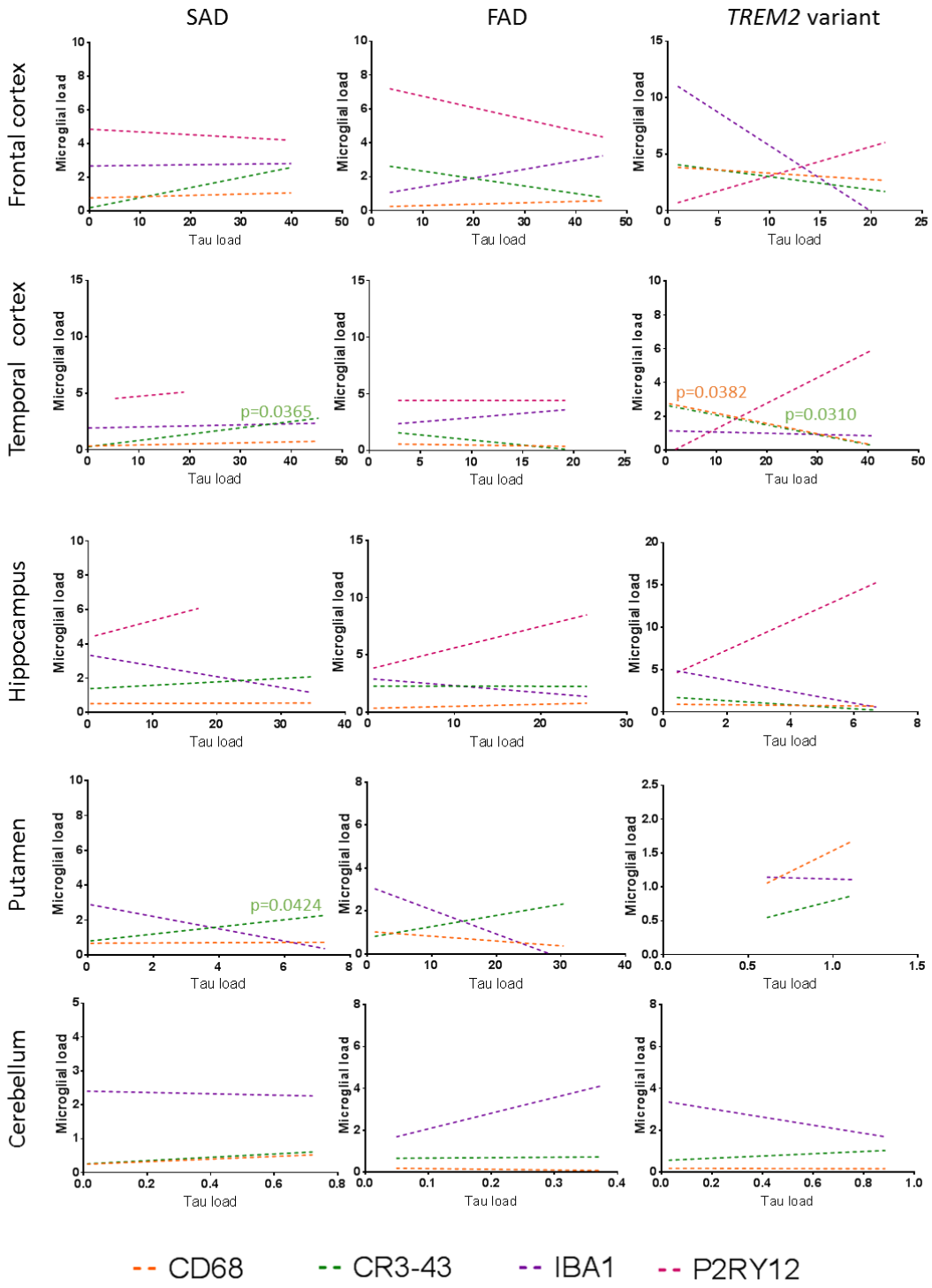

Figure 4.4: Correlations between tau load and microglial load. Each graph highlights the correlations between AT8 load and each microglial marker as indicated by colour in the key shown. Each graph is individual for disease group and region. Linear regression analysis was performed and any significant deviations of the line from zero are indicated with their p value with significance $p<0.05$.

4.4.2 Microglial circularity in *TREM2* variant cases compared to Alzheimer's disease

As microglia have a spectrum of different morphological phenotypes, ranging from a ramified, surveillance phenotype to a more amoeboid phagocytic phenotype the shape of the microglia was also investigated across the different disease groups to determine whether one phenotype was more prominent in any of the disease groups. This was measured as an index of circularity in which a perfect circle would score 1 and an imperfect shape would be 0. Ramified microglia would have a score closer to 0 whereas amoeboid microglia would have a score closer to 1 (Figure 4.2a-d).

TREM2 variant AD cases had significantly more circular Iba1 microglia than controls in the temporal cortex (*p=0.0248*) and more circular microglia in both the SAD (*p=0.0342*) and FAD groups (*p=0.0302*) in the cerebellum (Figure 4.5e). This trend followed suit in the frontal cortex and putamen. However, the hippocampus appeared to have more circular microglia in the controls compared to other regions.

TREM2 variant AD cases also have significantly more circular CR3-43 microglia than the SAD cases (*p=0.0128*) in the frontal cortex and more circular microglia than the controls (*p=0.0064*) in the temporal cortex (Figure 4.5f).

Furthermore, TREM2 variant AD cases had significantly more circular CD68 microglia than the controls in the frontal cortex (*p=0.0296*, Figure 4.5g). A similar trend to this can be seen in the putamen.

As expected P2RY12 microglia generally had a circularity score closer to 0 than Iba1, CD68 and CR3-43 microglia (Figure 4.5h). No major differences were observed between disease groups for P2RY12 circularity scores either with all groups scoring a small amount above or below 0.3.

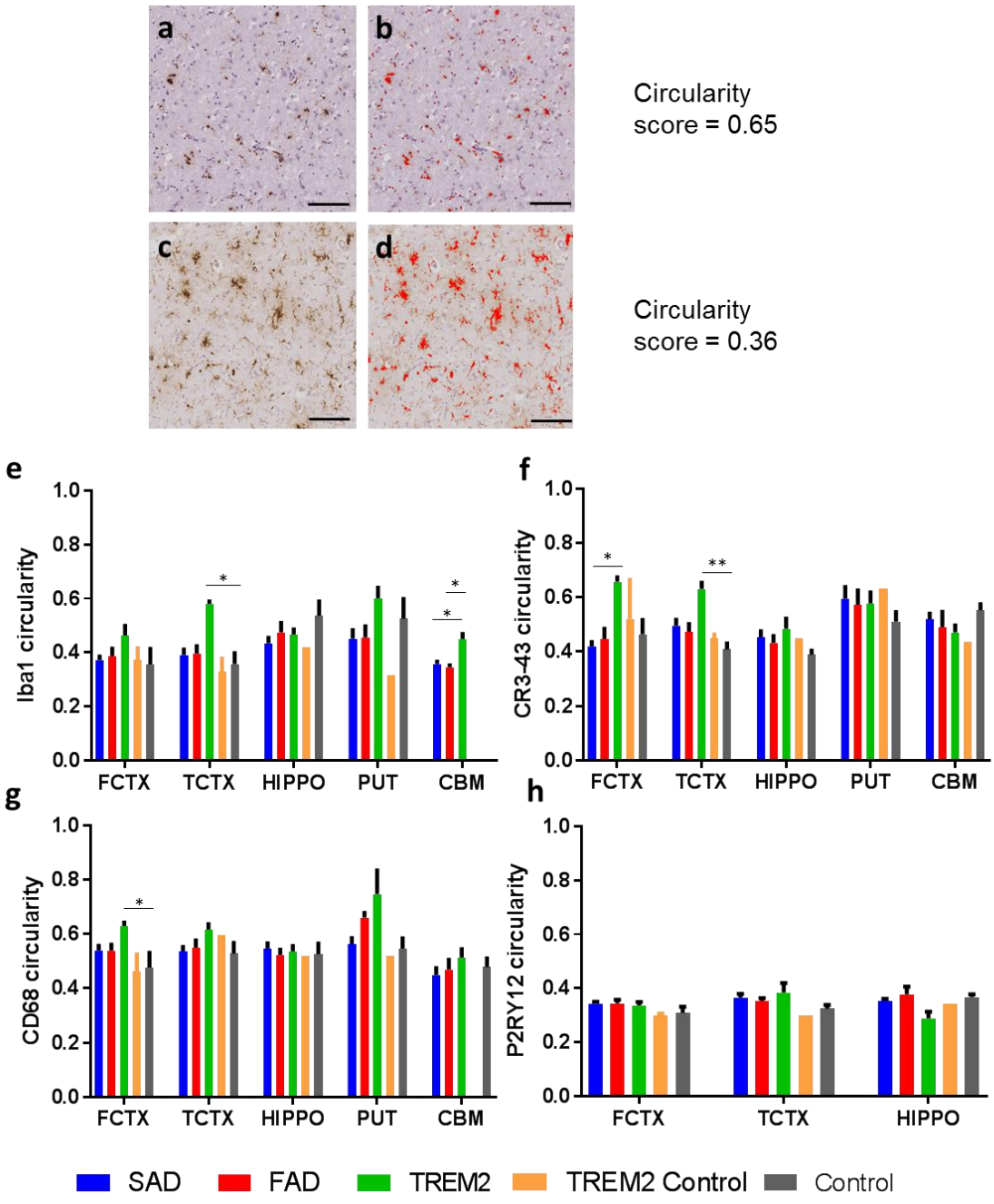

Figure 4.5: Microglial circularity in *TREM2* variant cases compared to AD and controls. Measured using different microglial markers in frontal cortex (FCTX), temporal cortex (TCTX), hippocampus (HIPPO), putamen (PUT) and cerebellum (CBM) and compared in disease groups; SAD, FAD, *TREM2* AD, *TREM2* Control and Control. A score of 1 is a perfect circle whereas a score of 0 is an imperfect shape. Mean values were taken from each case in a disease group. Two representative randomly selected squares are shown for case 2 (a) and case 14 (c). The corresponding circularity scores for these squares are shown (b, d). Iba1 circularity (e), CD68 circularity (g), CR3-43 circularity (f), and P2RY12 circularity (h). Key is shown to show colour for each disease group. Scale bar represents 50um. Kruskal-Wallis one way ANOVA was performed with Dunn's multiple comparison to assess significance. Significance is shown as * for $p<0.05$, ** for $p<0.005$, *** for $p<0.0005$, ****$p<0.0001$. Error bars represent SEM.

4.4.3 Microglial perimeter in *TREM2* variant cases

The load and shape of the microglia have been investigated; with the macro developed by Yau Lim, the size of the individual microglia could also be investigated. The perimeters of the microglia were assessed to determine if the size changed according to disease group (Figure 4.6a-d). The overall perimeter of the microglia across the different markers does not differ drastically; with only CD68 having smaller perimeters than the rest of the markers (Figure 4.3g) and this was most likely due to the lack of processes on these microglia. However, as CD68 and Iba1 are markers in which their target antigen is not on the plasma membrane, the stain may not take into account the whole size of the cell.

TREM2 variant AD cases have significantly reduced perimeter of Iba1 microglia in the temporal cortex compared to SAD cases (*p=0.0293*), with this trend following suit in the putamen (Figure 4.6e). The *TREM2* variant AD cases have significantly reduced perimeter of CR3-43 microglia compared to SAD cases in the frontal cortex (*p=0.0054*) and controls in the temporal cortex (*p=0.0293,* Figure 4.6f). No significant differences in the perimeter of CD68 microglia were found (Figure 4.6g). As CD68 microglia are predominantly amoeboid in shape, the size of the microglia may not differ greatly. Similarly, no significant differences in perimeter were detected in P2RY12 microglia (Figure 4.6h).

The SAD and FAD cases have the same size perimeter throughout all of the markers and all regions excluding the frontal cortex of CR3-43 microglia suggesting that although they may have differences in load and shape between the different AD subtypes, the size of the microglia does not differ greatly.

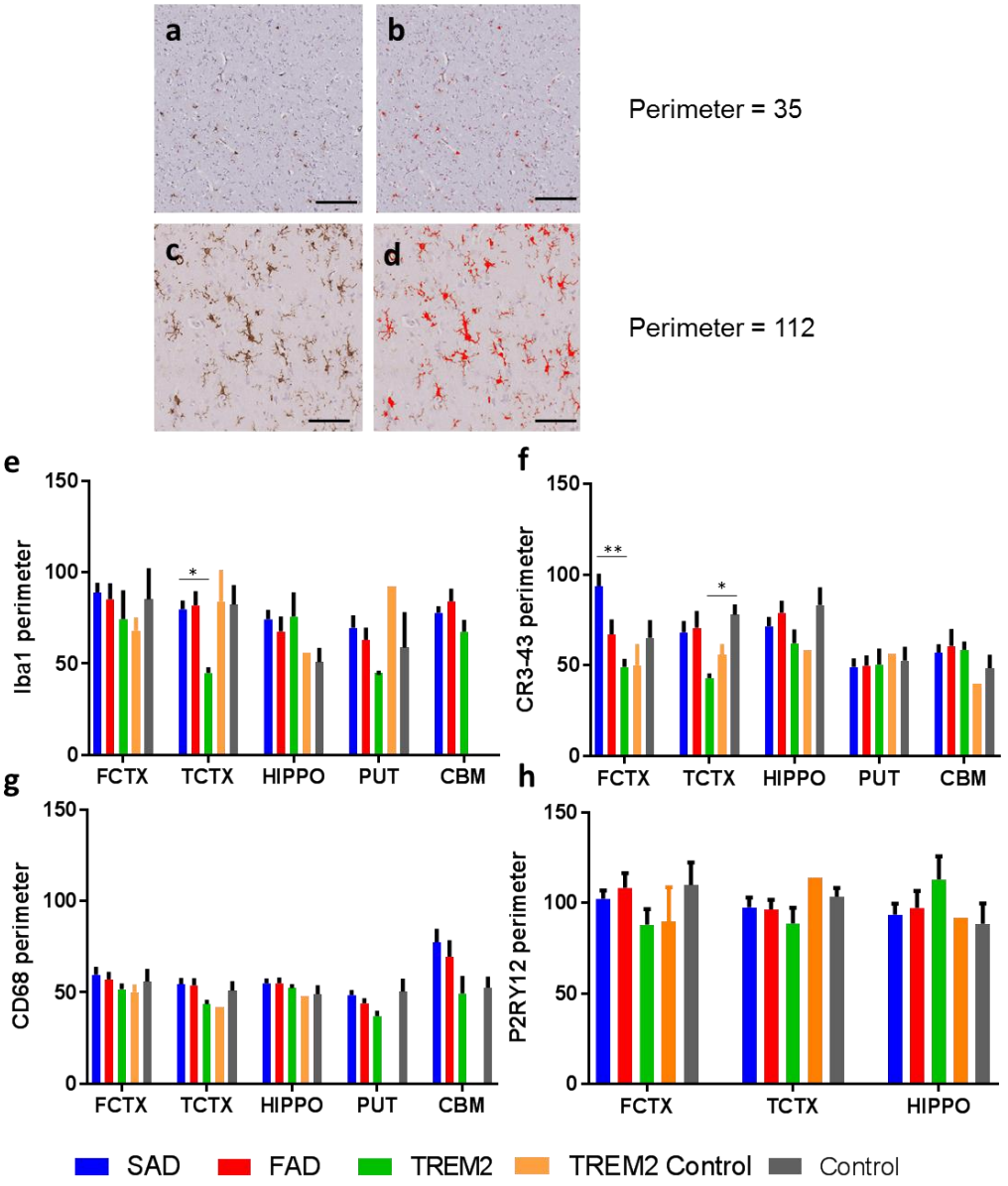

Figure 4.6: Microglial perimeter in *TREM2* variant cases compared to AD and controls. Measured using different microglial markers in frontal cortex (FCTX), temporal cortex (TCTX), hippocampus (HIPPO), putamen (PUT) and cerebellum (CBM) and compared in disease groups; SAD, FAD, *TREM2* AD, *TREM2* Control and Control. Mean values were taken from each case in a disease group. Two representative randomly selected squares are shown for case 13 (a) and case 33 (c). The corresponding perimeters for these squares are shown (b, d). Iba1 perimeter (e), CD68 perimeter (g), CR3-43 perimeter (f), and P2RY12 perimeter (h). Key is shown to show colour for each disease group. Scale bar represents 50µm. Kruskal-Wallis one way ANOVA was performed with Dunn's multiple comparison to assess significance. Significance is shown as * for $p<0.05$, ** for $p<0.005$, *** for $p<0.0005$, ****$p<0.0001$. Error bars represent SEM.

4.4.4 *APOE* genotype effect on microglia

As discussed in Chapter 3, *TREM2* variant AD cases all were found to have at least one *ApoE4* allele, whereas the *TREM2* variant controls had no *ApoE4* alleles. It was therefore hypothesised that there is a potential link between *TREM2* variants and *APOE* genotype. To investigate this link further, the microglial load, shape and size was investigated according to *APOE* genotype as illustrated in Figure 4.4, Figure 4.8, and Figure 4.6.

No significant differences in microglial load were observed for any of the microglial markers. However, Iba1 load appeared to be increased in the *ApoE3/4* group in the frontal cortex and hippocampus (Figure 4.7a). CR3-43 load appears to have showed decreased load in the *ApoE2/2* group compared to other groups and a pattern in *ApoE2/2*< *ApoE2/4*< *ApoE3/3*< *ApoE3/4*< *ApoE4/4* in the hippocampus, putamen and cerebellum (Figure 4.7b). CD68 load also showed a pattern of increasing load as less *ApoE2* and more *ApoE4* was present (Figure 4.7c). This pattern followed throughout all the regions for CD68. However, the *ApoE4/4* group does have large error bars which may account for this difference. There was no marked difference in the P2RY12 load in frontal cortex but the load in the temporal cortex followed the pattern *ApoE2/2*> *ApoE3/3*> *ApoE3/4*> *ApoE4/4*, whereas the hippocampus showed a decrease in the *ApoE2/2* load compared to other groups (Figure 4.7d). Therefore, the activated microglial markers (CD68 and CR3-43) showed a decrease in *ApoE2/2* in cortical areas aside from P2RY12 in which *ApoE2/2* has the highest load in the temporal cortex. This suggests that the P2RY12+ve resting microglia are more abundant in *ApoE2/2* cases than other *APOE* genotypes.

Microglial circularity comparisons between *APOE* genotypes also showed no significant differences. Nevertheless, Iba1 microglia do appear to be more circular in shape in the *ApoE4/4* group compared to other groups in the frontal cortex and temporal cortex (Figure 4.8a). Although the hippocampus shows the opposite with *ApoE2/2* being more circular in that region. CR3-43 microglia on the other hand, show more circular microglia in the *ApoE2/2* group in the frontal cortex and putamen (Figure 4.8b), though the *ApoE2/4* microglia appear to be less circular in the putamen. Similarly to Iba1 load, *ApoE2/2* CD68 microglia were less circular than other groups in the frontal cortex (Figure 4.5c). P2RY12

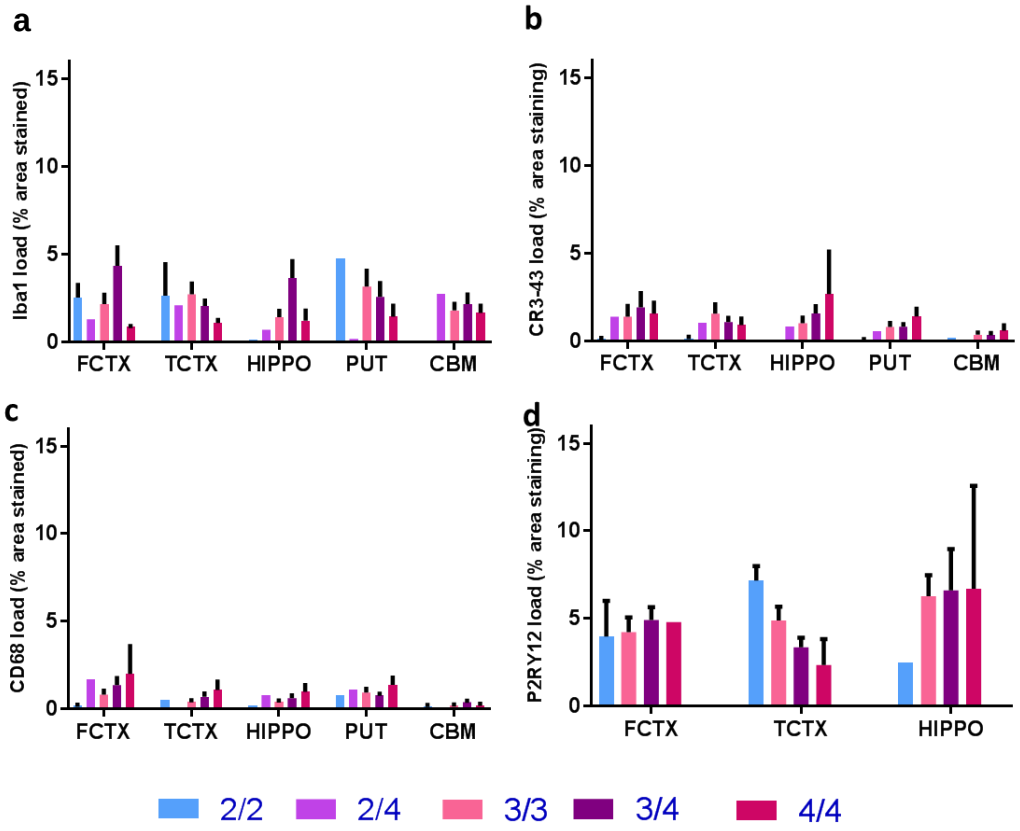

Figure 4.7: Microglial load compared between *APOE* genotypes. Measured using different microglial markers in frontal cortex (FCTX), temporal cortex (TCTX), hippocampus (HIPPO), putamen (PUT) and cerebellum (CBM). *APOE* genotypes were 2/2, 2/4, 3/3, 3/4 and 4/4. Load is measured as mean percentage of squares stained. (a) Iba1 load, (b) CD68 load, (c) CR3-43 load, (d) P2RY12 load. Key is shown to show colour for each *APOE* genotype. Kruskal-Wallis one way ANOVA was performed with Dunn's multiple comparison to assess significance. Significance is shown as * for $p<0.05$, ** for $p<0.005$, *** for $p<0.0005$, ****$p<0.0001$. Error bars represent SEM.

microglia are consistent in microglial load throughout regions (Figure 4.8d).

Further to this, there were no significant differences found in the Iba1 or P2RY12 microglial perimeter. The perimeter of the Iba1 microglia appeared to be decreased in the *ApoE4/4* group in the frontal cortex but increased compared to the *ApoE2/2* group in the hippocampus (Figure 4.6a). CR3-43 and CD68 microglia with *ApoE2/2* microglia were significantly decreased in perimeter in the frontal cortex compared to the *ApoE2/4* group (CR3-43 *p=0.0298*, Figure 4.6b, CD68 *p=0.0249*, Figure 4.6c). P2RY12 microglia had slightly elevated perimeter in *ApoE2/2* cases in the temporal cortex, whereas a decrease was seen in this group in the hippocampus (Figure 4.6d).

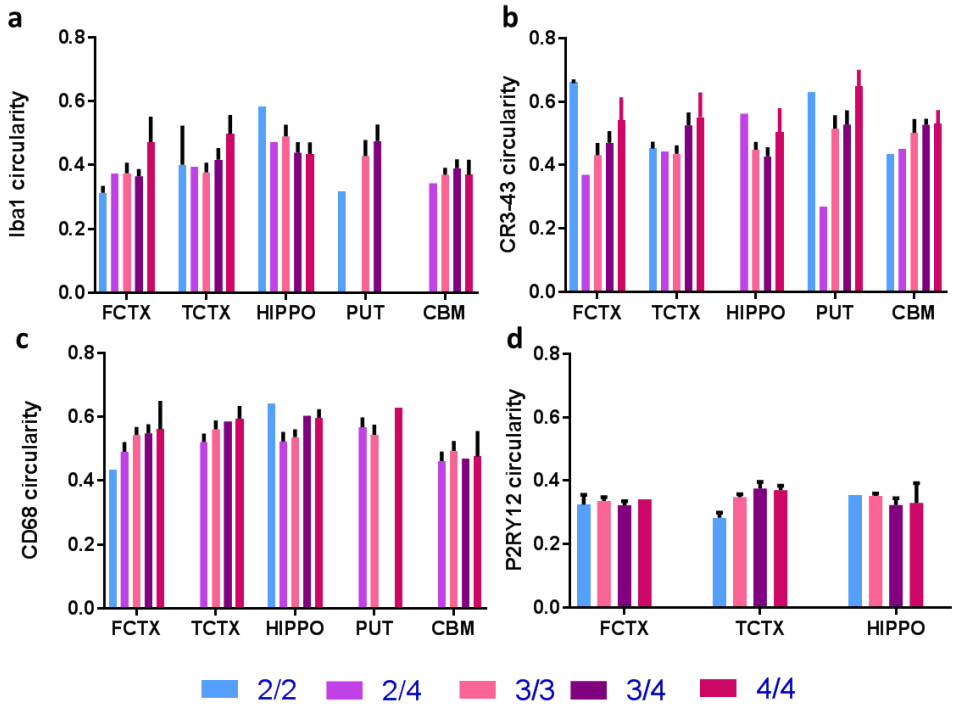

Figure 4.8: Microglial circularity compared between *APOE* genotypes. Measured using different microglial markers in frontal cortex (FCTX), temporal cortex (TCTX), hippocampus (HIPPO), putamen (PUT) and cerebellum (CBM). *APOE* genotypes were 2/2, 2/4, 3/3, 3/4 and 4/4. A score of 1 is a perfect circle whereas a score of 0 is an imperfect shape. Mean values were taken from each case in a disease group. (a) Iba1 circularity, (b) CD68 circularity, (c) CR3-43 circularity, (d) P2RY12 circularity. Key is shown to show colour for each *APOE* genotype. Kruskal-Wallis one way ANOVA was performed with Dunn's multiple comparison to assess significance. Significance is shown as * for $p<0.05$, ** for $p<0.005$, *** for $p<0.0005$, ****$p<0.0001$. Error bars represent SEM.

4.4.5 TREM2 antibody optimisation

The aim of this optimisation was to identify a reliable commercially available TREM2 antibody to investigate the TREM2 distribution levels across the different regions of the brain and compare this between *TREM2* variant cases and other sporadic and familial AD cases. Reports from the literature using TREM2 antibodies show the antibodies work well in mouse brain tissue but in human formalin fixed tissue the results are variable and are therefore not reliable. In this study six TREM2 antibodies were available and were tested to determine which antibody would be most optimal. The TREM2 antibodies (Table 4.4.2) were optimised in both formalin-fixed paraffin embedded and frozen tissue and liver sections were used as a positive control. Table 4.1 shows the details of each antibody in detail, including the epitope that they target. A summary of the findings with each antibody can be seen in Table 4.2.

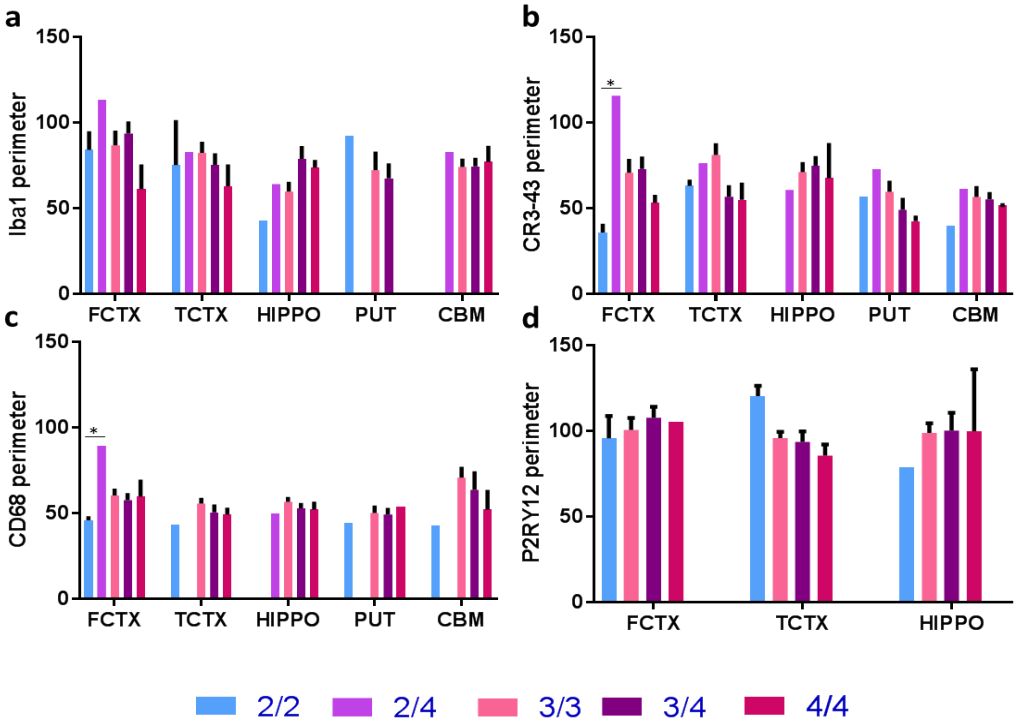

Figure 4.9: Microglial perimeter compared between *APOE* genotypes. Measured using different microglial markers in frontal cortex (FCTX), temporal cortex (TCTX), hippocampus (HIPPO), putamen (PUT) and cerebellum (CBM). *APOE* genotypes were 2/2, 2/4, 3/3, 3/4 and 4/4. Mean values were taken from each case in a disease group. (a) Iba1 perimeter, (b) CD68 perimeter, (c) CR3-43 perimeter, (d) P2RY12 perimeter. Key is shown to show colour for each *APOE* genotype. Kruskal-Wallis one way ANOVA was performed with Dunn's multiple comparison to assess significance. Significance is shown as * for p<0.05, ** for p<0.005, *** for p<0.0005, ****p<0.0001. Error bars represent SEM.

Antibody	Company	Epitope length	Epitope	Species	Clonality
TREM2	Abcam (ab117645)	168	1-168	goat	pAb
TREM2	Abgent (AP5469a)	28	22-50	rabbit	pAb
TREM2	SantaCruz (sc-373828)	160	1-160	mouse	mAb
TREM2	Sigma (HPA010917)	35	196-230	rabbit	pAb
TREM2	Sigma (HPA012571)	112	33-144	rabbit	pAb
TREM2	R&D (AF1828)	155	19-174	goat	pAb
TREM2	Proteintech (13483-1-AP)	200	22-222	rabbit	pAb

Table 4.2: Features of TREM2 antibodies

The Abcam antibody showed a small amount of staining in the control liver section (Figure 4.11a). Positive staining in the grey matter showed neuronal cells but the white matter remained negative (Figure 4.11). Staining worked better in the frozen tissue than the paraffin tissue. Acetone and PFA fixations gave rise to different staining patterns.

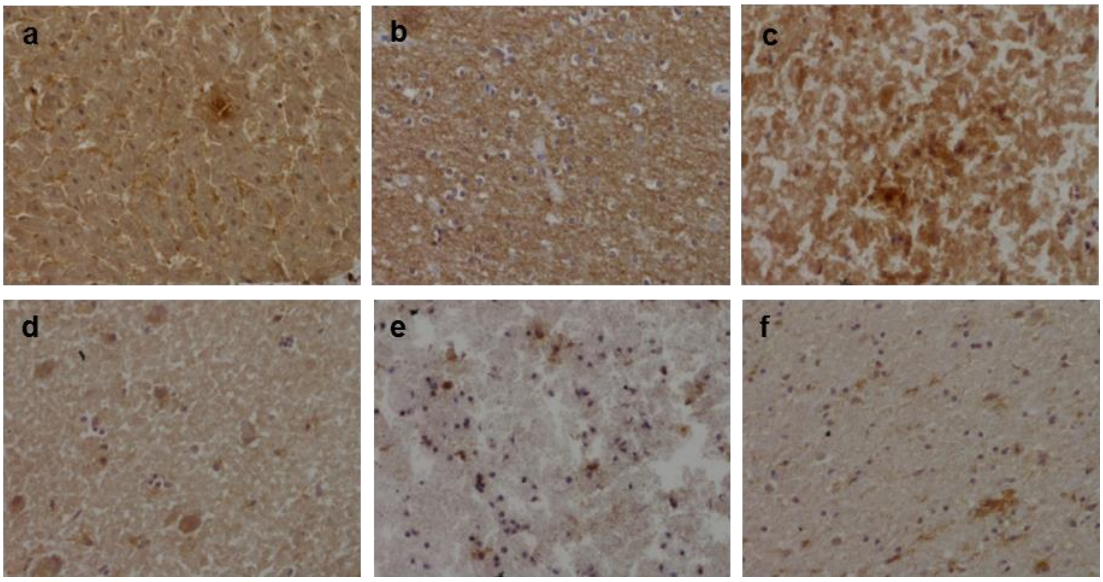

Figure 4.11: TREM2 antibody optimisation – Abcam (ab117645). Sections were tested under the following conditions: (a) Liver; (b) paraffin, grey matter; (c) frozen acetone, grey matter; (d) frozen PFA, grey matter; (e) frozen acetone, white matter; (f) frozen PFA, white matter. (b) 1:100 dilution, (a, c-f) 1:50 dilution. Images at 40x magnification.

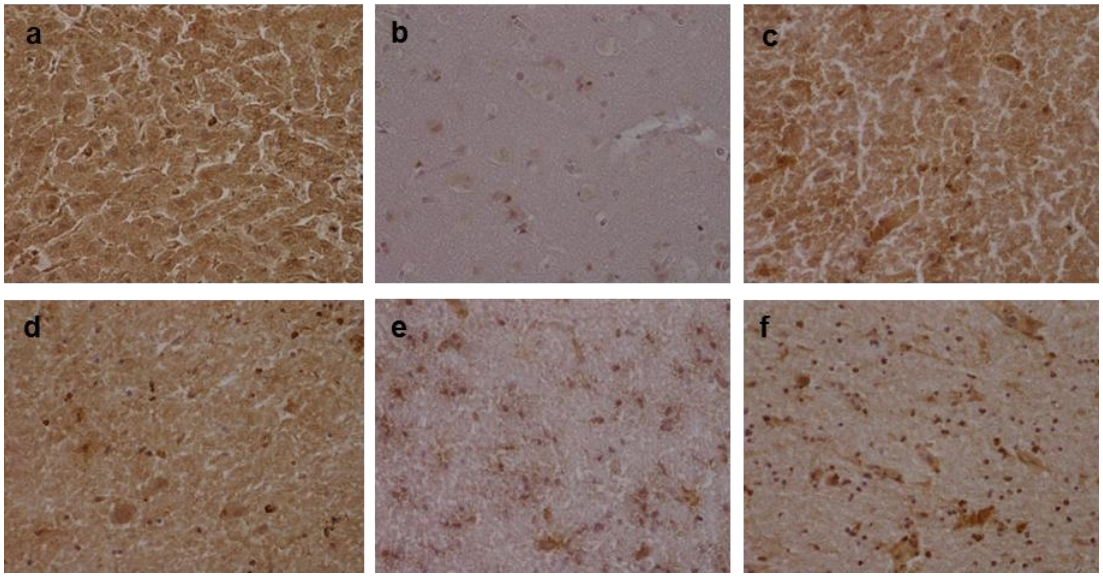

Figure 4.10: TREM2 antibody optimisation – Abgent (AP5469a). Sections were tested under the following conditions: (a) Liver; (b) paraffin, grey matter; (c) frozen acetone, grey matter; (d) frozen PFA, grey matter; (e) frozen acetone, white matter; (f) frozen PFA, white matter. (b) 1:200 dilution, (a, c-f) 1:50 dilution. Images at 40x magnification.

The Abgent antibody showed no clear staining in the liver section possibly indicating that the staining seen in the brain is non-specific (Figure 4.10a). The staining resembled neurons, however in the white matter it looked as if there was some glial nuclei staining (Figure 4.10). Better staining was seen in the frozen tissue with the acetone and PFA fixations giving different results.

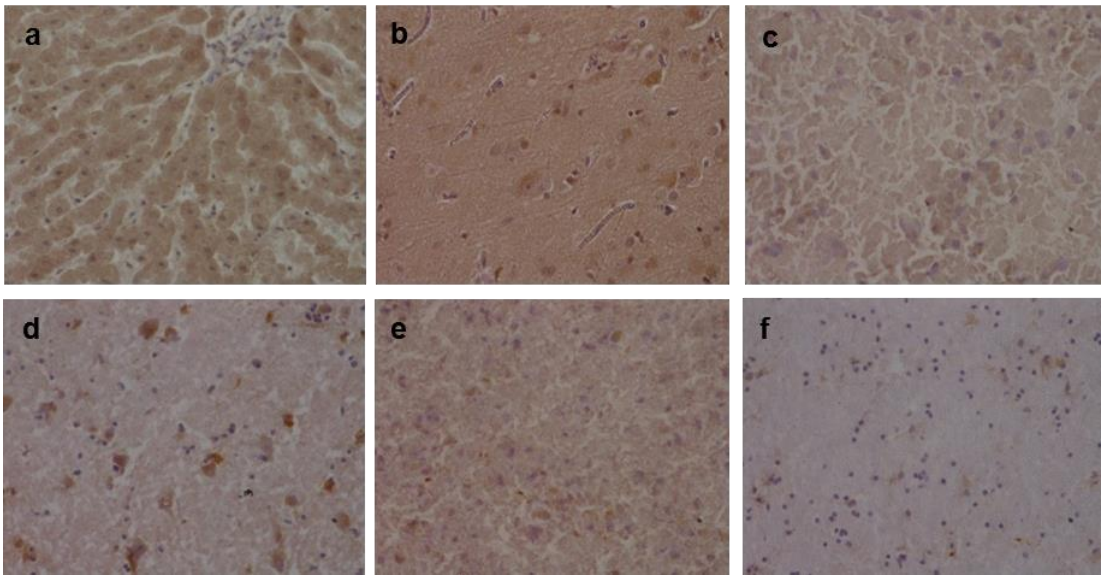

Figure 4.12: TREM2 antibody optimisation – SantaCruz (sc-373838). Sections were tested under the following conditions: (a) Liver; (b) paraffin, grey matter; (c) frozen acetone, grey matter; (d) frozen PFA, grey matter; (e) frozen acetone, white matter; (f) frozen PFA, white matter. All sections were stained with a 1:50 dilution. Images at 40x magnification.

The SantaCruz antibody showed staining that was neuronal in nature (Figure 4.12). Different pre-treatments did not work, with the PFA fixation in the frozen tissue white matter, the only image to show any real staining. Therefore, this antibody is not reliable.

The HPA010917 antibody showed no real staining in the liver section (Figure 4.14a). It had stronger staining in the white matter compared to the grey matter and very little staining was evident in the paraffin sections (Figure 4.14). In the PFA fixed frozen tissue, the staining resembled cellular processes, however, in the acetone fixed section the staining was more compact and perhaps would include the nuclei as well as some processes.

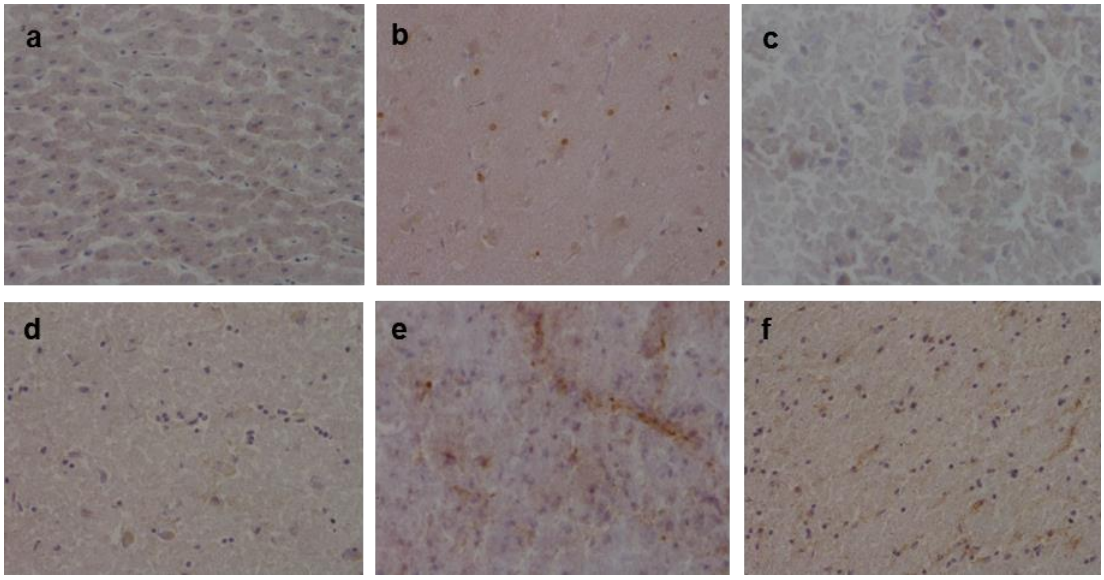

Figure 4.14: TREM2 antibody optimisation – HPA010917. Sections were tested under the following conditions: (a) Liver; (b) paraffin, grey matter; (c) frozen acetone, grey matter; (d) frozen PFA, grey matter; (e) frozen acetone, white matter; (f) frozen PFA, white matter. All sections were stained with a 1:100 dilution. Images at 40x magnification.

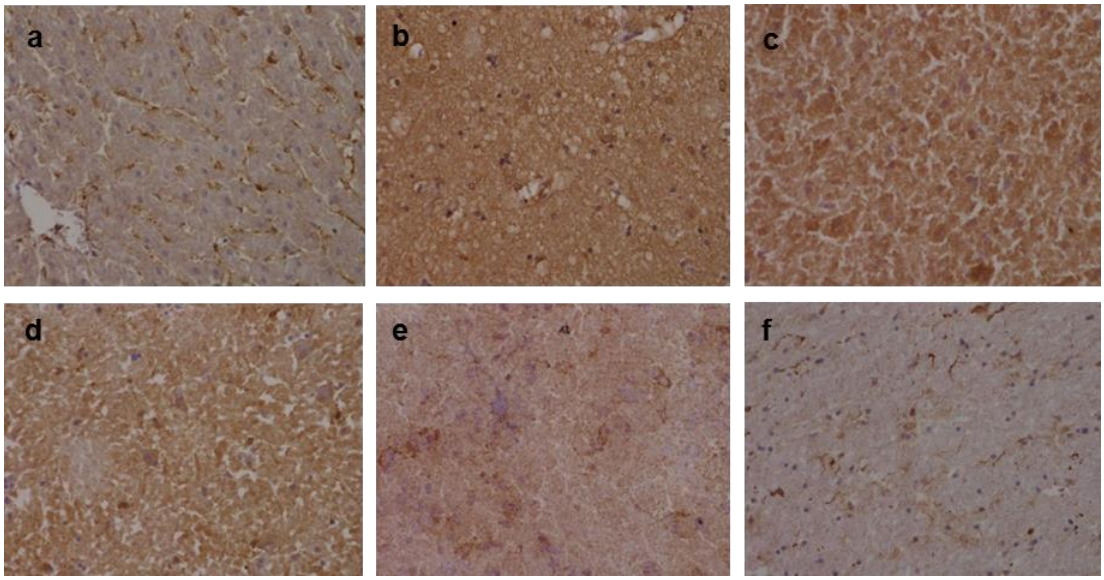

Figure 4.13: TREM2 antibody optimisation – HPA012571. Sections were tested under the following conditions: (a) Liver; (b) paraffin, grey matter; (c) frozen acetone, grey matter; (d) frozen PFA, grey matter; (e) frozen acetone, white matter; (f) frozen PFA, white matter. (b) 1:200 dilution, (a, c-f) 1:100 dilution. Images at 40x magnification.

Staining of the HPA012571 antibody showed more promising results. The liver control section showed staining that looked more specific to the Kupffer cells that we would expect to stain with TREM2 (Figure 4.13a). Paraffin sections had a large amount of background staining but no specific staining. However, in the frozen sections, staining that resembled

microglia was observed. The section that had been fixed in PFA looked to be the correct morphology (Figure 4.13).

The R&D antibody control liver section appears to show specific staining of the Kupffer cells (Figure 4.15a). Unlike with the other antibodies, the paraffin sections look to have staining that could be specific as do the frozen sections (Figure 4.15). However, some of the staining does look neuronal whereas other parts look similar to glial pathology. Some of the glial-looking staining looks to be potentially more of an astrocyte morphology than the microglial pathology.

The Proteintech antibody staining does not show any specific staining in the liver control section (Figure 4.16a). Conversely, in the brain tissue sections staining can be observed (Figure 4.16). Whether it is specific or not remains to be answered but the paraffin with pressure cooking treatment only and the frozen sections, both PFA and acetone fixed, would suggest that there could be. The morphology seen could be indicative of a more activated form of microglia.

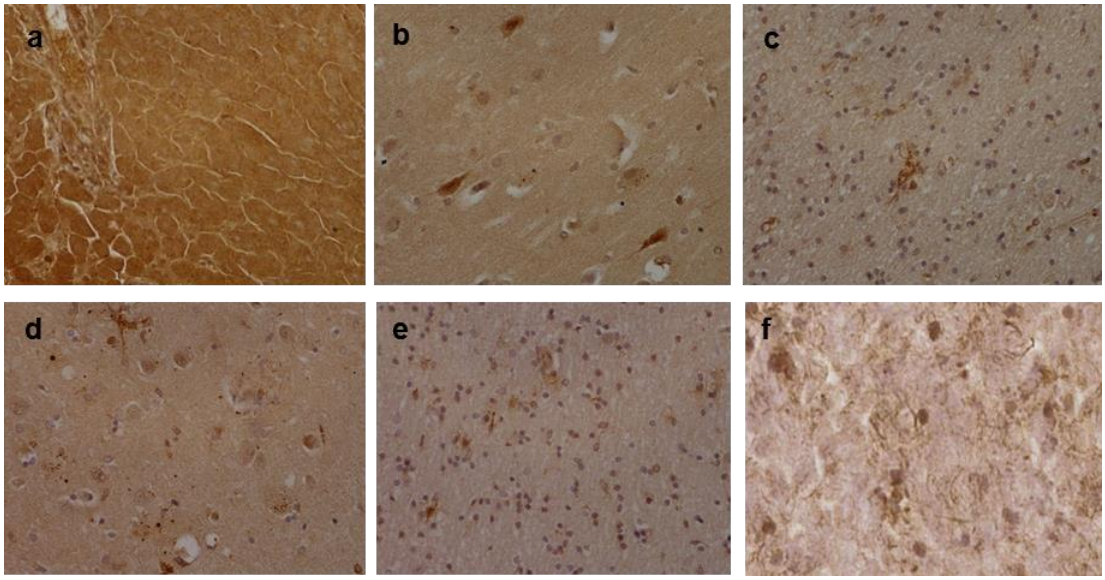

Figure 4.15: TREM2 antibody optimisation – R&D (AF1828). Sections were tested under the following conditions: (a) Liver, PC; (b) paraffin, grey matter, PC; (c) paraffin, white matter, PC; (d) paraffin, grey matter, PC+FA; (e) paraffin, white matter, PC+FA; (f) frozen PFA, white matter. All sections stained at 1:40 dilution. Images at 40x magnification. PC, pressure cooked in citrate buffer; FA, formic acid pretreatment.

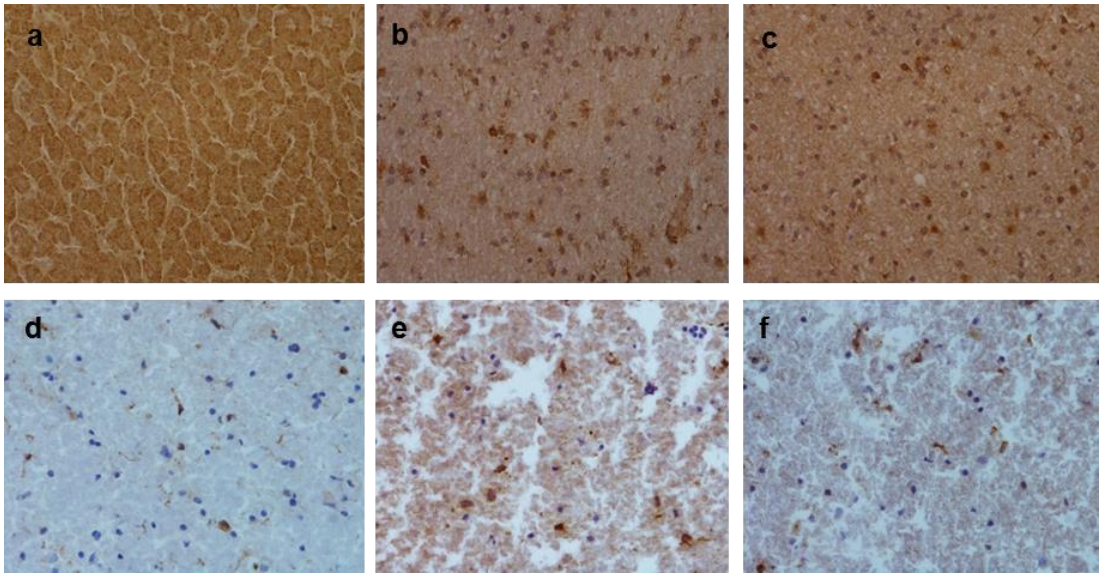

Figure 4.16: TREM2 antibody optimisation – Proteintech (13483-1-AP). Sections were tested under the following conditions: (a) Liver, PC; (b) paraffin, white matter, PC; (c) paraffin, white matter, PC+FA; (d) frozen PFA, white matter; (e, f) frozen acetone, white matter. (a-e) 1:100 dilution, (f) 1:200 dilution. Images at 40x magnification. PC, pressure cooked in citrate buffer; FA, formic acid pretreatment.

Antibody	Epitope length	Liver	Paraffin	Frozen PFA	Frozen acetone	Cell type
Abcam (Ab117645)	168	Y	N	Y	Y	Neuronal/glial
Abgent (AP5469a)	28	N	Y	Y	Y	Neuronal
SantaCruz (sc-373838)	160	N	N	N	Y	Neuronal
Sigma (HPA010917)	35	N	N	Y	Y	Glial
Sigma (HPA012571)	112	Y	N	Y	Y	Glial
R&D (AF1828)	155	Y	Y	Y	Y	Neuronal/glial
Proteintech (13483-1-AP)	200	N	Y	Y	Y	Glial

Table 4.3: Summary of TREM2 antibody optimisation

4.5 Discussion

4.5.1 Microglial phenotype in *TREM2* variant cases

In this study, the microglial phenotype of the *TREM2* variant AD cases was investigated using different microglial markers to assess load, shape and size of the microglia. The effect

of *APOE* genotype on the microglial phenotype was also investigated and seven TREM2 antibodies were analysed for their potential in staining microglial cells.

The microglial phenotype of the *TREM2* variant AD cases have an increased amoeboid morphology, suggesting that the microglia are activated in these cases to higher levels than other AD groups and controls. This is due to increased loads of CD68 across all regions tested, a general increase in circularity across microglial markers and a decrease in the perimeter of microglia, indicative of smaller amoeboid shaped microglial cells. Additionally, decreased P2RY12 levels in the temporal cortex are indicative of less ramified parenchymal microglia. CD68 is a lysosomal marker and is well established to be a marker of phagocytic microglia (Boche et al., 2013; Fadini et al., 2013; Holness and Simmons, 1993; Korzhevskii and Kirik, 2016; Shikuma et al., 2014; Smith et al., 2013; Zotova et al., 2011). The microglia in *TREM2* variant AD cases are more capable of phagocytosis as the microglia are more circular and have a smaller perimeter. TREM2 is thought to act through both loss and gain of function. Many *TREM2* deficient models have highlighted that deficiencies in TREM2 decrease the levels of phagocytosis and that overexpression of TREM2 can increase phagocytosis levels, this may suggest that *TREM2* variant models do not have a loss of function but instead a gain of function (Jay et al., 2015, 2017; Jiang et al., 2014, 2016b; Wang et al., 2015, 2016).

However, previous studies investigating the *R47H* or *D87N* variant have suggested that these *TREM2* variants are indeed loss of function mutations. It has been shown that the *R47H* variant alters the structure of the TREM2 protein so that it can no longer bind to anionic lipids or alternative ligands (Abduljaleel et al., 2014; Wang et al., 2015). *R47H* variants have also been shown to have an increased load of AD pathology, suggesting that clearance mechanisms may be inefficient or that Aβ is deposited at a quicker rate in these cases (Korvatska O et al., 2015; Roussos et al., 2015). However, our data show a higher number of activated microglia, indicating increased phagocytosis and therefore clearance of Aβ would be more efficient. Reasons for this could be due to the lack of cases that have been tested. Replication of this study in a wider sample cohort would determine if this is the case. Furthermore, other clinical features of AD such as seizures in individual cases could

affect the level of microglial activation and influence the results. Further clinic-pathological correlation on a case to case basis would need to be done to rule this out. If the *R47H* variant does have a loss of function, perhaps the variant causes the process of phagocytosis and clearance to slow down and become less efficient and as a compensatory mechanism, more microglia are recruited and activated into an amoeboid morphology to try and increase the clearance of Aβ. If this was the case, the pathology would increase as clearance slows down and disease would be exacerbated, putting the *TREM2* variant carriers at risk. *TREM2* deficiency would then have the same effect as there would be lower levels of phagocytosis in both cases.

Interestingly, the *TREM2* variant cases that were neurologically normal at time of death and did not have any underlying AD pathology, had a different phenotype to that observed in *TREM2* variant AD cases. Although not many changes were seen in the microglia size or shape in these cases, they did have a different level of abundance than the *TREM2* variant AD cases. They appear to have an opposite pattern of Iba1 load due to the fact that if *TREM2* variant AD cases had an increased load then the *TREM2* variant controls had a decreased load and vice versa throughout several regions. They also appear to have a more inactivated form of microglia, especially lacking antigen presenting cells (those represented by CR3-43 staining) and increased levels of P2RY12 microglia compared to *TREM2* variant AD cases. Therefore, having a *TREM2* variant can have varying effects in different people and there may be other factors involved in the TREM2 pathway that also need to be present for the variant to have a pathogenic effect and increase risk. At present, there are no published studies that look at carriers of the *TREM2* variants that did not develop AD. Further investigations into the differences might elucidate the role TREM2 is playing in disease.

Although different *APOE* genotypes showed no significance between varying microglial phenotypes, the *ApoE2/2* group appear to have a more inactivated phenotype with a decreased load, more ramified shape and a smaller perimeter when observing trend patterns. They also appear to have increased P2RY12 load, indicative of more homeostatic parenchymal microglia (Butovsky et al., 2013). *ApoE4/4* cases look to have a similar

microglial phenotype to that of the *TREM2* variant AD cases with increased CD68 load compared to other groups and are more amoeboid in shape. As the *ApoE4/4* is known as a risk factor in AD patients and *ApoE2/2* is thought to be protective, the fact they have different phenotypes may not be unexpected. However, as with the *TREM2* variant AD results, we see what should be a more activated phenotype typical of phagocytosis in the *ApoE4/4* cases suggesting there should be more clearance of Aβ in these cases. Microglial clearance could be enhanced in these cases but other clearance mechanisms could be impaired causing a cumulative effect that results in no difference. APOE has been shown to bind to LRP1 and also be involved in intramural periarterial drainage (IPAD) and could potentially be having an effect on this clearance system (Bu, 2009; Kim et al., 2009; Rebeck et al., 1995). It has been reported that *ApoE4* blocks the receptor mediated endocytosis employed by LRP1 which is part of a lipid transport pathway and therefore reduces the elimination of Aβ and causes increased Aβ in the vessel walls (Deane et al., 2008; Huynh et al., 2017).

It has previously been suggested that the *ApoE4* allele may cause its pathogenic effect through inflammatory mechanisms due to the fact that it does not protect against microglial activation as some of the other alleles do (Barger and Harmon, 1997; Gahtan and Overmier, 1999). Recently, Shi et al., (2017) found that in a P301S tau transgenic AD mouse model, *ApoE4* mice exhibit greater levels of neuroinflammation. This provides evidence that TREM2 and APOE are linked in their pathway and that the theory provided by Krasemann et al., (2017), which suggests *APOE* is upregulated which then triggers the TREM2 pathway, may be true.

As well as highlighting decreased levels of phagocytosis in *TREM2* deficient models, they also showed that in these models, an alternative method of inflammation and phagocytosis was used, through toll like receptors (Blander and Medzhitov, 2004; Frank et al., 2008; Guerreiro et al., 2013a; Jonsson et al., 2012b; Piccio et al., 2007; Takahashi et al., 2005). This method causes higher levels of toxic cytokines such as TNFα, nitric oxide synthase 2 and IL-1β. Therefore, it could be possible that in the *TREM2* variant models, microglia still become activated, perhaps through the APOE pathway. However, the classic phagocytic mechanism is reduced due to ineffective ligand binding, meaning that this alternative method

of phagocytosis is utilised, toxic cytokines are produced, which in turn cause a more toxic environment and causes disease to be exacerbated.

4.5.2 TREM2 antibody characterisation

There have been reports that show testing of TREM2 antibodies in formalin-fixed, paraffin-embedded tissue showed a small amount of staining observed with multiple antibodies (Satoh et al., 2013). This led to the question of whether TREM2 is widely expressed in the brain and if in fact it was more likely expressed on infiltrating peripheral macrophages or on monocytes rather than the resident microglia in the brain (Fahrenhold et al., 2017; Jay et al., 2015). Subsequently, direct RNA sequencing and qPCR analysis deciphering the similarities and differences in microglia and peripheral macrophages has taken place and confirmed that TREM2 is expressed only on microglia (Hickman et al., 2013).

The immunohistochemical staining carried out here shows a more comprehensive look at a larger range of antibodies. None of the TREM2 antibodies have previously been tested on frozen tissue and although the frozen tissue lacks morphology compared to paraffin embedded sections, the staining with the anti-TREM2 antibodies appeared more positive. In the case of some antibodies, Abcam, HPA010917, HPA012571, R&D and Proteintech, staining patterns resembled microglial processes. However, there still remains to be large variation in the staining between cases. This could be because the TREM2 protein level is only just detectable by the sensitivity of the immunohistochemical methods. Further development and validation of TREM2 antibodies needs to occur for this to be addressed. This would need to include characterisation using western blots, immunocytochemistry and testing with mutants to see if when TREM2 is absent the staining in abolished. Using frozen tissue for morphological studies is challenging, so ideally antibodies that could be used in paraffin should be developed.

4.5.3 Conclusions

In summary, *TREM2* variant cases have a different microglial profile to those in SAD or FAD cases. *TREM2* variant AD cases have more activated microglia, that should lead to more phagocytosis and increased clearance but previous literature suggests this is not the case. A

complicated inflammatory cascade is occurring in these cases which can cause these *TREM2* variant cases to be at risk of AD. The reason this is a risk and not inevitable though, is due to other factors that stops or slows some of these cases getting AD and alters their microglial phenotype. One of these factors could be *APOE* genotype, because as indicated previously, TREM2 and APOE act along the same pathway and TREM2 variant AD cases all have an ApoE4 allele. Better TREM2 antibodies will enable us to look at the distribution of TREM2 and help to elucidate what is occurring in these *TREM2* variant cases and therefore what role TREM2 plays in the pathogenesis of SAD or FAD.

Chapter 5

The genetic and proteomic profiles of *TREM2* variant cases

5 The genetic and proteomic profiles of *TREM2* variant cases

5.1. Abstract

Introduction: Neuroinflammation has long been known to play a role in AD. However, the findings that several genes associated with inflammation were identified as hits in AD GWAS studies brought closer attention to neuroinflammatory mechanisms in AD. The finding that *TREM2* was a genetic risk factor for late onset AD with a similar odds ratio to *APOE4* gave further insight that neuroinflammation may be important. TREM2 is expressed on microglia and microglia play a large role in the inflammatory cascades in the brain. Previous genetic and proteomic studies had identified the immune response to be an altered pathway, but whether it was a cause of the disease or consequence was still to be determined. Here the genetic profile of neuroinflammation in *TREM2* variant cases compared to SAD, FAD and normal controls was investigated and then compared to the protein expression in the same cases.

Materials and methods: Frontal cortex was taken from SAD (n=10), FAD *PSEN1* (n=7), FAD *APP* (n=3), *TREM2* variant SAD (n=3), *TREM2* variant FAD (n=1), *TREM2* variant controls (n=2) and normal controls (n=6). RNA was extracted using the Qiagen RNeasy kit and samples were sent for Nanostring nCounter analysis using the Human Inflammation panel consisting of 256 genes and an added 30 specific neurodegenerative genes. Data was analysed with nSolver software and fold changes compared to controls were calculated. Secondly, the protein was extracted, trypsin digested and analysed using 2D nanoUPLC coupled to a QTOF mass spectrometer (Synapt G2 Si). Proteins were quantitated and identified using label free proteomics (MSe). Data was processed using Progenesis software and fold-changes compared to controls were calculated. Both sets of data were analysed using Ingenuity Pathway Analysis software to determine the canonical pathways and disease functions highly represented in the datasets.

Results: The neuroinflammatory signalling pathway was found to be altered in all AD subgroups with *TREM2* variant SAD cases displaying greater levels of upregulation in genes involved than SAD cases. *TREM2* variant controls however, showed large levels of downregulation in this pathway. Genes involved in the TLR response were increased in the *TREM2* variant SAD cases. The top pathways changing in the proteomic data were involved with cell proliferation, cytoskeletal organisation and amyloid processing. Proteins involved with neurodegeneration were upregulated at the highest levels in the *TREM2* variant AD cases. *APOE* protein levels differed by 6-fold between *TREM2* variant SAD and *TREM2* variant controls.

Conclusions: Many genes, proteins and pathways are changing throughout the duration of AD. Some pathways such as cell proliferation and cytoskeletal organisation appear to be affected no matter which AD subtype is present. However, neuroinflammation differs between subtypes, with the *TREM2* variants displaying the greatest differences. As *TREM2* variant SAD and *TREM2* variant controls have such contrasting profiles, another factor must be needed in order for AD to take place. The lack of an *ApoE4* allele in the *TREM2* variant controls and the presence of one in the *TREM2* variant SAD cases, indicate that *APOE* genotype could be this factor or have its own independent effects. *APOE* and *TREM2* both affect the TLR pathway leading to increased pro-inflammatory cytokine release and increased cell death. Further investigation into these pathways and mechanisms may help elucidate the reasons that TREM2 variants confer a risk to AD.

5.2. Introduction

5.2.1. Inflammation in AD

Inflammation has been shown previously to be involved in the pathogenesis of AD. However, it was brought to closer attention when a number of GWAS studies identified several inflammatory genes as GWAS hits for AD, indicating that the inflammatory pathway may play a prominent role in AD pathogenesis. These hits included *TREM2, HLA-DR, INPP5D, MEF2C, CR1* and *CLU* (Zhang et al., 2015).

Inflammation in AD has been studied extensively to assess the role that it plays. As both pro-inflammatory and anti-inflammatory pathways have been shown to be present in AD brains, deciphering what is occurring as a cause of AD and what is occurring simply as an effect of disease is a complex matter and makes the study of inflammation a challenging one.

Cytokines such as Il-1, Il-6 and TNF-α have been shown to be involved with Aβ deposition via the processing of APP (Akiyama et al., 2000; Buxbaum et al., 1992; Dickson et al., 1993; Eikelenboom and Gool, 2004; Goldgaber et al., 1989; Griffin et al., 1989; Huell et al., 1995; Vandenabeele and Fiers, 1991). There is also evidence that C1q from the complement pathway can aid fibril formation through binding of several Aβ molecules in close proximity to each other, therefore promoting fibrillisation (Akiyama et al., 2000; Webster and Rogers, 1996; Webster et al., 1994, 1995). However, as these pro-inflammatory cytokines are shown to be released and the complement pathway activated upon Aβ fibrillisation, a cycle of inflammation and Aβ deposition ensue.

Microglia are thought to be the specialised macrophages of the CNS. It was therefore hypothesised that their main role in AD would be involving inflammation. The activation of microglia has been shown to occur as one of the earliest changes in AD and numbers of activated microglia correlate with disease severity using clinicopathological correlations and different model systems to show when microglial pathology appears in line to amyloid plaque deposition (Arends et al., 2000; Gentleman, 2013; Giulian, 1999; Martin et al., 1994; Mattiace et al., 1990b; Paresce et al., 1997; Rogers et al., 1988; Wegiel and Wisniewski, 1990; Wisniewski et al., 1989).

Microglia produce the cytokines Il-1, Il-6 and TNF-α and are shown to cluster around neuritic amyloid plaques (Dickson et al., 1993; Eikelenboom and Gool, 2004; Griffin et al., 1989; Huell et al., 1995). However, activated microglia do not cluster around diffuse amyloid plaques, suggesting that through release of these cytokines, Aβ fibrillisation into neuritic or dense core plaques occurs (Arends et al., 2000; Giulian, 1999; Mattiace et al., 1990a; Paresce et al., 1997; Rogers et al., 1988; Wegiel and Wisniewski, 1990; Wisniewski et al., 1989). One study observed that although the cerebellum is affected by AD pathology, no cerebellar functions are typically clinically impaired in AD. They linked that the cerebellum

has predominantly diffuse plaques rather than neuritic plaques and suggested that inflammation is needed, in the form of microglial clustering around the plaques, for neuritic plaque formation to occur, initiating a cascade of pro-inflammatory mediators leading to neurodegeneration that results in clinical symptoms (Eikelenboom et al., 1998; Joachim et al., 1989). Alternatively, the plaques may not have time to mature into neuritic plaques due to the cerebellum being the last Thal phase region to accumulate Aβ plaques.

In addition to cytokines, various other inflammatory mediators have been identified in Aβ plaques, such as other cytokines, chemokines, a range of complement factors and many acute phase proteins (Akiyama et al., 2000; Eikelenboom and Gool, 2004). Aβ is thought to act similarly to bacteria and elicit a strong pro-inflammatory response via these molecules, leading to the production of reactive oxygen species, synaptic loss and neurotoxicity. Activating and recruiting more microglia to the amyloid plaques (Akiyama et al., 2000; Eikelenboom and Gool, 2004; Eikelenboom et al., 1998).

Not all microglia have a pro-inflammatory role, many have anti-inflammatory properties. As the cascade of pro-inflammatory mediators occurs, anti-inflammatory cascades are triggered which initially mediate the clearance of Aβ and any neuronal debris (Akiyama et al., 2000). This is completed through phagocytic mechanisms in which the Aβ binds to receptors on the microglial cells, thereby transforming the cells into a phagocytic phenotype. It is hypothesised that this clearance becomes less efficient as the disease progresses, with microglia no longer being able to degrade the Aβ at an efficient rate (Paresce et al., 1997).

Microglia have roles both in forming and clearing amyloid plaques, indicating that the inflammation in AD can be both causative as well as an effect. Familial AD cases have mutations in the *APP, PSEN1* or *PSEN2* genes which effect APP processing and this is known to cause AD. However, in late onset sporadic AD, the cause of disease is unknown with multiple risk factors being discovered. The major risk factor for sporadic AD is age and microglia have been shown to become primed as we age (Hoeijmakers et al., 2016; Lane et al., 2017). This means that they require fewer stimuli in order to elicit an inflammatory response. Holtman et al., (2015) showed that primed microglia have an over-representation of genes involved with phagosomes, lysosomes, antigen presentation and AD signalling. It is

hypothesised that these primed microglia are stimulated easily and through APP processing and plaque formation, microglia help to initiate the pathogenesis of AD using inflammatory cascades (Perry and Holmes, 2014).

Multiple studies have looked at the gene expression and proteomic expression profiles in AD. Genetic expression studies using whole homogenate brain samples with microarray data or RNA sequencing data highlight pathways involved in: NF-κB signalling, complement and integrin, NADPH oxidase complex, phagocytic processes, IFN-γ –related pathways, metabolism, protein ubiquitination, vasculature development, synaptic signalling, synaptic transmission, synaptic plasticity, protein biosynthesis, protein trafficking, protein turnover and mitochondrial energy generation (Berchtold et al., 2014; Bossers et al., 2010; Chen et al., 2013; Holtman et al., 2015).

Other studies have isolated the microglia or astrocytes in AD and these studies revealed that pathways involved in immune response were unsurprisingly highlighted. Astrocytes showed decreased expression in genes involved with neuronal support and neuronal communication, whereas microglia showed decreased expression in genes involved with phagocytosis and endocytosis (Orre et al., 2014; Sekar et al., 2015). Furthermore, gene expression studies showed differences between different models of AD. Cells overexpressing APP highlighted changes in pathways in cell cycle, cell proliferation and p53 signalling (Wu et al., 2016). Transcriptomics on 5xFAD Tg AD mice showed complement and integrin overexpression, NADPH oxidase complex, phagocytic processes and IFN-γ related pathways (Landel et al., 2014). Similarly, gene expression in the rTg4S10 mouse model overexpressing mutant human tau highlighted predominantly inflammatory processes and alterations in neuronal network activity (Wes et al., 2014). Overall, there is a large range of processes or pathways that seem to be changing at the genetic level in AD, although numerous pathways involved in inflammation are present.

Proteomic studies also show similar pathways to be involved in different data sets in AD. Post-mortem brain proteomic studies have highlighted pathways involved in ubiquitin signalling and the ubiquitin proteasome system, energy metabolism, glycolysis, oxidative stress, apoptosis, signal transduction and synaptic functioning (Gentier and van Leeuwen,

2015; Musunuri et al., 2014). When senile plaques were isolated proteins involved with neuronal transport and cytoskeletal components were present in the plaques (Liao et al., 2004). Similarly, a study looking at the proteomics of LAN5 neuroblastoma cells that had been incubated with Aβ42 revealed changes in cytoskeletal dynamics, ribosomal biogenesis and spliceosome dysregulation, indicating that the many pathways that are changing in AD, may not all be related to the amyloid plaque pathology (Nuzzo et al., 2017). Proteomics in the AβPPswe/PS1dE9 mice additionally had genes changing that were involved in cytoskeletal structure, energy metabolism, synaptic components and protein degradation, much in line with what was observed in the human brain (Fu et al., 2015). Matarin et al., (2015) provided a comprehensive study using a microarray to study gene expression in several transgenic AD mouse models that had either mutant human *APP, PSEN1, APP/PSEN1* or mutant tau and compared these to wildtype mice. They found that in mice producing Aβ plaques the immune response correlated with plaque load, whereas the older mice that produced neurofibrillary tangles showed an increased immune response but additionally had decreased gene expression associated with synaptic function (Matarin et al., 2015).

The pathways that are found in genetic expression studies do not always correlate with protein expression data, thus making it hard to determine the real changes that are occurring to cause AD pathogenesis. As the immune system is adaptive and constantly changing to match its environment, it is difficult to predict changes that occur with genetic expression data. Although many studies have investigated either the genetic expression or the proteomic expression, limited studies have investigated both together to compare the differences at the transcriptional level to the translational level. In the cases where multi-omics has been performed, it has been proven to highlight novel network biology data that can be utilised to find biomarkers. A combination of transcriptomics and proteomics revealed the MAPK/ERK was reduced in AD and that the clathrin-mediated receptor endocytosis pathway was increased (Hallock and Thomas, 2012; Santiago et al., 2017). Similarly, there are limited sets of data that have compared the genetic or proteomic expression profiles of different AD groups directly to each other. Berchtold et al., (2014) compared MCI to AD samples and Conejero-Goldberg et al., (2011) identified differences in gene expression

based on *APOE* genotypes. However, there hasn't been a comprehensive comparison of gene or protein expression between SAD and FAD, other than multiple studies being discussed in a review (Lista et al., 2015).

5.2.2. Inflammation and TREM2

TREM2 was identified by GWAS studies as a hit for AD and subsequently was identified as a genetic risk factor for late onset AD with a similar odds ratio to *ApoE4* (Guerreiro et al., 2013a; Jonsson et al., 2012b). TREM2 is expressed on microglia and is known to have its own role in inflammatory processes. It was therefore of interest to examine whether the risk associated with *TREM2* variants was due to an altered inflammatory profile.

TREM2 was found to be a regulator of phagocytosis and therefore has a role in the clearance of Aβ. *TREM2* deficiency models showed reduced phagocytosis compared to wildtype (Jay et al., 2015; Jones et al., 2014; Kleinberger et al., 2014; Satoh et al., 2013; Ulrich and Holtzman, 2016; Wang et al., 2015; Zhao and Lukiw, 2013). It is therefore hypothesised that *TREM2* heterozygous variants that have the increased risk of AD, have a loss of function and are less able to clear the Aβ. *R47H* variants have reduced levels of ligand binding which is thought to stop the signalling cascade TREM2 performs once bound via its signalling partner, TYROBP, to occur (Abduljaleel et al., 2014; Wang et al., 2015).

The normal signalling cascade stimulates the microglial cell to go into an anti-inflammatory phagocytic phenotype, with minimal pro-inflammatory cytokines being produced (Blander and Medzhitov, 2004; Frank et al., 2008; Guerreiro et al., 2013a; Jonsson et al., 2012b; Takahashi et al., 2005). Reduced TREM2 expression has been shown to cause increased TLR activity (Yaghmoor et al., 2014). Furthermore, when TREM2 phagocytic mechanisms do not occur, an alternative method of phagocytosis via the TLRs can be initiated which in turn leads to increased pro-inflammatory mediators being released (Frank et al., 2008; Guerreiro et al., 2013a; Jonsson et al., 2012b; Piccio et al., 2007; Takahashi et al., 2005). This may indicate that although clearance is occurring, further Aβ deposition and neuronal death is being stimulated. Therefore, it is plausible that *TREM2* variants that have a loss of function

and can no longer signal via normal mechanisms, would use this alternative pathway, have reduced clearance of Aβ and a higher risk of AD.

An alternative theory to this is that microglia form a barrier around the Aβ plaques, encapsulating them, preventing them from causing any damage and that any uncovered parts are what cause neuronal toxicity (Yuan et al., 2016). One mechanism that this is thought to work is that TREM2 binds to APOE which in turn is part of the plaque. Through this interaction a pathway is activated which recruits microglia and forms a barrier. This barrier in *TREM2* deficient models is markedly reduced, leading to the thoughts that more Aβ plaque is uncovered in the variants, meaning further toxicity and a higher risk of AD occurring (Condello et al., 2017; Jay et al., 2015; Ulrich et al., 2014; Wang et al., 2015; Yuan et al., 2016).

There hasn't yet been any evidence to show differing propensities for different *APOE* alleles to bind to TREM2 with different affinities but a study that looked at the transcriptomics of *ApoE3* compared to *ApoE4* identified the pathways responsible for mitochondrial function, calcium regulation and cell cycle re-entry to differ between the two groups (Condello et al., 2017; Conejero-Goldberg et al., 2011). This could indicate that different mechanisms and pathways are activated or upregulated according to the *APOE* genotype present.

5.2.3. Aims

In this chapter, the genetic and proteomic expression profiles are compared between SAD, FAD and *TREM2* variant cases compared to controls. To identify any differences occurring in the inflammatory mechanisms, nanostring technology was used to assess 256 inflammatory genes and 30 AD specific markers between disease groups. This was then compared to label-free mass spectrometry proteomic data to determine if the same changes were observed at protein level. A direct comparison between all three groups and across two platforms has not been performed before so allows us to take an in-depth look at the mechanisms that are involved in each disease subgroup.

5.3. Materials and Methods

5.3.1. Case selection

All case demographics are detailed in Table 2.3. For nanostring analysis, the following cases were used for each group: SAD (cases 7, 9-15, 17-18); FAD (cases 26, 29-35); *TREM2* variant SAD (cases 1, 2, 5); *TREM2* variant FAD (case 6); *TREM2* variant control (cases 3-4); and controls (cases 37-42). Label-free mass spectrometry analysis cases were pooled into groups before running on the mass spectrometer. Two pools for each disease group were created where enough cases were available; otherwise only one pool was used. The cases used in each pool are outlined for each group: SAD (pool 1, cases 7,8 and 14; pool 2, cases 9, 12, 15, 17); FAD *PSEN1* (pool 1, 27, 33-34; pool 2, 26, 29, 32); FAD *APP* (pool 1, 30-31, 35); *TREM2* variant SAD (pool 1, cases 1, 2, 5); *TREM2* variant FAD (pool 1, case 6), *TREM2* variant control (pool 1, cases 3-4); and Controls (pool 1, cases 37-39; pool 2, cases 40-42).

5.3.2. Nanostring

RNA from chipped frontal cortex of cases stated above were extracted as per protocols described in 2.6.1 (SAD (n=10), FAD (n=8), *TREM2* SAD (n=3), *TREM2* FAD (n=1), *TREM2* control (n=2) and controls (n=6)). RNA was evaluated for quality using an Eppendorf spectrometer and only accepted if A260/A280 value was >1.8 and A260/A230 value was >1.5. Samples were diluted to 50ng/µl and analysed by Nanostring Technologies, Seattle. Full protocol details can be found in 0. Data was analysed using nSolver software provided by Nanostring Technologies. Fold changes compared to controls were calculated for each AD subgroup.

5.3.3. Proteomics

To assess the protein expression in the samples, proteins were extracted from the frontal cortex from each case (SAD (n=7), FAD *PSEN1* (n=8), FAD *APP* (n=3), *TREM2* SAD (n=3), *TREM2* FAD (n=6), *TREM2* controls (n=2), controls (n=6)) pooled, digested, and analysed using a Synapt G2-Si High Definition mass spectrometer using 2D fractionation to perform

quantitative label-free mass spectrometry. These methods are described in detail in 2.7.2, 2.7.3, 2.7.4, 2.7.5. Raw data was processed using Progenesis software, normalised and fold-change was calculated compared to controls for each AD subgroup.

5.3.4. Bioinformatics

Ingenuity Pathway Analysis (IPA) software was utilised to analyse the pathways and functions represented in both datasets. A comparison analysis for each dataset to compare AD subgroups was undertaken and a comparison for each subgroup across the different methods was done to assess the differences between genetic and proteomic profiles in these cases. Pathways and functions were predicted to be activated if they had a positive z-score and were coloured orange. They were predicted to be inhibited if they had a negative z-score and were coloured blue. Red genes represent genes upregulated in the datasets and green genes represent downregulated. Further details about the IPA software can be found in 2.8. To assess the level of overlap between over-represented biological processes in the datasets, Webgestalt was used to identify the GO terms and GOview was used to determine those that overlapped.

Nanostring (p<0.05)	SAD	FAD	*TREM2* FAD	*TREM2* SAD	*TREM2* Control
Upregulated	124	91	33	22	10
Downregulated	2	2	0	0	15

Table 5.1: Number of significantly changing genes in nanostring dataset. The number of genes that were changing with a p value <0.05 are indicated for each disease group and split into those that were upregulated or downregulated compared to controls.

5.4. Results

5.4.1. Genetic expression in *TREM2* variant cases

The full set of 286 genes both from NanoString Technologies Human Inflammation panel and 30 targeted genes more specific to AD were successfully processed and analysed. A full table of results are available in the Appendix Table 3, showing the average counts, ratios and p-values for all genes.

A total of 124 genes were upregulated significantly in SAD cases compared to controls at a significance level of p<0.05, of which 70 genes at p<0.01 and 24 genes at p<0.001 (Table

5.1, Table 5.2). Two genes were downregulated significantly in SAD, *MRC1* (macrophage mannose receptor 1) and *SNCA* (alpha-synuclein) ($p<0.05$). 91 genes were significantly upregulated in FAD cases compared to controls at level of $p<0.05$, 22 genes at $p<0.01$ and 2 genes, *NFKB1* (nuclear factor NF-kappa-B p105 subunit) and *TGFB2* (transforming growth factor beta-2) at $p<0.001$ (Table 5.1, Table 5.3). Two genes were downregulated significantly in FAD cases compared to controls, *PIK3C2G* (Phosphatidylinositol 4-phosphate 3-kinase C2 domain-containing subunit gamma) and *SNCA* ($p<0.05$). 22 genes were upregulated significantly in *TREM2* variant SAD cases compared to healthy controls at a level of $p<0.05$ (Table 5.1,Table 5.4). 11 genes were upregulated significantly and 14 genes were downregulated in *TREM2* variant controls to healthy controls ($p<0.05$). 33 genes were upregulated in the *TREM2* FAD variant compared to healthy controls ($p<0.05$).

Several genes show significantly altered expression in only one group (Table 5.5). For example, genes such as *APOE* (apolipoprotein E) and *PEN2* (Gamma-secretase subunit PEN-2), were only significantly upregulated in SAD compared to control but were not significant in any other groups. Similarly, *CD68* (Macrosialin), *IL6R* (Interleukin-6 receptor subunit alpha) and *TYROBP* (TYRO protein tyrosine kinase-binding protein) were only significantly up regulated in FAD compared to control. *TREM2* variant cases were the only group to have a significant upregulation of *GRB2* (Growth factor receptor-bound protein 2).

On the other hand, there were several genes that were significantly altered across all groups Table 5.6). These genes that demonstrated a more than 2-fold change in expression compared to controls across all three groups included *HSPB2* (Heat shock protein beta-2), *TGFB1* (Transforming growth factor beta-1), *CSF1* (Macrophage colony-stimulating factor 1) and *CXCR4* (C-X-C chemokine receptor type 4).

Investigating the data using Ingenuity Pathway Analysis software, the top-scoring pathway was the neuroinflammatory signalling pathway. This was expected as the neuroinflammation panel was used. However, the pathway was predicted to be activated in SAD, FAD, *TREM2* variant SAD and *TREM2* variant FAD but it was predicted to be inhibited in the *TREM2* variant controls when all cases were compared to controls (Figure 5.1). Figure 5.2 shows a diagram of this pathway and visualises the differences in gene expression across the

Gene symbol	Gene Name	Fold change compared to control	p-value
CCL2	C-C motif chemokine 2	3.53	0.0478
IRF7	Interferon regulatory factor 7	3.26	0.0141
MRC1	Macrophage mannose receptor 1	-3.08	0.0197
MYL2	Myosin regulatory light chain 2, ventricular/cardiac muscle isoform	2.88	0.0051
IRF1	Interferon regulatory factor 1	2.78	0.0292
TGFB3	Transforming growth factor beta-3	2.77	0.0014
HSPB1	Heat shock protein beta-1	2.68	0.0044
NOX4	NADPH oxidase 4	2.58	0.0223
TNF	Tumor necrosis factor	2.57	0.004
HSPB2	Heat shock protein beta-2	2.51	0.0008
C4A	Complement C4-A	2.47	0.0358
TGFB1	Transforming growth factor beta-1	2.46	0.0024
CSF1	Macrophage colony-stimulating factor 1	2.35	0.0053
CXCR4	C-X-C chemokine receptor type 4	2.29	0.0307
TNFSF14	Tumor necrosis factor ligand superfamily member 14	2.27	0.0117
TSPO	Translocator protein	2.20	0.0465
PTGDR2	Prostaglandin D2 receptor 2	2.04	0.053
TREM2	Triggering receptor expressed on myeloid cells 2	2.03	0.0139
GFAP	Glial fibrillary acidic protein	1.99	0.0132
ELK1	ETS domain-containing protein Elk-1	1.98	0.0128
OAS2	2'-5'-oligoadenylate synthase 2	1.96	0.0079
IL23R	Interleukin-23 receptor	1.96	0.0395
MAPKAPK 2	MAP kinase-activated protein kinase 2	1.95	0.0019
RELA	Transcription factor p65	1.95	0.0024
CCL22	C-C motif chemokine 22	1.89	0.0121
BCL6	B-cell lymphoma 6 protein	1.85	0.0226
IL10	Interleukin-10	1.83	0.0225
TRADD	Tumor necrosis factor receptor type 1-associated DEATH domain protein	1.80	0.0376
CCL20	C-C motif chemokine 20	1.79	0.004
CD40LG	CD40 ligand	1.78	0.0015

Table 5.2: Top 30 genes significantly changing in expression in SAD compared to control. Top 30 decided on greatest fold change of expression with a significance of $p<0.05$. (-) represents downregulated compared to control.

Gene symbol	Gene Name	Fold change compared to control	p-value
CXCR2	C-X-C chemokine receptor type 2	9.22	0.015
HSPB1	Heat shock protein beta-1	5.74	0.0041
CCL2	C-C motif chemokine 2	4.82	0.0288
MAFF	Transcription factor MafF	4.38	0.0059
TLR8	Toll-like receptor 8	4.32	0.0403
NOX4	NADPH oxidase 4	3.44	0.0269
IRF1	Interferon regulatory factor 1	3.43	0.018
PTGER4	Prostaglandin E2 receptor EP4 subtype	3.23	0.0313
FOS	Proto-oncogene c-Fos	3.17	0.0536
IL1R1	Interleukin-1 receptor type 1	3.06	0.026
IL10	Interleukin-10	3.05	0.0387
TGFB1	Transforming growth factor beta-1	2.88	0.0141
CSF1	Macrophage colony-stimulating factor 1	2.87	0.0123
MASP1	Mannan-binding lectin serine protease 1	2.81	0.0363
IL12A	Interleukin-12 subunit alpha	2.72	0.0176
HSPB2	Heat shock protein beta-2	2.69	0.009
CXCR4	C-X-C chemokine receptor type 4	2.62	0.0442
BCL6	B-cell lymphoma 6 protein	2.52	0.0096
MAPKAPK2	MAP kinase-activated protein kinase 2	2.43	0.0054
GFAP	Glial fibrillary acidic protein	2.34	0.0119
C4A	Complement C4-A	2.32	0.0477
MYD88	Myeloid differentiation primary response protein MyD88	2.29	0.021
CEBPB	CCAAT/enhancer-binding protein beta	2.27	0.0122
SHC1	SHC-transforming protein 1	2.22	0.0073
TGFB2	Transforming growth factor beta-2	2.20	0.0004
TREM2	Triggering receptor expressed on myeloid cells 2	2.16	0.0081
RELA	Transcription factor p65	2.12	0.0023
CCL8	C-C motif chemokine 8	2.09	0.0474
DDIT3	DNA damage-inducible transcript 3 protein	2.06	0.0085
NFE2L2	Nuclear factor erythroid 2-related factor 2	2.03	0.0014

Table 5.3: Top 30 genes significantly changing in expression in FAD compared to control. Top 30 decided on greatest fold change of expression with a significance of $p<0.05$. (-) represents downregulated compared to control.

Gene symbol	Gene Name	Fold change compared to control	p-value
KLK6	Kallikrein-6	3.26	0.0496
MASP2	Mannan-binding lectin serine protease 2	3.01	0.017
CSF1	Macrophage colony-stimulating factor 1	2.73	0.0213
TGFB1	Transforming growth factor beta-1	2.67	0.041
TNFSF14	Tumor necrosis factor ligand superfamily member 14	2.62	0.0145
HSPB2	Heat shock protein beta-2	2.55	0.0129
TSPO	Translocator protein	2.42	0.0543
RELA	Transcription factor p65	2.39	0.0059
MAPKAPK2	MAP kinase-activated protein kinase 2	2.34	0.0223
CXCR4	C-X-C chemokine receptor type 4	2.28	0.0419
TGFB3	Transforming growth factor beta-3	2.13	0.0317
BCL6	B-cell lymphoma 6 protein	2.03	0.0542
NFKB1	Nuclear factor NF-kappa-B p105 subunit	2.02	0.0156
IL17A	Interleukin-17A	1.98	0.0388
C6	Complement component C6	1.94	0.0205
KEAP1	Kelch-like ECH-associated protein 1	1.84	0.0173
STAT3	Signal transducer and activator of transcription 3	1.79	0.0501
RHOA	Transforming protein RhoA	1.78	0.0029
TRADD	Tumor necrosis factor receptor type 1-associated DEATH domain protein	1.78	0.0411
MAFK	Transcription factor MafK	1.74	0.0537
NFE2L2	Nuclear factor erythroid 2-related factor 2	1.70	0.0135
CTSD	Cathepsin D	1.70	0.0162
IRF3	Interferon regulatory factor 3	1.69	0.018
IL12B	Interleukin-12 subunit beta	1.69	0.0549
HDAC4	Histone deacetylase 4	1.68	0.0308
DAXX	Death domain-associated protein 6	1.67	0.0147
CCL20	C-C motif chemokine 20	1.67	0.0272
SMAD7	Mothers against decapentaplegic homolog 7	1.66	0.0214
P2RX7	P2X purinoceptor 7	1.64	0.0072
CD55	Complement decay-accelerating factor	1.64	0.0089

Table 5.4: Top 30 genes significantly changing in expression in *TREM2* variant cases compared to controls. Top 30 decided on greatest fold change of expression with a significance of $p<0.05$. (-) represents downregulated compared to control.

Gene symbol	Gene Name	Fold change compared to control	p-value
Only significantly changing in SAD			
IRF7	Interferon regulatory factor 7	3.26	0.0141
IL23R	Interleukin-23 receptor	1.96	0.0395
OAS2	2'-5'-oligoadenylate synthase 2	1.96	0.0079
CCL22	C-C motif chemokine 22	1.89	0.0121
C3AR1	C3a anaphylatoxin chemotactic receptor	1.74	0.0472
APOE	Apolipoprotein E	1.72	0.005
AGER	Advanced glycosylation end product-specific receptor	1.70	0.0069
FASLG	Tumor necrosis factor ligand superfamily member 6	1.70	0.0012
FXYD2	Sodium/potassium-transporting ATPase subunit gamma	1.64	0.0056
IRF5	Interferon regulatory factor 5	1.63	0.04
TGFBR1	TGF-beta receptor type-1	1.62	0.0144
C8A	Complement component C8 alpha chain	1.60	0.0008
PTGS1	Prostaglandin G/H synthase 1	1.59	0.0411
CRP	C-reactive protein	1.57	0.0298
PTGIR	Prostacyclin receptor	1.55	0.0493
CCL17	C-C motif chemokine 17	1.51	0.0033
HMGN1	Non-histone chromosomal protein HMG-14	1.39	0.0165
TCF4	Transcription factor 4	1.35	0.0053
HIF1A	Hypoxia-inducible factor 1-alpha	1.33	0.0421
PTK2	Focal adhesion kinase 1	1.32	0.0027
GNAQ	Guanine nucleotide-binding protein G(q) subunit alpha	1.30	0.0008
IL9	Interleukin-9	1.30	0.0474
PEN2	Gamma-secretase subunit PEN-2	1.30	0.0537
MAFG	Transcription factor MafG	1.26	0.0248
MAP2K6	Dual specificity mitogen-activated protein kinase kinase 6	1.24	0.0086
Only significantly changing in FAD			
HSPB1	Heat shock protein beta-1	5.74	0.0041
MAFF	Transcription factor MafF	4.38	0.0059
FOS	Proto-oncogene c-Fos	3.17	0.0536
MYD88	Myeloid differentiation primary response protein MyD88	2.29	0.021
MYC	Myc proto-oncogene protein	2.00	0.0414
CD68	Macrosialin	1.90	0.0182
TYROBP	TYRO protein tyrosine kinase-binding protein	1.87	0.0371
IL6R	Interleukin-6 receptor subunit alpha	1.77	0.0465
Only significantly changing in TREM2			
GRB2	Growth factor receptor-bound protein 2	1.35	0.0225

Table 5.5: Genes only significantly changing in either SAD, FAD or *TREM2* variant cases compared to controls.

Gene symbol	Gene Name	SAD		FAD		*TREM2*	
		Fold change compared to control	p-value	Fold change compared to control	p-value	Fold change compared to control	p-value
HSPB2	Heat shock protein beta-2	2.51	0.0008	2.69	0.009	2.55	0.0129
MAP3K1	Mitogen-activated protein kinase kinase kinase 1	1.40	0.0025	1.70	0.0162	1.54	0.0321
ADAM10	Disintegrin and metalloproteinase domain-containing protein 10	1.42	0.0005	1.32	0.0056	1.52	0.0129
CYSLTR2	Cysteinyl leukotriene receptor 2	1.61	0.0021	1.65	0.0269	1.41	0.0511
MAX	Protein max	1.40	0.0035	1.49	0.0172	1.55	0.0284
MEF2A	Myocyte-specific enhancer factor 2A	1.33	0.0002	1.32	0.0105	1.28	0.0256
NFATC3	Nuclear factor of activated T-cells, cytoplasmic 3	1.62	0.0005	1.84	0.0018	1.56	0.0172
RAF1	RAF proto-oncogene serine/threonine-protein kinase	1.42	0.0046	1.60	0.0027	1.63	0.003
BIRC2	Baculoviral IAP repeat-containing protein 2	1.20	0.0201	1.27	0.0046	1.33	0.0061
DDIT3	DNA damage-inducible transcript 3 protein	1.32	0.017	2.06	0.0085	1.55	0.0135
NFKB1	Nuclear factor NF-kappa-B p105 subunit	1.67	0.006	1.84	0.0004	2.02	0.0156
TGFB3	Transforming growth factor beta-3	2.77	0.0014	1.89	0.0411	2.13	0.0317
BCL6	B-cell lymphoma 6 protein	1.85	0.0226	2.52	0.0096	2.03	0.0542
C5	Complement C5	1.66	0.0127	1.58	0.0185	1.46	0.0382
C6	Complement component C6	1.66	0.0127	1.81	0.0275	1.94	0.0205
CoQ2	4-hydroxybenzoate polyprenyltransferase, mitochondrial	1.29	0.0434	1.37	0.0078	1.38	0.0444
CREB1	Cyclic AMP-responsive element-binding protein 1	1.38	0.0072	1.38	0.0236	1.39	0.0192
CSF1	Macrophage colony-stimulating factor 1	2.35	0.0053	2.87	0.0123	2.73	0.0213
CXCR4	C-X-C chemokine receptor type 4	2.29	0.0307	2.62	0.0442	2.28	0.0419
DAXX	Death domain-associated protein 6	1.62	0.0008	1.61	0.0205	1.67	0.0147
HDAC4	Histone deacetylase 4	1.56	0.0095	1.61	0.0541	1.68	0.0308
HMGB1	High mobility group protein B1	1.21	0.0131	1.16	0.0429	1.29	0.0186
IRF3	Interferon regulatory factor 3	1.57	0.0093	1.84	0.0092	1.69	0.018
MAP3K7	Mitogen-activated protein kinase kinase kinase 7	1.19	0.0033	1.21	0.026	1.25	0.0004
MAPKAPK2	MAP kinase-activated protein kinase 2	1.95	0.0019	2.43	0.0054	2.34	0.0223

Gene symbol	Gene Name	SAD		FAD		*TREM2*	
		Fold change compared to control	p-value	Fold change compared to control	p-value	Fold change compared to control	p-value
MAPKAPK5	MAP kinase-activated protein kinase 5	1.50	0.0006	1.40	0.0375	1.45	0.0307
NFE2L2	Nuclear factor erythroid 2-related factor 2	1.44	0.0257	2.03	0.0014	1.70	0.0135
PDGFA	Platelet-derived growth factor subunit A	1.39	0.0103	1.61	0.0057	1.50	0.0146
RAC1	Ras-related C3 botulinum toxin substrate 1	1.17	0.0239	1.23	0.0235	1.30	0.0025
RELA	Transcription factor p65	1.95	0.0024	2.12	0.0023	2.39	0.0059
RIPK1	Receptor-interacting serine/threonine-protein kinase 1	1.46	0.0164	1.53	0.0402	1.57	0.0349
SMAD7	Mothers against decapentaplegic homolog 7	1.59	0.002	2.01	0.0036	1.66	0.0214
SNCA	Alpha-synuclein	-1.18	0.0309	-1.63	0.0262	-1.44	0.0032
STAT3	Signal transducer and activator of transcription 3	1.54	0.0289	2.02	0.0177	1.79	0.0501
TGFB1	Transforming growth factor beta-1	2.46	0.0024	2.88	0.0141	2.67	0.041
TRAF2	TNF receptor-associated factor 2	1.45	0.0146	1.90	0.0197	1.55	0.029

Table 5.6: Genes that are significantly changing in all disease groups compared to control. (-) represents downregulated compared to control.

different disease groups. Both the SAD and *TREM2* SAD diagrams show predominant red genes, indicating large amounts of upregulation in neuroinflammatory genes, as also indicated by the highest changing genes in Table 5.2 (Figure 5.2a and b). The *TREM2* variant control diagram however, shows predominantly green genes, indicating large levels of downregulation in neuroinflammatory genes. This pattern also followed suit throughout the rest of the canonical pathways visualised in the heatmap (Figure 5.1), indicating that although the *TREM2* variant controls have the same variant in *TREM2*, they have an altered inflammatory gene expression profile when compared to controls. The *APOE* genotype in the *TREM2* variant controls do not include any *ApoE4* alleles whereas the *TREM2* SAD cases all contain an *ApoE4* allele. Therefore, this could be one factor explaining this difference.

The next canonical pathways that scored highest indicate which out of the many inflammatory pathways are the most activated or inhibited. These include TREM1-signalling, role of pattern recognition receptors (Figure 5.3), NF-κB signalling and p38 MAPK signalling pathways (Figure 5.1). The individual pathway gene expression heat maps for these can be found in Appendix Figure 2, 3, 4. In all four pathways, *TREM2* SAD cases have an increased level of upregulation compared to SAD cases when both groups are compared to normal controls. This may indicate that *TREM2* variant cases have a more severe inflammatory phenotype than SAD cases. However, no significant differences between these TREM2 variant SAD cases and SAD cases in age of onset or disease duration are observed.

Assessing the most represented bio functions that were scored by IPA analysis revealed that the top diseases and functions changing were migration of cells, cell movement, cell movement of tumour cell lines, leukocyte migration and cell movement of leukocytes indicating that activating the genes involved in the migration of cells may be involved in the disease pathogenesis (Figure 5.1b). Again, the *TREM2* variant controls had a predicted inhibition for all of these functions listed, whereas all other groups were predicted to be activated.

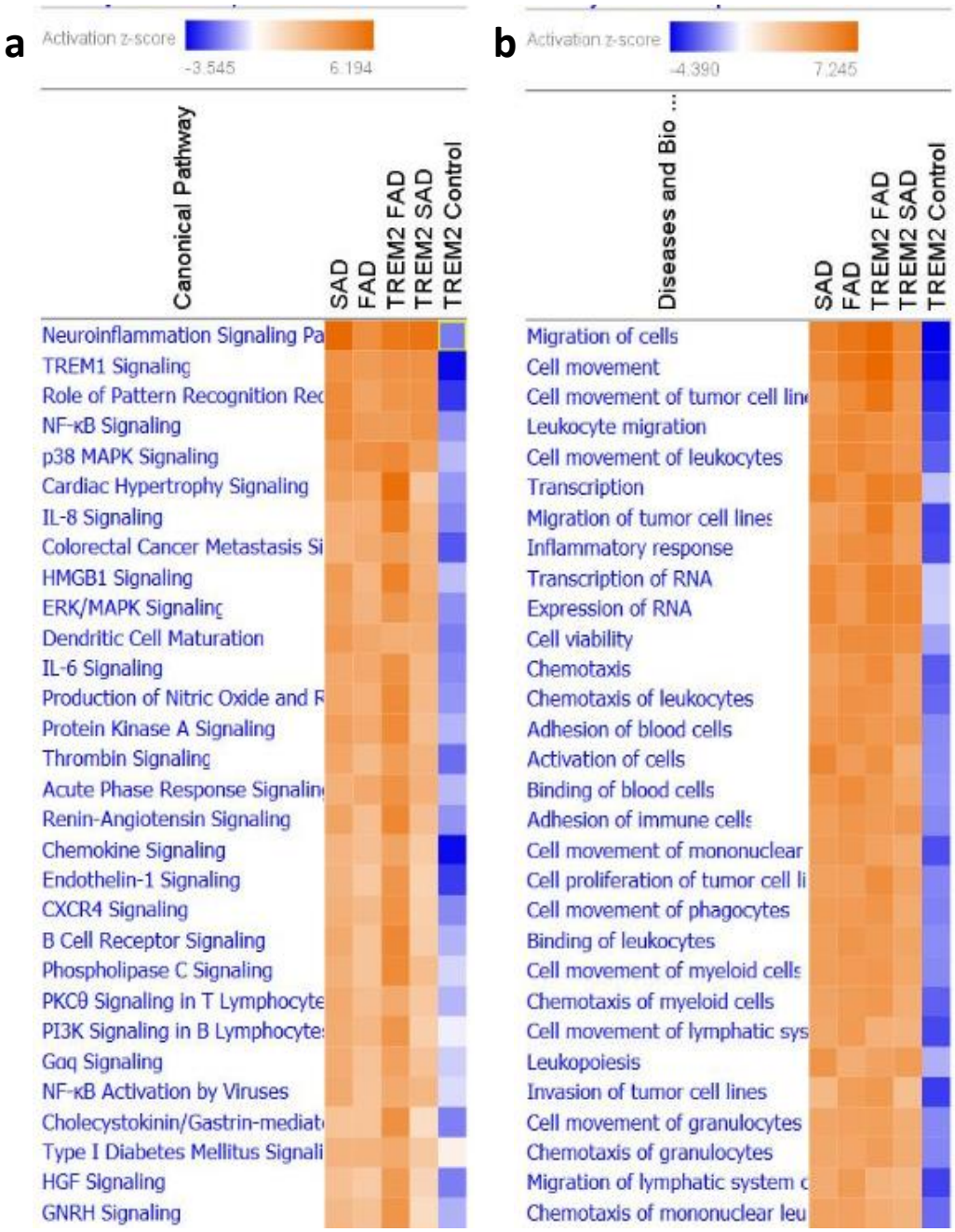

Figure 5.1: Top pathways and functions represented in nanostring data. (a) List of top 30 canonical pathways in nanostring data listed according to the z-score given by IPA software. (b) List of top diseases and functions represented in nanostring data according to z-score given by IPA software. Orange represents a predicted activation of the pathway and blue represents a predicted inhibition of the pathway based on expression values found in the data. Intensity of colour relates to how activated or inhibited the pathway is predicted to be.

a

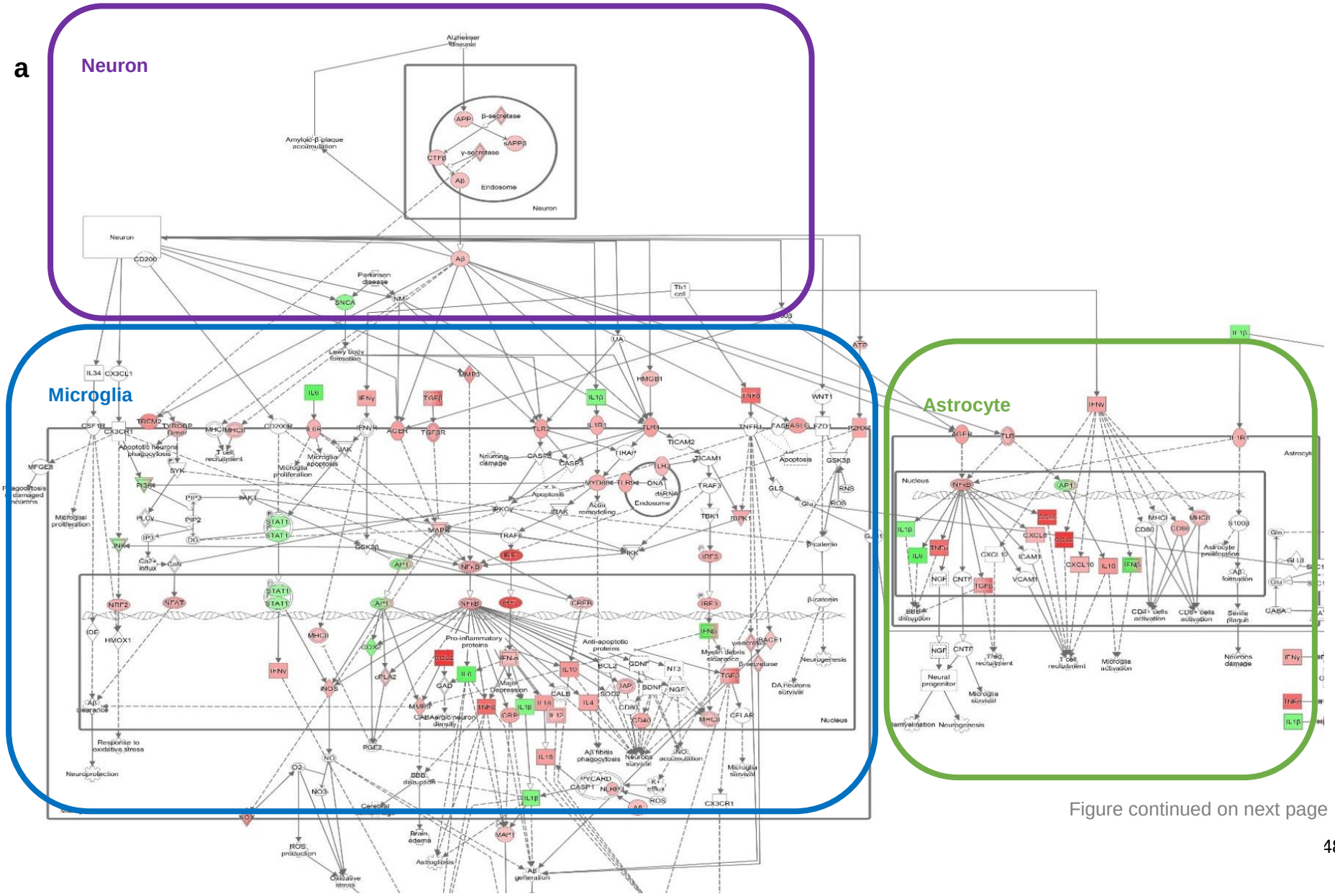

Figure continued on next page

b

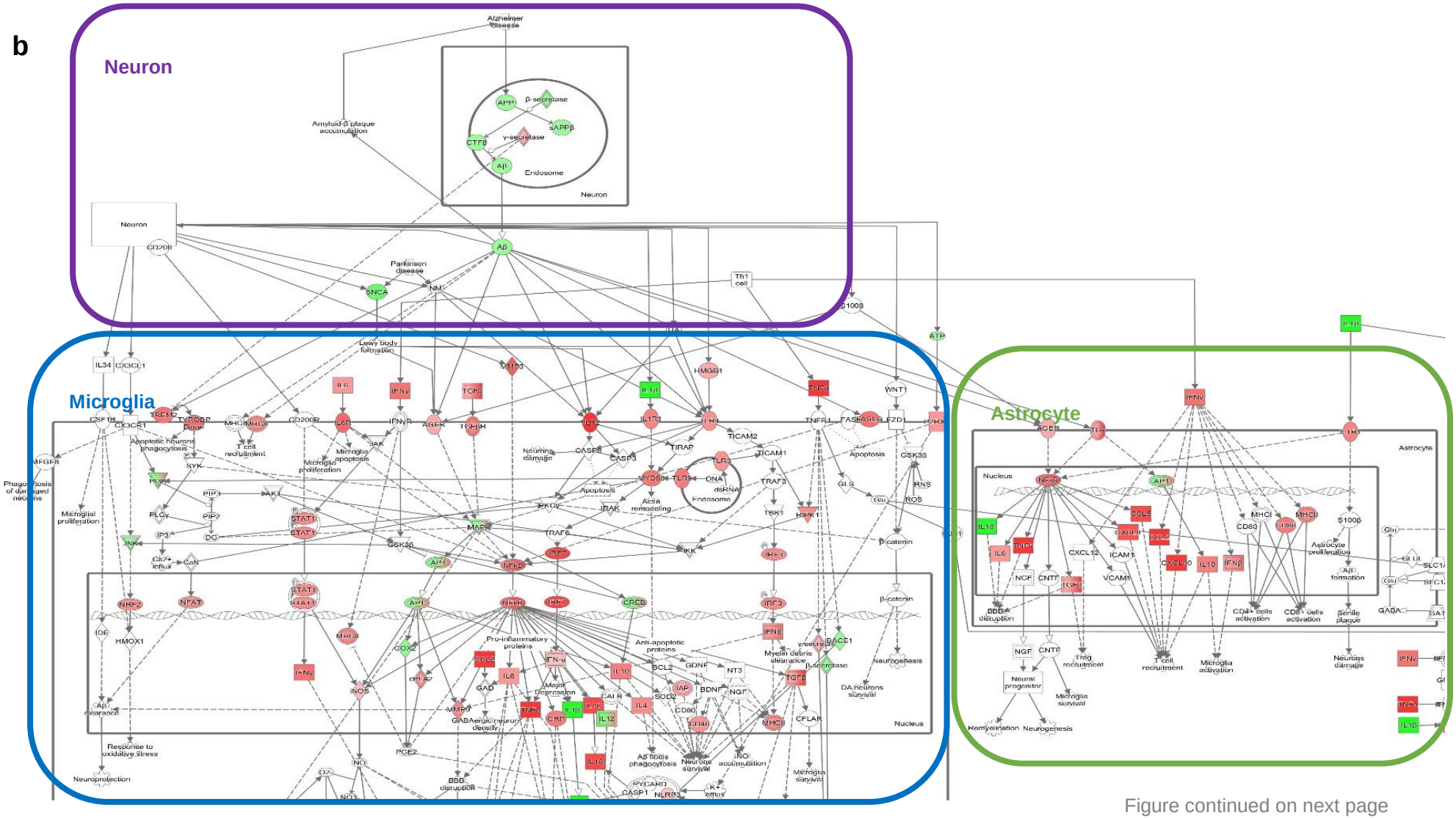

Figure continued on next page

c

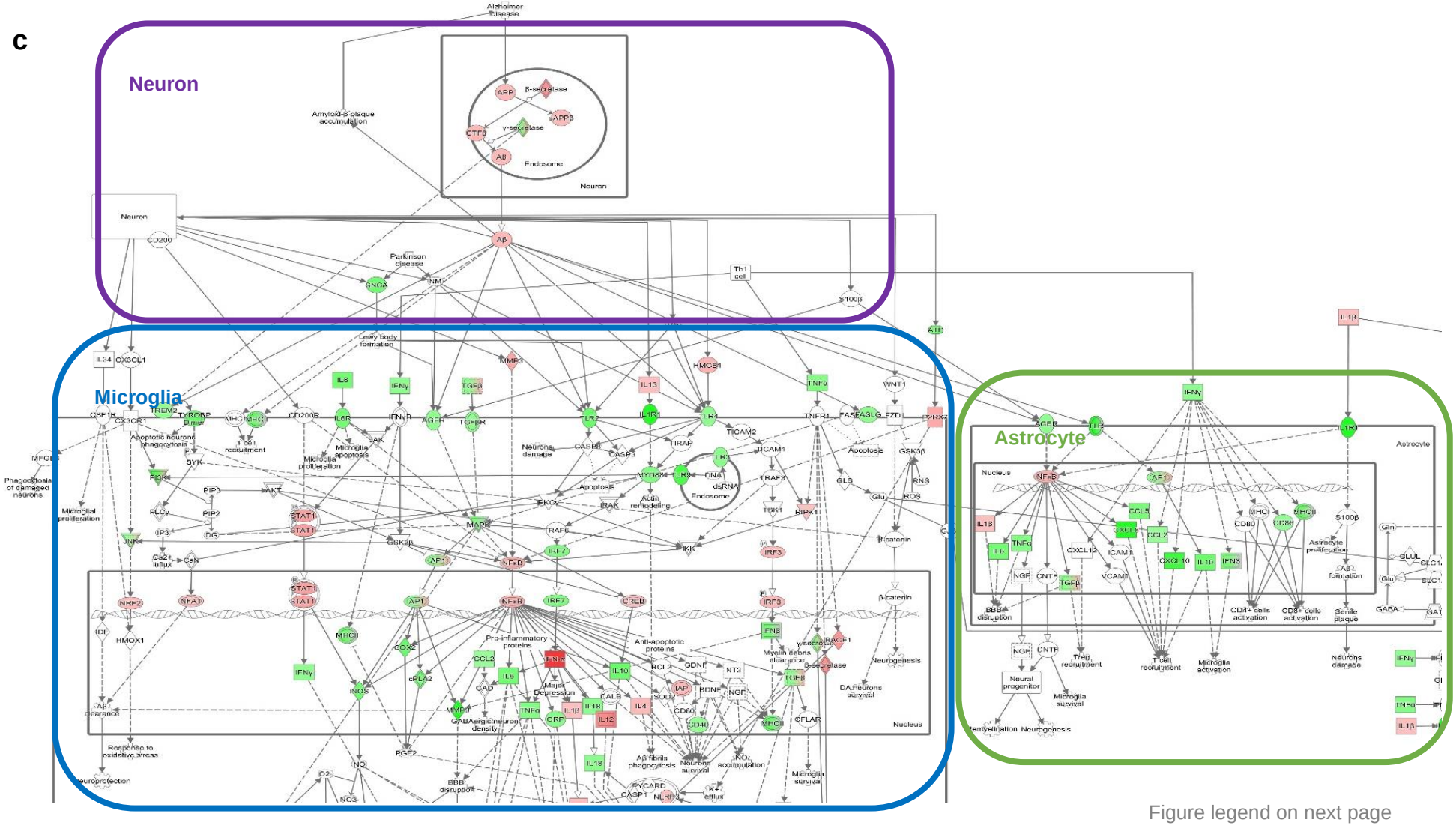

Figure legend on next page

Figure 5.2: Diagram depicting neuroinflammation signalling pathways. (a) Gene expression for SAD overlaid on pathway, (b) gene expression for *TREM2* variant SAD cases overlaid on pathway and (c) gene expression for *TREM2* variant control cases overlaid on pathway. Red genes are upregulated in dataset and green genes are downregulated. Intensity of colour shows level of up- or down-regulation with greater intensity meaning higher expression changes. Details of the pathway are difficult to see but overall difference of up- and downregulation of genes between disease groups is evident.

5.4.2. Proteomic expression in the frontal cortex of *TREM2* variant cases

To determine if the genetic expression changes also occur at the translational level, label-free mass spectrometry was performed to determine changes in protein expression. A total of 6012 proteins were detected in the soluble supernatant fraction and 5571 in the insoluble pellet fraction. Proteins were either detected in both the soluble and insoluble fraction (3269 proteins) or they were unique to the soluble fraction (2743 proteins) or insoluble fraction (2302 proteins). Most proteomic studies only look at the soluble fraction. However, assessing the proteins that are normally insoluble allows for the detection of proteins that precipate in vivo and may be involved in pathological inclusions. Only proteins that were changing >1.5 fold compared to controls were considered as changing in analysis. Both the up- and down-regulation of proteins were observed in every disease group when compared to controls, with the *TREM2* FAD group having the highest number of proteins changing in both directions and the least changing in the SAD group (Table 5.7).

The largest changes in protein expression according to fold change are listed for each disease group, the highest 20 upregulated, and the 20 most downregulated proteins are shown. A full list of all proteins detected can be found on Supplementary CD Table 1.

Proteomics (fold change >1.5)	**SAD**	**FAD *PSEN1***	**FAD *APP***	***TREM2* FAD**	***TREM2* SAD**	***TREM2* Control**
Upregulated	195	325	363	651	361	430
Downregulated	158	349	289	555	235	419

Table 5.7: Number of proteins changing in expression in mass spectrometry dataset. The number of proteins that were changing with greater than 1.5 fold change compared to control are indicated for each disease group and split into those that were upregulated or downregulated.

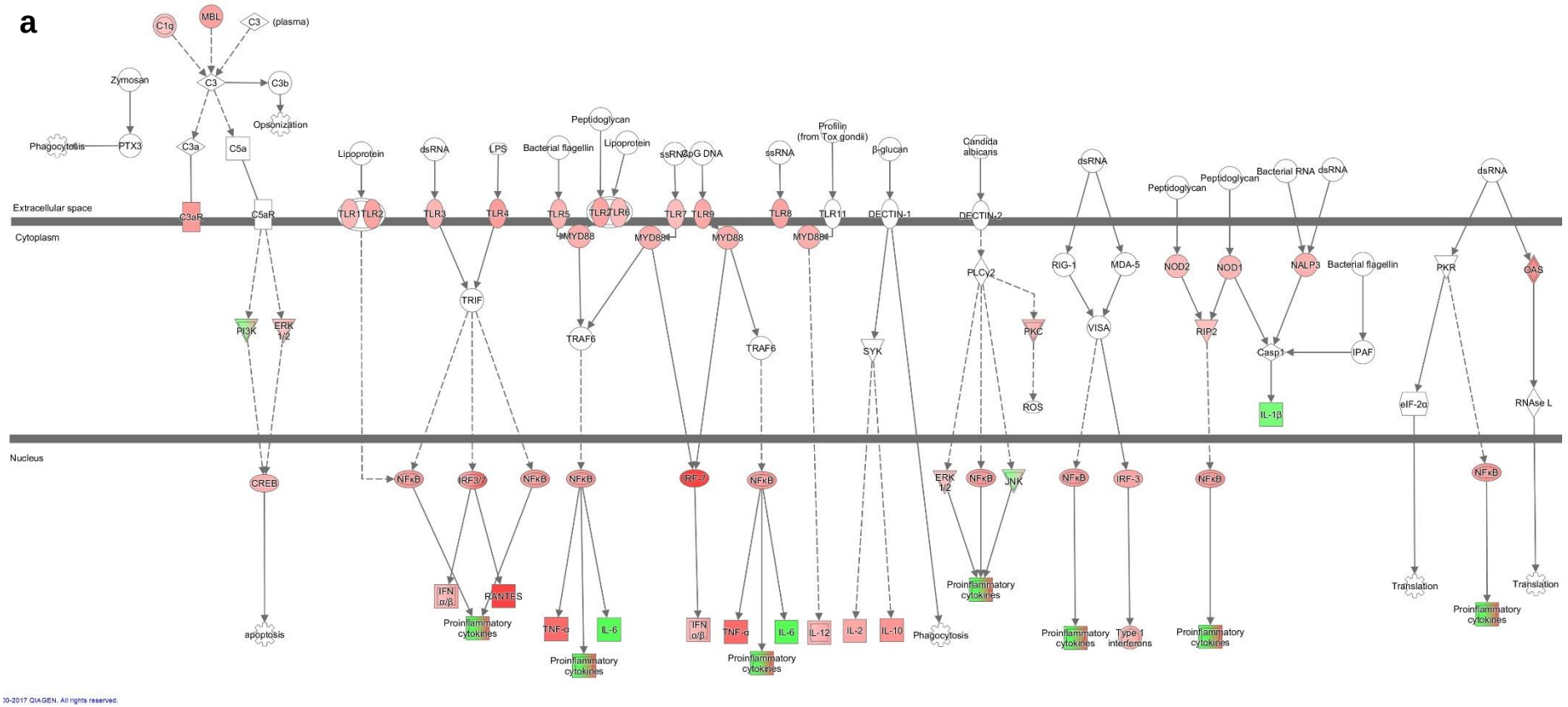

Figure continued on next page

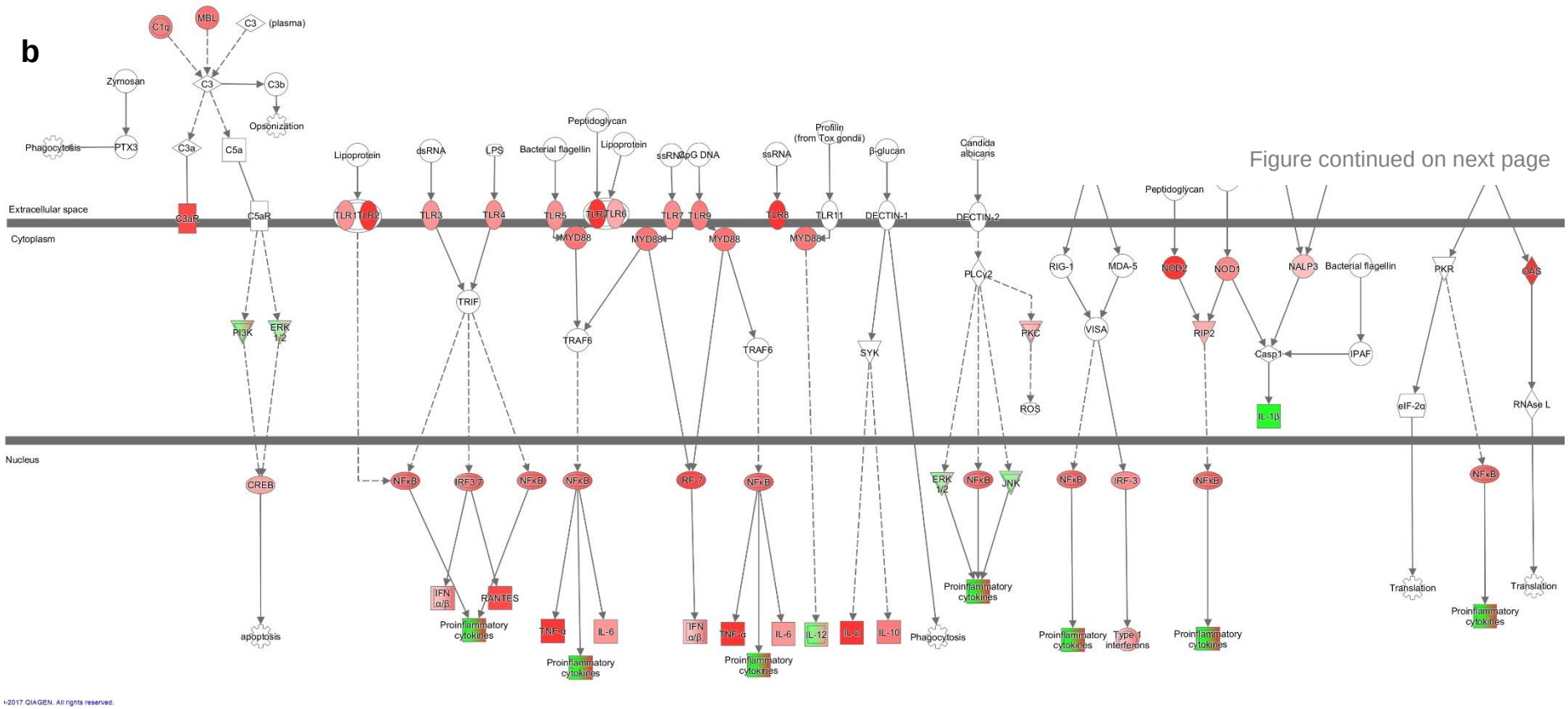

Figure continued on next page

Figure continued on next page

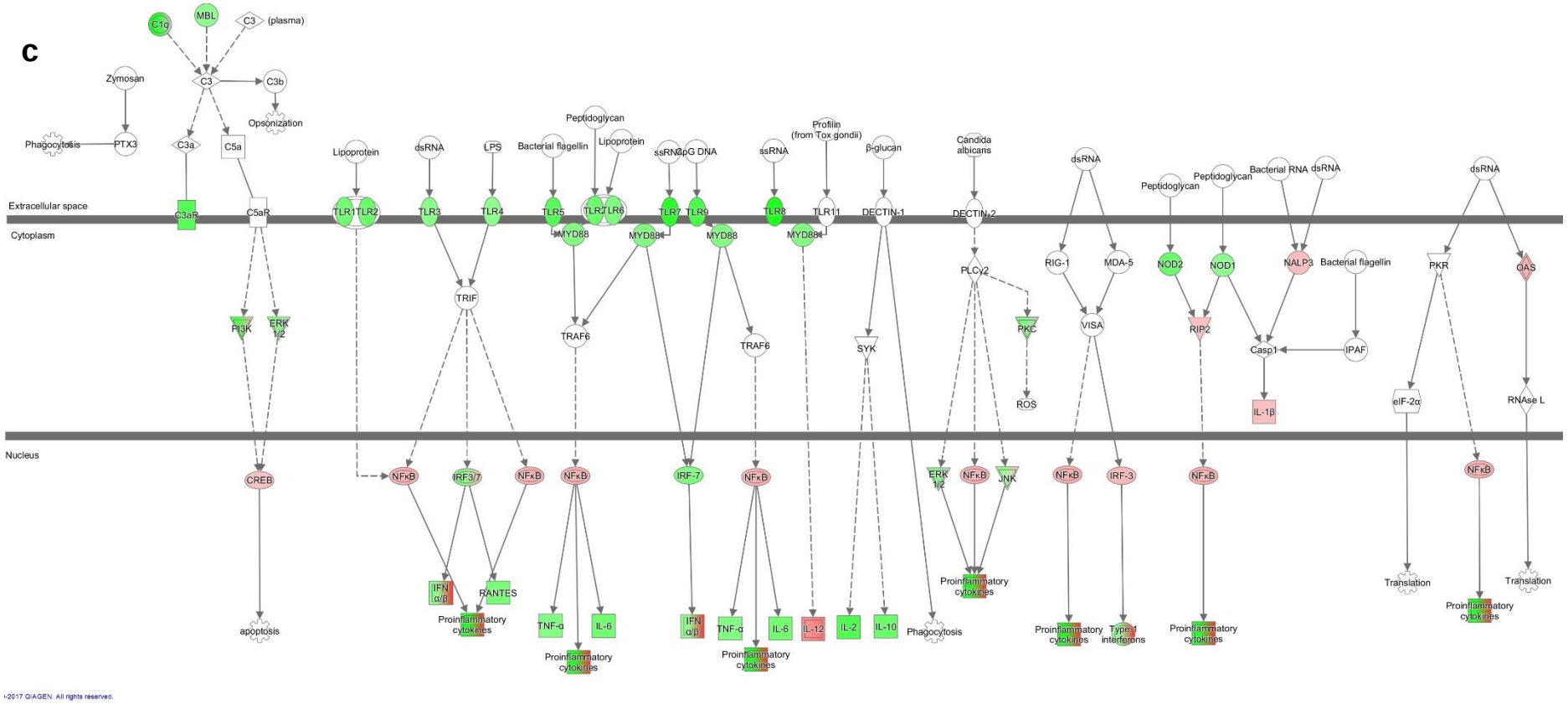

Figure 5.3: Diagram depicting role of pattern recognition receptor pathways. (a) Gene expression for SAD overlaid on pathway, (b) gene expression for *TREM2* variant SAD cases overlaid on pathway and (c) gene expression for *TREM2* variant control cases overlaid on pathway. Red genes are upregulated in dataset and green genes are downregulated. Intensity of colour shows level of up- or down-regulation with greater intensity meaning higher expression changes

These proteins identified in this study demonstrating the largest changes in expression have already been linked to AD in other studies. For SAD (Table 5.8), the highest upregulated protein was KRT6A (Keratin, type II cytoskeletal 6A) at a level of 25.3-fold increase in the insoluble fraction. KRT6A is a cytoskeletal protein and a number of cytoskeletal proteins have been identified previously to be present with Aβ plaques (Liao et al., 2004). DSC1 (Desmocollin-1) was found to be upregulated 8.5-fold in the insoluble fraction compared to controls and is associated with the adrenergic signalling system (Ramos et al., 2006). A polymorphism of this gene has been found in AD cases, linking the adrenergic signalling pathway to AD (Ramos et al., 2006). COL25A1 (Collagen alpha-1(XXV) chain) was upregulated 7.9-fold in the insoluble fraction and has been identified previously to provide increased risk of AD in a Swedish population (Forsell et al., 2010). It has also been shown to bind to amyloid fibrils and facilitate the formation of plaques by increasing the protease resistance of the Aβ (Tong et al., 2010). CRTC1 (CREB-regulated transcription coactivator 1) is upregulated 6.1-fold in the insoluble fraction and has been linked to memory function transcription in AD, with reports that it is differentially methylated in the AD hippocampus (Mendioroz et al., 2016; Parra-Damas et al., 2014; Saura, 2012). C4A (Complement C4-A) is upregulated 4.3-fold in the insoluble fraction and has also been observed to increase in other blood and brain proteomic studies (Khan et al., 2016). VGF, a neurosecretory protein, is downregulated 4.3-fold in the soluble fraction compared to controls and has already been identified as a CSF biomarker for AD (Busse et al., 2015; Hendrickson et al., 2015; Spellman et al., 2015). Additionally, it has been shown to have decreased levels in AD using immunohistochemistry (Cocco et al., 2010). KPNA6 (Importin subunit alpha-7) is downregulated 2.5-fold in the insoluble fraction and has also been shown to be decreased in another RNA sequencing study on AD (Roy et al., 2017). SYNPO (Synaptopodin) is downregulated 2.4-fold in the insoluble fraction and is involved in synaptic transmission. It has been shown to be downregulated in Parkinson's with dementia and Dementia with lewy bodies (Datta et al., 2017). PRIM1 (DNA primase small subunit) is downregulated 2.3-fold in the insoluble fraction and is involved in proliferation and cell cycle. It has been shown to be downregulated in a Down's syndrome mouse model (Hewitt et al., 2010).

Gene symbol	Protein Name	Fold change compared to control
KRT6A	*Keratin, type II cytoskeletal 6A*	25.32
KRT6C	*Keratin, type II cytoskeletal 6C*	8.93
DSC1	*Desmocollin-1*	8.47
COL25A1	*Collagen alpha-1(XXV) chain*	7.94
KRT5	*Keratin, type II cytoskeletal 5*	6.57
KRT16	*Keratin, type I cytoskeletal 16*	6.50
CRTC1	*CREB-regulated transcription coactivator 1*	6.07
APOE	*Apolipoprotein E*	6.01
KRT17	*Keratin, type I cytoskeletal 17*	5.40
MAPT	*Microtubule-associated protein*	4.49
C4A	*Complement C4-A*	4.29
IRF2BP1	*Interferon regulatory factor 2-binding protein 1*	3.78
OBSCN	*Obscurin*	3.37
QARS	Glutamine--tRNA ligase	3.35
COL9A2	*Collagen alpha-2(IX) chain*	3.29
KRT1	*Keratin, type II cytoskeletal 1*	3.13
ASAP2	*Arf-GAP with SH3 domain, ANK repeat and PH domain-containing protein 2*	3.10
UBN1	*Ubinuclein-1*	3.08
ARFGEF1	Brefeldin A-inhibited guanine nucleotide-exchange protein 1	3.03
DCTN2	*Dynactin subunit 2*	2.96

Gene symbol	Protein Name	Fold change compared to control
ASAP3	*Arf-GAP with SH3 domain, ANK repeat and PH domain-containing protein 3*	-7.45
VGF	Neurosecretory protein VGF	-4.32
TBC1D8B	*TBC1 domain family member 8B*	-4.16
SCG2	*Secretogranin-2*	-3.16
USP4	*Ubiquitin carboxyl-terminal hydrolase 4*	-2.91
VPS51	Vacuolar protein sorting-associated protein 51 homolog	-2.80
HIST1H1E	*Histone H1.4*	-2.55
KPNA6	*Importin subunit alpha-7*	-2.52
TCEAL3	*Transcription elongation factor A protein-like 3*	-2.48
TPM2	Tropomyosin beta chain	-2.47
FARSA	*Phenylalanine--tRNA ligase alpha subunit*	-2.44
SYNPO	*Synaptopodin*	-2.43
ALDH3A2	*Fatty aldehyde dehydrogenase*	-2.40
IRF2BP2	Interferon regulatory factor 2-binding protein 2	-2.38
TNRC18	*Trinucleotide repeat-containing gene 18 protein*	-2.35
TAGLN	Transgelin	-2.31
PRIM1	*DNA primase small subunit*	-2.30
KSR1	*Kinase suppressor of Ras 1*	-2.29
SENP6	Sentrin-specific protease 6	-2.21
SLC12A7	*Solute carrier family 12 member 7*	-2.20

Table 5.8: Top 20 up- and down- regulated proteins changing in expression in SAD compared to controls. Italics represent proteins that were in the insoluble fraction.

In FAD (*PSEN1* Table 5.9, *APP* Table 5.10), CTGF (Connective tissue growth factor) is upregulated 4-fold in the insoluble fractions in *PSEN1* variants. Its levels were shown to correlate with neuritic plaques and it is thought to increase Aβ production but increase Aβ degradation within glial cells (Yang et al., 2017a; Zhao et al., 2005). GRIA2 (Glutamate receptor 2) is upregulated in *APP* cases 5.3-fold in the insoluble fraction and this protein has been shown to differ in expression according to *APOE* genotype (Conejero-Goldberg et al., 2011). COL25A1 is upregulated in *APP* variant cases at 4.8-fold in the insoluble fraction so a further increase is seen in SAD cases. CRABP1 (Cellular retinoic acid-binding protein 1) is upregulated 4.6-fold in the insoluble fraction in *APP* cases and this has been shown previously to be upregulated in cells with increased Aβ42/Aβ40 ratio (Uhrig et al., 2008). C4B (Complement C4-B) is upregulated 3.3-fold in the insoluble fraction in *APP* cases and has previously been identified to increase in an AD CSF proteomic study (Finehout et al., 2005). CRK, an adaptor molecule, is upregulated 3.2-fold in the insoluble fraction in *APP* cases and is involved in regulating APP processing. BGN (Biglycan) is downregulated in PSEN1 cases 2.7-fold in the soluble fraction but was found to be upregulated in FAD fibroblasts (Bellucci et al., 2007). It is a proteoglycan that has been found with Aβ plaque cores and alters APP splicing (Bjelik et al., 2007). EPC2 (Enhancer of polycomb homolog 2) is downregulated in *APP* cases 3.3-fold in the soluble fraction and is associated with AD CSF biomarkers (Kim et al., 2011) GAP43 (Neuromodulin) is downregulated 2.9-fold in the insoluble fraction in APP cases and is thought to be involved with the sprouting response seen in AD (Masliah et al., 1992). GAP43 levels have been reported to decline as synaptic degeneration occurs (Bogdanovic et al., 2000; de la Monte et al., 1995).

In *TREM2* variant SAD cases (Table 5.11), the highest upregulated protein observed was GOLGA8R (Golgin subfamily A member 8R) at a level of 60.8-fold in the insoluble fraction and is a part of the golgi apparatus. C4A is also upregulated 6.8-fold in the insoluble fraction compared to controls, similarly to SAD cases. ANXA2 (annexin A2) is upregulated 4.4-fold in the insoluble fraction and has been found to interact with tau and play a role in inflammation (Gauthier-Kemper et al., 2011; Pineda et al., 2012).

Gene symbol	Protein Name	Fold change compared to control
SEC31A	*Protein transport protein Sec31A*	9.26
APOE	*Apolipoprotein E*	7.40
MRPL46	*39S ribosomal protein L46, mitochondrial*	6.76
RAB5C	*Ras-related protein Rab-5C*	6.72
TMC6	*Transmembrane channel-like protein 6*	6.38
NDUFA7	*NADH dehydrogenase [ubiquinone] 1 alpha subcomplex subunit 7*	5.84
JAKMIP3	*Janus kinase and microtubule-interacting protein 3*	5.61
BRAF	*Serine/threonine-protein kinase B-raf*	4.89
MPI	*Mannose-6-phosphate isomerase*	4.70
FAF2	*FAS-associated factor 2*	4.64
APOL2	*Apolipoprotein L2*	4.54
NONO	*Non-POU domain-containing octamer-binding protein*	4.35
USP15	*Ubiquitin carboxyl-terminal hydrolase 15*	4.19
PPEF2	*Serine/threonine-protein phosphatase with EF-hands 2*	4.16
RIC8A	*Synembryn-A*	4.15
CTGF	*Connective tissue growth factor*	3.95
FAM169A	*Soluble lamin-associated protein of 75 kDa*	3.91
GMPR	GMP reductase 1	3.73
HIP1	*Huntingtin-interacting protein 1*	3.67
DNPEP	*Aspartyl aminopeptidase*	3.57

Gene symbol	Protein Name	Fold change compared to control
ARMC9	*LisH domain-containing protein ARMC9*	-5.88
WNK2	*Serine/threonine-protein kinase WNK2*	-5.32
SPIRE1	*Protein spire homolog 1*	-4.94
SLFN11	*Schlafen family member 11*	-4.82
APC2	Adenomatous polyposis coli protein 2	-4.50
CAMSAP1	*Calmodulin-regulated spectrin-associated protein 1*	-3.98
TPM2	Tropomyosin beta chain	-3.78
ARID4A	*AT-rich interactive domain-containing protein 4A*	-3.31
SNW1	*SNW domain-containing protein 1*	-3.16
GDA	*Guanine deaminase*	-2.99
CELSR1	*Cadherin EGF LAG seven-pass G-type receptor 1*	-2.95
ARHGEF9	*Rho guanine nucleotide exchange factor 9*	-2.89
TNIK	*TRAF2 and NCK-interacting protein kinase*	-2.82
TAGLN	*Transgelin*	-2.81
CNN1	Calponin-1	-2.74
LSM14B	*Protein LSM14 homolog B*	-2.73
BGN	Biglycan	-2.72
MYH13	*Myosin-13*	-2.71
CASKIN1	*Caskin-1*	-2.67
IGHG2	*Ig gamma-2 chain C region*	-2.67

Table 5.9: Top 20 up- and down- regulated proteins changing in expression in FAD *PSEN1* compared to controls. Italics represent proteins that were in the insoluble fraction.

Gene symbol	Protein Name	Fold change compared to control
APOE	*Apolipoprotein E*	6.97
GRIA2	*Glutamate receptor 2*	5.28
COL25A1	*Collagen alpha-1(XXV) chain*	4.76
CRABP1	*Cellular retinoic acid-binding protein 1*	4.56
MAPT	*Microtubule-associated protein*	4.53
CTNND1	*Catenin delta-1*	4.42
SH3GL1	*Endophilin-A2*	3.60
DCTN2	*Dynactin subunit 2*	3.57
C4B	*Complement C4-B*	3.28
RBP1	*Retinol-binding protein 1*	3.28
LTN1	*E3 ubiquitin-protein ligase listerin*	3.20
CRK	*Adapter molecule crk*	3.15
SH3GL2	*Endophilin-A1*	3.13
DNAH10	*Dynein heavy chain 10, axonemal*	2.98
EPN3	*Epsin-3*	2.86
CLIC4	*Chloride intracellular channel protein 4*	2.85
ALDH6A1	*Methylmalonate-semialdehyde dehydrogenase [acylating], mitochondrial*	2.82
GSTM2	*Glutathione S-transferase Mu 2*	2.82
PDP1	*[Pyruvate dehydrogenase [acetyl-transferring]]-phosphatase 1, mitochondrial*	2.81
GPSM2	*G-protein-signaling modulator 2*	2.81

Gene symbol	Protein Name	Fold change compared to control
CXXC1	*CXXC finger 1 (PHD domain), isoform CRA_c*	-4.39
MPDZ	*Multiple PDZ domain protein*	-4.22
ASAP3	*Arf-GAP with SH3 domain, ANK repeat and PH domain-containing protein 3*	-3.98
CAMSAP1	*Calmodulin-regulated spectrin-associated protein 1*	-3.80
DEPDC4	DEP domain-containing protein 4	-3.28
EPC2	Enhancer of polycomb homolog 2	-3.26
HSP90AB2P	*Putative heat shock protein HSP 90-beta 2*	-3.25
SLC17A7	Vesicular glutamate transporter 1	-3.12
SEC16A	*Protein transport protein Sec16A*	-3.11
AVPR1B	*Vasopressin V1b receptor*	-3.06
FAM71F1	*Protein FAM71F1*	-2.85
GAP43	*Neuromodulin*	-2.85
NKTR	NK-tumor recognition protein	-2.84
ARFGEF3	*Brefeldin A-inhibited guanine nucleotide-exchange protein 3*	-2.81
CA1	*Carbonic anhydrase 1*	-2.73
PRPH	*Peripherin*	-2.72
SIRPA	*Tyrosine-protein phosphatase non-receptor type substrate 1*	-2.69
HIST1H1E	*Histone H1.4*	-2.59
CADM3	*Cell adhesion molecule 3*	-2.58
EPB42	*Erythrocyte membrane protein band 4.2*	-2.56

Table 5.10: Top 20 up- and down- regulated proteins changing in expression in FAD *APP* compared to controls. Italics represent proteins that were in the insoluble fraction.

This could demonstrate a difference between normal SAD and *TREM2* variant SAD. GRIA2 is upregulated 4.09-fold in the insoluble fraction, similarly to the FAD *APP* cases and EPC2 is also downregulated 2.64-fold in the soluble fraction, similar to FAD *APP* cases. The protein which demonstrated the most marked downregulation in these cases was CCNG1 (Cyclin-G1) at a level of 18.9-fold in the soluble fraction. It may be involved in the inhibition of cell proliferation and is associated with DNA damage. PXN (Paxillin) is downregulated 2.7-fold in the insoluble fraction and has been found to be a hub gene involved in age-related networks (Liang et al., 2012).

The *TREM2* variant FAD case (Table 5.12) had a different profile to the *TREM2* variant SAD cases. The highest upregulated protein is CRYZL1 (Quinone oxidoreductase-like protein 1) at 14.5-fold in the soluble fraction but not much is known about this protein at present. AHSG (Alpha-2-HS-glycoprotein) is upregulated 7.1-fold in the soluble fraction in this case and has been found to have a polymorphism in the gene associated with late onset AD in Italians (Geroldi et al., 2005). It has also been found to be downregulated in AD CSF. SERPINA3 (Alpha-1-antichymotrypsin) is upregulated 5.8-fold in the insoluble fraction and a polymorphism in this gene has been shown to effect age of onset and disease duration of AD (Kamboh et al., 2006). HBG2 (Haemoglobin subunit gamma-2) is upregulated 5.6-fold in the soluble fraction and a SNP association suggests it has a role in AD. Haemoglobin is also thought to bind to Aβ (Perry et al., 2008). The highest two downregulated proteins are XRCC5 (X-ray repair cross-complementing protein 5) at 99.3-fold in the soluble fraction and SCFD1 (Sec1 family domain-containing protein 1) at 27.3-fold in the soluble fraction. XCCR5 is a DNA repair protein and it has been shown to protect against oxidative stress damage associated with copper levels (Du et al., 2011). As TREM2 variant SAD cases have altered CCNG1 that is involved with DNA damage and the TREM2 variant FAD case has altered XCCR5, involved with DNA repair, DNA regulation may be important in these variants. SCFD1 is involved in the transport of proteins between the endoplasmic reticulum and the golgi apparatus and it has been suggested as a risk factor for ALS (van Rheenen et al., 2016). VGF was found to be downregulated 8.7-fold in the soluble fraction in this case, similarly to SAD cases. COL4A1 (Collagen alpha-1(IV) chain) is upregulated 4.9-fold in the soluble fraction and is known to provoke an inflammatory reaction (Marchesi, 2016).

Gene symbol	Protein Name	Fold change compared to control
GOLGA8R	*Golgin subfamily A member 8R*	60.79
APOE	*Apolipoprotein E*	7.77
MAPT	*Microtubule-associated protein*	7.74
ECT2	*Protein ECT2*	7.14
IFIT3	*Interferon-induced protein with tetratricopeptide repeats 3*	7.11
C4A	*Complement C4-A*	6.83
FHAD1	*Forkhead-associated domain-containing protein 1*	6.27
SPG7	*Paraplegin*	6.21
PHF5A	PHD finger-like domain-containing protein 5A	5.04
CPSF7	Cleavage and polyadenylation-specificity factor subunit 7	4.80
RIC8A	Synembryn-A	4.58
ANXA2	*Annexin A2*	4.41
STXBP6	Syntaxin-binding protein 6	4.41
HIST1H4A	Histone H4	4.23
ZBTB38	Zinc finger and BTB domain-containing protein 38	4.21
SQSTM1	Sequestosome-1	4.16
GRIA2	*Glutamate receptor 2*	4.09
RBM25	RNA-binding protein 25	3.98
APP	*Amyloid beta A4 protein*	3.91
PSMC4	*26S protease regulatory subunit 6B*	3.85

Gene symbol	Protein Name	Fold change compared to control
CCNG1	Cyclin-G1	-18.89
ASAP3	*Arf-GAP with SH3 domain, ANK repeat and PH domain-containing protein 3*	-12.19
GPATCH2	*G patch domain-containing protein 2*	-8.72
KSR1	*Kinase suppressor of Ras 1*	-4.69
EPB42	*Erythrocyte membrane protein band 4.2*	-4.30
ZEB2	*Zinc finger E-box-binding homeobox 2*	-4.22
SRRM2	*Serine/arginine repetitive matrix protein 2*	-3.66
FBF1	*Fas-binding factor 1*	-3.53
ASNS	*Asparagine synthetase [glutamine-hydrolyzing]*	-3.45
SI	Sucrase-isomaltase, intestinal	-3.27
CCDC51	Coiled-coil domain-containing protein 51	-3.10
TAGLN	Transgelin	-2.89
NUCKS1	*Nuclear ubiquitous casein and cyclin-dependent kinase substrate 1*	-2.84
CIRBP	Cold-inducible RNA-binding protein	-2.76
HNRNPUL1	Heterogeneous nuclear ribonucleoprotein U-like protein 1	-2.69
PXN	*Paxillin*	-2.67
C2CD3	*C2 domain-containing protein 3*	-2.65
EPC2	Enhancer of polycomb homolog 2	-2.64
PITPNM3	*Membrane-associated phosphatidylinositol transfer protein 3*	-2.60
WNK2	*Serine/threonine-protein kinase WNK2*	-2.60

Table 5.11: Top 20 up- and down- regulated proteins changing in expression in *TREM2* SAD cases compared to controls. Italics represent proteins that were in the insoluble fraction.

Gene symbol	Protein Name	Fold change compared to control
CRYZL1	Quinone oxidoreductase-like protein 1	14.54
PEX19	Peroxisomal biogenesis factor 19	7.14
AHSG	Alpha-2-HS-glycoprotein	7.08
IRF2BP2	Interferon regulatory factor 2-binding protein 2	6.40
SERPINA3	*Alpha-1-antichymotrypsin*	5.79
ARFGEF1	Brefeldin A-inhibited guanine nucleotide-exchange protein 1	5.66
HBG2	Hemoglobin subunit gamma-2	5.59
THAP4	THAP domain-containing protein 4	5.38
APOE	*Apolipoprotein E*	5.23
TXNDC17	Thioredoxin domain-containing protein 17	4.91
SHMT2	*Serine hydroxymethyltransferase, mitochondrial*	4.87
COL4A1	Collagen alpha-1(IV) chain	4.85
RGS3	Regulator of G-protein signaling 3	4.85
NAAA	N-acylethanolamine-hydrolyzing acid amidase	4.79
CCAR2	Cell cycle and apoptosis regulator protein 2	4.60
COL9A2	*Collagen alpha-2(IX) chain*	4.56
RPS4X	40S ribosomal protein S4, X isoform	4.47
KCNIP4	Kv channel-interacting protein 4	4.47
IQSEC2	*IQ motif and SEC7 domain-containing protein 2*	4.45
FEZ1	Fasciculation and elongation protein zeta-1	4.35

Gene symbol	Protein Name	Fold change compared to control
XRCC5	X-ray repair cross-complementing protein 5	-99.33
SCFD1	Sec1 family domain-containing protein 1	-27.33
HIST1H1E	*Histone H1.4*	-8.71
ASAP3	*Arf-GAP with SH3 domain, ANK repeat and PH domain-containing protein 3*	-8.70
VGF	Neurosecretory protein VGF	-8.66
RB1CC1	RB1-inducible coiled-coil protein 1	-8.14
ADAM11	Disintegrin and metalloproteinase domain-containing protein 11	-7.70
ZNF852	Zinc finger protein 852	-5.58
TBC1D8B	*TBC1 domain family member 8B*	-5.35
CORO1A	Coronin-1A	-4.94
ADGRB2	*Adhesion G protein-coupled receptor B2*	-4.86
PPFIA4	Liprin-alpha-4	-4.63
HTRA1	Serine protease HTRA1	-4.50
STXBP1	Syntaxin-binding protein 1	-4.19
CDH13	*Cadherin-13*	-4.13
HDGFRP3	*Hepatoma-derived growth factor-related protein 3*	-3.97
WDFY1	WD repeat and FYVE domain-containing protein 1	-3.93
SLC17A7	Vesicular glutamate transporter 1	-3.85
NCKIPSD	NCK-interacting protein with SH3 domain	-3.82
PPIL2	Peptidyl-prolyl cis-trans isomerase-like 2	-3.76

Table 5.12: Top 20 up- and down- regulated proteins changing in expression in *TREM2* FAD compared to controls. Italics represent proteins that were in the insoluble fraction.

KCNIP4 (Kv channel-interacting protein 4) is upregulated 4.8-fold in the soluble fraction and is known to cause increased Aβ42 via affecting γ-secretase activity (Massone et al., 2011). RB1CC1 (RB1-inducible coiled-coil protein 1) is downregulated 8.1-fold in the soluble fraction and is thought to have a role in AD as insufficiency of this protein causes neuronal atrophy to occur (Chano et al., 2007). HTRA1, a serine protease, is downregulated 4.5-fold in the soluble fraction and is involved with Aβ and tau clearance. It can degrade APP and cleave tau, as well as selectively degrading *ApoE4* more efficiently than *ApoE3* (Chu et al., 2016; Grau et al., 2005; Tennstaedt et al., 2012). PPIL2 (Peptidyl-prolyl cis-trans isomerase-like 2) is downregulated 3.8-fold in the soluble fraction in this case and was found to regulate BACE-1 activity in a cell-based assay (Beyer et al., 2014).

TREM2 variant controls (Table 5.13) only share one protein in the highest 20 proteins demonstrating changes in expression with the *TREM2* SAD group. PXN is downregulated 6.3-fold in the insoluble fraction compared to normal controls. The highest upregulated protein observed in the *TREM2* controls is PSMB7 (Proteasome subunit beta type-7) at 13.1-fold in the soluble fraction. Downregulation of this protein has shown inhibited cell proliferation in AD (Wu et al., 2016). An opposite effect here may be an indication of a mechanism that is involved in the risk effect of *TREM2* variants. On the other hand, NEDD8 is upregulated 9.6-fold in the soluble fraction in these cases but this protein was observed to be in neurofibrillary tangle pathology (Mori et al., 2005). PARP1 (Poly [ADP-ribose] polymerase 1) is upregulated 3.3-fold in the insoluble fraction. PARP1 activity is activated by oxidative stress and it induces cell death. Aβ has also been shown to induce PARP1 activity (Wencel et al., 2017). MAP1B (Microtubule-associated protein 1B) is upregulated 3.1-fold in the insoluble fraction and is present in sites where neurofibrillary tangles are deposited in AD (Iqbal et al., 2005). The most downregulated protein in these cases was ASAP3, Arf-GAP with SH3 domain, ANK repeat and PH domain-containing protein 3, at 54.57-fold difference in the insoluble fraction, which promotes cell proliferation (Tian et al., 2017). CDH8 (cadherin-8) is also highly downregulated in the *TREM2* variant controls at 48.1-fold in the soluble fraction. It is a cell-adhesion protein and they are thought to have a role in cell sorting due to them being able to connect cells together (Suzuki and Takeichi, 2008).

Gene symbol	Protein Name	Fold change compared to control
PSMB7	Proteasome subunit beta type-7	13.12
NEDD8	NEDD8	9.55
WDR19	*WD repeat-containing protein 19*	9.32
SLC14A1	Urea transporter 1	5.92
C2CD3	C2 domain-containing protein 3	5.37
SHTN1	*Shootin-1*	4.89
PGBD5	*PiggyBac transposable element-derived protein 5*	4.13
WDR47	WD repeat-containing protein 47	4.05
IGHA2	*Ig alpha-2 chain C region*	3.88
LAMA5	*Laminin subunit alpha-5*	3.81
SCYL1	*N-terminal kinase-like protein*	3.73
MAP2K1	Dual specificity mitogen-activated protein kinase kinase 1	3.63
SLC25A5	*ADP/ATP translocase 2*	3.61
PSAP	*Prosaposin*	3.50
NEB	*Nebulin*	3.50
PARP1	*Poly [ADP-ribose] polymerase 1*	3.29
KRT10	*Keratin, type I cytoskeletal 10*	3.27
LAMA2	*Laminin subunit alpha-2*	3.25
CCDC30	Coiled-coil domain-containing protein 30	3.16
MAP1B	*Microtubule-associated protein 1B*	3.14

Gene symbol	Protein Name	Fold change compared to control
ASAP3	*Arf-GAP with SH3 domain, ANK repeat and PH domain-containing protein 3*	-54.57
CDH8	Cadherin-8	-48.09
WDFY1	*WD repeat and FYVE domain-containing protein 1*	-11.28
COX6A1	Cytochrome c oxidase subunit 6A1, mitochondrial	-9.54
SRRM2	*Serine/arginine repetitive matrix protein 2*	-8.96
AGFG1	*Arf-GAP domain and FG repeat-containing protein 1*	-7.18
RAB24	*Ras-related protein Rab-24*	-6.49
MKRN1	*E3 ubiquitin-protein ligase makorin-1*	-6.47
PXN	*Paxillin*	-6.28
PANK4	Pantothenate kinase 4	-6.08
GC	Vitamin D-binding protein	-5.48
H3F3A	Histone H3.3	-5.42
HBB	Hemoglobin subunit beta	-4.95
FDFT1	*Squalene synthase*	-4.82
TECPR1	*Tectonin beta-propeller repeat-containing protein 1*	-4.75
CA1	Carbonic anhydrase 1	-4.52
PTPRE	*Receptor-type tyrosine-protein phosphatase epsilon*	-4.50
CUX2	Homeobox protein cut-like 2	-4.43
ERO1A	*ERO1-like protein alpha*	-4.40
VARS	Valine--tRNA ligase	-4.28

Table 5.13: Top 20 up- and down- regulated proteins changing in expression in *TREM2* controls compared to controls. Italics represent proteins that were in the insoluble fraction.

In addition to these proteins changing in the different disease groups, several proteins related to AD or neurodegeneration in general were also altered (Table 5.14). APP and MAPT are the proteins directly related to AD pathology and in both cases these were upregulated in all groups other than the *TREM2* variant controls, in which they were downregulated when compared to normal controls. For APP, the greatest fold change was observed in the *TREM2* variant FAD case (4.2-fold, insoluble fraction), followed by the *TREM2* variant SAD case (3.9-fold, insoluble fraction) in which it was one of the highest 20 proteins observed to be upregulated (Table 5.11). For MAPT, the greatest fold change difference was observed in the *TREM2* variant SAD cases (7.7-fold, insoluble fraction) with an increase of 3.2-fold above the next highest group. It was in the highest 20 proteins upregulated for SAD (Table 5.8), FAD *APP* (Table 5.10) and *TREM2* SAD (Table 5.11). The same pattern was observed with the GFAP (Glial fibrillary acidic protein) which is normally used as a reactive astrocyte marker. GFAP was upregulated across all groups but the greatest level of upregulation was observed in the TREM2 variant SAD group in both the soluble and insoluble fractions (3.8-fold soluble, 3.2-fold insoluble). *APOE* was upregulated across all groups in the insoluble fraction, being in the highest 20 proteins upregulated for all groups other than *TREM2* variant controls. Again, the highest level of upregulation was observed in the *TREM2* variant SAD cases (7.8-fold, insoluble fraction). SNCA (alpha-synuclein) was shown to be upregulated in SAD, *TREM2* variant SAD and *TREM2* variant controls but downregulated in all FAD cases for both soluble and insoluble fractions.

Ingenuity pathway analysis highlighted that the top canonical pathways (predicted to be activated or inhibited by the expression of genes represented in them) differ between the soluble and insoluble fractions (Figure 5.4). The top pathways in the soluble fraction are HIPPO signalling, Melatonin signalling, LXR/RXR activation, amyloid processing, actin cytoskeleton signalling and neuroinflammation signalling. HIPPO signalling, amyloid processing and neuroinflammation signalling are predicted predominantly to be activated across the disease groups, whereas melatonin signalling, LXR/RXR activation and actin cytoskeleton signalling are more a mixture of predicted activation and inhibition between groups. The *TREM2* variant FAD case appears to have a more activated pathway phenotype

Gene symbol	Protein name	Fold change compared to control					
		SAD	FAD PSEN1	FAD APP	TREM2 FAD	TREM2 SAD	TREM2 Control
Soluble fraction							
ADAM10	Disintegrin and metalloprotease domain-containing protein 10	1.36	1.38	1.13	2.15	1.48	-
ABCA7	ATP-binding cassette sub-family A member 8	-	-	1.09	-	1.27	-
APOE	apolipoprotein e	1.05	1.26	1.07	1.64	1.24	1.12
APP	Amyloid beta A4 protein	-	1.17	1.24	-	1.06	1.15
CLU	Clusterin	1.33	1.30	1.47	1.75	1.27	1.16
CTSD	Cathepsin D	1.02	1.08	1.05	1.12	1.16	1.08
GFAP	Glial fibrillary acidic protein	1.98	2.04	1.64	2.36	3.76	1.04
MAPT	Microtubule-associated protein tau	1.46	2.86	1.77	2.36	1.04	1.44
P2RX7	P2X purinoreceptor 7	-	1.05	1.01	1.12	1.31	-
SNCA	Alpha-synuclein	1.08	1.05	1.61	1.29	1.03	1.36
Insoluble fraction							
ABCA7	*ATP-binding cassette sub-family A member 7*	*1.14*	*1.96*	-	*1.13*	*2.04*	*2.04*
APOE	*apolipoprotein e*	*6.01*	*7.40*	*6.97*	*5.23*	*7.77*	*1.16*
APP	*Amyloid beta A4 protein*	*2.92*	*2.88*	*2.78*	*4.21*	*3.91*	*1.34*
CLU	*Clusterin*	*1.32*	*1.65*	*1.27*	*1.70*	*1.49*	*1.05*
CTSD	*Cathepsin D*	*1.04*	*1.21*	*1.27*	*1.20*	*1.17*	*1.55*
GFAP	*Glial fibrillary acidic protein*	*1.55*	*1.50*	*1.30*	*1.92*	*3.23*	*1.93*
MAPT	*Microtubule-associated protein tau*	*4.49*	*3.00*	*4.53*	*3.51*	*7.74*	*1.24*
SNCA	*Alpha-synuclein*	*1.57*	*1.10*	*2.37*	*2.21*	*1.41*	*2.34*

Table 5.14: Protein expression in genes associated with neurodegeneration. Red represents upregulation and green represents downregulation compared to controls. Italics represent proteins that were in the insoluble fraction.

compared to other disease groups. The top pathways in the insoluble fraction are EIF2 signalling, RhoA signalling, signalling by Rho family GTPases, ERK5 signalling, glioma signalling and ephrin receptor signalling. EIF2 signalling and glioma signalling are predominantly predicted to be inhibited across the disease groups with *TREM2* variant controls having the opposite prediction. RhoA signalling, signalling by Rho family GTPases, ERK5 signalling and ephrin receptor signalling have a more activated prediction. The *TREM2* variant control group has a different pattern showing predominantly predicted activation throughout the top canonical pathways, whereas the other groups are more varied between activation and inhibition.

Bio function analysis on the IPA software had greater similarity between soluble and insoluble fractions (Figure 5.5). Top functions represented in the soluble fraction were viral infection, infection by RNA virus, infection of cells, cell viability of tumour cell lines and infection of tumour cell lines. Whereas in the insoluble fraction they were cell movement, migration of cells, infection by RNA virus, infection of epithelial cell line and infection of embryonic cell line. Infection was the main function represented from both fractions, with a prediction of inhibition across most groups being observed. This may indicate that a loss of infection markers for infection may play a role in AD. However, *TREM2* variant control groups had activation of this function. The other top function represented was cell migration and movement and in contrast this function was predicted to be activated in all groups. *TREM2* variant groups had a higher amount of functions predicted to be activated than the cases without a *TREM2* variant, particularly in the soluble fraction. *TREM2* variant cases especially had an activated profile predicted throughout the top functions listed in the soluble fraction. The dementia disease/function was on the list of top diseases and bio functions listed for the insoluble fraction. It is predicted to be activated in all groups, although the *TREM2* variant controls had a lower z-score. This is a good validation of the methods and analyses used in this work.

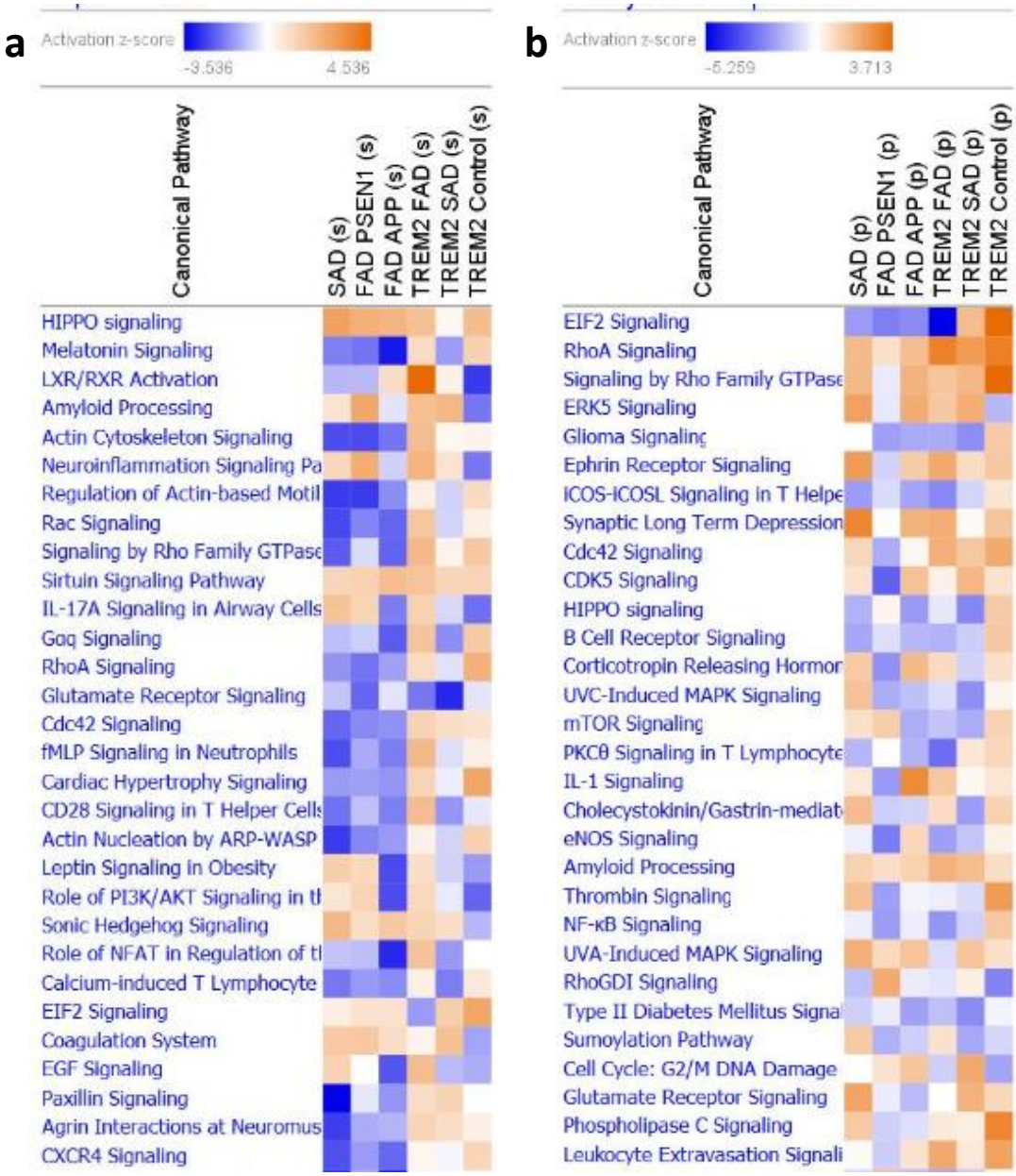

Figure 5.4: Canonical pathways represented in proteomic data. (a)Canonical pathways found in the soluble fraction according to z-score given by IPA software, (b) canonical pathways found in the insoluble fraction according to z-score given by IPA software. Orange represents a predicted activation of the pathway and blue represents a predicted inhibition of the pathway based on expression values found in the data. Intensity of colour relates to how activated or inhibited the pathway is predicted to be.

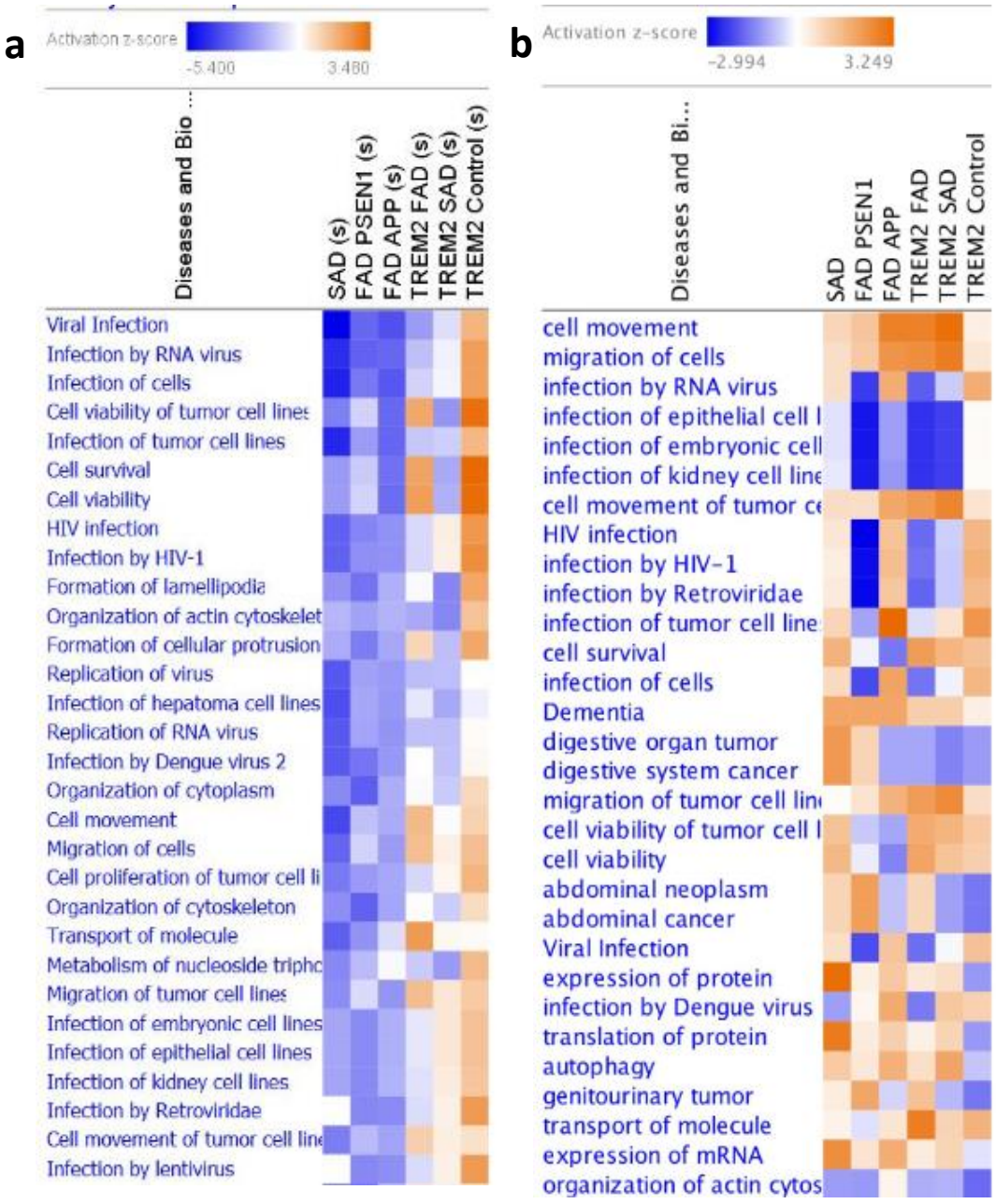

Figure 5.5: Diseases and functions represented in proteomic data. (a)Diseases and functions found in the soluble fraction according to z-score given by IPA software, (b) diseases and functions found in the insoluble fraction according to z-score given by IPA software. Orange represents a predicted activation of the pathway and blue represents a predicted inhibition of the pathway based on expression values found in the data. Intensity of colour relates to how activated or inhibited the pathway is predicted to be.

5.4.3. Comparative analysis

When comparing the genetic expression data obtained through nanostring methods and the protein expression data from the label-free mass spectrometry, it must be performed with limitations in mind. As the nanostring data only investigated 256 neuroinflammatory genes and 30 genes specific to neurodegeneration, neuroinflammatory pathways are more likely to appear as represented when comparing the two data sets. It is therefore, no surprise that when the top canonical pathways represented in each disease group and using each experiment were compared, the neuroinflammatory signalling pathway was present in all but the *TREM2* variant control group (Figure 5.7). However, this pathway was one of the top canonical pathways represented in the insoluble fraction of the proteomics showing that neuroinflammation is still a major factor at the protein level and should be investigated thoroughly. The neuroinflammation signalling pathway is predicted to be activated in both the nanostring and proteomic data of all groups apart from the proteomics of the FAD group, in which it is inhibited.

The general pattern when comparing the canonical pathways is that the pathways are predicted to be activated in the genetic expression data but inhibited in many of the proteomic data. The *TREM2* variant FAD case is different to this pattern in the fact that it has a higher level of activated pathways predicted in the soluble fraction compared to other groups. Additionally, the *TREM2* variant control group once again has a different profile in that the pathways most highly represented in this group are predicted to be inhibited at the

Figure 5.6: Overlap of over-represented GO biological process terms between disease groups when compared to controls between genetic and proteomic analysis. (a) nanostring data represented, (b) soluble fraction of proteomics, (c) insoluble fraction of proteomics. FAD sections include GO terms for both *PSEN1* and *APP* cases, *TREM2* sections include GO terms for *TREM2* SAD, *TREM2* FAD and *TREM2* controls.

genetic level but activated at the protein expression level. This again highlights how different the *TREM2* variant control group are to not only the other AD groups but the other cases that have a *TREM2* variant.

To look at the specific amount of overlap between different disease groups, the genes and proteins that had greater than 1.5 fold expression difference were entered into Webgestalt and represented GO biological processes were determined. The amount of overlap was then decided using the GOview online software. As depicted in Figure 5.6, the nanostring data had both a large amount of overlap of terms between groups and terms that were specifically over-represented in each disease group. However, when the same analysis was undertaken with the proteomic data, a large amount of terms were specifically seen in the *TREM2* variant group with fewer terms in the SAD and FAD groups and very minimal terms being overlapped between groups. This was true for both soluble and insoluble fractions and highlights that there are many differences in the expression seen at the genetic and proteomic levels.

5.5. Discussion

In this chapter, both the genetic and proteomic expression profiles have been investigated in SAD, FAD, *TREM2* SAD, *TREM2* FAD and *TREM2* controls and have been compared to controls before being compared to each other. Both sets of data give us an insight into the disease processes occurring in AD. The majority of the findings in this study confirm previous genetic or proteomic studies. However, here, the cases could be additionally split into cohorts of sporadic and genetically determined AD.

Using nanostring nCounter technology the gene expression of 256 Human inflammation genes and 30 neurodegenerative specific genes were investigated to determine the neuroinflammatory profiles of the different AD subgroups. Neuroinflammation was shown to be affected in all of the subgroups with *TREM2* SAD having a significantly upregulated neuroinflammatory profile in comparison to SAD. *TREM2* variant controls had the opposite profile with largely downregulated genes being observed compared to controls.

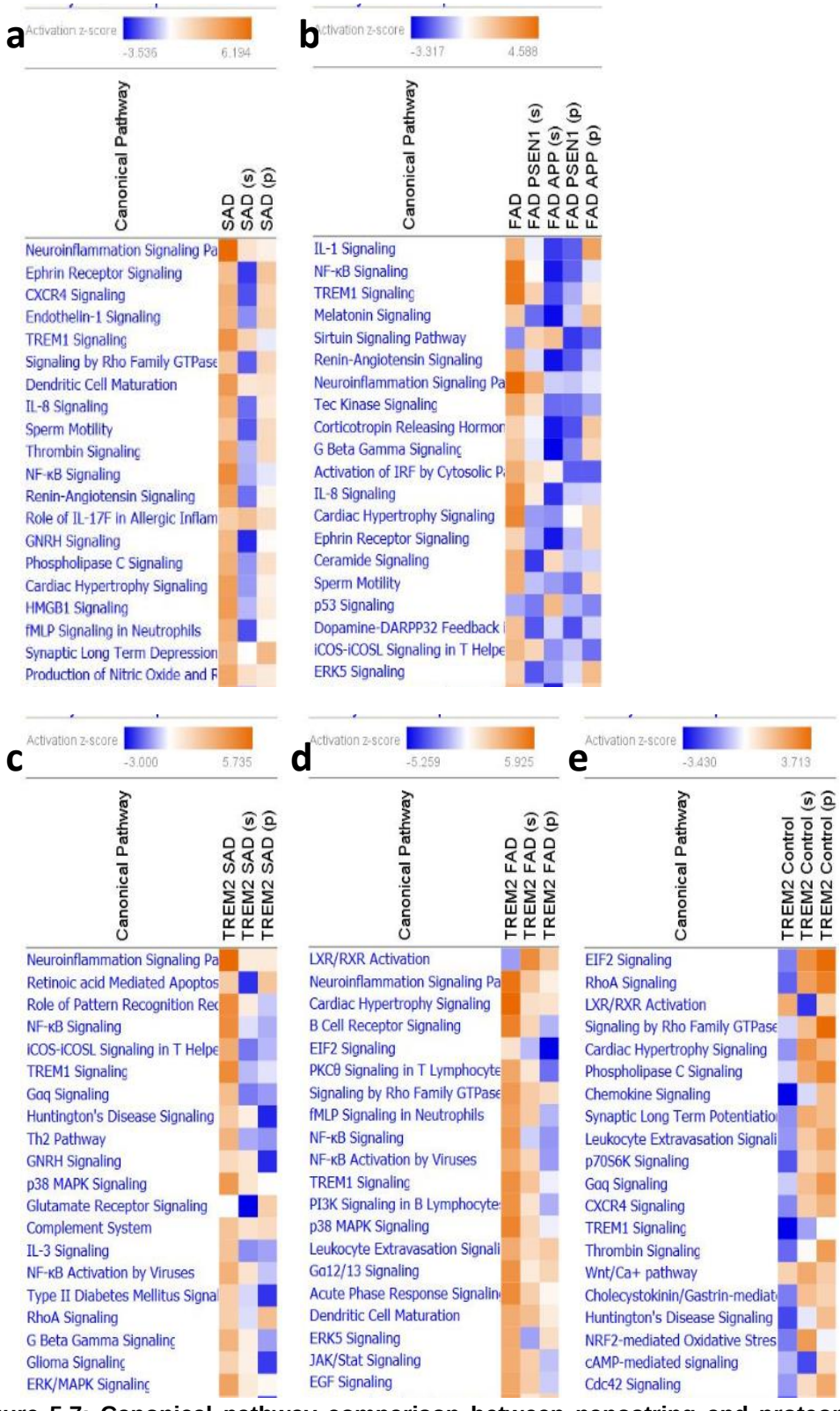

Figure 5.7: Canonical pathway comparison between nanostring and proteomic data sets. (a) comparison of top canonical pathways in SAD, (b) FAD, (c) *TREM2* SAD, (d) *TREM2* FAD and (e) *TREM2* controls compared to controls ordered by z-score determine by IPA software. First column is nanostring data, second column the soluble fraction of proteomics (s) and third the insoluble pellet fraction of proteomics (p). Orange represents a predicted activation of the pathway and blue represents a predicted inhibition of the pathway based on expression values found in the data. Intensity of colour relates to how activated or inhibited the pathway is predicted to be.

When looking in closer detail at the canonical pathways represented, we can see many pathways that may be implicated in AD pathogenesis. One of these, the role of pattern recognition receptors, highlights the role that TLR's may play between the different AD subgroups. TLR1-8 were upregulated in the SAD group but TLR2 and TLR4 were upregulated to a higher level in the *TREM2* variant SAD group. TREM2 acts via the ITAM motif present on its adapter protein DAP12. DAP12 negatively regulates the TLR response (Boutajangout and Wisniewski, 2013; Ito and Hamerman, 2012). Consequently, it is accepted that TREM2 inhibits the TLR response and therefore suppresses the pro-inflammatory cytokines produced (Boutajangout and Wisniewski, 2013; Hamerman et al., 2005). As *TREM2 R47H* variants are thought to have a loss-of-function mutation and not bind to its ligands as effectively, the TLR response is no longer suppressed, further pro-inflammatory cytokines are released and cell death continues to occur. As an increase is seen in the TLR gene expression in *TREM2* variant SAD cases compared to SAD cases without a *TREM2* variant, the TLR response may be exacerbated in these variants, leading to more neuroinflammation than normal which may play a role in why *TREM2* variants cause a risk to late onset AD. However, these TLR's are downregulated in *TREM2* variant controls, meaning that another factor must be needed for TLR's to become upregulated in the presence of a *TREM2* variant.

Label-free proteomics was utilised to determine the proteomic profile of any proteins in these different cases and determine if the genetic expression data translated to the protein level. Neuroinflammation was not found to be the most highly represented canonical pathway at the protein level but it was one of the top pathways represented in the insoluble fraction, highlighting that neuroinflammatory mechanisms are important in AD pathogenesis. As plaques are likely to be in the insoluble fraction, this could indicate that neuroinflammation plays a role in amyloid plaque pathology.

Astrocytes are also thought to play a part in the neuroinflammatory processes observed in the brain and in neurodegenerative disease. An upregulation of the *GFAP* gene, a marker for reactive astrocytes, was observed in the SAD and FAD groups as well as an upregulation of this protein across all groups. The *TREM2* variant SAD group however, had a larger

increase than any other group. This would suggest that although TREM2 is found on microglia, the downstream signalling cascades that stem from it also affect the neuroinflammatory processes that are found within astrocytes.

As would be expected in AD brain, the proteomic data showed increases in genes associated with amyloid and tau pathology, with amyloid processing being one of the top canonical pathways represented in both the soluble and insoluble fractions of the proteomics. Most of the proteins that were involved with amyloid processing or in Aβ fibrillisation (*COL25A1, CTGF, CRABP1, CRK, BGN, HBG2, KCNIP4, HTRA1, PPIL2*) were observed to change in the FAD cases. As the pathogenic mutations in either *PSEN1* or *APP* cause an increased production of Aβ, the fact other proteins involved in these processes are affected most in these cases is logical. APP had the highest fold change compared to controls in *TREM2* variant FAD and *TREM2* variant SAD, suggesting the production of APP alters in these *TREM2* variant cases. The same was true for MAPT, with the highest upregulation occurring in the *TREM2* variant SAD cases. The loss of function of *TREM2* variants may lead to an altered pro-inflammatory microglial phenotype, which then results in increased production of APP and MAPT.

Two proteins commonly found in the presence of neurofibrillary tangles, NEDD8 and MAP1B were both found to be upregulated in the *TREM2* variant control cases. NEDD8 is a ubiquitin-like protein and promotes proteasomal degradation. As these are upregulated in *TREM2* controls, it may suggest that these cases do still have the potential for neurofibrillary tangle pathology to occur but another factor is stopping the process from occurring or progressing.

Cytoskeletal signalling cascades have been identified previously to be affected in AD, with both actin and microtubule organisation being affected (Henriques et al., 2015). The results here suggest that these pathways are changing the most within AD, at least at the protein level. Actin cytoskeleton signalling was in the top five canonical pathways represented in the soluble fraction of the proteomic data with a prediction that it was inhibited in most AD subgroups. However, the pathways RhoA signalling, signalling by Rho family GTPases and ERK5 signalling were all in the top five canonical pathways represented in the insoluble

fraction of the proteomics, with a prediction that they are activated across AD subgroups. Breakdown of the cytoskeleton in the neurons, leads to impaired axonal transport, synaptic dysfunction and ultimately cell loss (Henriques et al., 2015). Unlike other changes observed, these pathways were affected in all AD subgroups in a similar manner. There were no differences observed in the *TREM2* variant cases. This could indicate that although cytoskeletal abnormalities are an important factor for AD pathogenesis, it does not contribute to the risk of developing the disease in *TREM2* variants carriers.

Other pathways and proteins that are affected are those involved with cell proliferation. The top represented canonical pathway in the soluble fraction of proteomics was HIPPO signalling. HIPPO signalling is a pathway involved in controlling cell proliferation as well as apoptosis. Inhibition of this pathway has been shown to cause cancer due to increased proliferation and decreased cell death (Wang and Wang, 2016). In AD, it has been suggested this pathway becomes hyperactivated, acts through binding to APP and causes decreased cell proliferation (Wang and Wang, 2016). This study has confirmed that as HIPPO signalling is predicted to be activated across all the disease subgroups. As further evidence of cell proliferation being affected, the protein ASAP3 was one of the top downregulated proteins in all groups other than the FAD *PSEN1* group and this protein promotes cell proliferation. Also, PSMB7 is upregulated in *TREM2* variant controls but inhibits cell proliferation. CCNG1, on the other hand, is downregulated in *TREM2* variant SAD cases but also inhibits cell proliferation. Although differences are not observed between disease subgroups, the regulation of cell proliferation is clearly important in AD and needs to be investigated further.

APOE was another protein upregulated compared to controls across all disease subgroups in the insoluble fraction. As APOE can bind to Aβ plaques that would precipitate in the insoluble fraction, this may explain the increase. However, the amount of upregulation was much higher in all groups compared to the *TREM2* variant controls and was highest in the *TREM2* variant SAD cases. *APOE* is also a risk factor for late onset AD with similar odds to that of *TREM2*. Therefore, determining what effect is had by *APOE* genotype and which effect by *TREM2* risk variants can be difficult to decipher. As individual cases were pooled

for proteomic analysis, a separate analysis based on *APOE* genotype is not possible. However, the *TREM2* variant controls did not contain any *ApoE4* alleles and the *TREM2* variant SAD cases all contain at least one *ApoE4* allele. It is therefore interesting that the *TREM2* variant controls have a markedly different neuroinflammatory profile compared to *TREM2* variant SAD cases. An *ApoE4* allele could be the additional factor that is required for the *TREM2* variant effect on the pathways discussed above. Age of onset and disease duration do not significantly differ between *TREM2* variants with an *ApoE4* allele and SAD cases with an *ApoE4* allele. Therefore, it is feasible that these cases are working along similar mechanisms.

TREM2 and APOE have been shown to bind and Krasemann et al., (2017) suggest that APOE triggers the TREM2 signalling pathway (Atagi et al., 2015; Bailey et al., 2015; Jendresen et al., 2017). These results may support this theory in part. TLR activators have been shown to also reduce microglial expression of TREM2 with further reduction seen in *ApoE4/4* carriers compared to other genotypes (Li et al., 2015). As mentioned previously, reduced TREM2 leads to an increased TLR response and release of further pro-inflammatory cytokines which exacerbate disease. APOE is a lipoprotein and lipoproteins are responsible for activating TLR2. TLR2 was found to be upregulated in *TREM2* variant SAD cases at a greater level to SAD cases. As the *TREM2* variant SAD cases all carry one *ApoE4* allele, a greater reduction of TREM2 expression may be seen, leading to increased TLR activation and a pro-inflammatory signalling cascade to ensue. As the *TREM2* variant controls do not contain an *ApoE4* allele, this cascade may not occur in these cases, leading to the different profile of TLR activation and neuroinflammation that is observed.

Comparisons between the nanostring data and the proteomic data highlights multiple approaches are needed to decipher the underlying pathological mechanisms in these diseases and that we will gain the most accurate information if we continue to complete multi-omic datasets and look at network biology. Furthermore, stratifying the cases we investigate according to their pathological and genetic background will enable us to visualise the whole picture. Large differences between expression at the genetic and proteomic levels could be explained as either compensatory mechanisms at the translational level for

differences occurring at the transcriptional level or alternative splicing regulation/dysregulation. A proteomic study identified that cells exposed to Aβ42 displayed spliceosome dysregulation, suggesting that this could be a possibility (Nuzzo et al., 2017). Additionally, a number of miRNA's have been reported to be reduced in AD, such as miR-339-5p found to regulate expression of BACE1 and miR-132/212 found to regulate tau expression (Long et al., 2014; Smith et al., 2015). Further investigation into the different isoforms expressed for the proteins changing in the greatest amounts would help us to understand these changes in greater detail.

5.5.1. Conclusions

In summary, pathways involved in neuroinflammation, cytoskeletal organisation, cell proliferation and amyloid processing have been shown to change in AD compared to controls at either the genetic or proteomic level across multiple cell types. *TREM2* variant SAD cases appear to have an altered genetic neuroinflammatory profile compared to SAD and FAD cases. Particular changes in TLR gene expression in *TREM2* variant SAD groups compared to other AD groups lacking a *TREM2* variant are apparent and indicate a mechanism in which *TREM2* variants could confer risk of AD. *TREM2* variant controls have a strikingly different neuroinflammatory genetic profile and altered proteomic expression of proteins associated with AD pathology and reactive astrocytes when compared to normal controls. This indicates that changes do occur in these TREM2 variants but they do not have the same effect as in *TREM2* variant SAD cases. These *TREM2* variant controls lack an *ApoE4* allele and have the opposite effect to *TREM2* variant SAD cases with an *ApoE4* allele. *APOE* genotype could be important to determine which effect a *TREM2* variant may have. Further investigation to determine if these effects are independent of each other or not need to be undertaken for us to fully elucidate the role of *TREM2* variants and why they confer risk of AD. Whilst this investigation does not decide whether inflammation is causing AD or just a consequence, it points towards it having a role in the pathogenesis of *TREM2* variants.

Chapter 6

Could the presubiculum be protected from neurodegeneration observed in AD and *TREM2* variant cases?

6 Could the presubiculum be protected from neurodegeneration observed in AD and *TREM2* variant cases?

6.1 Abstract

Introduction: One of the most severely affected regions of the brain in AD is the hippocampal formation and parahippocampal region. This region can be divided into subregions, which include the presubiculum. The presubiculum is medially adjacent to the entorhinal cortex and is shown to connect anatomically with both the entorhinal cortex, the hippocampus and deeper brain nuclei. Over a decade ago, it was observed that the adjacent regions, subiculum and entorhinal cortex, have differing Aβ composition/appearance. Both the entorhinal cortex and the subiculum contain Aβ plaques, whereas the presubiculum has one large diffuse 'cloud' of Aβ. Here some of the variables that influence the formation of the Aβ deposits found in the presubiculum were investigated and analysed to determine if there was an identifiable factor in this region that made it resistant to further AD pathogenesis.

Materials and methods: Immunohistochemistry was carried out with Aβ, AT8, Iba1, CD68, CR3-43 antibodies on the hippocampus, taken at the level of the lateral geniculate body. This level contained both the presubiculum and entorhinal cortex of SAD (n=19), FAD (n=11) and *TREM2* variant AD (n=3) cases and immunohistochemistry was performed to make pathological comparisons between the areas. Fluorescent Aβ immunohistochemistry combined with Thioflavin-S histological staining was also performed to visualise the Aβ conformational state in both regions. Tau and microglial density were calculated with Image J analysis of random squares from both the presubiculum and entorhinal cortex. The number of NFT's were counted manually. The specific Aβ peptides present within the presubiculum and entorhinal cortex were determined following laser-capture microdissection (LCM) paired with matrix assisted laser desorption ionisation time-of-flight mass spectrometry analysis. Immunohistochemistry using antibodies against N-terminally truncated and pyroglutamate

modified Aβ peptides was performed to validate results. Label-free quantitative mass spectrometry using a Synapt G2-Si High Definition QToF with 2D fractionation was used to determine if there were any proteomic differences between the two regions.

Results: Aβ immunohistochemistry showed a large non-fibrillar Aβ deposit in the presubiculum and fibrillar dense core Aβ plaques in the entorhinal cortex of SAD, FAD and *TREM2* variant cases. Significantly less hyperphosphorylated tau and significantly less NFT's were observed in the presubiculum compared to entorhinal cortex in both SAD and FAD cases. Iba1 microglial levels only changed in SAD cases with significantly more microglia being observed in the presubiculum and with other disease groups showing no difference. Activated microglial markers, CD68 and CR3-43 both show significantly less microglial activation in the presubiculum compared to the entorhinal cortex. Aβ peptide analysis identified more N-terminally truncated and pyroglutamate modified Aβ peptides present in the entorhinal cortex compared to minimal unmodified Aβ peptides present in the presubiculum. However, immunohistochemistry with antibodies for varying Aβ peptides was detected in both regions. Proteomic analysis revealed many changes in expression between the presubiculum and entorhinal cortex. Changes were observed in APP processing, Aβ deposition, Aβ clearance, Aβ toxicity, tau accumulation and microglial activation.

Conclusions: This study demonstrated that the Aβ deposition/composition and the microglial response in the presubiculum is morphologically and proteomically diverse from its neighbouring region, the entorhinal cortex. The changes observed in the presubiculum result in less aggregation of Aβ and tau and reduced microglial activation. Why this area responds differently to AD pathogenesis remains unclear. Further biochemical analysis of this area and the proteins mentioned here are needed to elucidate what causes this phenomenon and its effect. Understanding what factor(s) are the key to this neuroprotective mechanism, could lead to therapeutic neuroprotection that can be applied to the whole brain and halt AD disease progression.

6.2 Introduction

6.2.1 Parahippocampal anatomy and connections

One of the most severely affected regions in AD is the hippocampal region (Akiyama et al., 1990; Wisniewski et al., 1998). The hippocampus is an important region for memory function and memory loss is one of the first symptoms of AD. It is also an important area for navigation, shown by the discovery that place cells, grid cells and head direction cells provide a navigational map (Nassar et al., 2015; O'Keefe and Nadel, 1978; Simonnet et al., 2017; Tukker et al., 2015).

The neuroanatomy and connectivity of this region of the brain has been studied in great detail and has several sub-regions as depicted in Figure 6.1. The hippocampal formation is formed of the dentate gyrus, the CA3/4, CA2, CA1 areas and the subiculum. Directly adjacent to this is the parahippocampal region which is connected with the hippocampal formation through a pathway known as the perforant pathway (Augustinack et al., 2010; Caballero-Bleda and Witter, 1994; van Strien et al., 2009). The parahippocampal region is made up of the pre- and para- subiculum, the transsubiculum and the entorhinal cortex (Drexel et al., 2013). In rodents, the presubiculum area is further classified into the presubiculum and the postsubiculum (Ding, 2013).

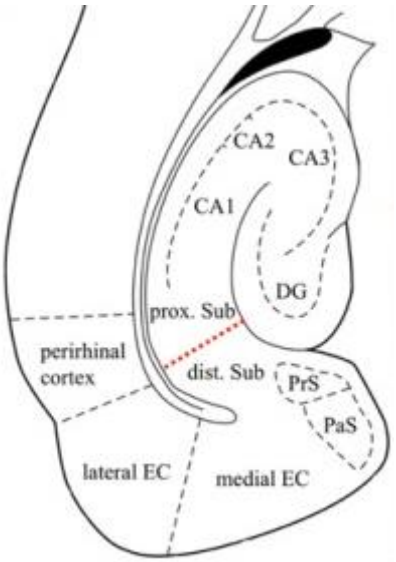

Figure 6.1: Anatomy of the hippocampus and parahippocampal region. Modified from Drexel et al. 2013. DG, dentate gyrus; Sub, Subiculum; PrS, Presubiculum; EC, entorhinal cortex

Originally it was thought that the only connection between the parahippocampus and the hippocampal formation were the projections arising from the entorhinal cortex via the perforant pathway. However, it is now known that a number of other subregions in the parahippocampus send efferent fibres to the hippocampal formation, with the presubiculum being one (Caballero-Bleda and Witter, 1994). The presubiculum has several afferent and efferent connections both within the hippocampal/parahippocampal area and to further areas of the brain (van Groen and Wyss, 1990). There is evidence that the presubiculum sends projections to the; dentate gyrus, CA3, CA1, subiculum, parasubiculum, septum, anterior thalamic nuclei, retrosplenial cortex and most prominently the entorhinal cortex (Akiyama et al., 1990; van Groen and Wyss, 1990; van Strien et al., 2009). For example, Simonnet et al., (2017) report that thalamic afferents recruit presubicular principal neurons and Martinotti interneurons and that these projections have a role in head direction signals. Reports show that these interneurons have a wide variation in their physiological properties (Nassar et al., 2015; Tukker et al., 2015). The parasubiculum also sends projections to the entorhinal cortex, however they are quite distinct in the fact that the parasubiculum sends projection to layer II of the entorhinal cortex, whereas the presubiculum sends projections to layer III of the entorhinal cortex (Caballero-Bleda and Witter, 1994). The fact that these layers project on to different areas of the hippocampal formation could be important for function (Caballero-Bleda and Witter, 1994). The presubiculum differs from its neighbouring areas, such as the medial entorhinal cortex, due to the fact its superficial layers do not have large amounts of excitatory connectivity (Couey et al., 2013; Dhillon and Jones, 2000; Fuchs et al., 2016; Pastoll et al., 2013; Peng et al., 2017).

Furthermore, James Papez noted in 1937 that there was a direct connection between the hippocampus and the hypothalamus involving a number of brain regions (Papez JW, 1937). This was later proved to be true and referred to as the Papez circuit (Figure 6.2) (Shipley, 1974). The presubiculum forms part of this circuit with connections arising from the supramamillary region onto the anterior thalamic nuclei to the cingulate cortex before the presubiculum (Akiyama et al., 1990; van Groen and Wyss, 1990; Shipley, 1974). The presubiculum then connects this to the perforant pathway via the entorhinal cortex and is often referred to as the “relay centre” (Akiyama et al., 1990; Kalus et al., 1989).

6.2.2 Pathological observations in the presubiculum

Over two decades ago, a few groups observed that the presubiculum showed different pathological properties in AD when compared to the other subdivisons of the hippocampal formation and the parahippocampal region (Akiyama et al., 1990; Kalus et al., 1989; Wisniewski et al., 1998). They observed that this area did not contain Aβ plaques but instead had a 'cloud' or 'lake-like' pattern of diffuse Aβ staining that seemed to fill the presubiculum (Kalus et al., 1989).

Nissl staining was used to identify the presubiculum, as the parvopyramidal layer of the presubiculum is formed of small densely packed pyramidal neurons that have large nuclei, which are easily identified from the larger, less densely packed neurons of the parvopyramidal layer of the parasubiculum (Akiyama et al., 1990; Braak, 1978; Ding, 2013; van Groen and Wyss, 1990; Kalus et al., 1989). Acetylcholine esterase staining also

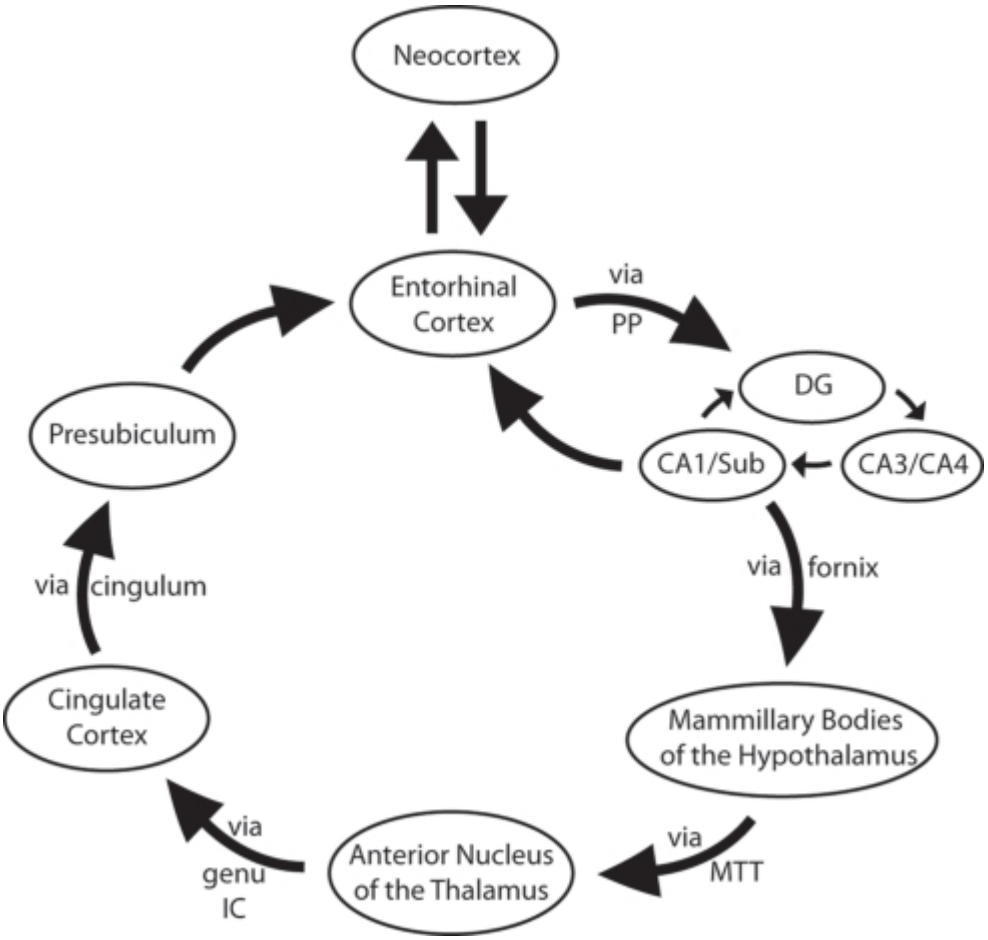

Figure 6.2: Papez circuit and the connections between the regions involved. Modified from Augustinack et. al 2010. PP, perforant pathway; DG, dentate gyrus; genu IC, genu of the internal capsule; MMT, mamillothalamic tract; Sub, Subiculum.

produced a different pattern between the parasubiculum and the presubiculum, resulting in a further method of identification (Ding, 2013; van Groen and Wyss, 1990).

Comparing the Nissl staining with either Aβ immunohistochemistry or Thioflavin-S and Congo-red stains showed that only diffuse amyloid was identified within this area as the presubiculum was negative for amyloid in the β-sheet conformation (Akiyama et al., 1990; Wisniewski et al., 1998). Additionally, Ji et al., (2015) highlighted that the PiB radioligands, used as a PET ligand to detect amyloid, did not bind to the presubiculum in AD, further confirming that the Aβ in the presubiculum is not in an amyloid conformational state. Wisniewski et al., (1998) however, did note that there may actually be a higher total percentage of Aβ load in the presubiculum compared to other hippocampal areas. Only sparse NFTs were seen in the presubiculum, considerably lower amounts than that of the subiculum or CA1 areas (Akiyama et al., 1990; Kalus et al., 1989; Wisniewski et al., 1998). Additionally, no activated glial staining was present in the presubiculum, which led to suggestions that the Aβ production/clearance mechanisms may be impaired in this region (Akiyama et al., 1990; Wisniewski et al., 1998). No amyloid- associated proteins were detected here either; neither proteins that promote amyloid fibrilisation e.g. ApoE, or proteins that inhibit amyloid fibrillisation e.g. ApoJ (Wisniewski et al., 1998). In contrast, the entorhinal cortex shows severe neuronal loss, dense core amyloid plaques, frequent NFT's, activated microglia and activated astrocytes (Akiyama et al., 1990; Ji et al., 2015; Kalus et al., 1989; Wisniewski et al., 1998).

Imaging studies have shown that both the presubiculum and subiculum areas show prominent atrophy from early stages in the disease, namely mild cognitive impairment (MCI) stage, which progressively worsens with disease progression (Carlesimo et al., 2015). The authors suggest that this may be because of degeneration of the perforant pathway, which the presubiculum is a part of. Mizutani and Kasahara, (1997) have shown previously that this pathway is degenerated in AD and that this starts in the entorhinal cortex and is spread through the subiculum and into the hippocampus. However, they made no mention as to whether this affects the presubiculum in this pathway.

Further to this, McCuUoch and Dewar, (1991) report that the presubiculum has six times the amount of galanin binding sites than the other hippocampal or parahippocampal regions. Galanin is thought to inhibit the acetylcholine release in rats (Girotti et al., 1993). As acetylcholine release is reduced in AD brains, the presence of more galanin binding sites could be one way in which the presubiculum is protected from the effects of AD (Kása et al., 1997).

This phenomenon of diffuse amyloid deposits in the presubiculum is not unique to AD. However, this has not previously been reported in the literature. The pathological 'cloud' hallmark is visualised in the presubiculum in other forms of dementia such as Familial British Dementia and Familial Danish Dementia as well as some forms of Prion disease (Murray et. Al, manuscript in preparation).

Although the presubiculum was previously overlooked as an important region within the parahippocampus, its high connectivity with other important regions, both for memory and navigation, suggest otherwise. The different type of pathology in this region compared with the traditional pathology seen in the other hippocampal and parahippocampal regions indicate that the presubiculum has different properties. Diffuse amyloid deposits are seen from early in disease (Thal phases 2 and 3) and do not change through to end stage disease, with reports of these large deposits being seen in non-demented aging cases (Akiyama et al., 1990; Wisniewski et al., 1998).

6.2.3 Amyloid plaque composition

The amyloid plaques that are present in AD are composed of aggregated Aβ protein. Aβ is formed when cleavage of the amyloid precursor protein (APP) occurs by the secretases (Russo et al., 2002). Aβ peptides of varying length occur due to the secretases cleaving at different points at both the N-terminus and the C-terminus (Chávez-Gutiérrez et al., 2012; Russo et al., 2002; Szaruga et al., 2015).

The four most dominant Aβ peptides are Aβ1-42, Aβ1-40, Aβ4-42 and pGluAβ3-42 (Bouter et al., 2013; Portelius et al., 2010, 2015; Russo et al., 2002). The full-length Aβ protein is formed of residues Aβ1-42 however; the Aβ1-40 peptide is also highly abundant and has

been shown to be less prone to aggregation (Pike et al., 1995). The β-sheet formation of the fibrils is due in part to pGluAβ3-42 affecting the α-helix structure and in mice it has been shown that Aβ4-42 is linked to behavioural memory deficits (Bouter et al., 2013; Goldblatt et al., 2015). A range of N-terminally truncated and pyroglutamate-modified Aβ peptides have been detected and shown to be more toxic than the full length peptides (Miller et al., 1993; Pike et al., 1995; Portelius et al., 2010, 2015; Russo et al., 2002). Russo et al., (2002) reports that cleavages at the N-terminus make the peptide more prone to toxicity which affects its degradation properties, whereas cleavages at the C-terminus affect the fibril morphology.

Portelius et al., (2015) determined that AD patients have a higher amount of N-terminally truncated and pyroglutamate-modified peptides than pathological aging cases (AD pathology without cognitive decline). N-terminally truncated peptides have been detected both in familial and sporadic forms of AD, however, they appear to be observed earlier in familial cases and in Down syndrome cases, with the protein load being linked to disease severity (Portelius et al., 2010; Russo et al., 2002).

6.2.4 Aims

In this chapter, Aβ immunohistochemistry was used to determine the pathological differences that are observed between the presubiculum and the entorhinal cortex. In this study SAD, FAD and *TREM2* variant AD cases were compared to determine if the presubiculum differs between different AD subgroups. Laser-capture microdissection paired with mass spectrometry was employed to identify the Aβ peptide species present in the presubiculum and entorhinal cortex. Various antibodies for different N-terminally truncated and pyroglutamate modified Aβ isoforms were used with immunohistochemistry to determine if the composition of Aβ differed between the presubiculum and the entorhinal cortex.

To understand whether this area is fully protected from AD pathology, the density of hyper-phosphorylated tau and microglia using multiple microglial markers were determined as well as the number of NFT's counted.

To assess which proteins are present in the presubiculum and determine their expression levels compared to those in the entorhinal cortex, quantitative label- free mass spectrometry was performed. These results were analysed to determine if the presubiculum has specific tissue factors or pathways altered in comparison to the neighbouring entorhinal cortex.

6.3 Materials and Methods

6.3.1 Case selection

All case demographics are detailed in Table 2.3. Cases 1, 2, and 5-36 were used for Aβ immunohistochemical comparison between the presubiculm and entorhinal cortex (SAD (n=19), FAD (n=11), *TREM2* SAD (n=3)). Case 25 was used for fluorescent immunohistochemistry and histological Thioflavin-S staining. All cases were used for pathological analysis of tau and microglia using the antibodies, AT8, Iba1, CD68 and CR3-43. Cases 1, 5, 9, 25, 27 and 30 were used to determine the type of Aβ peptide present (SAD (n=2), FAD (n=2), *TREM2* SAD (n=2)). Case 29 was used for immunohistochemistry with a range of N-terminally truncated and pyroglutamate modified Aβ isoforms. Cases 1, 5, 9, 13, 14, 16, 33 and 34 were used for quantitative label-free mass spectrometry (SAD (n=4), FAD (n=2), *TREM2* SAD (n=2)).

6.3.2 Immunohistochemistry

Immunohistochemistry with Aβ, AT8, Iba1, CD68, CR3-43, 1-57 (N-terminal AβpE3), 2-48 (N-terminal AβpE3) and pE (pyroglutamate) antibodies was performed, as described in 2.4, on the parahippocampus region. Details of the antibodies used in this study are listed in Table 2.6. Sequential sections of the same region were taken for each antibody. The Aβ immunohistochemistry was used to determine where the presubiculum was, the large diffuse area of staining, and this was used to select the same area on the other sequential sections.

Thioflavin-S staining was performed, as described in 2.4.4, alongside fluorescent Aβ immunohistochemistry.

6.3.3 Pathological analysis

Density analysis for AT8, Iba1, CD68, and CR3-43 was calculated using methods described in 2.5. The number of NFT's were then manually counted after cases were blinded.

6.3.4 LCM

Laser-capture microdissection was used as described in 2.7.1 to capture the presubiculum and three-hundred amyloid plaques from the entorhinal cortex for each case analysed. Individual plaques were used here as we were directly comparing the Aβ species distributed in the regions. Secondly, the presubiculum and an area of the entorhinal cortex of the same size were captured and used for quantitative label- free mass spectrometry. Here the whole region was captured as we were looking for any proteomic changes.

6.3.5 Proteomics

To assess the type of Aβ peptides present in the presubiculum and entorhinal cortex, laser-captured samples were taken and sent to Prof. Henrik Zetterberg's lab for matrix assisted laser desorption ionisation time-of-flight mass spectrometry analysis using the methods described in 2.7.6.

To assess which proteins were present and their expression in both the presubiculum and entorhinal cortex, laser-captured samples were protein extracted, digested, and run on a Synapt G2-Si High Definition machine with 2D fractionation to perform quantitative label-free mass spectrometry. These methods are described in more detail in 2.7.2, 2.7.3, 2.7.4, 2.7.5. Fold change was calculated by dividing one region by the other for each protein.

6.3.6 Statistics

Wilcoxon paired rank tests were used to determine significance between the presubiculum and entorhinal cortex for each disease group with the AT8, Iba1, CD68 and CR3-43 antibodies. GraphPad Prism v7 was used to complete this analysis.

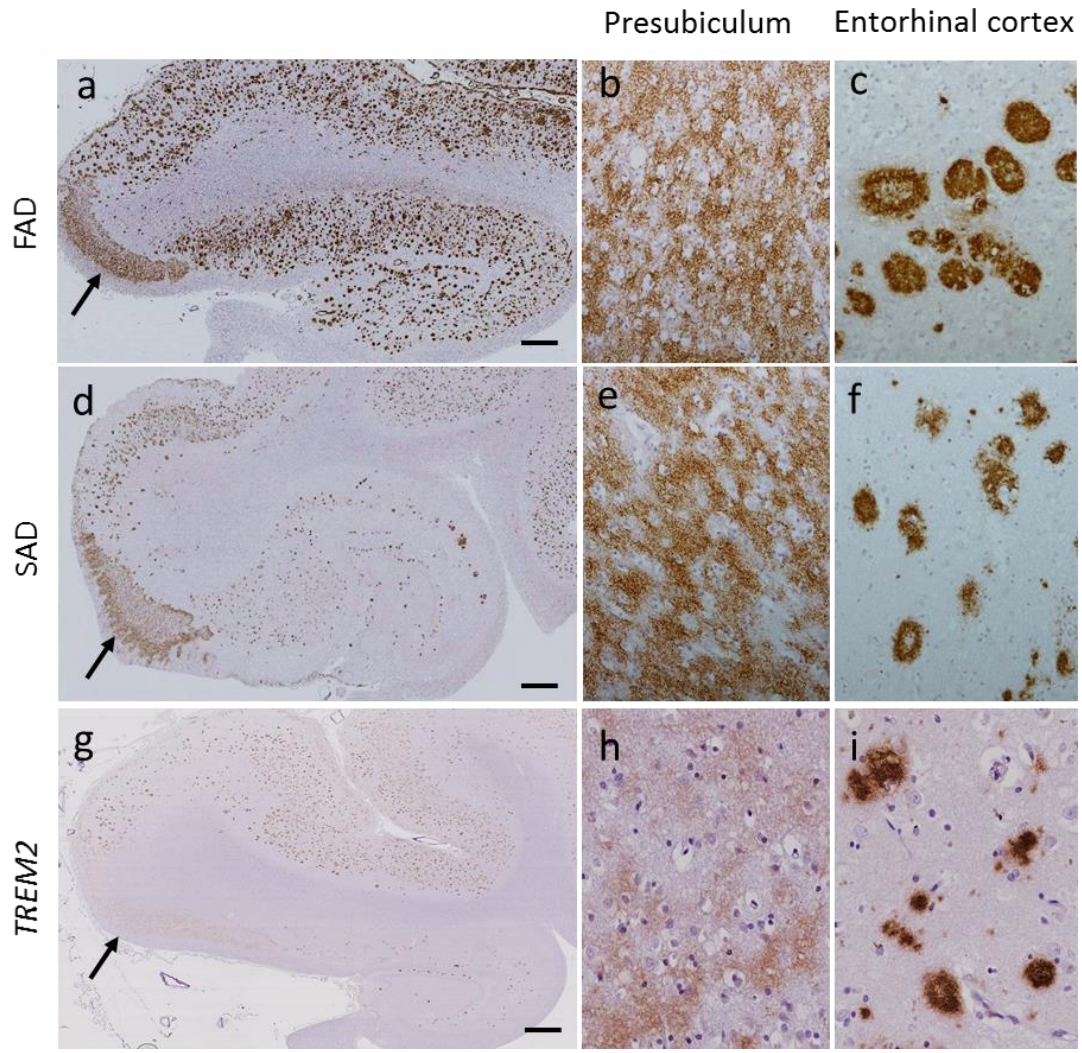

Figure 6.3: Pathological analysis of the presubiculum in familial (FAD, case 33, a-c), sporadic (SAD, case 8, d-f), and *TREM2* variant (case 1, g-i) Alzheimer's disease. Aβ immunohistochemistry demonstrated the presence of a large diffuse deposit in the presubiculum (a, d, g, black arrow) and can be seen at higher magnification (b, e, h). The adjacent entorhinal cortex showed mature Aβ plaques (c, f, i) Bar in a, d and g represents 1000 µm and it represents 50 µm in all remaining images.

6.4 Results

6.4.1 Amyloid pathology in the presubiculum

Aβ immunohistochemistry identified that the morphology of the Aβ deposits in the presubiculum is different to the Aβ morphology in the neighbouring regions, the subiculum and the entorhinal cortex in AD. The presubiculum contained a 'lake-like' diffuse Aβ deposit

and the entorhinal cortex contained mature Aβ plaques. This large diffuse area of staining in the presubiculum was observed in all SAD, FAD and *TREM2* variant AD cases (Figure 6.3) and did not differ when comparing different disease durations or stages of pathology.

To show that the Aβ being deposited in the presubiculum is diffuse in nature, and not in an amyloid conformational state, fluorescent Aβ immunohistochemistry alongside Thioflavin staining was performed. The large deposit found in the presubiculum was identifiable with fluorescent Aβ immunohistochemistry (Figure 6.4b, white arrow) but was Thioflavin-S negative (Figure 6.4d), indicating that the Aβ in this region is in a pre-amyloid conformational state. The Aβ plaques in the entorhinal cortex, however, were Aβ-positive and Thioflavin-S positive (Figure 6.4c and e), demonstrating that they have the β-pleated structure required for an amyloid conformation.

6.4.2 Tau pathology in the presubiculum

To determine if a similar pattern could be observed for both AD pathological hallmarks, the amounts of phosphorylated tau in the presubiculum and entorhinal cortex were determined using AT8 immunohistochemistry. AT8 staining includes NFT's, neuropil threads and neurites. When determining the density of the tau immunohistochemistry there was significantly less AT8 staining in the presubiculum than in the entorhinal cortex (Figure 6.5) in both SAD ($p<0.0001$) and FAD ($p=0.001$) groups, with the same trend being observed in the *TREM2* variant AD cases (Figure 6.6a). Further to this, the number of NFT's were quantified with significantly less NFT's being observed in the presubiculum compared to the entorhinal cortex in SAD ($p<0.0001$) and FAD ($p=0.001$), with the *TREM2* variant AD cases also following the same trend.

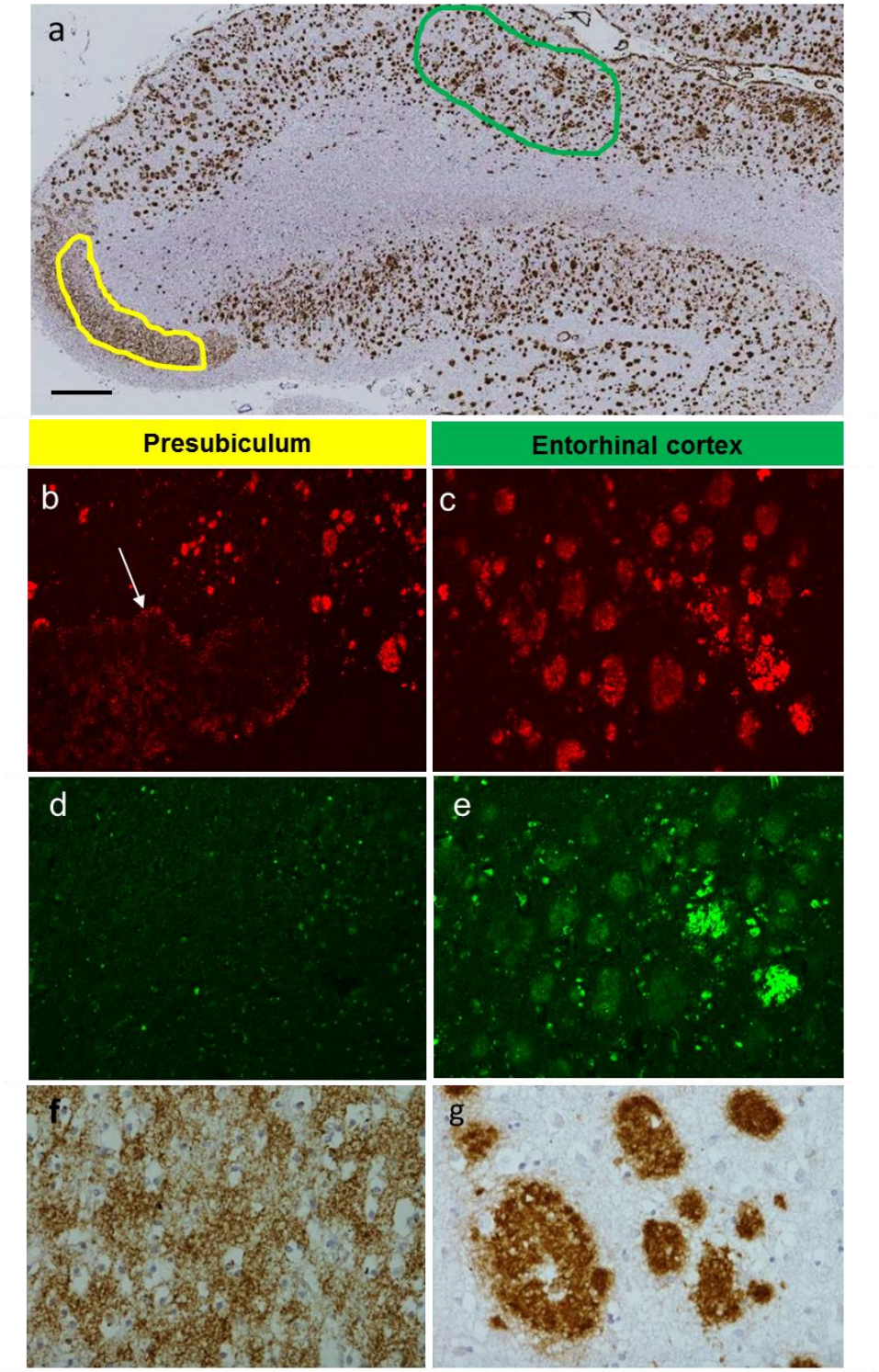

Figure 6.4: Pathological comparisons of the presubiculum and entorhinal cortex in Alzheimer's disease. Aβ immunohistochemistry in an AD case where the presubiculum area is highlighted with yellow and the entorhinal cortex green (a, case 25). Higher magnification images can be seen of the presubiculum (f) and the entorhinal cortex (g). Fluorescent Aβ immunohistochemistry highlights the contrast between the diffuse nature of the presubiculum (b, white arrow) and the entorhinal cortex (c) which is confirmed by negative Thioflavin staining of the presubiculum (d) and positive staining in the entorhinal cortex (e). Bar in (a) represents 1000μm in a; 100μm in b, c, d, and e; 50μm in f and g.

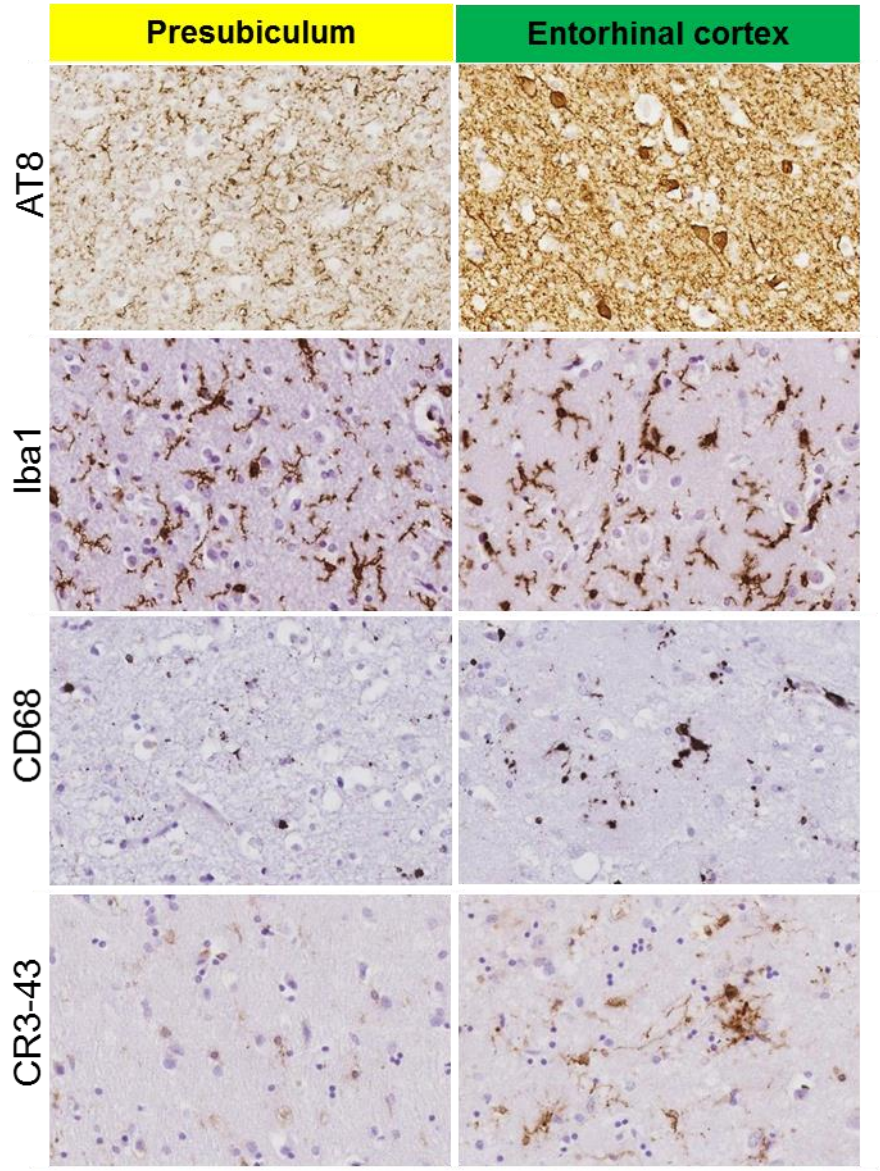

Figure 6.5: Tau and microglial comparisons between the presubiculum and entorhinal cortex in Alzheimer's disease. Tau immunohistochemistry shows the difference between the density of neuropil threads and neurofibrillary tangles in the presubiculum and entorhinal cortex. The microglial marker, Iba1, shows the number of microglia being similar between the two regions, whereas CD68 and CR3-43 highlight the increase in the number of activated microglia in the entorhinal cortex compared to the presubiculum.

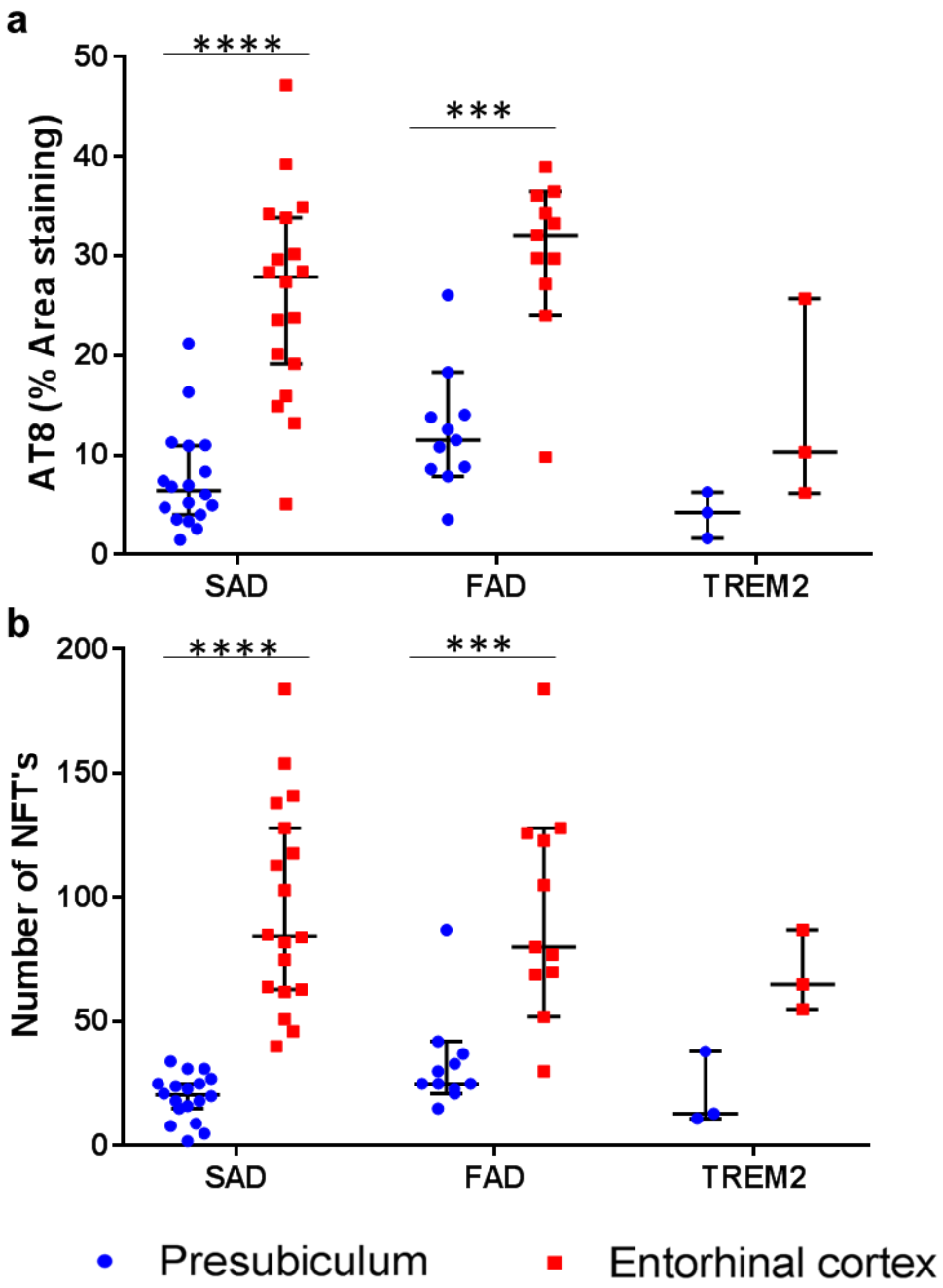

Figure 6.6: Quantification of tau immunohistochemistry in the presubiculum and entorhinal cortex. The density of the tau immunohistochemistry observed in the entorhinal cortex and presubiculum was quantitated (a). The overall density included NFTs and neuropil threads were significantly higher in the entorhinal cortex compared to the presubiculum in SAD and FAD. The number of NFTs was also significantly higher in the entorhinal cortex compared to the presubiculum in SAD and FAD (b). Presubiculum is shown by blue circles and entorhinal cortex by red squares. FAD; Familial Alzheimer's disease: SAD; Sporadic Alzheimer's disease: TREM2; *TREM2* variant AD cases. Significance was identified by Wilcoxon paired ranks test and is shown as * for $p<0.05$, ** for $p<0.005$, *** for $p<0.0005$, ****$p<0.0001$. Bars represent median with 95% confidence intervals.

6.4.3 Microglial pathology in the presubiculum

To assess the level of microglial activation in the presubiculum deposit, three different microglial markers were used to determine the amount of microglia and their activation states between the two regions. Iba1 was used to assess the number of microglia as it is a pan microglial marker that recognises both surveillant microglia and activated microglia. CD68 and CR3-43 were used to assess the level of microglial activation as they recognise phagocytic microglia and antigen presenting cells respectively. Immunohistochemistry showed that levels of Iba1 positive microglia were largely unchanged between the two areas except for the SAD group in which there were significantly more microglia in the presubiculum than the entorhinal cortex in the sporadic AD group (Figure 6.7a, $p=0.0323$). Conversely, the activated microglial stains CD68 and CR3-43 were decreased in the presubiculum compared to the entorhinal cortex in SAD (CD68 $p<0.0001$, CR3-43 $p=0.0003$) and FAD groups (CD68 $p=0.0195$, CR3-43 $p=0.0195$). *TREM2* variant AD cases showed no difference (Figure 6.7b and c).

Although *TREM2* variant AD cases did not show any significant changes throughout any of the immunohistochemical stains, there is a reduced number of Iba1 positive microglia in both the presubiculum and entorhinal cortex compared to sporadic and familial cases (Figure 6.7a). This may indicate that there are less microglia overall in the *TREM2* variant cases, and may mean that the effect of different pathology in the presubiculum could be less prominent in these cases when compared to SAD or FAD cases.

6.4.4 Amyloid peptides in the presubiculum

To identify the biochemical profile of Aβ peptides in the presubiculum compared to the entorhinal cortex, a combination of laser-capture microdissection and matrix-assisted laser desorption ionisation time-of-flight mass spectrometry (MALDI-MS) was used to identify the different Aβ isoforms. Figure 6.8 depicts a representative mass spectra that was typically observed. As indicated in Table 6.21, all cases from SAD, FAD and *TREM2* variant AD cases had many more N-terminally truncated and pyroglutamate modified Aβ isoforms in the

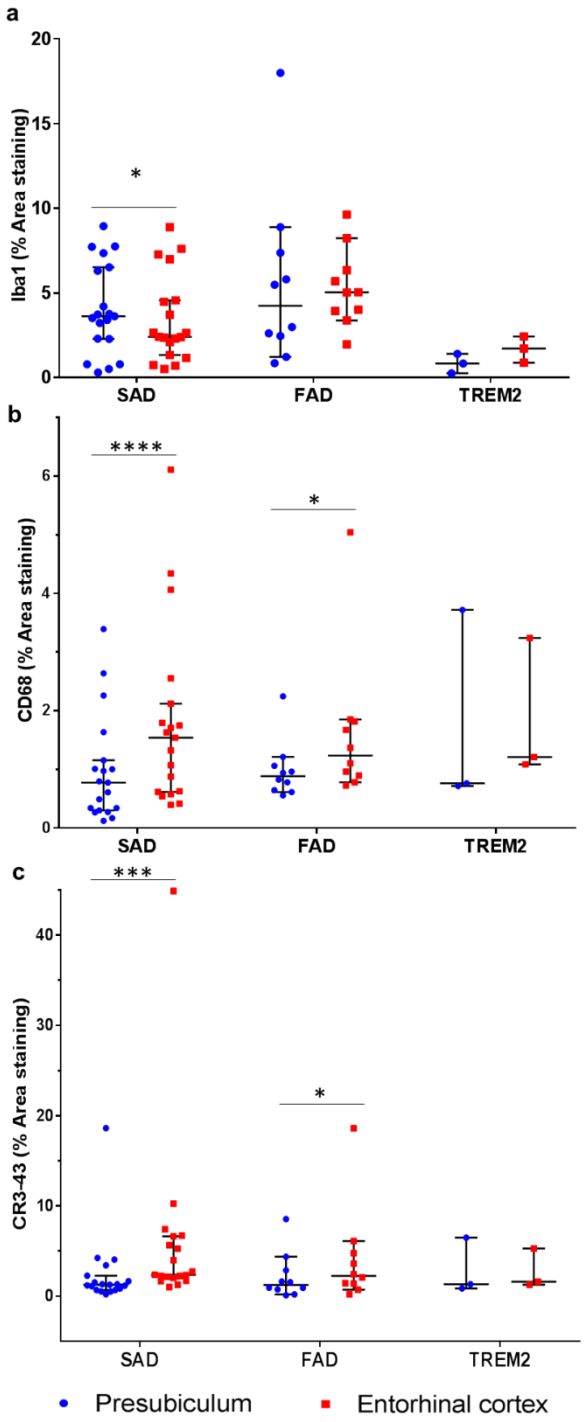

Figure 6.7: Quantification of microglial immunohistochemistry in the presubiculum and entorhinal cortex. The density of microglial staining was calculated using the microglial antibodies Iba1 (a), CD68 (b) and CR3-43 (c). Iba1 density was similar in FAD and TREM2 but significantly less in the entorhinal cortex of SAD. Both CD68 and CR3-43 densities showed significantly less microglia in the SAD and FAD groups. FAD; Familial Alzheimer's disease: SAD; Sporadic Alzheimer's disease: TREM2; *TREM2* variant AD cases. Significance was identified by Wilcoxon paired ranks test and is shown as * for $p<0.05$, ** for $p<0.005$, *** for $p<0.0005$, ****$p<0.0001$. Bars represent median with 95% confidence intervals.

entorhinal cortex than the presubiculum. The full length Aβ1-42 and the N-terminally truncated Aβ4-42 isoforms were the only isoforms detected in the presubiculum other than one SAD case which also detected pyroglutamate modified pGluAβ3-42.

To identify whether this result was also observed pathologically, previously published N-terminally truncated and pyroglutamate modified Aβ isoform antibodies were used for further pathological comparison between the two areas (Wittnam et al., 2012). However, all the antibodies followed the same morphological pattern as the previous Aβ immunohistochemistry (Figure 6.9). This is contradictory to the mass spectrometry results but may indicate that while these isoforms are present as indicated by immunohistochemistry, the levels vary dramatically and were undetectable using these MALDI-MS methods.

6.4.5 Proteomic expression in the presubiculum

Further exploration of the protein expression differences between the presubiculum and entorhinal cortex were performed using laser-capture microdissection and quantitative label free mass spectrometry analysis. Homogenised samples were split into a soluble and insoluble fraction during the extraction process and run separately on the mass spectrometer. A total of 561 proteins were detected in the soluble supernatant fraction and 1824 proteins in the insoluble pellet fraction. Proteins were detected either in both fractions (303 proteins) or in just the soluble fraction (254 proteins) or the insoluble fraction (1488 proteins). The fold change in expression was calculated for each protein for one region compared to the other (2.7.5).

An average of all AD cases (SAD, FAD and TREM2 combined) was used to determine the main differences occurring between the two regions with a more detailed analysis of the different disease subgroups completed later. The complete list of proteins, their expression and fold change expression can be found in Supplementary CD Table 2.

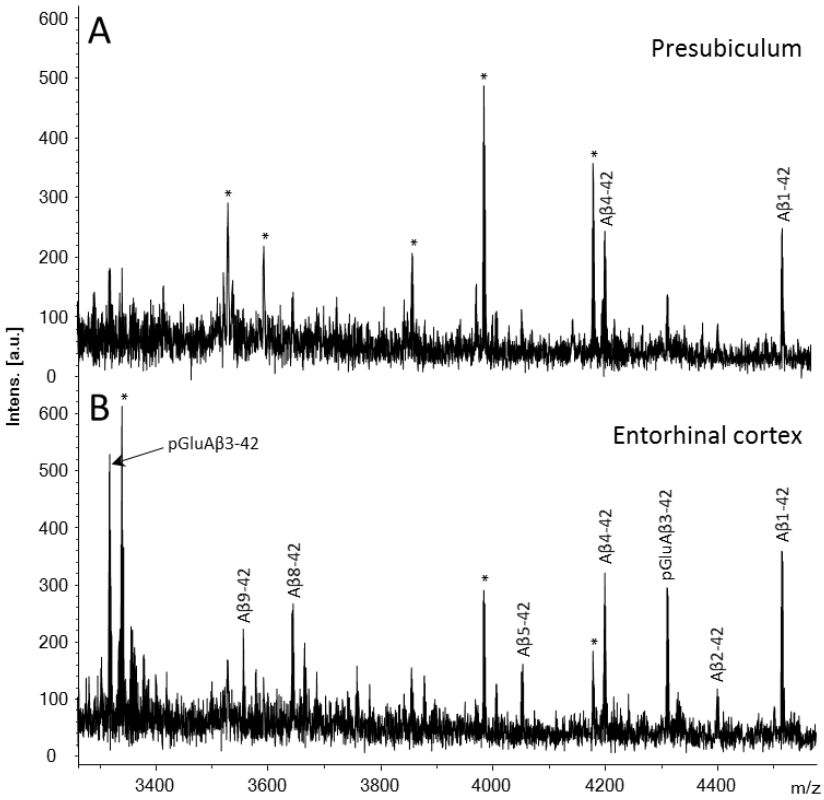

Figure 6.8: Mass spectra of the Aβ peptide pattern from the presubiculum and entorhinal cortex. Representative mass spectra from case 9 highlights the differences between the full length Aβ species identified in the presubiculum (A) compared to the truncated and post-translationally modified Aβ species identified in the entorhinal cortex (B). * represent unidentified non-Aβ related peaks. A peak was considered as identified if the signal-to-noise was > 2.

Presubiculum

Case type	5-42	7-42	8-42	9-42	10-42	4-42	1-40	2-42	2-43	1-42	p3-40	p3-42	p11-42
SAD						Y				Y			
SAD						Y				Y		Y	
FAD													
FAD						Y							
TREM2 AD													
TREM2 AD										Y			

Entorhinal cortex

Case type	5-42	7-42	8-42	9-42	10-42	4-42	1-40	2-42	2-43	1-42	p3-40	p3-42	p11-42
SAD	Y		Y	Y	Y	Y		Y		Y		Y	Y
SAD						Y				Y			Y
FAD	Y	Y	Y	Y	Y	Y		Y		Y		Y	Y
FAD	Y	Y	Y	Y	Y	Y	Y			Y	Y	Y	Y
TREM2 AD										Y			Y
TREM2 AD	Y	Y	Y	Y		Y		Y		Y		Y	Y

Table 6.1: Aβ isoforms present in the presubiculum and entorhinal cortex of SAD, FAD and TREM2 variant AD cases. Different lengths of isoform are shown in each column with p indicating pyroglutamate modified Aβ isoforms. SAD (cases 9 and 25); FAD (cases 27 and 30); TREM2 variant AD (cases 1 and 5).

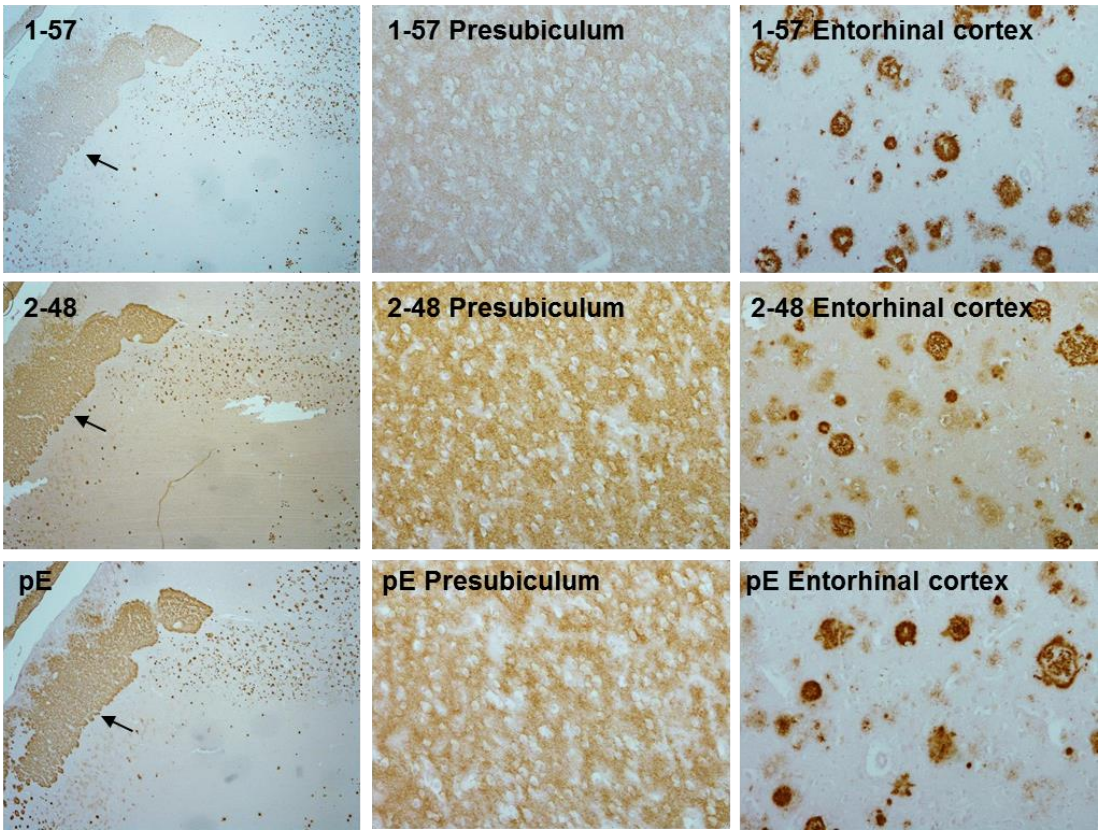

Figure 6.9: Comparison of different Aβ isoforms in the presubiculum and entorhinal cortex. Antibodies for 1-57, 2-48 and pE were tested. The presubiculum can be identified in each as shown in the first column of images by the black arrow (2x magnification). The second column shows the presubiculum with each antibody at 20x magnification and the third depicts the entorhinal cortex at 20x magnification.

When averaging the results from all AD cases, a total of 107 proteins had a fold change of 1.5 or greater increase in the presubiculum compared to the entorhinal cortex in the soluble fraction and 221 in the insoluble fraction. The most altered 30 proteins in each instance are shown in Table 6.2 and Table 6.3. The number of gene ontology terms that were over-represented from these proteins were determined using Webgestalt, with the top biological processes all indicating biosynthetic and biogenetic processes (Table 6.7).

Among the list of proteins found to be increased in the presubiculum were proteins that already have been shown to be associated with AD. DOCK2 (Dedicator of cytokinesis protein 2, Table 6.2, row 7), had an 11-fold average increase in the presubiuclum and is known to modulate microglial cytokine secretion, phagocytosis and paracrine neurotoxicity

(Cimino et al., 2009, 2013). HSPA9 (Heat shock 70kDa protein 9, Table 6.2, row 9), had a 9-fold average increase in the presubiculum and it has been shown that this protein could regulate Aβ toxicity (Flachbartová and Kovacech, 2013). LDHA (L-lactate dehydrogenase A chain, Table 6.2, row 11) has a 5-fold increase in the presubiculum and its overexpression is linked to resisting the toxic effects of Aβ (Newington et al., 2012). NSG1 (Neuron-specific protein family member 1, Table 6.2, row 20), has an average increase of 3-fold in the presubiculum and has been shown to have a role in the proteolytic processing of APP (Muthusamy et al., 2015). AGPS (Alkyldihydroxyacetonephosphate synthase, Table 6.3, row 4) has an average increase of 19-fold in the presubiculum and is a rate limiting enzyme that can alter APP levels (Grimm et al., 2011). Lastly, INPP5D (phosphatidylinositol 3_4_5-trisphosphate 5-phosphatase 1, Table 6.3, row 25), is increased by an average of 4.5-fold in the presubiculum and is a negative regulator of the innate immune system (Efthymiou and Goate, 2017).

Additionally, there were 2 proteins that were only detected in the presubiculum, Annexin A1 in the soluble fraction and TUSC5 in the insoluble fraction (Table 6.6). Annexin A1 plays a role in the innate immune system and is involved in the resolution of inflammation and wound healing. It was detected with a count of 13.2 in SAD and 273 in the *TREM2* variant AD cases. TUSC5 (tumour suppressor candidate 5) is thought to be involved in fat metabolism.

109 proteins had a 1.5 or greater fold change increase in the entorhinal cortex compared to the presubiculum in the soluble fraction and 559 in the insoluble fraction. The most altered 30 of these proteins in each instance are found in Table 6.4 and Table 6.5. The number of gene ontology terms that were over-represented from these proteins were determined using Webgestalt, with the top biological processes indicating that cell organisation and cell signalling are affected (Table 6.8). This was validated with Ingenuity Pathway analysis which also showed the top canonical pathways that were altered in the insoluble fraction were a number of cell signalling pathways (Figure 6.10).

Gene ID	Gene name	Average	SAD	FAD	TREM2
DHCR7	7-dehydrocholesterol reductase	49.60	N/A	N/A	124.71
SATB1	DNA-binding protein SATB1	41.63	4.58	5.96	93.12
SLC24A3	Sodium/potassium/calcium exchanger 3	20.93	8.88	N/A	24.22
SMARCA4	Transcription activator BRG1	17.94	N/A	N/A	196.05
CD2	T-cell surface antigen CD2	15.98	4.81	N/A	162.09
PRKCSH	Glucosidase 2 subunit beta	12.87	N/A	N/A	19.21
DOCK2	Dedicator of cytokinesis protein 2	11.68	7.65	N/A	N/A
RPL30	60S ribosomal protein L30	9.47	1.58	N/A	31.92
HSPA9	Stress-70 protein_ mitochondrial	9.39	3.05	1.04	53.17
SLC12A9	Solute carrier family 12 member 9	6.26	2.13	3.32	36.80
LDHA	L-lactate dehydrogenase A chain	5.10	19.10	1.25	1.24
DLAT	Acetyltransferase component of pyruvate dehydrogenase complex	4.70	2.21	2.71	14.91
ANXA5	Annexin A5	4.52	1.12	1.34	15.53
ABCA8	ATP-binding cassette sub-family A member 8	4.20	1.50	3.84	N/A
USP35	Ubiquitin carboxyl-terminal hydrolase 35	4.20	1.43	14.19	N/A
CCDC88C	Protein Daple	3.98	1.27	69.86	2.75
R3HDM1	R3H domain-containing protein 1	3.79	1.45	9.49	14.37
RERE	Arginine-glutamic acid dipeptide repeats protein	3.76	1.64	1.38	12.44
ATRIP	ATR-interacting protein	3.44	1.50	2.80	12.78
NSG1	Neuron-specific protein family member 1	3.33	1.67	2.43	7.32
VAT1	Synaptic vesicle membrane protein VAT-1 homolog	3.13	1.59	1.01	6.40
PTK2	Focal adhesion kinase 1	3.01	3.67	1.40	11.35
TUBB1	Tubulin beta-1 chain	2.93	1.09	9.91	4.18
TUBA3C	Tubulin alpha-3C/D chain	2.84	10.65	3.45	2.31
BCS1L	Mitochondrial chaperone BCS1	2.80	1.81	5.38	1.12
EHD2	EH domain-containing protein 2	2.77	1.04	1.83	7.26
PFN1	Profilin-1	2.74	1.08	1.29	5.26
NXPH3	Neurexophilin-3	2.74	2.66	3.62	1.53
CDON	Cell adhesion molecule-related/down-regulated by oncogenes	2.73	1.82	10.39	2.00
TBC1D1	TBC1 domain family member 1	2.61	1.27	2.73	10.89

Table 6.2: Top 30 proteins with greatest average fold change increase in the presubiculum for the soluble fraction. Fold change for average of all cases (SAD, FAD and *TREM2* combined) as well as the fold change for each disease group (SAD, FAD, *TREM2*) is shown. Yellow indicates a fold change where increase is in presubiculum whereas green indicates fold change where increase is in entorhinal cortex. N/A is shown where the protein was found in only one region, the region that was found is indicated by colour.

Gene ID	Gene name	Average	SAD	FAD	TREM2
CTDSPL	CTD small phosphatase-like protein	217.36	29.26	N/A	431.19
PRR12	Proline-rich protein 12	36.36	N/A	6.37	N/A
ZFP30	Zinc finger protein 30 homolog	27.09	340.01	N/A	N/A
AGPS	Alkyldihydroxyacetonephosphate synthase_ peroxisomal	19.10	49.12	9.46	8.29
SLC38A10	Putative sodium-coupled neutral amino acid transporter 10	18.78	23.76	5.04	29.46
IFT122	Intraflagellar transport protein 122 homolog	16.58	61.79	N/A	N/A
LRRC70	Leucine-rich repeat-containing protein 70	12.64	57.57	4.21	N/A
ZNF540	Zinc finger protein 540	11.61	29.52	3.44	15.96
ZBTB48	Zinc finger and BTB domain-containing protein 48	10.71	18.20	9.46	3.80
S100A9	Protein S100-A9	9.96	38.49	N/A	N/A
CEP55	Centrosomal protein of 55 kDa	9.20	39.35	N/A	28.29
PRSS2	Trypsin-2	8.49	131.53	10.58	2.45
GNB3	Guanine nucleotide-binding protein G(I)/G(S)/G(T) subunit beta-3	6.71	1.28	23.33	12.02
KRT16	Keratin_ type I cytoskeletal 16	6.54	9.05	3.15	6.44
CWC27	Peptidyl-prolyl cis-trans isomerase CWC27 homolog	6.29	50.39	1.44	2.14
MTERF2	Transcription termination factor 2_ mitochondrial	5.99	1.03	8.23	N/A
ADAMTS15	A disintegrin and metalloproteinase with thrombospondin motifs 15	5.77	N/A	4.68	N/A
DDX56	Probable ATP-dependent RNA helicase DDX56	5.77	22.81	8.10	361.36
DDX19A	ATP-dependent RNA helicase DDX19A	5.63	1.44	2.14	14.53
ZNF267	Zinc finger protein 267	5.61	8.94	N/A	3.54
VAT1	Synaptic vesicle membrane protein VAT-1 homolog	5.51	3.74	N/A	24.30
KRT9	Keratin_ type I cytoskeletal 9	5.47	3.01	11.07	5.24
FMO2	Dimethylaniline monooxygenase [N-oxide-forming] 2	5.21	59.44	4.82	1.59
TRPM1	Transient receptor potential cation channel subfamily M member 1	5.16	25.33	N/A	7.70
INPP5D	Phosphatidylinositol 3_4_5-trisphosphate 5-phosphatase 1	4.49	676.90	N/A	N/A
C2CD2	C2 domain-containing protein 2	4.40	20.38	1.81	3.48
BTAF1	TATA-binding protein-associated factor 172	4.25	4.12	9.93	1.25
ESRP2	Epithelial splicing regulatory protein 2	4.21	28.85	1.11	1.46
ACTN2	Alpha-actinin-2	4.00	5.42	1.96	21.91
KRT14	Keratin_ type I cytoskeletal 14	4.00	2.92	5.91	5.17

Table 6.3: Top 30 proteins with greatest average fold change increase in the presubiculum for the insoluble fraction. Fold change for average of all cases (SAD, FAD and *TREM2* combined) as well as the fold change for each disease group (SAD, FAD, *TREM2*) is shown. Yellow indicates a fold change where increase is in presubiculum whereas green indicates fold change where increase is in entorhinal cortex. N/A is shown where the protein was found in only one region, the region that was found is indicated by colour. White indicates it was not detected for either.

Of particular interest, PSAP (Prosaposin, Table 6.4, row 3), has a 21-fold average increase in the entorhinal cortex compared to the presubiculum. It has been indicated to be involved with progranuluin neuroprotection mechanisms that are activated in models of AD and degradation of glycosphingolipids in lysosomes (Nicholson et al., 2016). Upregulation of this protein in the entorhinal cortex may indicate a defect in lysosomal catabolism. S100A8 (Table 6.4, row 4), has a 17.6 fold increase in the entorhinal cortex and this protein has links to Aβ production (Lodeiro et al., 2017). OTUB1 (ubiquitin thioesterase, Table 6.4, row 16), has a 5-fold increase in the entorhinal cortex and is a tau deubiquitinating enzyme (Wang et al., 2017). XPO1 (exportin-1, Table 6.5, row 10), has a 39-fold increase in the entorhinal cortex and is known to be an Aβ toxicity modifier (Rosenthal et al., 2012). AQP4 (aquaporin 4, Table 6.5, row 19), has a 21-fold increase in the entorhinal cortex. AQP4 is an astrocytic water channel protein and it has been identified to be distributed in the proximity of Aβ plaques and may have a role in Aβ clearance (Hoshi et al., 2012; Xu et al., 2015). LRP1 (Prolow-density lipoprotein receptor-related protein 1, Table 6.5, row 23), has a 15.5-fold increase in the entorhinal cortex and is involved in clearance of Aβ, as referred to in Chapter 3 (Ismail et al., 2017; Storck and Pietrzik, 2017; Zandl-Lang et al., 2017). C3, a complement protein (Table 6.5, row 26), has a 13-fold increase in the entorhinal cortex and this has been shown to be elevated in AD and contributes to Aβ clearance (Shi et al., 2017). Lastly, despite not being one of the most altered 30 changing proteins, APOE (apolipoprotein E) still has an 8.6-fold increase in the entorhinal cortex compared to the presubiculum. Having an *ApoE4* allele confers increased risk of having AD and APOE is thought to play roles in Aβ clearance and microglial recruitment as discussed in previous chapters.

A greater number of proteins were only detected in the entorhinal cortex than in the presubiculum, with 48 being listed (Table 6.6). For example, CXCR3, was detected in the entorhinal cortex of all three AD subgroups, whereas SFTPC, PRMT5, PURA, SNX6 and RAB21 were only detected in the entorhinal cortex of SAD and FAD cases. CX3CR3 (C-X-C chemokine receptor type 3, Table 6.6, row 6), has a role in microglial activation and has an impact on Aβ plaque burden (Krauthausen et al., 2014, 2015). SFTPC (Pulmonary

Gene ID	Gene name	Average	SAD	FAD	TREM2
DNALI1	Axonemal dynein light intermediate polypeptide 1	36.52	N/A	1.26	86.91
SERPINB5	Serpin B5	29.92	N/A	N/A	N/A
PSAP	Prosaposin	21.16	N/A	17.47	N/A
S100A8	Protein S100-A8	17.64	40.50	1.93	69.12
GSDMD	Gasdermin domain containing 1_ isoform CRA_d	15.15	5.44	N/A	N/A
CDK5RAP2	CDK5 regulatory subunit-associated protein 2	9.59	4.95	2.05	26.67
EPN3	EPN3 protein	9.45	2.14	9.48	62.64
SMARCA2	Probable global transcription activator SNF2L2	8.16	N/A	N/A	N/A
CKAP5	Cytoskeleton-associated protein 5	7.52	1.26	1.02	30.87
EIF2AK4	Eukaryotic translation initiation factor 2-alpha kinase 4	7.01	5.18	8.11	21.02
CKMT1A	Creatine kinase U-type_ mitochondrial	6.52	4.87	N/A	N/A
LGALS7	Galectin-7	6.42	11.64	2.18	2.42
PGAM1	Phosphoglycerate mutase 1	5.46	3.53	1.39	91.14
ADGRE2	Adhesion G protein-coupled receptor E2	5.26	28.93	N/A	3.80
MXRA8	Matrix-remodeling-associated protein 8	4.98	1.49	620.99	4.81
OTUB1	Ubiquitin thioesterase OTUB1	4.75	N/A	N/A	N/A
DPYSL2	Dihydropyrimidinase-related protein 2	4.73	1.43	3.02	33.45
SNAP25	Synaptosomal-associated protein 25	4.47	1.29	6.20	37.93
PCDHGA1	Protocadherin gamma-A1	4.41	6.20	7.76	109.56
MMP8	Neutrophil collagenase	4.31	N/A	N/A	45.29
CLIP2	CAP-Gly domain-containing linker protein 2	4.29	7.42	N/A	N/A
S100A9	Protein S100-A9	4.20	9.29	1.26	2.11
GFAP	Glial fibrillary acidic protein	3.93	1.35	9.27	6.33
YARS	Tyrosine--tRNA ligase	3.93	1.60	3.71	27.44
SLC6A17	Sodium-dependent neutral amino acid transporter SLC6A17	3.81	1.40	8.18	2.75
CALM2	Calmodulin	3.58	1.73	4.15	9.97
CALML3	Calmodulin-like protein 3	3.51	4.00	2.76	10.96
FAM109A	Sesquipedalian-1	3.41	8.25	4.00	1.16
TRAP1	Heat shock protein 75 kDa_ mitochondrial	3.22	1.24	4.32	17.84
MTFR1	Mitochondrial fission regulator 1	3.19	N/A	N/A	N/A

Table 6.4: Top 30 proteins with greatest average fold change increase in the entorhinal cortex for the soluble fraction. Fold change for average of all cases (SAD, FAD and *TREM2* combined) as well as the fold change for each disease group (SAD, FAD, *TREM2*) is shown. Yellow indicates a fold change where increase is in presubiculum whereas green indicates fold change where increase is in entorhinal cortex. N/A is shown where the protein was found in only one region, the region that was found is indicated by colour. White indicates it was not detected for either.

Gene ID	Gene name	Average	SAD	FAD	TREM2
OR6M1	Olfactory receptor 6M1	234.71	132.14	2270.51	235.48
ANXA4	Annexin A4	151.09	1.59	N/A	N/A
SH3GL1	Endophilin-A2	141.46	106.03	N/A	N/A
ATP6V1D	V-type proton ATPase subunit D	95.62	0.00	N/A	1.85
C9orf172	Uncharacterized protein C9orf172	78.34	2.16	N/A	N/A
SQSTM1	Sequestosome-1	61.44	17.10	N/A	N/A
NAGLT1	Sodium-dependent glucose transporter 1	51.13	13.33	9.00	217.03
TUBGCP6	Gamma-tubulin complex component 6	44.26	16.59	150.94	29.57
PITPNA	Phosphatidylinositol transfer protein alpha isoform	40.75	31.17	96.02	25.87
XPO1	Exportin-1	39.29	4.44	N/A	N/A
ENPP6	Ectonucleotide pyrophosphatase/phosphodiesterase family member 6	38.36	N/A	N/A	N/A
SLC19A3	Thiamine transporter 2	30.85	377.55	25.65	1.03
NDUFB9	NADH dehydrogenase [ubiquinone] 1 beta subcomplex subunit 9	29.92	30.91	N/A	N/A
PSMD1	26S proteasome non-ATPase regulatory subunit 1	27.06	N/A	N/A	N/A
ZSCAN18	Zinc finger and SCAN domain-containing protein 18	25.93	2.77	N/A	N/A
PCSK6	Proprotein convertase subtilisin/kexin type 6	24.92	N/A	N/A	N/A
GNPTAB	N-acetylglucosamine-1-phosphotransferase subunits alpha/beta	24.72	24.13	N/A	3.83
SLC35E3	Solute carrier family 35 member E3	21.61	12.83	127.25	154.01
AQP4	Aquaporin-4	20.81	18.44	164.78	1.48
GFAP	Glial fibrillary acidic protein	18.38	3.60	172.48	2.79
UQCRB	Cytochrome b-c1 complex subunit 7	16.14	28.44	N/A	N/A
C1QBP	Complement component 1 Q subcomponent-binding protein_ mitochondrial	16.01	N/A	N/A	N/A
LRP1	Prolow-density lipoprotein receptor-related protein 1	15.57	N/A	N/A	1.24
DAAM2	Disheveled-associated activator of morphogenesis 2	14.67	5.36	N/A	2.21
HOMEZ	Homeobox and leucine zipper protein Homez	14.13	8.16	N/A	1.55
C3	Complement C3	13.23	15.29	N/A	N/A
WDR7	WD repeat-containing protein 7	12.44	5.44	N/A	N/A
NADK2	NAD kinase 2_ mitochondrial	12.43	N/A	N/A	N/A
THBS2	Thrombospondin-2	12.11	N/A	10.12	N/A
TWF2	Twinfilin-2	12.05	1.56	N/A	N/A

Table 6.5: Top 30 proteins with greatest average fold change increase in the entorhinal cortex for the insoluble fraction. Fold change for average of all cases (SAD, FAD and *TREM2* combined) as well as the fold change for each disease group (SAD, FAD, *TREM2*) is shown. Yellow indicates a fold change where increase is in presubiculum whereas green indicates fold change where increase is in entorhinal cortex. N/A is shown where the protein was found in only one region, the region that was found is indicated by colour. White indicates it was not detected for either.

surfactant-associated protein C, Table 6.6, row 10), is also able to fibrillise into the amyloid conformational state (Johansson et al., 2004). PRMT5 (protein arginine N-methyltransferase 5, Table 6.6, row 20), is known to have a role in Aβ toxicity (Quan et al., 2015). PURA (transcriptional activator protein Pur-alpha, Table 6.6, row 24), is known to regulate APP transcription (Darbinian et al., 2008). SNX6 (sorting nexin 6, Table 6.6, row 28), is involved in APP cleavage regulation (Okada et al., 2010). RAB21 (ras-related protein Rab-21, Table 6.6, row 46), is involved in γ- secretase activity (Sun et al., 2017).

Interestingly, many of the proteins only detected in the entorhinal cortex were not detected at all in the *TREM2* variant AD cases (Table 6.6). Furthermore, the gene ontology terms that are specifically being over-represented in each disease subgroup are markedly variable. The biological processes show very little overlap between disease groups in either soluble or insoluble conditions or where these proteins are higher in the presubiculum or higher in the entorhinal cortex (Figure 6.11). The same can be seen when looking at the heatmap of canonical pathways identified to be represented in these cases. The TREM2 group has an opposite level of activation or inhibition when compared to SAD and FAD (Figure 6.10).

Gene ID	Gene name	Presubiculum			Entorhinal cortex		
		SAD	FAD	TREM2	SAD	FAD	TREM2
Soluble fraction							
ANXA1	Annexin A1	13.23	0	272.97	0	0	0
Insoluble fraction							
REV1	DNA repair protein REV1	0	0	0	0	25.40	0
IL18R1	Interleukin-18 receptor 1	0	0	0	146.97	41.69	20.44
MATR3	Matrin-3	0	0	0	16.79	80.66	0
MGAT5B	Alpha-1_6-mannosylglycoprotein 6-beta-N-acetylglucosaminyltransferase B	0	0	0	0	47.84	0
CXCR3	C-X-C chemokine receptor type 3	0	0	0	120.05	32.83	16.35
KPNA4	Importin subunit alpha-3	0	0	0	29.88	154.19	0
FES	Tyrosine-protein kinase Fes/Fps	0	0	0	0	141.58	0
ADAM23	Disintegrin and metalloproteinase domain-containing protein 23	0	0	0	261.58	313.14	0
SFTPC	Pulmonary surfactant-associated protein C	0	0	0	7.49	36.46	0
HLA-C	HLA class I histocompatibility antigen_ Cw-6 alpha chain	0	0	0	5.71	109.15	0
IRS4	Insulin receptor substrate 4	0	0	0	31.66	103.96	0
F10	Coagulation factor X	0	0	0	0	46.64	0
UBE3C	Ubiquitin-protein ligase E3C	0	0	0	4.76	154.69	0
KPNA5	Importin subunit alpha-6	0	0	0	0	64.52	0
SNX3	Sorting nexin-3	0	0	0	66.40	192.78	0
FRYL	Protein furry homolog-like	0	0	0	4.97	92.82	0
PARVA	Alpha-parvin	0	0	0	0	92.10	0
SHB	SH2 domain-containing adapter protein B	0	0	0	175.43	0	0
PRMT5	Protein arginine N-methyltransferase 5	0	0	0	18.15	61.53	0
KCNRG	Potassium channel regulatory protein	0	0	0	0	30.91	0
SFXN5	Sideroflexin-5	0	0	0	29.32	103.02	0
LANCL2	LanC-like protein 2	0	0	0	54.68	168.97	0
PURA	Transcriptional activator protein Pur-alpha	0	0	0	214.74	475.79	0

PGLYRP2	N-acetylmuramoyl-L-alanine amidase	0	0	0	120.23	37.64	17.65
RPS17	40S ribosomal protein S17	0	0	0	49.15	94.80	0
DBNL	Drebrin-like protein	0	0	0	0	86.94	0
SNX6	Sorting nexin 6_ isoform CRA_b	0	0	0	0	58.57	0
PTRF	Polymerase I and transcript release factor	0	0	0	24.72	363.85	0
ASPSCR1	Tether-containing UBX domain for GLUT4	0	0	0	0	100.34	0
PLCD3	1-phosphatidylinositol 4_5-bisphosphate phosphodiesterase delta-3	0	0	0	0	91.18	0
EIF2S1	Eukaryotic translation initiation factor 2 subunit 1	0	0	0	0.58	68.89	1.03
AP1S1	AP-1 complex subunit sigma-1A	0	0	0	16.06	106.38	0
HPCAL4	Hippocalcin-like protein 4	0	0	0	89.90	278.02	0
NARS	Asparagine--tRNA ligase_ cytoplasmic	0	0	0	56.47	342.24	0
GALK1	Galactokinase	0	0	0	3.94	146.20	0
MPP2	MAGUK p55 subfamily member 2	0	0	0	0	103.68	22.75
DCLK2	Serine/threonine-protein kinase DCLK2	0	0	0	45.18	186.62	0
MYBBP1A	Myb-binding protein 1A	0	0	0	11.14	286.39	0
ARHGEF2	Rho guanine nucleotide exchange factor 2	0	0	0	19.97	90.59	0
CENPJ	Centromere protein J	0	0	0	0	50.32	0
RNPEP	Aminopeptidase B	0	0	0	0	125.99	0
MST1R	Macrophage-stimulating protein receptor	0	0	0	0	146.84	0
GIT1	ARF GTPase-activating protein GIT1	0	0	0	10.31	72.13	0
CALU	Calumenin	0	0	0	65.71	129.02	0.06
RAB21	Ras-related protein Rab-21	0	0	0	18.83	80.71	0
PDXP	Pyridoxal phosphate phosphatase	0	0	0	0	223.36	0
RCN2	Reticulocalbin-2	0	0	0	32.74	153.52	0
POGZ	Pogo transposable element with ZNF domain	0	0	0	0	56.31	0
TUSC5	Tumor suppressor candidate 5	0	0	141.22	0	0	0

Table 6.6: Proteins only detected in either the presubiculum or the entorhinal cortex. Raw counts for each disease group are shown for both the presubiculum and the entorhinal cortex.

Soluble fraction

Molecular function	
GO ID	**GO term**
GO:0004111	creatine kinase activity
GO:0004859	phospholipase inhibitor activity
GO:0016775	phosphotransferase activity, nitrogenous group as acceptor
GO:0055102	lipase inhibitor activity
GO:0004857	enzyme inhibitor activity
GO:0046915	transition metal ion transmembrane transporter activity
GO:0005546	phosphatidylinositol-4,5-bisphosphate binding
GO:0005544	calcium-dependent phospholipid binding
GO:0017016	Ras GTPase binding
GO:0031267	small GTPase binding

Insoluble fraction

Biological process		**Molecular function**		**Cellular component**	
GO ID	**GO term**	**GO ID**	**GO term**	**GO ID**	**GO term**
GO:0044281	small molecule metabolic process	GO:0043168	anion binding	GO:0005856	cytoskeleton
GO:0009152	purine ribonucleotide biosynthetic process	GO:0005198	structural molecule activity	GO:0044430	cytoskeletal part
GO:0022607	cellular component assembly	GO:0036094	small molecule binding	GO:0044444	cytoplasmic part
GO:0034329	cell junction assembly	GO:0036094	small molecule binding	GO:0005737	cytoplasm
GO:0043269	regulation of ion transport	GO:0000166	nucleotide binding	GO:0033267	axon part
GO:0010035	response to inorganic substance	GO:1901265	nucleoside phosphate binding	GO:0030424	axon
GO:0009260	ribonucleotide biosynthetic process	GO:0032549	ribonucleoside binding	GO:0005882	intermediate filament
GO:0046390	ribose phosphate biosynthetic process	GO:0032550	purine ribonucleoside binding	GO:0044463	cell projection part
GO:0044085	cellular component biogenesis	GO:0016462	pyrophosphatase activity	GO:0045111	intermediate filament cytoskeleton
GO:0034330	cell junction organization	GO:0001882	nucleoside binding	GO:0043005	neuron projection

Table 6.7: Top 10 over-represented gene ontology terms from proteins that had greater than 1.5 fold change increase in the presubiculum compared to entorhinal cortex in the categories Biological processes, Molecular function and cellular components.

Soluble fraction

Biological process		Molecular function		Cellular component	
GO ID	**GO term**	**GO ID**	**GO term**	**GO ID**	**GO term**
GO:0035637	multicellular organismal signaling	GO:0005200	structural constituent of cytoskeleton	GO:0033267	axon part
GO:0019226	transmission of nerve impulse	GO:0005198	structural molecule activity	GO:0043005	neuron projection
GO:0006836	neurotransmitter transport	GO:0050786	RAGE receptor binding	GO:0044463	cell projection part
GO:0007268	synaptic transmission	GO:0005515	protein binding	GO:0045202	synapse
GO:0007267	cell-cell signaling	GO:0005509	calcium ion binding	GO:0005829	cytosol
GO:0048812	neuron projection morphogenesis	GO:0008022	protein C-terminus binding	GO:0005882	intermediate filament
GO:0045103	intermediate filament-based process	GO:0042287	MHC protein binding	GO:0030424	axon
GO:0050877	neurological system process	GO:0005504	fatty acid binding	GO:0033269	internode region of axon
GO:0045104	intermediate filament cytoskeleton organization	GO:0019829	cation-transporting ATPase activity	GO:0045111	intermediate filament cytoskeleton
GO:0032990	cell part morphogenesis			GO:0005856	cytoskeleton

Insoluble fraction

Biological process		Molecular function		Cellular component	
GO ID	**GO term**	**GO ID**	**GO term**	**GO ID**	**GO term**
GO:0048666	neuron development	GO:0005515	protein binding	GO:0005737	cytoplasm
GO:0071842	cellular component organization at cellular level	GO:0043168	anion binding	GO:0044444	cytoplasmic part
GO:0071841	cellular component organization or biogenesis at cellular leve	GO:0000166	nucleotide binding	GO:0005622	intracellular
GO:0071840	cellular component organization or biogenesis	GO:1901265	nucleoside phosphate binding	GO:0044424	intracellular part
GO:0016043	cellular component organization	GO:0032553	ribonucleotide binding	GO:0005829	cytosol
GO:0051649	establishment of localization in cell	GO:0032555	purine ribonucleotide binding	GO:0005856	cytoskeleton
GO:0030030	cell projection organization	GO:0017076	purine nucleotide binding	GO:0044430	cytoskeletal part
GO:0009056	catabolic process	GO:0036094	small molecule binding	GO:0032991	macromolecular complex
GO:0022008	neurogenesis	GO:0001883	purine nucleoside binding	GO:0043234	protein complex
GO:0051641	cellular localization	GO:0032549	ribonucleoside binding	GO:0044422	organelle part

Table 6.8: Top 10 over-represented gene ontology terms from proteins that had greater than 1.5 fold change increase in the entorhinal cortex compared to the presubiculum in the categories Biological processes, Molecular function and cellular components.

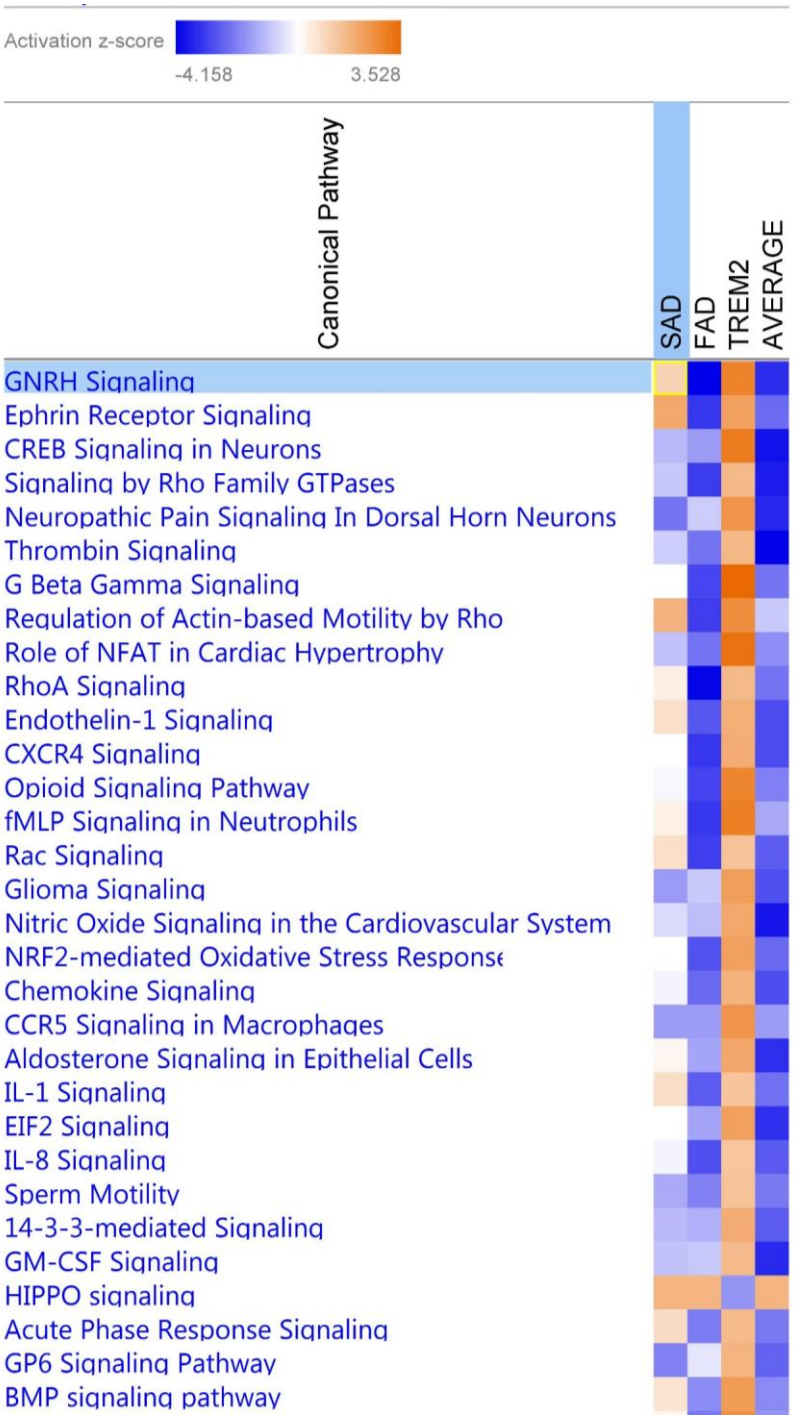

Figure 6.10: Canonical pathways represented in insoluble fraction of presubiculum proteomic data. Pathways found according to z-score given by IPA software. Orange represents a predicted activation of the pathway and blue represents a predicted inhibition of the pathway based on expression values found in the data. Intensity of colour relates to how activated or inhibited the pathway is predicted to be.

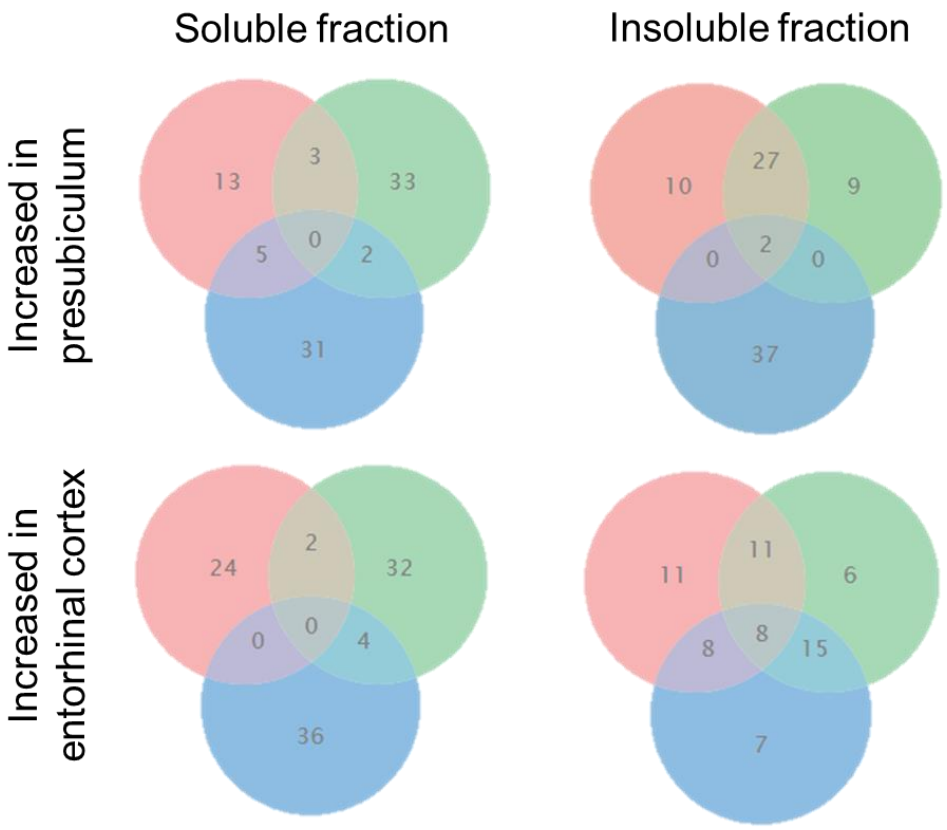

Figure 6.11: Comparison of overlapping over-represented gene ontology biological process terms between different disease groups. Venn diagram for each condition, both soluble and insoluble fractions and for the proteins that were increased in the presubiculum and those that were increased in the entorhinal cortex. Pink represents SAD, Blue represents FAD, Green represents TREM2 variant cases. Numbers indicate how many GO terms are in that category.

6.5 Discussion

In this chapter, the morphological differences in the presubiculum compared to the neighbouring entorhinal cortex in sporadic AD cases were confirmed and these results were built upon with the discovery that these morphological differences are also present in familial AD and *TREM2* variant cases. Therefore indicating that these changes are not specific to one subtype of AD. Not only does the presubiculum have a large non-fibrillar Aβ deposit compared with the fibrillar dense-core Aβ plaques of the entorhinal cortex, there was also significantly reduced tau accumulation, significantly less microglial activation and less N-

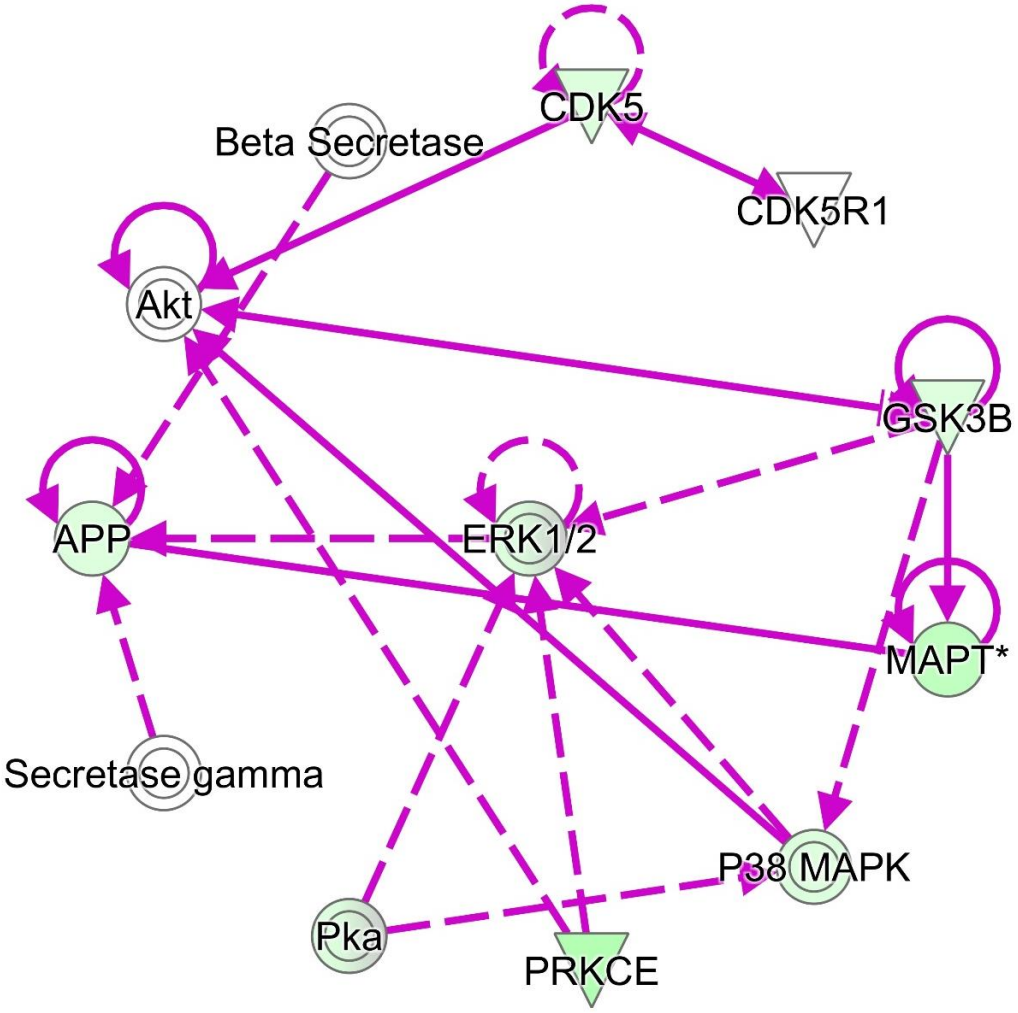

Figure 6.12: Amyloid processing pathway proteins with presubiculum proteomic expression data overlaid. Green represents downregulation of that protein in the presubiculum compared to the entorhinal cortex. Pathway generated using Ingenuity Pathway Analysis software.

terminally truncated and pyro-glutamate modified Aβ peptides present than in the entorhinal cortex. Furthermore, the proteomic expression profile of the presubiculum varies dramatically from the entorhinal cortex region.

Through fluorescent immunohistochemistry and Thioflavin-S staining it was confirmed that the large deposit of the presubiculum is not of a fibrillar amyloid conformational state, in agreement with previous studies that also showed Thioflavin and congo red negative staining and no PiB ligand binding (Akiyama et al., 1990; Ji et al., 2015; Wisniewski et al., 1998). Numerous studies predict that non-fibrillar Aβ will mature into fibrillar Aβ in time,

indicating that diffuse plaques mature into dense-core fibrillar plaques during disease progression (Cork et al., 1990; Iwatsubo et al., 1996; Mann et al., 1992; Pappolla et al., 1991; Probst et al., 1991). However, the diffuse non-fibrillar Aβ deposits found in the presubiculum are present from an early disease stage (Thal phase 2 or 3) and do not mature into dense-core plaques with disease progression, with the diffuse deposits even seen at end- stage disease (Thal et al., 2000). Therefore, the presubiculum must have different properties that do not allow the diffuse Aβ to mature into dense-core Aβ plaques. There may be a factor or multiple factors that are stopping this process from occuring.

To determine if the Aβ peptide species in each region differed and whether it could explain the differences in the conformational state of the amyloid present, both the presubiculum and Aβ plaques from the entorhinal cortex were laser-capture microdissected and analysed by mass spectrometry. Aβ peptides are formed from cleavage of the amyloid precursor protein, APP (Ghiso and Frangione, 2002; Hébert et al., 2004; Shirotani et al., 2004). It is cleaved at both the N-terminal and the C-terminal. However, in both instances the cleavage can occur at different points in the protein and by different secretases. A beta-secretase known as BACE1 is the secretase that cleaves APP at the N-terminus, whereas a γ-secretase complex, made up of presenilin-1, presenilin-2, nicastrin, APH-1 and PEN-2 is responsible for cleaving at the C-terminus (Niimura et al., 2005; Thinakaran and Koo, 2008). C-terminal cleavage results in cleavage either at residue 40 or 42. Both Aβ1-40 and Aβ1-42 are thought to have pathogenic roles and both exist in Aβ plaques (Alonzo et al., 1998; Iwatsubo et al., 1994). However, the Aβ1-40 peptide is more commonly linked to amyloid deposition in CAA than AD (Alonzo et al., 1998). It is thought that the ratio between these two peptides is more indicative of disease status (Spies et al., 2010). Many N-terminally truncated Aβ peptides can be formed and a combination of these are reported to be found in dense-core Aβ plaques (Portelius et al., 2010). In addition, several Aβ peptides can be modified by pyroglutamate and this process is thought to mature the Aβ plaques (Wittnam et al., 2012). Only the Aβ1-42, Aβ4-42 and pGluAβ3-42 peptides were found in the presubiculum, and these were not all present in each case. On the other hand, a whole range of N-terminally truncated and pyroglutamate modified peptides were detected in the plaques from the entorhinal cortex. This finding suggests that a variety of N-terminally truncated or

pyroglutamate-modified Aβ peptides need to be present for fibrillisation to occur and that cleavage of APP in the presubiculum may differ and stop this occurring.

However, when a range of antibodies for various N-terminally truncated and pyroglutamate modified Aβ peptides that were previously characterised were used immunohistochemically to identify Aβ1-57, Aβ2-48, pE-Aβ peptides, all were present in the presubiculum (Wittnam et al., 2012). This suggests that these peptides do exist in the presubiculum, so the reason fibrillisation does not occur may not only be down to the differing APP cleavage. Reasons for the discrepancies between the mass spectrometry analysis and immunohistochemistry analysis may be down to sensitivity in the different methods. Even though the various Aβ peptides exist in the presubiculum, they may not be present in the same quantities as they are in the entorhinal cortex and are therefore below a detectable level using MS due to the concentration of the full length Aβ peptides. The proteins could alter in their solubility or post-translational modifications and these possible differences could also explain the variation observed here.

In addition, some of the proteins that had markedly different levels of expression between the presubiculum and entorhinal cortex in the label-free proteomic data, were proteins involved in APP cleavage or Aβ deposition and fibrillisation (Figure 6.12). Both SNX6 and NSG1 are involved in BACE1 mechanisms. SNX6 negatively regulates BACE1 cleavage of APP and this protein was only detected in the entorhinal cortex of samples (Okada et al., 2010). NSG1 is a neuronal vesicle trafficking protein and it affects the proteolytic processing of APP through BACE1 with its endocytic and recycling functions (Muthusamy et al., 2015). NSG1 expression was markedly increased in the presubiculum compared to entorhinal cortex. The lack of SNX6 and the increase of NSG1 in the presubiculum could indicate that greater amounts of BACE1 are internalised into endosomes, and that the BACE1 that is left is not regulated by SNX6, therefore producing less N-terminally truncated Aβ peptides.

Conversely, RAB21 regulates γ-secretase activity via interaction with presenilin-1. Overexpression of RAB21 results in greater Aβ production, whereas silencing of this gene reduced Aβ levels (Sun et al., 2017). RAB21 was only detected in the entorhinal cortex,

suggesting that its absence in the presubiculum could lead to decreased Aβ production in this region.

Aβ production levels in the presubiculum are also highlighted by the proteins PURA and S100A8. PURA is a transcription factor and it has multiple consensus binding sites within the APP promoter. It therefore regulates the transcription of APP and when PURA is bound, transcription of APP is downregulated (Darbinian et al., 2008). Although PURA is only found in the entorhinal cortex, indicative of APP transcription being downregulated in this area, it may in fact indicate that there is dysregulation of APP transcription in the presubiculum. S100A8 is thought to aggregate itself prior to Aβ plaque formation and treatment of a neuronal cell line with S100A8 leads to increased Aβ1-42 but decreased levels of Aβ1-40 (Lodeiro et al., 2017). S100A8 was increased in the entorhinal cortex which may indicate that Aβ in the presubiculum is not able to mature into dense-core plaques as S100A8 is not present in the correct levels to stimulate aggregation, through its own aggregation.

The results show that Aβ generation/processing is different in the presubiculum compared to the entorhinal cortex and this may go some way to explaining the reason that the Aβ deposits in the presubiculum do not go on to form mature plaques. However, this phenomenon is not unique to AD. A similar observation of a large diffuse amyloid deposit can be seen in the presubiculum of both Familial British Dementia (FBD) and Familial Danish Dementia (FDD) (Murray et al, in preparation). Both of these diseases have amyloid that fibrillises to form amyloid deposits, as in AD, but in these diseases it is formed from the ABri and ADan proteins, respectively, due to mutations in the *BRI2* gene. This may suggest that mechanisms other than Aβ generation/processing may occur here and lead to a hypothesis that other factors in the tissue environment are causing these protein expression levels to change.

Previous studies identified the presubiculum had decreased tau accumulation and lacked neurofibrillary degeneration, in contrast to the entorhinal cortex which displayed many NFT's (Akiyama et al., 1990; Bobinski et al., 1995; Fukutani et al., 1997; Kalus et al., 1989). This study also confirmed these observations with significantly less phosphorylated tau and significantly less NFT's in the presubiculum than in the entorhinal cortex. This would suggest

that the mechanisms affecting accumulation of either Aβ or tau are not present or are disrupted in the presubiculum. It has been argued that since Aβ plaques can promote tau aggregation, the relative lack of Aβ plaques observed in the presubiculum has a downstream effect by halting tau aggregation or provoking less hyperphosphorylation of tau (Bennett et al., 2017). The proteomic results revealed that OTUB1 (OTU Deubiquitinase, Ubiquitin Aldehyde Binding 1), a tau deubiquitinating enzyme is increased in the entorhinal cortex compared to the presubiculum. OTUB1 has been shown to increase AT8 positive tau accumulation and to increase tau-seeded tau aggregation (Wang et al., 2017). The fact that OTUB1 is not seen in high levels in the presubiculum, strengthens the possibility that tau is not able to form aggregates as well or as quickly in the presubiculum as it does in the entorhinal cortex.

Inflammation also occurs in AD and is thought to be a part of the pathogenic mechanism. Microglia play a large role in this, with reports of microglia becoming activated, clustering around Aβ plaques and phagocytosing to clear Aβ (see chapter 4 for more detail) (Boche et al., 2013; Gahtan and Overmier, 1999; Gentleman, 2013; Giulian et al., 1996; Griffin et al., 1989, 1995; Itagaki et al., 1989; Meda et al., 1995; Rogers and Lue, 2001; Rogers et al., 1992a, 1992b; Sheng et al., 1998; Yin et al., 2017). Additionally, they are known to release a selection of toxic cytokines that have a pro-inflammatory effect and lead to further cell death (Blasko et al., 2004; Goldgaber et al., 1989). Previous reports have identified that the presubiculum contains no activated microglia compared to many activated microglia in the entorhinal cortex (Akiyama et al., 1990; Wisniewski et al., 1998). This was also confirmed in this study with significantly less microglia positive for activated microglial markers CD68 and CR3-43 in the presubiculum than in the entorhinal cortex. However, microglia were present in both areas, as shown by the Iba1 microglial marker that detects both activated and non-activated microglia.

Proteomic results also suggest that the microglia in the presubiculum act differently to the microglia in the entorhinal cortex. DOCK2 is part of the prostaglandin pathway and has been shown to modulate microglial cytokine secretion and phagocytosis (Cimino et al., 2009). DOCK2 deficient AD mice do not have morphologically different microglia but do have

reduced Aβ plaque size (Cimino et al., 2013). DOCK2 was found only to affect fibrillar Aβ with no change occurring in soluble Aβ levels (Cimino et al., 2013). As DOCK2 is increased in the presubiculum, where no mature Aβ plaques are forming, this increase in expression could be due to increased modulation of the microglia, rather than its effect on Aβ. INPP5D is a negative regulator of the innate immune system and has been linked to AD in GWAS studies (Efthymiou and Goate, 2017; Gjoneska et al., 2015; McKeever et al., 2017). INPP5D mRNA expression was shown to be increased in early stage AD but to decrease as cognitive decline worsens (Yoshino et al., 2017). The increase of INPP5D in the presubiculum suggests that negative regulation of the immune system is more likely to occur here than in the entorhinal cortex. This may explain why microglia do not become activated in this region. Additionally, CX3CR3 is a fractalkine receptor and is involved in neuroinflammatory modulation. APP/PS1 CX3CR3$^{-/-}$ mouse models have been reported to have reduced plaque burden with microglia being less associated with plaques (Krauthausen et al., 2015). Furthermore, this deficiency caused the attenuation of activated microglia and astrocytes with activated microglial markers CD45 and CD11b being absent and reduced levels of pro-inflammatory cytokines being released (Krauthausen et al., 2014, 2015). As CX3CR3 was only found in the entorhinal cortex, the presubiculum could be modelling a CX3CR3 deficiency, leading to reduced activation of the microglia and reduced association with the Aβ present. ANXA1 promotes resolution of inflammation by supressing microglial activation and inhibiting secretion of their pro-inflammatory cytokines (Ries et al., 2016). ANXA1 was only detected in the presubiculum suggesting that a protective role in attenuating the microglial response to Aβ.

Whilst protein changes heavily influence the generation of Aβ/ tau inclusions, there are other cellular mechanisms that are likely to contribute to aberrant protein accumulation. For example, the difference in Aβ morphology could be due to altered clearance mechanisms of Aβ. The proteins C3, AQP4, LRP1 and APOE are all increased in the entorhinal cortex and have an effect on Aβ clearance. C3 is part of the complement cascade and has been shown to be elevated in AD (Shi et al., 2017). C3 deficient mice confer protection against hippocampal synapse loss and alter the microglial phenotype (Shi et al., 2017). Blockage of C3 resulted in Aβ- induced synapse loss rescue before Aβ plaques could accumulate (Shi et

al., 2017). AQP4 has been linked to lymphatic drainage as well as transcytosis mechanisms of clearance of Aβ (Yang et al., 2016). It is commonly found associated with Aβ plaques (Yang et al., 2017b). LRP1 is involved in the endocytosis and transcytosis of Aβ (Kanekiyo et al., 2012, 2013; Nazer et al., 2008; Shibata et al., 2000; Storck and Pietrzik, 2017; Zandl-Lang et al., 2017). Overexpression of LRP1 has been shown to lead to increased Aβ production, however, deletion of LRP1 in multiple AD mouse models show an increase in soluble Aβ and a decrease in clearance (Cam et al., 2005; Pietrzik et al., 2002; Storck and Pietrzik, 2017; Zerbinatti et al., 2004). Interestingly, LRP1 binds to APOE and both are found to be upregulated in the entorhinal cortex (Bell et al., 2007). C3 also has been shown to bind to the *ApoE4* allele (Bonham et al., 2016). Additionally, APOE has been reported to aid Aβ clearance by helping to transport Aβ to the blood vessels (Cirrito et al., 2005; Huynh et al., 2017). Although these results are indicative of less clearance occurring in the presubiculum, this could be down to these proteins playing different roles or having their activity altered in some way. For example, LRP1 can only clear Aβ when it is membrane bound but cleavage by beta and gamma secretases, similar to APP, can cause the protein to be released extracellularly (Arnim et al., 2005; Shackleton et al., 2016; Storck and Pietrzik, 2017). Conversely, less Aβ clearance could be a consequence of the absence of fibrillar Aβ, with these mechanisms of clearance only occurring in the presence of mature Aβ plaques.

Another downstream effect of the presubiculum only containing the non-fibrillar Aβ is less Aβ toxicity. Both HSPA9 and LDHA were upregulated in the presubiculum but are normally shown to be downregulated in AD (Newington et al., 2012; Silva et al., 2014). HSPA9 is a chaperone protein and an expression study identified the isoforms of this protein to be differentially expressed in the hippocampal region, and it is thought to regulate the Aβ toxicity pathway (Flachbartová and Kovacech, 2013). LDHA confers a resistance to Aβ toxicity by decreasing ROS production and mitochondrial respiration (Newington et al., 2012). Reduction in Aβ toxicity may not be the cause of the different deposits in the presubiculum but could add to the neuroprotective nature of the region, allowing it stay in this conformation even as disease progresses.

There are limitations to this study that also need to be considered. Firstly, the number of cases analysed by mass spectrometry is low and these results could not be confirmed until the same methods were applied to a larger cohort. Secondly, the absence of a protein in one of the regions does not necessarily indicate that it is absent from this region. It could be due to technical variability of the mass spectrometer. Therefore, further validation of proteins of interest would be needed to be certain of this.

Although the results discussed were seen in all three AD subgroups, *TREM2* variant cases do appear to have an altered proteomic expression compared to SAD and FAD cases. The result is similar but fewer proteins appear to be causing this effect. As TREM2 is expressed on microglia and mediates its effects through microglia, this could point to the microglial changes observed here being the key to the neuroprotection that the presubiculum appears to have.

6.5.1 Conclusions

In summary, the presubiculum is morphologically and proteomically diverse from its neighbouring region, the entorhinal cortex. The anatomically driven, targeted proteomic screen has highlighted that many changes occur in this region and these associate with less aggregation of Aβ/tau and reduced microglial activation. The presubiculum has deep connections with both the entorhinal cortex, the hippocampus and other areas of the brain. It would therefore be expected that AD pathology would deposit in the same manner in the presubiculum. It remains unclear why this is the case but further biochemical analysis of this area and the proteins mentioned here is needed to elucidate what the cause of this phenomenon is and what is occurring as an effect. Understanding what factor is the key to this neuroprotective mechanism, could lead to therapeutic neuroprotection that can be applied to the whole brain and help halt the disease in its tracks.

Chapter 7

General discussion

7 General discussion

7.1 Summary

1. *TREM2* variant cases that had a diagnosis of AD had similar levels of amyloid plaques and neurofibrillary tangle pathology to sporadic cases and *TREM2* variant cases that were diagnosed as controls had no AD pathology, with no pathological aging present.

2. Five out of six *TREM2* variant cases had CAA pathology, including one case that had no AD pathology present.

3. All *TREM2* variant SAD cases were identified to have an *ApoE4* allele present whereas *TREM2* variant control cases did not.

4. Amyloid plaque load was significantly different between FAD cases and *TREM2* variant cases and SAD cases. However there were no differences in type of plaque between disease groups.

5. Tau load did not significantly differ between *TREM2* variant cases and other disease groups.

6. *TREM2* variant cases had more CD68+ve, circular microglia than other disease groups, indicative of a phenotype of a phagocytic state.

7. *TREM2* variant AD cases showed upregulation of many neuroinflammatory genes compared to other disease groups, whereas *TREM2* variant control cases showed downregulation in these genes.

8. Proteins known to be increased in AD were found to be further increased in *TREM2* variant AD cases and decreased in *TREM2* variant controls.

9. The presubiculum was identified to be pathologically and biochemically altered compared to its neighbouring region, the entorhinal cortex. The presubiculum contains diffuse amyloid deposits, significantly less neurofibrillary tangles, significantly less activated microglia and an altered proteomic profile.

TREM2 was discovered as a genetic risk factor for late onset AD with a similar odds ratio to *ApoE4*. Several variants were found to be pathogenic and having confirmed that TREM2 is expressed on microglia, it was speculated that inflammation may play a greater role in AD pathogenesis than was first thought. Various studies have been undertaken to determine what effect a *TREM2* variant may have on the brain, and its role in AD pathogenesis. However, those have predominantly been on animal or cell models, causing a deficiency or overexpression of *TREM2*. The aim of this thesis was to elucidate further the role *TREM2* variants may have on the brain compared to other sporadic and familial forms of AD and healthy controls. Using multiple techniques and methods the role of TREM2 has been investigated to understand how *TREM2* may confer a risk.

The *TREM2* variant cases that had a pathologically confirmed diagnosis of AD had similar macroscopic abnormalities to those seen in sporadic and familial forms of AD. The *TREM2* variant cases that were confirmed to be normal controls showed no marked differences to normal healthy controls at the macroscopic level. At the microscopic level, the pathology was indicative of AD with amyloid plaque deposition and neurofibrillary tangles present in *TREM2* variant AD cases and indicative of controls with no AD pathology in the *TREM2* variant control cases.

7.2 The effect of *TREM2* variants on amyloid deposition

Mouse models (*APPPS1*) overexpressing *TREM2* showed decreases in amyloid plaque deposition whereas models of *TREM2* deficiency showed conflicting results on the amount of amyloid load between cortical and hippocampal regions (Jay et al., 2015, 2017; Jiang et al., 2014, 2016b; Wang et al., 2015, 2016). On the other hand, amyloid plaques that were found in *TREM2* deficient mice and post-mortem *TREM2 R47H* variants were reported to be more

diffuse and less compact than those of wildtype mice (Yuan et al., 2016). Here, this was investigated by assessing the numbers of diffuse and dense core plaques between Thal phase regions and the different AD subgroups (SAD, FAD, *TREM2* SAD). Whilst there were significantly more diffuse plaques than dense-core plaques in all regions and in each disease group, there was no difference when comparing each disease group to each other. Therefore, this data conflicted with the experiment Yuan et al., (2016) performed previously. Yuan et. al, classified the plaques into a greater number of categories and only assessed the frontal gyrus so the conflicting data could be due to these results not having the same specificity and variation seen across regions.

The type of amyloid plaque deposition did not differ between the disease groups. However, the type of plaque is important in the process of AD pathogenesis. This was demonstrated by the presubiculum region showing a level of neuroprotection against neurodegeneration and the amyloid deposited in this region was shown to be Thioflavin-S negative and therefore in a non-amyloid conformational state. Further to this, the presence of N-terminally truncated and pyroglutamate modified Aβ peptides were observed to be decreased in the presubiculum, although still present when compared to the entorhinal cortex. These N-terminally truncated and pyro-glutamate modified forms of Aβ have been shown to be located in dense-core amyloid plaques and mature the plaques (Portelius et al., 2010; Wittnam et al., 2012). Additionally, the decreased expression of the S100A8 protein in the presubiculum compared to the entorhinal cortex, highlighted that the Aβ in the presubiculum may be stopped from maturing into dense core plaques (Lodeiro et al., 2017). These dense core plaques are also known to be more toxic than diffuse plaques (Serrano-Pozo et al., 2011) and proteins involved with the mechanisms of Aβ toxicity are differentially expressed in the presubiculum compared to the entorhinal cortex, showing reduced Aβ toxicity mediated effects in this region.

From these observations, it can be hypothesised that fibrillar dense cored plaques encourage the toxic effects and neurodegeneration that ensue in the AD brain. As the *TREM2* variant AD cases do not show differences in the levels of diffuse and dense cored

plaques when compared to SAD and FAD, it might be suggested that *TREM2* variants do not confer risk through the fibrillisation of Aβ plaques.

When the total Aβ load was determined, there were differences between regions and a difference in the amount of Aβ load in the FAD cases. FAD cases had significantly more Aβ load in the later Thal phases than SAD and *TREM2* variant SAD cases. Proteins involved with APP cleavage and Aβ production were also found in the top proteins changing in expression of the FAD cases when comparing levels to controls. As FAD cases have pathogenic mutations in the genes that produce Aβ, this is logical. However, the larger levels of Aβ and the pathways involved with it may be the main mechanism in this group, meaning other mechanisms found in SAD may not work in the same way. This would be important to remember if any treatments come to light.

Although FAD cases had the highest Aβ load and the largest variation of amyloid processing genes changing in expression compared to controls, the amyloid processing pathway in the proteomic data was predicted to be activated in all groups other than the *TREM2* variant control group in which it was predicted to be inhibited. *TREM2* variant AD cases had the highest levels of upregulation of APP protein and *TREM2* variant controls were the only group to show downregulation of APP compared to controls. Proteins involved in this pathway also changed in expression in the presubiculum when compared to the entorhinal cortex. The amyloid processing pathway is therefore clearly important in AD pathogenesis and differences in this pathway between *TREM2* variant SAD cases to SAD cases indicate that changes in Aβ production may increase risk, even if how the Aβ is then fibrillised doesn't show a difference.

7.3 The effect of *TREM2* variants on tau deposition

In the same way to Aβ, hyperphosphorylated tau only increased in load in FAD cases in the frontal cortex and putamen compared to other disease groups, otherwise no differences in tau load were observed. This gives further indication that the *TREM2* variant SAD cases act similarly to SAD cases along the mechanisms forming the pathological hallmarks of AD. However, *TREM2* deficient mouse models showed that tau was increased compared to

wildtypes, suggesting that a difference in tau accumulation is only partially observed in heterozygous variants (Jiang et al., 2015, 2016a). On the other hand, *TREM2* variant SAD cases had the highest increase of MAPT protein expression compared to controls whereas *TREM2* variant controls were the only group to show downregulation. A pattern that was also seen with APP. This data allows us to hypothesise that although there may be increased production of amyloid and tau, the mechanisms that are involved with causing their aggregation are no different in the *TREM2* variant SAD cases to SAD cases but play a larger role in FAD cases.

As *TREM2* variant controls have a downregulation of tau at the protein level compared to controls without a *TREM2* variant, they may lack the ability to produce tau as well as the mechanisms involved with *TREM2* aggregation being no different. Therefore, resulting in no build-up of neurofibrillary tangles. The proteins NEDD8 and MAP1B were two of the top upregulated proteins in the *TREM2* variant controls and they have both been reported to be located with neurofibrillary tangles (Iqbal et al., 2005; Mori et al., 2005). This suggests that there is the propensity for neurofibrillary tangles to occur, however another factor is stopping this, potentially less tau being produced.

TREM2 variant controls may have similar mechanisms to the neuroprotection observed in the presubiuclum of AD cases. Significantly less hyperphosphorylated tau and neurofibrillary tangles are present in this area compared to the neighbouring entorhinal cortex. Additionally, a protein OTUB1 known to increase tau accumulation and aggregation was shown to be decreased in the presubiculum compared to the entorhinal cortex (Wang et al., 2017). Less production and aggregation of tau in both the presubiculum and the *TREM2* variant controls may be one way in which these cases or region is protected from the effects/risk of AD.

7.4 Inflammatory response in *TREM2* variant cases

Microglia are known as surveillant cells that detect any foreign substances or cell debris and initiate an inflammatory reaction to reduce it. One way that they do this is by being activated into a phagocytic phenotype. Microglia in AD are thought to be responsible for clearing Aβ plaques via phagocytic mechanisms and TREM2 is thought to have a role in these

mechanisms (Boche et al., 2013; Gahtan and Overmier, 1999; Guerreiro et al., 2013a; Jonsson et al., 2012b; Shaffer et al., 1995; Weldon et al., 1998; Wu et al., 2014).

TREM2 deficiency models observed a decreased level of phagocytosis, whereas *TREM2* overexpression models observed an increased level of phagocytosis (Jay et al., 2015; Jones et al., 2014; Kleinberger et al., 2014; Satoh et al., 2013; Ulrich and Holtzman, 2016; Wang et al., 2015; Zhao and Lukiw, 2013). It was therefore hypothesised that *TREM2* variants would have a loss of function that would result in less clearance of Aβ and hence a higher risk of AD. When in the phagocytic phenotype, the microglia display an amoeboid morphology, which are CD68 positive. When assessing the microglial morphology of the microglia in these cases, it was observed that the *TREM2* variant SAD cases had more of an amoeboid morphology as they had increased CD68 microglial load, increased circularity across microglial markers and a reduced perimeter, indicative of the smaller rounder amoeboid microglia. This would suggest that the microglia in the *TREM2* variant SAD cases are more capable of phagocytosis. This either would conflict with the data from the *TREM2* deficiency models or suggest that even though the microglia are in the phagocytic amoeboid morphology, the process of phagocytosis is not as efficient or reduced. Mazaheri et al., (2017) show that TREM2 deficient microglia have reduced chemotaxis and response to neuronal injury. Alterations in the phagocytic mechanisms in these *TREM2* variant microglia may play a part in their reduced response to neuronal injury.

Although TREM2 is thought to initiate a cascade in which phagocytosis occurs, an alternative mechanism of phagocytosis also exists via toll-like receptors (Blander and Medzhitov, 2004; Frank et al., 2008; Guerreiro et al., 2013a; Jonsson et al., 2012b; Piccio et al., 2007; Takahashi et al., 2005). This alternative mechanism also promotes release of pro-inflammatory cytokines that go on to cause further neuronal damage and exacerbate the inflammatory reaction (Blander and Medzhitov, 2004; Frank et al., 2008; Guerreiro et al., 2013a; Jonsson et al., 2012b; Takahashi et al., 2005). This pathway was shown to be activated in the *TREM2* deficient models and this could therefore lead to the increased risk seen in these *TREM2* variant cases (Takahashi et al., 2005). Further evidence of this alternative mechanism being used was found in the genetic expression data, using

nanostring technology. This pathway was shown to be upregulated in all AD cases. However, the *TREM2* variant SAD cases had higher levels of upregulation than SAD cases, especially of TLR2 and TLR4. As this pathway is activated at higher levels in *TREM2* variant SAD cases, this could lead to increased phagocytosis using this mechanism. Thus, explaining the more amoeboid phagocytic morphology that is seen in these cases. These cases with a *TREM2* variant would then be at increased risk of AD, as higher levels of pro-inflammatory cytokines would be released, leading to increased neuronal loss.

The TLR pathway is not the only neuroinflammatory pathway to be affected in AD. The importance of inflammation in AD was observed when the presubiculum, the region not affected by AD pathology, showed significantly less activated microglia than the entorhinal cortex and protein expression levels showed altered modulation, regulation, activation of microglia and a reduced association of microglia with Aβ plaques. Suggestive that in an area with little neurodegeneration, the inflammatory profile is changed markedly.

Further to this, the whole neuroinflammatory pathway was predicted to be activated in all of the AD groups, with inhibition only predicted in the *TREM2* variant control group. However, as observed in the TLR pathway, the *TREM2* variant SAD cases have an increased amount of activation as more genes in this overall pathway are upregulated.

The *TREM2* variant control group observed large levels of downregulation of genes involved in the overall neuroinflammatory pathway, showing a striking difference from the healthy controls, which also have no AD pathology. They also show downregulation across the whole TLR pathway. The microglia in these cases had a different pattern of morphology to that seen in the *TREM2* variant SAD cases; exhibiting an opposite pattern of Iba1 load, microglia lacking antigen presenting cells in a more surveillant phenotype, and increased P2RY12 homeostatic microglia. These cases have the same variant of *TREM2* as the *TREM2* variant SAD cases but have opposing microglial and inflammatory phenotypes and little AD pathology present. Therefore, another factor other than the *TREM2* variant must have an effect in order to determine the effects the variant has on the brain and how much risk of AD is present.

7.5 *APOE* genotype effect on *TREM2* variant cases

APOE is the major known risk factor for late onset AD and confers different levels of risk dependent on its genotype (Allen D. Roses, 1996). The presence of two *ApoE4* alleles confer the greatest risk with *ApoE2* allele's having more of a protective role (Yu et al., 2015). *ApoE4* additionally causes risk of CAA (Alonzo et al., 1998; Pfeifer et al., 2002). However, for CAA, *ApoE2* has been shown to cause vascular changes so not be protective of CAA (Yu et al., 2015). This is evident within these *TREM2* variant cases. The *APOE* genotype was determined for each case and it was found that the *TREM2* variant cases that had a SAD diagnosis all had at least one *ApoE4* allele, whereas the *TREM2* variants that were diagnosed as controls, having no AD pathology, had no *ApoE4* allele. Five out of six of these cases all had CAA, indicating that the *ApoE* genotype may determine the presence of CAA, regardless of *TREM2* variant. As a case that no AD pathology had CAA, it may suggest a link between TREM2 and the failure of intramural periarterial drainage (IPAD) and CAA. As these cases have an altered extracelleular matrix composition as shown in the proteomic study, the basement membrane could be impaired leading to CAA.

The finding that all *TREM2* variant SAD cases had an *ApoE4* allele could also be seen throughout the cases identified with *TREM2* variants in the literature (Korvatska O et al., 2015; Krasemann et al., 2017; Yuan et al., 2016). Therefore, the hypothesis that both an *ApoE4* genotype and a *TREM2 R47H* variant are needed to cause AD was introduced (Murray et al, in press). APOE has been shown to be a ligand for TREM2 and it has been reported that APOE binding to TREM2 initiates the TREM2 signalling pathway, via its signalling adaptor protein, TYROBP/DAP12 (Atagi et al., 2015; Bailey et al., 2015; Jendresen et al., 2017; Krasemann et al., 2017). To date there has been no confirmation that different *ApoE* alleles bind to TREM2 at different affinities. However, as *TREM2* variants, *R47H* in particular, have been shown to have reduced ligand binding, including lipoproteins, the binding to APOE in these variants may be reduced or changed (Abduljaleel et al., 2014; Wang et al., 2015).

Where possible, a separate analysis based on *APOE* genotype rather than disease group was completed, to determine if the effect we are seeing between disease groups was

independent of *APOE* genotype or not. *ApoE4* is reported to increase Aβ deposition and decrease its clearance (Castellano et al., 2011). However, in this data, no difference was found between genotypes for Aβ load, leading to the conclusion that APOE may have an effect on the way the Aβ is deposited rather than how much is deposited.

Within the microglia, in which TREM2 binding to the APOE associated with plaques is reported to trigger phagocytic mechanisms, the *ApoE2/2* microglia appeared to have an inactivated phenotype with decreased microglial load, a more ramified, surveillant shape and a smaller perimeter. In particular, they had an increased P2RY12 load that is indicative of larger amounts of homeostatic microglia. On the other hand, the *ApoE4/4* microglia had a similar phenotype to that found in *TREM2* variant SAD cases with increased CD68 load and a more amoeboid morphology. These results therefore indicate that *APOE* genotype has a larger effect on microglial phenotype than the deposition of AD pathology and hence may be an important link to inflammation.

Furthermore, APOE is upregulated at the protein level of the insoluble fraction across all groups. This upregulation is highest in the *TREM2* variant SAD group and markedly higher fold changes were observed in all groups compared to the *TREM2* variant controls, in which the neuroinflammatory pathway is downregulated instead of upregulated. Similarly, APOE is increased in the entorhinal cortex compared to the presubiculum. As APOE is upregulated in areas or cases in which neuroinflammation is not activated, its role in inflammation is more convincing.

ApoE4 genotypes have been shown to have increased neuroinflammation in *P301S* tau transgenic mouse models (Shi et al., 2017). The link between *TREM2* and *APOE* may be modulated through the neuroinflammatory route. The TLR pathway had higher levels of upregulation in *TREM2* variant SAD cases compared to other SAD cases. TLR activators have been shown to reduce microglial expression of TREM2 with further reduction observed in *ApoE4/4* carriers compared to other genotypes. APOE itself is an upstream regulator of TLR2, which is one of the genes increased in *TREM2* variant SAD cases. *APOE* and its individual phenotypes, may be causing decreased expression of TREM2, leading to reduced inhibition of the TLR response pathway and an increase in pro-inflammatory cytokines being

released. As *TREM2* variant controls have no *ApoE4* allele present, this effect would be reduced, leading to further inhibition of the TLR pathway, shown by downregulation of these genes, and the conventional phagocytosis triggered by TREM2 occurs with less inflammatory cascades. If this hypothesis is true, it would show that the effect of *APOE* genotype and *TREM2* variants are linked, adding notion to the hypothesis that the *TREM2* variant cannot cause AD unless an *ApoE4* allele is present.

7.6 General conclusions

Overall, this thesis has shown that *TREM2* variant cases have differences in microglial phenotype, genetic and proteomic expression compared to either sporadic or familial AD cases but do not show changes in amyloid plaque or neurofibrillary tangle deposition analysed through semi-quantiative assessments or through diagnostic criteria.

Previous literature suggested that *TREM2* variants have a loss of function and they have reduced function in clearing amyloid plaques via phagocytic mechanisms. This study did not find a change in the amyloid load in *TREM2* variants compared to AD and the *TREM2* variant cases did not show a difference in the number of diffuse and dense core plaques, this may not be the case. Instead, the microglial actions and inflammatory cascades that ensue may be having the effect in order to cause risk of AD. The most distinct changes in *TREM2* variant SAD cases here is in the changes seen in the neuroinflammatory pathway.

The observation that *TREM2* variant cases that do not have any AD pathology at time of death, have a different profile not only to other *TREM2* variants and AD cases but also to normal controls, suggests that another factor is needed to promote a different route of pathogenesis to AD cases. TREM2's link to APOE and the fact that the *APOE* genotype lacks an *ApoE4* allele in these cases, indicates that APOE may be exerting this change between *TREM2* variants, leading us to question whether the *TREM2 R47H* variant is acting independently.

Limitations to this study include the small number of cases due to the rarity of the *TREM2* mutations that come to brain donation and the fact only late stage AD post-mortem brains have been investigated. This makes it harder to determine whether the changes we observe

are cause or consequence of the disease and the results need to be repeated in larger cohorts. Putting these limitations aside, I would propose the hypothesis that TREM2 and APOE work closely together, having an impact on the pro-inflammatory cascades that lead to further neuronal damage and death and lead to exacerbation of disease. Further investigations into these pathways and the differences between *TREM2* variants that develop disease and those that don't may lead us to the mechanisms that can be targeted for treatments.

7.7 Future directions

Human studies	**Experimental work**
Repeat these experiments on a larger set of cases. Although there wasn't wide variation between the *TREM2* variants, whilst split into their AD/control groups, this could be by chance. Therefore, studying these effects observed in a greater number of cases would allow us to be certain these differences are true.	Assess the pathology in the same way in different *TREM2* mouse models to determine if the methods are producing different results or whether the pathology differs greatly between rodents and humans.
To further establish what changes may occur with Aβ plaques in the *TREM2* variants, the size of the plaques could be determined and additionally the microglia that are seen to surround the dense core plaques could be counted, with the physical interactions between the two verified using a range of markers.	iPSC models from patients with a *TREM2* variant could be used to determine when the Aβ plaques appear and when they do, what size they are and a microglial cell dish could be used to determine how they react when Aβ is introduced to the culture.

Further validation of new commercial TREM2 antibodies would help elucidate this connection between amyloid plaques and microglia. These studies would help to determine why TREM2 models do see differences in amyloid plaque deposition and in this study, we do not.	If failure to find a reproducible commercial antibody in human tissue, the TREM2 distribution between different regions could be determined using pathology found in *TREM2* haplosufficient mouse models.
Validating the proteomic data with western blots to determine the increased protein level of APP, MAPT, APOE and GFAP in the *TREM2* variant SAD cases would also be beneficial.	Proteomics on *TREM2* mouse models could be performed to determine if the same differences in protein expression can be observerd. This would help elucidate how reliable these mouse models are.
As the genes within astrocytes in the neuroinflammation signalling pathway were shown to be altered and the protein levels of reactive astrocytes appear to be increased in *TREM2* variant SAD cases, the astrocyte phenotype and morphology could be determined in a similar way to the microglial phenotype in this study. Results from this experiment could help elucidate the role of TREM2 further and how it interacts with all cell types, not just microglia.	iPSC models from patients with a *TREM2* variant could be made into astrocytic cultures and the way that the astrocytes behave could be studied. Their reaction to Aβ being introduced could be measured.
It would be interesting to see if the same differences found at the genetic and proteomic levels in the frontal cortex of these	Mouse models that are *TREM2* deficient could also have other inflammatory genes knocked out/inhibited and the accumulative

cases were also found in other regions affected by AD pathology and also in the regions that do not contain AD pathology. The results from the study on the presubiculum, an area protected from neurodegeneration, suggest that changes in the inflammatory proteins are key to neuroprotection so investigating these proteins in multiple other regions may help to reveal proteins that could be targeted to stop AD progression.	effect could be observed. Assays to detect inflammatory proteins in these models could also be performed to determine if the same effects are seen in the mouse models.
The differences between different AD subgroups in these datasets could also be further investigated to isolate which mechanisms are particular to each disease group and what the common mechanisms are. These findings should also be validated with immunohistochemistry, RT-PCR or western blotting techniques.	Once uncommon/common pathways and mechanisms have been discovered between the different disease groups, inhibitors to molecules within the pathways could be used on mouse models and the effects observed.
If the proteomics could be repeated on AD cases without a *TREM2* variant but with a range of *APOE* genotypes it would allow us to better determine whether the *APOE* genotype is the main cause of the changes we observe in this study and whether these changes are independent or dependent on *TREM2*. Assessing the APOE load with immunohistochemistry and determining what	The *APOE* genotype found in the different *TREM2* mouse models in which they have measured pathology should be investigated to determine if the same links can be seen in these models.

cells it is located with would also help to further understand this link between APOE and TREM2. However, as APOE has multiple functions this could be a difficult task.	
APOE also has a role in the transport of Aβ to the blood vessels and is also known to confer risk to CAA. Five out of six of the *TREM2* variant cases also have CAA pathology, so further investigation into whether the prevalence of CAA is higher in *TREM2* variants compared with other AD cases would help us to also understand the full role that APOE is playing in these brains.	Investigating the difference clearance mechanisms in *TREM2* mouse models would help establish whether microglial clearance is the only clearance mechanism impaired. In particular, the IPAD mechanisms could be investigated in these mouse models to investigate the high prevalence of CAA in these *TREM2* variant cases and to determine if APOE is linked to TREM2 mechanisms via this pathway.

As always, studying post-mortem brain tissue predominantly means studying late stage disease when changes have already occurred and picking out what is causing disease and what is occurring as a result of the disease can be confusing. The main alternative to this is using different models to look at these investigations. The caveat with this is that most models can only model one aspect of the disease so it is difficult to determine if the whole effect is seen. Ideally, these experiments could be repeated on post-mortem brains in a set of cases that have early stage disease.

This thesis has highlighted that further investigation towards inflammation in AD needs pursuing and that there is still more to be discovered about the TREM2 signalling pathway and the link it has to APOE. Through some of these mentioned future directions, we could find answers to some of these questions, making us closer to understanding AD pathogenesis and finding targets for treatments.

Chapter 8

References

8 References

Abduljaleel, Z., Al-Allaf, F.A., Khan, W., Athar, M., Shahzad, N., Taher, M.M., Elrobh, M., Alanazi, M.S., and El-Huneidi, W. (2014). Evidence of Trem2 Variant Associated with Triple Risk of Alzheimer's Disease. PLoS ONE *9*, e92648.

Abramov, E., Dolev, I., Fogel, H., Ciccotosto, G.D., Ruff, E., and Slutsky, I. (2009). Amyloid-β as a positive endogenous regulator of release probability at hippocampal synapses. Nat. Neurosci. *12*, 1567.

Ahmed, Z., Cooper, J., Murray, T.K., Garn, K., McNaughton, E., Clarke, H., Parhizkar, S., Ward, M.A., Cavallini, A., Jackson, S., et al. (2014). A novel in vivo model of tau propagation with rapid and progressive neurofibrillary tangle pathology: the pattern of spread is determined by connectivity, not proximity. Acta Neuropathol. (Berl.) *127*, 667–683.

Akiyama, H., Tago, H., Itagaki, S., and McGeer, P.L. (1990). Occurrence of diffuse amyloid deposits in the presubicular parvopyramidal layer in Alzheimer's disease. Acta Neuropathol. (Berl.) *79*, 537–544.

Akiyama, H., Barger, S., Barnum, S., Bradt, B., Bauer, J., Cole, G.M., Cooper, N.R., Eikelenboom, P., Emmerling, M., Fiebich, B.L., et al. (2000). Inflammation and Alzheimer's disease. Neurobiol. Aging *21*, 383–421.

Albright, A.V., Shieh, J.T., O'Connor, M.J., and González-Scarano, F. (2000). Characterization of cultured microglia that can be infected by HIV-1. J. Neurovirol. *6 Suppl 1*, S53-60.

Allcock, R.J.N., Barrow, A.D., Forbes, S., Beck, S., and Trowsdale, J. (2003). The human TREM gene cluster at 6p21.1 encodes both activating and inhibitory single IgV domain receptors and includes NKp44. Eur. J. Immunol. *33*, 567–577.

Allen D. Roses, M.D. (1996). Apolipoprotein E Alleles as Risk Factors in Alzheimer's Disease. Annu. Rev. Med. *47*, 387–400.

Alonzo, N.C., Hyman, B.T., Rebeck, G.W., and Greenberg, S.M. (1998). Progression of Cerebral Amyloid Angiopathy: Accumulation of Amyloid-β40 in Affected Vessels. J. Neuropathol. Exp. Neurol. *57*, 353–359.

Altman, J. (1994). Microglia emerge from the fog. Trends Neurosci. *17*, 47–49.

Andjelkovic, A.V., Nikolic, B., Pachter, J.S., and Zecevic, N. (1998). Macrophages/microglial cells in human central nervous system during development: an immunohistochemical study. Brain Res. *814*, 13–25.

Aoki, N., Kimura, S., and Xing, Z. (2003). Role of DAP12 in Innate and Adaptive Immune Responses. Curr. Pharm. Des. *9*, 7–10.

Arends, Y.M., C., Rozemuller, J.M., Eikelenboom, P., and Hauw, J.-J. (2000). Microglia, amyloid and dementia in Alzheimer disease: A correlative study. Neurobiol. Aging *21*, 39–47.

Arnim, C.A.F. von, Kinoshita, A., Peltan, I.D., Tangredi, M.M., Herl, L., Lee, B.M., Spoelgen, R., Hshieh, T.T., Ranganathan, S., Battey, F.D., et al. (2005). The Low Density Lipoprotein Receptor-related Protein (LRP) Is a Novel β-Secretase (BACE1) Substrate. J. Biol. Chem. *280*, 17777–17785.

Atagi, Y., Liu, C.-C., Painter, M.M., Chen, X.-F., Verbeeck, C., Zheng, H., Li, X., Rademakers, R., Kang, S.S., Xu, H., et al. (2015). Apolipoprotein E is a Ligand for Triggering Receptor Expressed on Myeloid Cells 2 (TREM2). J. Biol. Chem. jbc.M115.679043.

Augustinack, J.C., Helmer, K., Huber, K.E., Kakunoori, S., Zöllei, L., and Fischl, B. (2010). Direct visualization of the perforant pathway in the human brain with ex vivo diffusion tensor imaging. Front. Hum. Neurosci. *4*, 42.

Bailey, C.C., DeVaux, L.B., and Farzan, M. (2015). The Triggering Receptor Expressed on Myeloid Cells 2 Binds Apolipoprotein E. J. Biol. Chem. jbc.M115.677286.

Bales, K.R., Verina, T., Cummins, D.J., Du, Y., Dodel, R.C., Saura, J., Fishman, C.E., DeLong, C.A., Piccardo, P., Petegnief, V., et al. (1999). Apolipoprotein E is essential for amyloid deposition in the APPV717F transgenic mouse model of Alzheimer's disease. Proc. Natl. Acad. Sci. U. S. A. *96*, 15233–15238.

Banati, R.B., Gehrmann, J., Czech, C., Mönning, U., Jones, L.L., König, G., Beyreuther, K., and Kreutzberg, G.W. (1993). Early and rapid de novo synthesis of Alzheimer βA4-Amyloid precursor protein (APP) in activated microglia. Glia *9*, 199–210.

Barger, S.W., and Harmon, A.D. (1997). Microglial activation by Alzheimer amyloid precursor protein and modulation by apolipoprotein E. Nature *388*, 42257.

Bell, R.D., Sagare, A., Friedman, A.E., Bedi, G., Holtzman, D.M., Deane, R., and Zlokovic, B.V. (2007). Transport pathways for clearance of human Alzheimer's amyloid β-peptide and apolipoproteins E and J in the mouse central nervous system. J. Cereb. Blood Flow Metab. Off. J. Int. Soc. Cereb. Blood Flow Metab. *27*, 909–918.

Bellucci, C., Lilli, C., Baroni, T., Parnetti, L., Sorbi, S., Emiliani, C., Lumare, E., Calabresi, P., Balloni, S., and Bodo, M. (2007). Differences in Extracellular Matrix Production and Basic Fibroblast Growth Factor Response in Skin Fibroblasts from Sporadic and Familial Alzheimer's Disease. Mol. Med. *13*, 542–550.

Bennett, R.E., DeVos, S.L., Dujardin, S., Corjuc, B., Gor, R., Gonzalez, J., Roe, A.D., Frosch, M.P., Pitstick, R., Carlson, G.A., et al. (2017). Enhanced Tau Aggregation in the Presence of Amyloid β. Am. J. Pathol. *187*, 1601–1612.

Berchtold, N.C., Sabbagh, M.N., Beach, T.G., Kim, R.C., Cribbs, D.H., and Cotman, C.W. (2014). Brain gene expression patterns differentiate Mild Cognitive Impairment from normal Aged and Alzheimer Disease. Neurobiol. Aging *35*, 1961–1972.

Bergeron, C., Ranalli, P.J., and Miceli, P.N. (1987). Amyloid angiopathy in Alzheimer's disease. Can. J. Neurol. Sci. *14*, 564–569.

Bertram, L., and Tanzi, R.E. (2012). Chapter 3 - The Genetics of Alzheimer's Disease. In Progress in Molecular Biology and Translational Science, David B. Teplow, ed. (Academic Press), pp. 79–100.

Beyer, N., Coulson, D.T.R., Quinn, J.G., Brockbank, S., Hellemans, J., Irvine, G.B., Ravid, R., and Johnston, J.A. (2014). mRNA levels of BACE1 and its interacting proteins, RTN3 and PPIL2, correlate in human post mortem brain tissue. Neuroscience *274*, 44–52.

Bhaskar, K., Konerth, M., Kokiko-Cochran, O.N., Cardona, A., Ransohoff, R.M., and Lamb, B.T. (2010). Regulation of Tau Pathology by the Microglial Fractalkine Receptor. Neuron *68*, 19–31.

Bisht, K., Sharma, K.P., Lecours, C., Gabriela Sánchez, M., El Hajj, H., Milior, G., Olmos-Alonso, A., Gómez-Nicola, D., Luheshi, G., Vallières, L., et al. (2016). Dark microglia: A new phenotype predominantly associated with pathological states. Glia n/a-n/a.

Bjelik, A., Pákáski, M., Bereczki, E., Gonda, S., Juhász, A., Rimanóczy, Á., Zana, M., Janka, Z., Sántha, M., and Kálmán, J. (2007). APP mRNA splicing is upregulated in the brain of biglycan transgenic mice. Neurochem. Int. *50*, 1–4.

Blander, J.M., and Medzhitov, R. (2004). Regulation of Phagosome Maturation by Signals from Toll-Like Receptors. Science *304*, 1014–1018.

Blasko, I., Stampfer-Kountchev, M., Robatscher, P., Veerhuis, R., Eikelenboom, P., and Grubeck-Loebenstein, B. (2004). How chronic inflammation can affect the brain and support the development of Alzheimer's disease in old age: the role of microglia and astrocytes. Aging Cell *3*, 169–176.

Bobinski, M., Wegiel, J., Wisniewski, H.M., Tarnawski, M., Reisberg, B., Mlodzik, B., de Leon, M.J., and Miller, D.C. (1995). Atrophy of hippocampal formation subdivisions correlates with stage and duration of Alzheimer disease. Dement. Basel Switz. *6*, 205–210.

Boche, D., Perry, V.H., and Nicoll, J. a. R. (2013). Review: Activation patterns of microglia and their identification in the human brain. Neuropathol. Appl. Neurobiol. *39*, 3–18.

Bogdanovic, N., Davidsson, P., Volkmann, I., Winblad, B., and Blennow, K. (2000). Growth-associated protein GAP-43 in the frontal cortex and in the hippocampus in Alzheimer's disease: an immunohistochemical and quantitative study. J. Neural Transm. *107*, 463–478.

Bogdanovic, N., Corder, E., Lannfelt, L., and Winblad, B. (2002). APOE polymorphism and clinical duration determine regional neuropathology in Swedish APP670, 671 mutation carriers: implications for late-onset Alzheimer's disease. J. Cell. Mol. Med. *6*, 199–214.

Bohm, C., Chen, F., Sevalle, J., Qamar, S., Dodd, R., Li, Y., Schmitt-Ulms, G., Fraser, P.E., and St George-Hyslop, P.H. (2015). Current and future implications of basic and translational research on amyloid-β peptide production and removal pathways. Mol. Cell. Neurosci. *66*, 3–11.

Bolmont, T., Haiss, F., Eicke, D., Radde, R., Mathis, C.A., Klunk, W.E., Kohsaka, S., Jucker, M., and Calhoun, M.E. (2008). Dynamics of the Microglial/Amyloid Interaction Indicate a Role in Plaque Maintenance. J. Neurosci. *28*, 4283–4292.

Bonham, L.W., Desikan, R.S., and Yokoyama, J.S. (2016). The relationship between complement factor C3, APOE ε4, amyloid and tau in Alzheimer's disease. Acta Neuropathol. Commun. *4*.

Borroni, B., Ferrari, F., Galimberti, D., Nacmias, B., Barone, C., Bagnoli, S., Fenoglio, C., Piaceri, I., Archetti, S., Bonvicini, C., et al. (2014). Heterozygous TREM2 mutations in frontotemporal dementia. Neurobiol. Aging *35*, 934.e7-934.e10.

Bossers, K., Wirz, K.T.S., Meerhoff, G.F., Essing, A.H.W., Dongen, V., W, J., Houba, P., Kruse, C.G., Verhaagen, J., and Swaab, D.F. (2010). Concerted changes in transcripts in the prefrontal cortex precede neuropathology in Alzheimer's disease. Brain *133*, 3699–3723.

Bouchon, A., Hernández-Munain, C., Cella, M., and Colonna, M. (2001). A Dap12-Mediated Pathway Regulates Expression of Cc Chemokine Receptor 7 and Maturation of Human Dendritic Cells. J. Exp. Med. *194*, 1111–1122.

Boutajangout, A., and Wisniewski, T. (2013). The Innate Immune System in Alzheimer's Disease.

Bouter, Y., Dietrich, K., Wittnam, J.L., Rezaei-Ghaleh, N., Pillot, T., Papot-Couturier, S., Lefebvre, T., Sprenger, F., Wirths, O., Zweckstetter, M., et al. (2013). N-truncated amyloid β (Aβ) 4-42 forms stable aggregates and induces acute and long-lasting behavioral deficits. Acta Neuropathol. (Berl.) *126*, 189–205.

Braak, P.D. med H. (1978). Pigment architecture of the human telencephalic cortex. Cell Tissue Res. *190*, 509–523.

Braak, H., and Braak, E. (1991). Neuropathological stageing of Alzheimer-related changes. Acta Neuropathol. (Berl.) *82*, 239–259.

Brecht, W.J., Harris, F.M., Chang, S., Tesseur, I., Yu, G.-Q., Xu, Q., Fish, J.D., Wyss-Coray, T., Buttini, M., Mucke, L., et al. (2004). Neuron-Specific Apolipoprotein E4 Proteolysis Is Associated with Increased Tau Phosphorylation in Brains of Transgenic Mice. J. Neurosci. *24*, 2527–2534.

Brenowitz, W.D., Nelson, P.T., Besser, L.M., Heller, K.B., and Kukull, W.A. (2015). Cerebral amyloid angiopathy and its co-occurrence with Alzheimer's disease and other cerebrovascular neuropathologic changes. Neurobiol. Aging *36*, 2702–2708.

Bu, G. (2009). Apolipoprotein E and its receptors in Alzheimer's disease: pathways, pathogenesis and therapy. Nat. Rev. Neurosci. *10*, 333–344.

Buchhave, P., Minthon, L., Zetterberg, H., Wallin, Å.K., Blennow, K., and Hansson, O. (2012). Cerebrospinal Fluid Levels ofβ-Amyloid 1-42, but Not of Tau, Are Fully Changed Already 5 to 10 Years Before the Onset of Alzheimer Dementia. Arch. Gen. Psychiatry *69*, 98–106.

Busse, S., Steiner, J., Glorius, S., Dobrowolny, H., Greiner-Bohl, S., Mawrin, C., Bommhardt, U., Hartig, R., Bogerts, B., and Busse, M. (2015). VGF expression by T lymphocytes in patients with Alzheimer's disease. Oncotarget *6*, 14843–14851.

Butovsky, O., Jedrychowski, M.P., Moore, C.S., Cialic, R., Lanser, A.J., Gabriely, G., Koeglsperger, T., Dake, B., Wu, P.M., Doykan, C.E., et al. (2013). Identification of a unique TGF-β–dependent molecular and functional signature in microglia. Nat. Neurosci. *17*, 131–143.

Buxbaum, J.D., Oishi, M., Chen, H.I., Pinkas-Kramarski, R., Jaffe, E.A., Gandy, S.E., and Greengard, P. (1992). Cholinergic agonists and interleukin 1 regulate processing and secretion of the Alzheimer beta/A4 amyloid protein precursor. Proc. Natl. Acad. Sci. U. S. A. *89*, 10075–10078.

Caballero-Bleda, M., and Witter, M.P. (1994). Projections from the presubiculum and the parasubiculum to morphologically characterized entorhinal-hippocampal projection neurons in the rat. Exp. Brain Res. *101*, 93–108.

Cady, J., Koval, E.D., Benitez, B.A., Zaidman, C., Jockel-Balsarotti, J., Allred, P., Baloh, R.H., Ravits, J., Simpson, E., Appel, S.H., et al. (2014). The TREM2 variant p.R47H is a risk factor for sporadic amyotrophic lateral sclerosis. JAMA Neurol. *71*, 449–453.

Cam, J.A., Zerbinatti, C.V., Li, Y., and Bu, G. (2005). Rapid Endocytosis of the Low Density Lipoprotein Receptor-related Protein Modulates Cell Surface Distribution and Processing of the β-Amyloid Precursor Protein. J. Biol. Chem. *280*, 15464–15470.

Camargo, L.M., Zhang, X.D., Loerch, P., Caceres, R.M., Marine, S.D., Uva, P., Ferrer, M., Rinaldis, E. de, Stone, D.J., Majercak, J., et al. (2015). Pathway-Based Analysis of Genome-Wide siRNA Screens Reveals the Regulatory Landscape of App Processing. PLoS ONE *10*, e0115369.

Cantoni, C., Bollman, B., Licastro, D., Xie, M., Mikesell, R., Schmidt, R., Yuede, C.M., Galimberti, D., Olivecrona, G., Klein, R.S., et al. (2015). TREM2 regulates microglial cell activation in response to demyelination in vivo. Acta Neuropathol. (Berl.) 1–19.

Carlesimo, G.A., Piras, F., Orfei, M.D., Iorio, M., Caltagirone, C., and Spalletta, G. (2015). Atrophy of presubiculum and subiculum is the earliest hippocampal anatomical marker of Alzheimer's disease. Alzheimers Dement. Diagn. Assess. Dis. Monit. *1*, 24–32.

Carpenter, A.F., Carpenter, P.W., and Markesbery, W.R. (1993). Morphometric analysis of microglia in Alzheimer's disease. J. Neuropathol. Exp. Neurol. *52*, 601–608.

Castellano, J.M., Kim, J., Stewart, F.R., Jiang, H., DeMattos, R.B., Patterson, B.W., Fagan, A.M., Morris, J.C., Mawuenyega, K.G., Cruchaga, C., et al. (2011). Human apoE isoforms differentially regulate brain amyloid-β peptide clearance. Sci. Transl. Med. *3*, 89ra57.

Chakrabarty, P., Li, A., Ceballos-Diaz, C., Eddy, J.A., Funk, C.C., Moore, B., DiNunno, N., Rosario, A.M., Cruz, P.E., Verbeeck, C., et al. (2015). IL-10 Alters Immunoproteostasis in APP Mice, Increasing Plaque Burden and Worsening Cognitive Behavior. Neuron *85*, 519–533.

Chan, G., White, C.C., Winn, P.A., Cimpean, M., Replogle, J.M., Glick, L.R., Cuerdon, N.E., Ryan, K.J., Johnson, K.A., Schneider, J.A., et al. (2015). CD33 modulates TREM2: convergence of Alzheimer loci. Nat. Neurosci. *advance online publication*.

Chano, T., Okabe, H., and Hulette, C.M. (2007). RB1CC1 insufficiency causes neuronal atrophy through mTOR signaling alteration and involved in the pathology of Alzheimer's diseases. Brain Res. *1168*, 97–105.

Chávez-Gutiérrez, L., Bammens, L., Benilova, I., Vandersteen, A., Benurwar, M., Borgers, M., Lismont, S., Zhou, L., Van Cleynenbreugel, S., Esselmann, H., et al. (2012). The mechanism of γ-Secretase dysfunction in familial Alzheimer disease. EMBO J. *31*, 2261–2274.

Chen, F., Guan, Q., Nie, Z.-Y., and Jin, L.-J. (2013). Gene Expression Profile and Functional Analysis of Alzheimer's Disease. Am. J. Alzheimers Dis. Dementiasr *28*, 693–701.

Chertoff, M., Shrivastava, K., Gonzalez, B., Acarin, L., and Giménez-Llort, L. (2013). Differential Modulation of TREM2 Protein during Postnatal Brain Development in Mice. PLoS ONE *8*, 1–14.

Cho, H.S., Hyman, B.T., Greenberg, S.M., and Rebeck, G.W. (2001). Quantitation of apoE Domains in Alzheimer Disease Brain Suggests a Role for apoE in Aß Aggregation. J. Neuropathol. Exp. Neurol. *60*, 342–349.

Chu, Q., Diedrich, J.K., Vaughan, J.M., Donaldson, C.J., Nunn, M.F., Lee, K.-F., and Saghatelian, A. (2016). HtrA1 Proteolysis of ApoE in vitro is Allele Selective. J. Am. Chem. Soc. *138*, 9473–9478.

Cimino, P.J., Sokal, I., Leverenz, J., Fukui, Y., and Montine, T.J. (2009). DOCK2 Is a Microglial Specific Regulator of Central Nervous System Innate Immunity Found in Normal and Alzheimer's Disease Brain. Am. J. Pathol. *175*, 1622–1630.

Cimino, P.J., Yang, Y., Li, X., Hemingway, J.F., Cherne, M.K., Khademi, S.B., Fukui, Y., Montine, K.S., Montine, T.J., and Keene, C.D. (2013). Ablation of the Microglial Protein DOCK2 Reduces Amyloid Burden in a Mouse Model of Alzheimer's Disease. Exp. Mol. Pathol. *94*, 366–371.

Cirrito, J.R., Deane, R., Fagan, A.M., Spinner, M.L., Parsadanian, M., Finn, M.B., Jiang, H., Prior, J.L., Sagare, A., Bales, K.R., et al. (2005). P-glycoprotein deficiency at the blood-brain barrier increases amyloid-β deposition in an Alzheimer disease mouse model. J. Clin. Invest. *115*, 3285–3290.

Cocco, C., D'Amato, F., Noli, B., Ledda, A., Brancia, C., Bongioanni, P., and Ferri, G.-L. (2010). Distribution of VGF peptides in the human cortex and their selective changes in Parkinson's and Alzheimer's diseases. J. Anat. *217*, 683–693.

Colonna, M. (2003). TREMs in the immune system and beyond. Nat. Rev. Immunol. *3*, 445–453.

Colonna, M., and Wang, Y. (2016). TREM2 variants: new keys to decipher Alzheimer disease pathogenesis. Nat. Rev. Neurosci. *17*, 201.

Condello, C., Yuan, P., and Grutzendler, J. (2017). Microglia-Mediated Neuroprotection, TREM2, and Alzheimer's Disease: Evidence From Optical Imaging. Biol. Psychiatry.

Conejero-Goldberg, C., Hyde, T., Chen, S., Dreses-Werringloer, U., Herman, M., Kleinman, J., Davies, P., and Goldberg, T. (2011). Molecular signatures in post-mortem brain tissue of younger individuals at high risk for Alzheimer's disease as based on APOE genotype. Mol. Psychiatry *16*, 836–847.

Cooper, A.D. (1997). Hepatic uptake of chylomicron remnants. J. Lipid Res. *38*, 2173–2192.

Corder, E.H., Saunders, A.M., Strittmatter, W.J., Schmechel, D.E., Gaskell, P.C., Small, G.W., Roses, A.D., Haines, J.L., and Pericak-Vance, M.A. (1993). Gene dose of apolipoprotein E type 4 allele and the risk of Alzheimer's disease in late onset families. Science *261*, 921–923.

Cotman, S.L., Halfter, W., and Cole, G.J. (2000). Agrin Binds to β-Amyloid (Aβ), Accelerates Aβ Fibril Formation, and Is Localized to Aβ Deposits in Alzheimer's Disease Brain. Mol. Cell. Neurosci. *15*, 183–198.

Couey, J.J., Witoelar, A., Zhang, S.-J., Zheng, K., Ye, J., Dunn, B., Czajkowski, R., Moser, M.-B., Moser, E.I., Roudi, Y., et al. (2013). Recurrent inhibitory circuitry as a mechanism for grid formation. Nat. Neurosci. *16*, nn.3310.

Cruchaga, C., Kauwe, J.S.K., Harari, O., Jin, S.C., Cai, Y., Karch, C.M., Benitez, B., Jeng, A.T., Skorupa, T., Carrell, D., et al. (2013). GWAS of cerebrospinal fluid tau levels identifies novel risk variants for Alzheimer's disease. Neuron *78*, 256–268.

Dandrea, M.R., Reiser, P.A., Gumula, N.A., Hertzog, B.M., and Andrade-Gordon, P. (2001). Application of triple immunohistochemistry to characterize amyloid plaque-associated inflammation in brains with Alzheimer's disease. Biotech. Histochem. Off. Publ. Biol. Stain Comm. *76*, 97–106.

Darbinian, N., Cui, J., Basile, A., Valle, L.D., Otte, J., Miklossy, J., Sawaya, B.E., Amini, S., Khalili, K., and Gordon, J. (2008). Negative Regulation of AβPP Gene Expression by Pur-alpha. J. Alzheimers Dis. *15*, 71–82.

Datta, A., Chai, Y.L., Tan, J.M., Lee, J.H., Francis, P.T., Chen, C.P., Sze, S.K., and Lai, M.K.P. (2017). An iTRAQ-based proteomic analysis reveals dysregulation of neocortical synaptopodin in Lewy body dementias. Mol. Brain *10*.

Daws, M.R., Sullam, P.M., Niemi, E.C., Chen, T.T., Tchao, N.K., and Seaman, W.E. (2003). Pattern Recognition by TREM-2: Binding of Anionic Ligands. J. Immunol. *171*, 594–599.

Deane, R., Sagare, A., Hamm, K., Parisi, M., Lane, S., Finn, M.B., Holtzman, D.M., and Zlokovic, B.V. (2008). apoE isoform–specific disruption of amyloid β peptide clearance from mouse brain. J. Clin. Invest. *118*, 4002–4013.

Dempsey, L.A. (2015). TREM2 function in microglia. Nat. Immunol. *16*, 447–447.

Dhillon, A., and Jones, R.S.G. (2000). Laminar differences in recurrent excitatory transmission in the rat entorhinal cortex in vitro. Neuroscience *99*, 413–422.

Dickson, D.W., Lee, S.C., Mattiace, L.A., Yen, S.-H.C., and Brosnan, C. (1993). Microglia and cytokines in neurological disease, with special reference to AIDS and Alzheimer's disease. Glia *7*, 75–83.

Ding, S.-L. (2013). Comparative anatomy of the prosubiculum, subiculum, presubiculum, postsubiculum, and parasubiculum in human, monkey, and rodent. J. Comp. Neurol. *521*, 4145–4162.

DiPatre, P.L., and Gelman, B.B. (1997). Microglial cell activation in aging and Alzheimer disease: partial linkage with neurofibrillary tangle burden in the hippocampus. J. Neuropathol. Exp. Neurol. *56*, 143–149.

Drexel, M., Kirchmair, E., and Sperk, G. (2013). Changes in the expression of GABAA receptor subunit mRNAs in parahippocampal areas after kainic acid-induced seizures. Front. Neural Circuits *7*, 142.

Du, T., Caragounis, A., Parker, S.J., Meyerowitz, J., La Fontaine, S., Kanninen, K.M., Perreau, V.M., Crouch, P.J., and White, A.R. (2011). A potential copper-regulatory role for cytosolic expression of the DNA repair protein XRCC5. Free Radic. Biol. Med. *51*, 2060–2072.

Efthymiou, A.G., and Goate, A.M. (2017). Late onset Alzheimer's disease genetics implicates microglial pathways in disease risk. Mol. Neurodegener. *12*.

Eikelenboom, P., and Gool, W.A. van (2004). Neuroinflammatory perspectives on the two faces of Alzheimer's disease. J. Neural Transm. *111*, 281–294.

Eikelenboom, P., Rozemuller, J.M., and van Muiswinkel, F.L. (1998). Inflammation and Alzheimer's Disease: Relationships between Pathogenic Mechanisms and Clinical Expression. Exp. Neurol. *154*, 89–98.

Ellis, R.J., Olichney, J.M., Thal, L.J., Mirra, S.S., Morris, J.C., Beekly, D., and Heyman, A. (1996). Cerebral amyloid angiopathy in the brains of patients with Alzheimer's disease: the CERAD experience, Part XV. Neurology *46*, 1592–1596.

Emi, M., Wu, L.L., Robertson, M.A., Myers, R.L., Hegele, R.A., Williams, R.R., White, R., and Lalouel, J.M. (1988). Genotyping and sequence analysis of apolipoprotein E isoforms. Genomics *3*, 373–379.

Emmerling, M.R., Watson, M.D., Raby, C.A., and Spiegel, K. (2000). The role of complement in Alzheimer's disease pathology. Biochim. Biophys. Acta BBA - Mol. Basis Dis. *1502*, 158–171.

Esiri, M.M., al Izzi, M.S., and Reading, M.C. (1991). Macrophages, microglial cells, and HLA-DR antigens in fetal and infant brain. J. Clin. Pathol. *44*, 102–106.

Fadini, G.P., Cappellari, R., Mazzucato, M., Agostini, C., Kreutzenberg, S.V. de, and Avogaro, A. (2013). Monocyte–macrophage polarization balance in pre-diabetic individuals. Acta Diabetol. *50*, 977–982.

Fahrenhold, M., Rakic, S., Classey, J., Brayne, C., Ince, P.G., Nicoll, J.A.R., Boche, D., and MRC-CFAS (2017). TREM2 expression in the human brain: a marker of monocyte recruitment? Brain Pathol. Zurich Switz.

Finehout, E.J., Franck, Z., and Lee, K.H. (2005). Complement Protein Isoforms in CSF as Possible Biomarkers for Neurodegenerative Disease. Dis. Markers *21*, 93–101.

Flachbartová, Z., and Kovacech, B. (2013). Mortalin – a multipotent chaperone regulating cellular processes ranging from viral infection to neurodegeneration. Acta Virol. *57*, 3–15.

Forabosco, P., Ramasamy, A., Trabzuni, D., Walker, R., Smith, C., Bras, J., Levine, A.P., Hardy, J., Pocock, J.M., Guerreiro, R., et al. (2013). Insights into TREM2 biology by network analysis of human brain gene expression data. Neurobiol. Aging *34*, 2699–2714.

Forsell, C., Björk, B.F., Lilius, L., Axelman, K., Fabre, S.F., Fratiglioni, L., Winblad, B., and Graff, C. (2010). Genetic association to the amyloid plaque associated protein gene COL25A1 in Alzheimer's disease. Neurobiol. Aging *31*, 409–415.

Frackowiak, J., Wisniewski, H.M., Wegiel, J., Merz, G.S., Iqbal, K., and Wang, K.C. (1992). Ultrastructure of the microglia that phagocytose amyloid and the microglia that produce beta-amyloid fibrils. Acta Neuropathol. (Berl.) *84*, 225–233.

Frank, S., Burbach, G.J., Bonin, M., Walter, M., Streit, W., Bechmann, I., and Deller, T. (2008). TREM2 is upregulated in amyloid plaque-associated microglia in aged APP23 transgenic mice. Glia *56*, 1438–1447.

Frautschy, S.A., Yang, F., Irrizarry, M., Hyman, B., Saido, T.C., Hsiao, K., and Cole, G.M. (1998). Microglial response to amyloid plaques in APPsw transgenic mice. Am. J. Pathol. *152*, 307–317.

Fu, Y., Zhao, D., Pan, B., Wang, J., Cui, Y., Shi, F., Wang, C., Yin, X., Zhou, X., and Yang, L. (2015). Proteomic Analysis of Protein Expression Throughout Disease Progression in a Mouse Model of Alzheimer's Disease. J. Alzheimers Dis. *47*, 915–926.

Fuchs, E.C., Neitz, A., Pinna, R., Melzer, S., Caputi, A., and Monyer, H. (2016). Local and Distant Input Controlling Excitation in Layer II of the Medial Entorhinal Cortex. Neuron *89*, 194–208.

Fukutani, Y., Sasaki, K., Mukai, M., Matsubara, R., Isaki, K., and Cairns, N.J. (1997). Neurons and extracellular neurofibrillary tangles in the hippocampal subdivisions in early-onset familial Alzheimer's disease: A case study. Psychiatry Clin. Neurosci. *51*, 227–231.

Gahtan, E., and Overmier, J.B. (1999). Inflammatory pathogenesis in Alzheimer's disease: biological mechanisms and cognitive sequeli. Neurosci. Biobehav. Rev. *23*, 615–633.

Gauthier-Kemper, A., Weissmann, C., Golovyashkina, N., Sebö-Lemke, Z., Drewes, G., Gerke, V., Heinisch, J.J., and Brandt, R. (2011). The frontotemporal dementia mutation R406W blocks tau's interaction with the membrane in an annexin A2–dependent manner. J. Cell Biol. *192*, 647–661.

Geiss, G.K., Bumgarner, R.E., Birditt, B., Dahl, T., Dowidar, N., Dunaway, D.L., Fell, H.P., Ferree, S., George, R.D., Grogan, T., et al. (2008). Direct multiplexed measurement of gene expression with color-coded probe pairs. Nat. Biotechnol. *26*, 317–325.

Gentier, R.J., and van Leeuwen, F.W. (2015). Misframed ubiquitin and impaired protein quality control: an early event in Alzheimer's disease. Front. Mol. Neurosci. 47.

Gentleman, S.M. (2013). Review: Microglia in protein aggregation disorders: friend or foe? Neuropathol. Appl. Neurobiol. *39*, 45–50.

Geroldi, D., Minoretti, P., Bianchi, M., Di Vito, C., Reino, M., Bertona, M., and Emanuele, E. (2005). Genetic association of alpha2-Heremans–Schmid glycoprotein polymorphism with late-onset Alzheimer's disease in Italians. Neurosci. Lett. *386*, 176–178.

Ghani, M., Sato, C., Kakhki, E.G., Gibbs, J.R., Traynor, B., St George-Hyslop, P., and Rogaeva, E. (2016). Mutation analysis of the MS4A and TREM gene clusters in a case-control Alzheimer's disease data set. Neurobiol. Aging *42*, 217.e7-217.e13.

Giraldo, M., Lopera, F., Siniard, A., Corneveaux, J.J., Schrauwen, I., Carvajal, J., Muñoz, C., Ramirez-Restrepo, M., Myers, A.J., Caselli, R.J., et al. (2013). Variants in triggering receptor expressed on myeloid cells 2 are associated with both behavioral variant frontotemporal lobar degeneration and Alzheimer's disease. Neurobiol. Aging *34*.

Girotti, P., Bertorelli, R., Fisone, G., Land, T., Langel, U., Consolo, S., and Bartfai, T. (1993). N-terminal galanin fragments inhibit the hippocampal release of acetylcholine in vivo. Brain Res. *612*, 258–262.

Gispert, J.D., Monté, G.C., Suárez-Calvet, M., Falcon, C., Tucholka, A., Rojas, S., Rami, L., Sánchez-Valle, R., Lladó, A., Kleinberger, G., et al. (2016). The APOE ε4 genotype modulates CSF YKL-40 levels and their structural brain correlates in the continuum of Alzheimer's disease but not those of sTREM2. Alzheimers Dement. Diagn. Assess. Dis. Monit. *6*, 50–59.

Giulian, D. (1999). Microglia and the immune pathology of Alzheimer disease. Am. J. Hum. Genet. *65*, 13–18.

Giulian, D., Haverkamp, L.J., Yu, J.H., Karshin, W., Tom, D., Li, J., Kirkpatrick, J., Kuo, Y.-M., and Roher, A.E. (1996). Specific Domains of β-Amyloid from Alzheimer Plaque Elicit Neuron Killing in Human Microglia. J. Neurosci. *16*, 6021–6037.

Gjoneska, E., Pfenning, A.R., Mathys, H., Quon, G., Kundaje, A., Tsai, L.-H., and Kellis, M. (2015). Conserved epigenomic signals in mice and humans reveal immune basis of Alzheimer/'s disease. Nature *518*, 365–369.

Glabe, C.G. (2006). Common mechanisms of amyloid oligomer pathogenesis in degenerative disease. Neurobiol. Aging *27*, 570–575.

Goldblatt, G., Matos, J.O., Gornto, J., and Tatulian, S.A. (2015). Isotope-edited FTIR reveals distinct aggregation and structural behaviors of unmodified and pyroglutamylated amyloid β peptides. Phys. Chem. Chem. Phys.

Goldgaber, D., Harris, H.W., Hla, T., Maciag, T., Donnelly, R.J., Jacobsen, J.S., Vitek, M.P., and Gajdusek, D.C. (1989). Interleukin 1 regulates synthesis of amyloid beta-protein precursor mRNA in human endothelial cells. Proc. Natl. Acad. Sci. U. S. A. *86*, 7606–7610.

Gomez-Nicola, D., Teeling, J., Guaza, C., Godbout, J.P., and Taub, D.D. (2013). The Role of Inflammatory Mediators in Immune-to-Brain Communication during Health and Disease. Mediators Inflamm. *2013*.

Grathwohl, S.A., Kälin, R.E., Bolmont, T., Prokop, S., Winkelmann, G., Kaeser, S.A., Odenthal, J., Radde, R., Eldh, T., Gandy, S., et al. (2009). Formation and maintenance of Alzheimer's disease β-amyloid plaques in the absence of microglia. Nat. Neurosci. *12*, 1361–1363.

Grau, S., Baldi, A., Bussani, R., Tian, X., Stefanescu, R., Przybylski, M., Richards, P., Jones, S.A., Shridhar, V., Clausen, T., et al. (2005). Implications of the serine protease HtrA1 in amyloid precursor protein processing. Proc. Natl. Acad. Sci. U. S. A. *102*, 6021–6026.

Griffin, W.S., Stanley, L.C., Ling, C., White, L., MacLeod, V., Perrot, L.J., White, C.L., and Araoz, C. (1989). Brain interleukin 1 and S-100 immunoreactivity are elevated in Down syndrome and Alzheimer disease. Proc. Natl. Acad. Sci. U. S. A. *86*, 7611–7615.

Griffin, W.S., Sheng, J.G., Roberts, G.W., and Mrak, R.E. (1995). Interleukin-1 expression in different plaque types in Alzheimer's disease: significance in plaque evolution. J. Neuropathol. Exp. Neurol. *54*, 276–281.

Grimm, M.O.W., Kuchenbecker, J., Rothhaar, T.L., Grösgen, S., Hundsdörfer, B., Burg, V.K., Friess, P., Müller, U., Grimm, H.S., Riemenschneider, M., et al. (2011). Plasmalogen

synthesis is regulated via alkyl-dihydroxyacetonephosphate-synthase by amyloid precursor protein processing and is affected in Alzheimer's disease. J. Neurochem. *116*, 916–925.

van Groen, T., and Wyss, J.M. (1990). The connections of presubiculum and parasubiculum in the rat. Brain Res. *518*, 227–243.

de Groot, C.J., Hulshof, S., Hoozemans, J.J., and Veerhuis, R. (2001). Establishment of microglial cell cultures derived from postmortem human adult brain tissue: immunophenotypical and functional characterization. Microsc. Res. Tech. *54*, 34–39.

Grösgen, S., Grimm, M.O.W., Frieß, P., and Hartmann, T. (2010). Role of amyloid beta in lipid homeostasis. Biochim. Biophys. Acta BBA - Mol. Cell Biol. Lipids *1801*, 966–974.

Guerreiro, R., Wojtas, A., Bras, J., Carrasquillo, M., Rogaeva, E., Majounie, E., Cruchaga, C., Sassi, C., Kauwe, J.S.K., Younkin, S., et al. (2013a). TREM2 Variants in Alzheimer's Disease. N. Engl. J. Med. *368*, 117–127.

Guerreiro, R.J., Lohmann, E., Brás, J.M., Gibbs, J.R., Rohrer, J.D., Gurunlian, N., Dursun, B., Bilgic, B., Hanagasi, H., Gurvit, H., et al. (2013b). Using Exome Sequencing to Reveal Mutations in TREM2 Presenting as a Frontotemporal Dementia–like Syndrome Without Bone Involvement. JAMA Neurol. *70*, 78–84.

Guillemin, G.J., and Brew, B.J. (2004). Microglia, macrophages, perivascular macrophages, and pericytes: a review of function and identification. J. Leukoc. Biol. *75*, 388–397.

Hallock, P., and Thomas, M.A. (2012). Integrating the Alzheimer's Disease Proteome and Transcriptome: A Comprehensive Network Model of a Complex Disease. OMICS J. Integr. Biol. *16*, 37–49.

Hamerman, J.A., Tchao, N.K., Lowell, C.A., and Lanier, L.L. (2005). Enhanced Toll-like receptor responses in the absence of signaling adaptor DAP12. Nat. Immunol. *6*, 579–586.

Hardy, J., and Selkoe, D.J. (2002). The Amyloid Hypothesis of Alzheimer's Disease: Progress and Problems on the Road to Therapeutics. Science *297*, 353–356.

Hardy, J.A., and Higgins, G.A. (1992). Alzheimer's Disease: The Amyloid Cascade Hypothesis. Science *256*, 184–185.

Harris, F.M., Brecht, W.J., Xu, Q., Tesseur, I., Kekonius, L., Wyss-Coray, T., Fish, J.D., Masliah, E., Hopkins, P.C., Scearce-Levie, K., et al. (2003). Carboxyl-terminal-truncated apolipoprotein E4 causes Alzheimer's disease-like neurodegeneration and behavioral deficits in transgenic mice. Proc. Natl. Acad. Sci. U. S. A. *100*, 10966–10971.

Hassan, N.F., Campbell, D.E., Rifat, S., and Douglas, S.D. (1991). Isolation and characterization of human fetal brain-derived microglia in in vitro culture. Neuroscience *41*, 149–158.

Hawkes, C.A., Gatherer, M., Sharp, M.M., Dorr, A., Yuen, H.M., Kalaria, R., Weller, R.O., and Carare, R.O. (2013). Regional differences in the morphological and functional effects of aging on cerebral basement membranes and perivascular drainage of amyloid-β from the mouse brain. Aging Cell *12*, 224–236.

He, Z., Guo, J.L., McBride, J.D., Narasimhan, S., Kim, H., Changolkar, L., Zhang, B., Gathagan, R.J., Yue, C., Dengler, C., et al. (2018). Amyloid-β plaques enhance Alzheimer's brain tau-seeded pathologies by facilitating neuritic plaque tau aggregation. Nat. Med. *24*, 29.

Hendrickson, R.C., Lee, A.Y.H., Song, Q., Liaw, A., Wiener, M., Paweletz, C.P., Seeburger, J.L., Li, J., Meng, F., Deyanova, E.G., et al. (2015). High Resolution Discovery Proteomics

Reveals Candidate Disease Progression Markers of Alzheimer's Disease in Human Cerebrospinal Fluid. PLoS ONE *10*.

Henriques, A.G., Oliveira, J.M., Carvalho, L.P., and Silva, O.A.B. da C. e (2015). Aβ Influences Cytoskeletal Signaling Cascades with Consequences to Alzheimer's Disease. Mol. Neurobiol. *52*, 1391–1407.

Herz, J., and Bock, and H.H. (2002). Lipoprotein Receptors in the Nervous System. Annu. Rev. Biochem. *71*, 405–434.

Heslegrave, A., Heywood, W., Paterson, R., Magdalinou, N., Svensson, J., Johansson, P., Öhrfelt, A., Blennow, K., Hardy, J., Schott, J., et al. (2016). Increased cerebrospinal fluid soluble TREM2 concentration in Alzheimer's disease. Mol. Neurodegener. *11*.

Hewitt, C.A., Ling, K.-H., Merson, T.D., Simpson, K.M., Ritchie, M.E., King, S.L., Pritchard, M.A., Smyth, G.K., Thomas, T., Scott, H.S., et al. (2010). Gene Network Disruptions and Neurogenesis Defects in the Adult Ts1Cje Mouse Model of Down Syndrome. PLoS ONE *5*.

Hickman, S.E., and El Khoury, J. (2014). TREM2 and the neuroimmunology of Alzheimer's disease. Biochem. Pharmacol. *88*, 495–498.

Hickman, S.E., Allison, E.K., and Khoury, J.E. (2008). Microglial Dysfunction and Defective β-Amyloid Clearance Pathways in Aging Alzheimer's Disease Mice. J. Neurosci. *28*, 8354–8360.

Hickman, S.E., Kingery, N.D., Ohsumi, T., Borowsky, M., Wang, L., Means, T.K., and Khoury, J.E. (2013). The Microglial Sensome Revealed by Direct RNA Sequencing. Nat. Neurosci. *16*, 1896–1905.

Hoeijmakers, L., Heinen, Y., van Dam, A.-M., Lucassen, P.J., and Korosi, A. (2016). Microglial Priming and Alzheimer's Disease: A Possible Role for (Early) Immune Challenges and Epigenetics? Front. Hum. Neurosci. *10*.

Holness, C.L., and Simmons, D.L. (1993). Molecular cloning of CD68, a human macrophage marker related to lysosomal glycoproteins. Blood *81*, 1607–1613.

Holtman, I.R., Raj, D.D., Miller, J.A., Schaafsma, W., Yin, Z., Brouwer, N., Wes, P.D., Möller, T., Orre, M., Kamphuis, W., et al. (2015). Induction of a common microglia gene expression signature by aging and neurodegenerative conditions: a co-expression meta-analysis. Acta Neuropathol. Commun. *3*, 31.

Hooli, B.V., Parrado, A.R., Mullin, K., Yip, W.-K., Liu, T., Roehr, J.T., Qiao, D., Jessen, F., Peters, O., Becker, T., et al. (2014). The rare TREM2 R47H variant exerts only a modest effect on Alzheimer disease risk. Neurology 10.1212/WNL.0000000000000855.

van Horssen, J., Otte-Höller, I., David, G., Maat-Schieman, M.L., van den Heuvel, L.P., Wesseling, P., de Waal, R.M., and Verbeek, M.M. (2001). Heparan sulfate proteoglycan expression in cerebrovascular amyloid beta deposits in Alzheimer's disease and hereditary cerebral hemorrhage with amyloidosis (Dutch) brains. Acta Neuropathol. (Berl.) *102*, 604–614.

Hoshi, A., Yamamoto, T., Shimizu, K., Ugawa, Y., Nishizawa, M., Takahashi, H., and Kakita, A. (2012). Characteristics of Aquaporin Expression Surrounding Senile Plaques and Cerebral Amyloid Angiopathy in Alzheimer Disease. J. Neuropathol. Exp. Neurol. *71*, 750–759.

Hsieh, C.L., Koike, M., Spusta, S.C., Niemi, E.C., Yenari, M., Nakamura, M.C., and Seaman, W.E. (2009). A role for TREM2 ligands in the phagocytosis of apoptotic neuronal cells by microglia. J. Neurochem. *109*, 1144–1156.

Huang, Y. (2011). Roles of apolipoprotein E4 (ApoE4) in the pathogenesis of Alzheimer's disease: lessons from ApoE mouse models. Biochem. Soc. Trans. *39*, 924–932.

Huang, Y., and Mahley, R.W. (2014). Apolipoprotein E: Structure and function in lipid metabolism, neurobiology, and Alzheimer's diseases. Neurobiol. Dis. *72*, 3–12.

Huang, Y., and Mahley, R.W. Apolipoprotein E: Structure and Function in Lipid Metabolism, Neurobiology, and Alzheimer's Diseases. Neurobiol. Dis.

Huang, Y., Liu, X.Q., Wyss-Coray, T., Brecht, W.J., Sanan, D.A., and Mahley, R.W. (2001). Apolipoprotein E fragments present in Alzheimer's disease brains induce neurofibrillary tangle-like intracellular inclusions in neurons. Proc. Natl. Acad. Sci. U. S. A. *98*, 8838–8843.

Huell, M., Strauss, S., Volk, B., Berger, M., and Bauer, J. (1995). Interleukin-6 is present in early stages of plaque formation and is restricted to the brains of Alzheimer's disease patients. Acta Neuropathol. (Berl.) *89*, 544–551.

Hulette, C.M., Downey, B.T., and Burger, P.C. (1992). Macrophage markers in diagnostic neuropathology. Am. J. Surg. Pathol. *16*, 493–499.

Humphries, C., and Kohli, M.A. (2014). Rare Variants and Transcriptomics in Alzheimer disease. Curr. Genet. Med. Rep. *2*, 75–84.

Huynh, T.-P.V., Davis, A.A., Ulrich, J.D., and Holtzman, D.M. (2017). Apolipoprotein E and Alzheimer's disease: the influence of apolipoprotein E on amyloid-β and other amyloidogenic proteins. J. Lipid Res. *58*, 824–836.

Hyman, B.T., Marzloff, K., and Arriagada, P.V. (1993). The lack of accumulation of senile plaques or amyloid burden in Alzheimer's disease suggests a dynamic balance between amyloid deposition and resolution. J. Neuropathol. Exp. Neurol. *52*, 594–600.

Imai, Y., Ibata, I., Ito, D., Ohsawa, K., and Kohsaka, S. (1996). A Novel Geneiba1in the Major Histocompatibility Complex Class III Region Encoding an EF Hand Protein Expressed in a Monocytic Lineage. Biochem. Biophys. Res. Commun. *224*, 855–862.

Iqbal, K., del C. Alonso, A., Chen, S., Chohan, M.O., El-Akkad, E., Gong, C.-X., Khatoon, S., Li, B., Liu, F., Rahman, A., et al. (2005). Tau pathology in Alzheimer disease and other tauopathies. Biochim. Biophys. Acta BBA - Mol. Basis Dis. *1739*, 198–210.

Ishii, T., and Haga, S. (1984). Immuno-electron-microscopic localization of complements in amyloid fibrils of senile plaques. Acta Neuropathol. (Berl.) *63*, 296–300.

Ismail, N., Ismail, M., Azmi, N.H., Bakar, M.F.A., Yida, Z., Abdullah, M.A., and Basri, H. (2017). Thymoquinone-rich fraction nanoemulsion (TQRFNE) decreases Aβ40 and Aβ42 levels by modulating APP processing, up-regulating IDE and LRP1, and down-regulating BACE1 and RAGE in response to high fat/cholesterol diet-induced rats. Biomed. Pharmacother. *95*, 780–788.

Itagaki, S., McGeer, P.L., Akiyama, H., Zhu, S., and Selkoe, D. (1989). Relationship of microglia and astrocytes to amyloid deposits of Alzheimer disease. J. Neuroimmunol. *24*, 173–182.

Ito, H., and Hamerman, J.A. (2012). TREM-2, triggering receptor expressed on myeloid cell-2, negatively regulates TLR responses in dendritic cells. Eur. J. Immunol. *42*, 176–185.

Ito, D., Imai, Y., Ohsawa, K., Nakajima, K., Fukuuchi, Y., and Kohsaka, S. (1998). Microglia-specific localisation of a novel calcium binding protein, Iba1. Mol. Brain Res. *57*, 1–9.

Iwatsubo, T., Odaka, A., Suzuki, N., Mizusawa, H., Nukina, N., and Ihara, Y. (1994). Visualization of Aβ42(43) and Aβ40 in senile plaques with end-specific Aβ monoclonals: Evidence that an initially deposited species is Aβ42(43). Neuron *13*, 45–53.

Jay, T.R., Miller, C.M., Cheng, P.J., Graham, L.C., Bemiller, S., Broihier, M.L., Xu, G., Margevicius, D., Karlo, J.C., Sousa, G.L., et al. (2015). TREM2 deficiency eliminates TREM2+ inflammatory macrophages and ameliorates pathology in Alzheimer's disease mouse models. J. Exp. Med. *212*, 287–295.

Jay, T.R., Hirsch, A.M., Broihier, M.L., Miller, C.M., Neilson, L.E., Ransohoff, R.M., Lamb, B.T., and Landreth, G.E. (2017). Disease Progression-Dependent Effects of TREM2 Deficiency in a Mouse Model of Alzheimer's Disease. J. Neurosci. *37*, 637–647.

Jendresen, C., Årskog, V., Daws, M.R., and Nilsson, L.N.G. (2017). The Alzheimer's disease risk factors apolipoprotein E and TREM2 are linked in a receptor signaling pathway. J. Neuroinflammation *14*, 59.

Ji, B., Chen, C.-J., Bando, K., Ashino, H., Shiraishi, H., Sano, H., Kasahara, H., Minamizawa, T., Yamada, K., Ono, M., et al. (2015). Distinct binding of amyloid imaging ligands to unique amyloid-β deposited in the presubiculum of Alzheimer's disease. J. Neurochem. *135*, 859–866.

Jiang, T., Yu, J.-T., Zhu, X.-C., and Tan, L. (2013). TREM2 in Alzheimer's disease. Mol. Neurobiol. *48*, 180–185.

Jiang, T., Tan, L., Zhu, X.-C., Zhang, Q.-Q., Cao, L., Tan, M.-S., Gu, L.-Z., Wang, H.-F., Ding, Z.-Z., Zhang, Y.-D., et al. (2014). Up-regulation of TREM2 Ameliorates Neuropathology and Rescues Spatial Cognitive Impairment in a Transgenic Mouse Model of Alzheimer's Disease. Neuropsychopharmacology.

Jiang, T., Tan, L., Zhu, X.-C., Zhou, J.-S., Cao, L., Tan, M.-S., Wang, H.-F., Chen, Q., Zhang, Y.-D., and Yu, J.-T. (2015). Silencing of TREM2 exacerbates tau pathology, neurodegenerative changes, and spatial learning deficits in P301S tau transgenic mice. Neurobiol. Aging *36*, 3176–3186.

Jiang, T., Zhang, Y.-D., Chen, Q., Gao, Q., Zhu, X.-C., Zhou, J.-S., Shi, J.-Q., Lu, H., Tan, L., and Yu, J.-T. (2016a). TREM2 modifies microglial phenotype and provides neuroprotection in P301S tau transgenic mice. Neuropharmacology *105*, 196–206.

Jiang, T., Wan, Y., Zhang, Y.-D., Zhou, J.-S., Gao, Q., Zhu, X.-C., Shi, J.-Q., Lu, H., Tan, L., and Yu, J.-T. (2016b). TREM2 Overexpression has No Improvement on Neuropathology and Cognitive Impairment in Aging APPswe/PS1dE9 Mice. Mol. Neurobiol. 1–11.

Jiao, B., Liu, X., Tang, B., Hou, L., Zhou, L., Zhang, F., Zhou, Y., Guo, J., Yan, X., and Shen, L. (2014). Investigation of TREM2, PLD3, and UNC5C variants in patients with Alzheimer's disease from mainland China. Neurobiol. Aging *35*, 2422.e9-2422.e11.

Jin, S.C., Carrasquillo, M.M., Benitez, B.A., Skorupa, T., Carrell, D., Patel, D., Lincoln, S., Krishnan, S., Kachadoorian, M., Reitz, C., et al. (2015). TREM2 is associated with increased risk for Alzheimer's disease in African Americans. Mol. Neurodegener. *10*, 19.

Joachim, C.L., Morris, J.H., and Selkoe, D.J. (1989). Diffuse senile plaques occur commonly in the cerebellum in Alzheimer's disease. Am. J. Pathol. *135*, 309–319.

Johansson, J., Weaver, T.E., and Tjernberg, L.O. (2004). Proteolytic generation and aggregation of peptides from transmembrane regions: lung surfactant protein C and amyloid β-peptide. Cell. Mol. Life Sci. CMLS *61*, 326–335.

Jones, B.M., Bhattacharjee, S., Dua, P., Hill, J.M., Zhao, Y., and Lukiw, W.J. (2014). Regulating amyloidogenesis through the natural triggering receptor expressed in myeloid/microglial cells 2 (TREM2). Front. Cell. Neurosci. *8*.

Jones, P.B., Adams, K.W., Rozkalne, A., Spires-Jones, T.L., Hshieh, T.T., Hashimoto, T., von Armin, C.A.F., Mielke, M., Bacskai, B.J., and Hyman, B.T. (2011). Apolipoprotein E: Isoform Specific Differences in Tertiary Structure and Interaction with Amyloid-β in Human Alzheimer Brain. PLoS ONE *6*.

Jonsson, T., Atwal, J.K., Steinberg, S., Snaedal, J., Jonsson, P.V., Bjornsson, S., Stefansson, H., Sulem, P., Gudbjartsson, D., Maloney, J., et al. (2012a). A mutation in APP protects against Alzheimer/'s disease and age-related cognitive decline. Nature *488*, 96–99.

Jonsson, T., Stefansson, H., Steinberg, S., Jonsdottir, I., Jonsson, P.V., Snaedal, J., Bjornsson, S., Huttenlocher, J., Levey, A.I., Lah, J.J., et al. (2012b). Variant of TREM2 Associated with the Risk of Alzheimer's Disease. N. Engl. J. Med. *368*, 107–116.

Kalus, P., Braak, H., Braak, E., and Bohl, J. (1989). The presubicular region in Alzheimer's disease: topography of amyloid deposits and neurofibrillary changes. Brain Res. *494*, 198–203.

Kamboh, M.I., Minster, R.L., Kenney, M., Ozturk, A., Desai, P.P., Kammerer, C.M., and DeKosky, S.T. (2006). Alpha-1-antichymotrypsin (ACT or SERPINA3) polymorphism may affect age-at-onset and disease duration of Alzheimer's disease. Neurobiol. Aging *27*, 1435–1439.

Kanekiyo, T., Liu, C.-C., Shinohara, M., Li, J., and Bu, G. (2012). LRP1 in Brain Vascular Smooth Muscle Cells Mediates Local Clearance of Alzheimer's Amyloid-β. J. Neurosci. Off. J. Soc. Neurosci. *32*, 16458–16465.

Kanekiyo, T., Cirrito, J.R., Liu, C.-C., Shinohara, M., Li, J., Schuler, D.R., Shinohara, M., Holtzman, D.M., and Bu, G. (2013). Neuronal Clearance of Amyloid-β by Endocytic Receptor LRP1. J. Neurosci. *33*, 19276–19283.

Karran, E., and Hardy, J. (2014). Antiamyloid Therapy for Alzheimer's Disease — Are We on the Right Road? N. Engl. J. Med. *370*, 377–378.

Kása, P., Rakonczay, Z., and Gulya, K. (1997). The cholinergic system in Alzheimer's disease. Prog. Neurobiol. *52*, 511–535.

Keren-Shaul, H., Spinrad, A., Weiner, A., Matcovitch-Natan, O., Dvir-Szternfeld, R., Ulland, T.K., David, E., Baruch, K., Lara-Astaiso, D., Toth, B., et al. (2017). A Unique Microglia Type Associated with Restricting Development of Alzheimer's Disease. Cell *169*, 1276-1290.e17.

Khan, A.T., Dobson, R.J.B., Sattlecker, M., and Kiddle, S.J. (2016). Alzheimer's disease: are blood and brain markers related? A systematic review. Ann. Clin. Transl. Neurol. *3*, 455–462.

Kierdorf, K., and Prinz, M. (2013). Factors regulating microglia activation. Front. Cell. Neurosci. *7*, 44.

Kim, J., Castellano, J.M., Jiang, H., Basak, J.M., Parsadanian, M., Pham, V., Mason, S.M., Paul, S.M., and Holtzman, D.M. (2009). Overexpression of Low Density Lipoprotein Receptor in the Brain Markedly Inhibits Amyloid Deposition and Increases Extracellular Aβ Clearance. Neuron *64*, 632–644.

Kim, S., Swaminathan, S., Shen, L., Risacher, S.L., Nho, K., Foroud, T., Shaw, L.M., Trojanowski, J.Q., Potkin, S.G., Huentelman, M.J., et al. (2011). Genome-wide association study of CSF biomarkers Aβ1-42, t-tau, and p-tau181p in the ADNI cohort. Neurology *76*, 69–79.

Kitazawa, M., Yamasaki, T.R., and Laferla, F.M. (2004). Microglia as a Potential Bridge between the Amyloid β-Peptide and Tau. Ann. N. Y. Acad. Sci. *1035*, 85–103.

Kleinberger, G., Yamanishi, Y., Suárez-Calvet, M., Czirr, E., Lohmann, E., Cuyvers, E., Struyfs, H., Pettkus, N., Wenninger-Weinzierl, A., Mazaheri, F., et al. (2014). TREM2 mutations implicated in neurodegeneration impair cell surface transport and phagocytosis. Sci. Transl. Med. *6*, 243ra86-243ra86.

Klesney-Tait, J., Turnbull, I.R., and Colonna, M. (2006). The TREM receptor family and signal integration. Nat. Immunol. *7*, 1266.

Kober, D.L., Wanhainen, K.M., Johnson, B.M., Randolph, D.T., Holtzman, M.J., and Brett, T.J. (2014). Preparation, crystallization, and preliminary crystallographic analysis of wild-type and mutant human TREM-2 ectodomains linked to neurodegenerative and inflammatory diseases. Protein Expr. Purif. *96*, 32–38.

Kober, D.L., Alexander-Brett, J.M., Karch, C.M., Cruchaga, C., Colonna, M., Holtzman, M.J., and Brett, T.J. (2016). Neurodegenerative disease mutations in TREM2 reveal a functional surface and distinct loss-of-function mechanisms. ELife *5*, e20391.

Kolev, M.V., Ruseva, M.M., Harris, C.L., Morgan, B.P., and Donev, R.M. (2009). Implication of Complement System and its Regulators in Alzheimer's Disease. Curr. Neuropharmacol. *7*, 1–8.

Korvatska O, Leverenz JB, Jayadev S, and et al (2015). R47h variant of trem2 associated with alzheimer disease in a large late-onset family: Clinical, genetic, and neuropathological study. JAMA Neurol.

Korzhevskii, D.E., and Kirik, O.V. (2016). Brain Microglia and Microglial Markers. Neurosci. Behav. Physiol. *46*, 284–290.

Krasemann, S., Madore, C., Cialic, R., Baufeld, C., Calcagno, N., Fatimy, R.E., Beckers, L., O'Loughlin, E., Xu, Y., Fanek, Z., et al. (2017). The TREM2-APOE Pathway Drives the Transcriptional Phenotype of Dysfunctional Microglia in Neurodegenerative Diseases. Immunity *47*, 566-581.e9.

Krauthausen, M., Saxe, S., Zimmermann, J., Emrich, M., Heneka, M.T., and Müller, M. (2014). CXCR3 modulates glial accumulation and activation in cuprizone-induced demyelination of the central nervous system. J. Neuroinflammation *11*, 109.

Krauthausen, M., Kummer, M.P., Zimmermann, J., Reyes-Irisarri, E., Terwel, D., Bulic, B., Heneka, M.T., and Müller, M. (2015). CXCR3 promotes plaque formation and behavioral deficits in an Alzheimer's disease model. J. Clin. Invest. *125*, 365–378.

LaDu, M.J., Munson, G.W., Jungbauer, L., Getz, G.S., Reardon, C.A., Tai, L.M., and Yu, C. (2012). Preferential Interactions between ApoE-containing Lipoproteins and Aβ Revealed by a Detection Method that Combines Size Exclusion Chromatography with Non-Reducing Gel-shift. Biochim. Biophys. Acta *1821*, 295–302.

Landel, V., Baranger, K., Virard, I., Loriod, B., Khrestchatisky, M., Rivera, S., Benech, P., and Féron, F. (2014). Temporal gene profiling of the 5XFAD transgenic mouse model highlights the importance of microglial activation in Alzheimer's disease. Mol. Neurodegener. *9*, 33.

Lane, C.A., Parker, T.D., Cash, D.M., Macpherson, K., Donnachie, E., Murray-Smith, H., Barnes, A., Barker, S., Beasley, D.G., Bras, J., et al. (2017). Study protocol: Insight 46 – a neuroscience sub-study of the MRC National Survey of Health and Development. BMC Neurol. *17*.

Lassmann, H., Schmied, M., Vass, K., and Hickey, W.F. (1993). Bone marrow derived elements and resident microglia in brain inflammation. Glia *7*, 19–24.

Lee, D.C., Rizer, J., Hunt, J.B., Selenica, M.-L.B., Gordon, M.N., and Morgan, D. (2013). Review: Experimental manipulations of microglia in mouse models of Alzheimer's pathology: activation reduces amyloid but hastens tau pathology. Neuropathol. Appl. Neurobiol. *39*, 69–85.

Lee, Y.B., Nagai, A., and Kim, S.U. (2002). Cytokines, chemokines, and cytokine receptors in human microglia. J. Neurosci. Res. *69*, 94–103.

Li, X., Montine, K.S., Keene, C.D., and Montine, T.J. (2015). Different mechanisms of apolipoprotein E isoform–dependent modulation of prostaglandin E2 production and triggering receptor expressed on myeloid cells 2 (TREM2) expression after innate immune activation of microglia. FASEB J. fj.14-262683.

Liang, D., Han, G., Feng, X., Sun, J., Duan, Y., and Lei, H. (2012). Concerted Perturbation Observed in a Hub Network in Alzheimer's Disease. PLoS ONE *7*.

Liao, F., Hori, Y., Hudry, E., Bauer, A.Q., Jiang, H., Mahan, T.E., Lefton, K.B., Zhang, T.J., Dearborn, J.T., Kim, J., et al. (2014). Anti-ApoE Antibody Given after Plaque Onset Decreases Aβ Accumulation and Improves Brain Function in a Mouse Model of Aβ Amyloidosis. J. Neurosci. *34*, 7281–7292.

Liao, L., Cheng, D., Wang, J., Duong, D.M., Losik, T.G., Gearing, M., Rees, H.D., Lah, J.J., Levey, A.I., and Peng, J. (2004). Proteomic Characterization of Postmortem Amyloid Plaques Isolated by Laser Capture Microdissection. J. Biol. Chem. *279*, 37061–37068.

Lill, C.M., Rengmark, A., Pihlstrøm, L., Fogh, I., Shatunov, A., Sleiman, P.M., Wang, L.-S., Liu, T., Lassen, C.F., Meissner, E., et al. (2015). The role of TREM2 R47H as a risk factor for Alzheimer's disease, frontotemporal lobar degeneration, amyotrophic lateral sclerosis, and Parkinson's disease. Alzheimers Dement. J. Alzheimers Assoc. *11*, 1407–1416.

Lista, S., O'Bryant, S.E., Blennow, K., Dubois, B., Hugon, J., Zetterberg, H., and Hampel, H. (2015). Biomarkers in Sporadic and Familial Alzheimer's Disease. J. Alzheimers Dis. *47*, 291–317.

Lodeiro, M., Puerta, E., Ismail, M.-A.-M., Rodriguez-Rodriguez, P., Rönnbäck, A., Codita, A., Parrado-Fernandez, C., Maioli, S., Gil-Bea, F., Merino-Serrais, P., et al. (2017). Aggregation of the Inflammatory S100A8 Precedes Aβ Plaque Formation in Transgenic APP Mice: Positive Feedback for S100A8 and Aβ Productions. J. Gerontol. Ser. A *72*, 319–328.

Long, J.M., Ray, B., and Lahiri, D.K. (2014). MicroRNA-339-5p Down-regulates Protein Expression of β-Site Amyloid Precursor Protein-Cleaving Enzyme 1 (BACE1) in Human Primary Brain Cultures and Is Reduced in Brain Tissue Specimens of Alzheimer Disease Subjects. J. Biol. Chem. *289*, 5184–5198.

Lu, Y., Liu, W., and Wang, X. (2015). TREM2 variants and risk of Alzheimer's disease: a meta-analysis. Neurol. Sci. 1–8.

Lue, L.-F., Brachova, L., Walker, D.G., and Rogers, J. (1996). Characterization of glial cultures from rapid autopsies of Alzheimer's and control patients. Neurobiol. Aging *17*, 421–429.

Lue, L.-F., Schmitz, C.T., Sorrano, G., Sue, L.I., Beach, T.G., and Walker, D.G. (2014). TREM2 protein expression changes correlate with Alzheimer's disease neurodegenerative pathologies in postmortem temporal cortices. Brain Pathol. Zurich Switz.

Lue, L.-F., Schmitz, C., and Walker, D.G. (2015). What happens to microglial TREM2 in Alzheimer's disease: Immunoregulatory turned into immunopathogenic? Neuroscience *302*, 138–150.

Luis, E.O., Ortega-Cubero, S., Lamet, I., Razquin, C., Cruchaga, C., Benitez, B.A., Lorenzo, E., Irigoyen, J., Pastor, M.A., and Pastor, P. (2014). Frontobasal gray matter loss is associated with the TREM2 p.R47H variant. Neurobiol. Aging *35*, 2681–2690.

Lynch, M.A. (2009). The multifaceted profile of activated microglia. Mol. Neurobiol. *40*, 139–156.

Ma, J., Jiang, T., Tan, L., and Yu, J.-T. (2014). TYROBP in Alzheimer's Disease. Mol. Neurobiol. 1–7.

Mahley, R.W. (1988). Apolipoprotein E: cholesterol transport protein with expanding role in cell biology. Science *240*, 622–630.

Mahley, R.W., and Huang, Y. (1999). Apolipoprotein E: from atherosclerosis to Alzheimer's disease and beyond. Curr. Opin. Lipidol. *10*, 207–217.

Mahley, R.W., and Ji, Z.-S. (1999). Remnant lipoprotein metabolism: key pathways involving cell-surface heparan sulfate proteoglycans and apolipoprotein E. J. Lipid Res. *40*, 1–16.

Malkki, H. (2015). Alzheimer disease: The involvement of TREM2 R47H variant in Alzheimer disease confirmed, but mechanisms remain elusive. Nat. Rev. Neurol. *11*, 307–307.

Mann, D.M., Iwatsubo, T., Fukumoto, H., Ihara, Y., Odaka, A., and Suzuki, N. (1995). Microglial cells and amyloid beta protein (A beta) deposition; association with A beta 40-containing plaques. Acta Neuropathol. (Berl.) *90*, 472–477.

Maphis, N., Xu, G., Kokiko-Cochran, O.N., Jiang, S., Cardona, A., Ransohoff, R.M., Lamb, B.T., and Bhaskar, K. (2015). Reactive microglia drive tau pathology and contribute to the spreading of pathological tau in the brain. Brain *138*, 1738–1755.

Marchesi, V.T. (2016). Gain-of-function somatic mutations contribute to inflammation and blood vessel damage that lead to Alzheimer dementia: a hypothesis. FASEB J. *30*, 503–506.

Martin, L.J., Pardo, C.A., Cork, L.C., and Price, D.L. (1994). Synaptic pathology and glial responses to neuronal injury precede the formation of senile plaques and amyloid deposits in the aging cerebral cortex. Am. J. Pathol. *145*, 1358–1381.

Martiskainen, H., Viswanathan, J., Nykänen, N.-P., Kurki, M., Helisalmi, S., Natunen, T., Sarajärvi, T., Kurkinen, K.M.A., Pursiheimo, J.-P., Rauramaa, T., et al. (2015). Transcriptomics and mechanistic elucidation of Alzheimer's disease risk genes in the brain and in vitro models. Neurobiol. Aging *36*, 1221.e15-1221.e28.

Masliah, E., Mallory, M., Hansen, L., Alford, M., DeTeresa, R., Terry, R., Baudier, J., and Saitoh, T. (1992). Localization of amyloid precursor protein in GAP43-immunoreactive aberrant sprouting neurites in Alzheimer's disease. Brain Res. *574*, 312–316.

Massone, S., Vassallo, I., Castelnuovo, M., Fiorino, G., Gatta, E., Robello, M., Borghi, R., Tabaton, M., Russo, C., Dieci, G., et al. (2011). RNA polymerase III drives alternative splicing of the potassium channel–interacting protein contributing to brain complexity and neurodegeneration. J. Cell Biol. *193*, 851–866.

Masters, C.L., and Selkoe, D.J. (2012). Biochemistry of Amyloid β-Protein and Amyloid Deposits in Alzheimer Disease. Cold Spring Harb. Perspect. Med. *2*, a006262.

Matarin, M., Salih, D.A., Yasvoina, M., Cummings, D.M., Guelfi, S., Liu, W., Nahaboo Solim, M.A., Moens, T.G., Paublete, R.M., Ali, S.S., et al. (2015). A Genome-wide Gene-Expression

Analysis and Database in Transgenic Mice during Development of Amyloid or Tau Pathology. Cell Rep. *10*, 633–644.

Mattiace, L.A., Davies, P., Yen, S.-H., and Dickson, D.W. (1990a). Microglia in cerebellar plaques in Alzheimer's disease. Acta Neuropathol. (Berl.) *80*, 493–498.

Mattiace, L.A., Davies, P., and Dickson, D.W. (1990b). Detection of HLA-DR on microglia in the human brain is a function of both clinical and technical factors. Am. J. Pathol. *136*, 1101–1114.

Mazaheri, F., Snaidero, N., Kleinberger, G., Madore, C., Daria, A., Werner, G., Krasemann, S., Capell, A., Trümbach, D., Wurst, W., et al. (2017). TREM2 deficiency impairs chemotaxis and microglial responses to neuronal injury. EMBO Rep. *18*, 1186–1198.

McCuUoch, M.I.J., and Deborah Dewar (1991). Preservation of [125I]galanin binding sites despite loss of cholinergic neurons to the hippocampus in Alzheimer's disease. Brain Res. *568*, 303–306.

McGeer, P.L., and McGeer, E.G. (1995). The inflammatory response system of brain: implications for therapy of Alzheimer and other neurodegenerative diseases. Brain Res. Rev. *21*, 195–218.

McGeer, P.L., Itagaki, S., and McGeer, E.G. (1988). Expression of the histocompatibility glycoprotein HLA-DR in neurological disease. Acta Neuropathol. (Berl.) *76*, 550–557.

McGeer, P.L., Kawamata, T., Walker, D.G., Akiyama, H., Tooyama, I., and McGeer, E.G. (1993). Microglia in degenerative neurological disease. Glia *7*, 84–92.

McKeever, P.M., Kim, T., Hesketh, A.R., MacNair, L., Miletic, D., Favrin, G., Oliver, S.G., Zhang, Z., St George-Hyslop, P., and Robertson, J. (2017). Cholinergic neuron gene expression differences captured by translational profiling in a mouse model of Alzheimer's disease. Neurobiol. Aging *57*, 104–119.

Meda, L., Cassatella, M.A., Szendrei, G.I., Jr, L.O., Baron, P., Villalba, M., Ferrari, D., and Rossi, F. (1995). Activation of microglial cells by β-amyloid protein and interferon-γ. Nature *374*, 374647a0.

Melchior, B., Garcia, A.E., Hsiung, B.-K., Lo, K.M., Doose, J.M., Cameron Thrash, J., Stalder, A.K., Staufenbiel, M., Neumann, H., and Carson, M.J. (2010). Dual induction of TREM2 and tolerance-related transcript, Tmem176b, in amyloid transgenic mice: implications for vaccine-based therapies for Alzheimer's disease. ASN NEURO *2*.

Mendioroz, M., Celarain, N., Altuna, M., Sánchez-Ruiz de Gordoa, J., Zelaya, M.V., Roldán, M., Rubio, I., Larumbe, R., Erro, M.E., Méndez, I., et al. (2016). CRTC1 gene is differentially methylated in the human hippocampus in Alzheimer's disease. Alzheimers Res. Ther. *8*.

Mengel, D., Thelen, M., Balzer-Geldsetzer, M., Söling, C., Bach, J.-P., Schaeffer, E., Herold, C., Becker, T., Liepelt, I., Becker, J., et al. (2016). TREM2 rare variant p.R47H is not associated with Parkinson's disease. Parkinsonism Relat. Disord. *23*, 109–111.

Miller, D.L., Papayannopoulos, I.A., Styles, J., Bobin, S.A., Lin, Y.Y., Biemann, K., and Iqbal, K. (1993). Peptide Compositions of the Cerebrovascular and Senile Plaque Core Amyloid Deposits of Alzheimer′s Disease. Arch. Biochem. Biophys. *301*, 41–52.

Mizutani, T., and Kasahara, M. (1997). Hippocampal atrophy secondary to entorhinal cortical degeneration in Alzheimer-type dementia. Neurosci. Lett. *222*, 119–122.

de la Monte, S.M., Ng, S.C., and Hsu, D.W. (1995). Aberrant GAP-43 gene expression in Alzheimer's disease. Am. J. Pathol. *147*, 934–946.

Montine, T.J., Phelps, C.H., Beach, T.G., Bigio, E.H., Cairns, N.J., Dickson, D.W., Duyckaerts, C., Frosch, M.P., Masliah, E., Mirra, S.S., et al. (2011). National Institute on Aging–Alzheimer's Association guidelines for the neuropathologic assessment of Alzheimer's disease: a practical approach. Acta Neuropathol. (Berl.) *123*, 1–11.

Mori, F., Nishie, M., Piao, Y.-S., Kito, K., Kamitani, T., Takahashi, H., and Wakabayashi, K. (2005). Accumulation of NEDD8 in neuronal and glial inclusions of neurodegenerative disorders. Neuropathol. Appl. Neurobiol. *31*, 53–61.

Mullan, M., Crawford, F., Axelman, K., Houlden, H., Lilius, L., Winblad, B., and Lannfelt, L. (1992). A pathogenic mutation for probable Alzheimer's disease in the APP gene at the N–terminus of β–amyloid. Nat. Genet. *1*, 345–347.

Murray, M.E., and Dickson, D.W. (2014). Is pathological aging a successful resistance against amyloid-beta or preclinical Alzheimer's disease? Alzheimers Res. Ther. *6*, 24.

Murray, C.E., King, A., Troakes, C., Hodges, A., and Lashley, T. APOE ε4 is also required in TREM2 R47H variant carriers for Alzheimer's disease to develop. Neuropathol. Appl. Neurobiol. *0*.

Musunuri, S., Wetterhall, M., Ingelsson, M., Lannfelt, L., Artemenko, K., Bergquist, J., Kultima, K., and Shevchenko, G. (2014). Quantification of the Brain Proteome in Alzheimer's Disease Using Multiplexed Mass Spectrometry. J. Proteome Res. *13*, 2056–2068.

Muthusamy, N., Chen, Y.-J., Yin, D.-M., Mei, L., and Bergson, C. (2015). Complementary roles of the neuron-enriched endosomal proteins NEEP21 and calcyon in neuronal vesicle trafficking. J. Neurochem. *132*, 20–31.

Nagai, A., Nakagawa, E., Hatori, K., Choi, H.B., McLarnon, J.G., Lee, M.A., and Kim, S.U. (2001). Generation and Characterization of Immortalized Human Microglial Cell Lines: Expression of Cytokines and Chemokines. Neurobiol. Dis. *8*, 1057–1068.

Namba, Y., Tomonaga, M., Kawasaki, H., Otomo, E., and Ikeda, K. (1991). Apolipoprotein E immunoreactivity in cerebral amyloid deposits and neurofibrillary tangles in Alzheimer's disease and kuru plaque amyloid in Creutzfeldt-Jakob disease. Brain Res. *541*, 163–166.

Nassar, M., Simonnet, J., Lofredi, R., Cohen, I., Savary, E., Yanagawa, Y., Miles, R., and Fricker, D. (2015). Diversity and overlap of Parvalbumin and Somatostatin expressing interneurons in mouse presubiculum. Front. Neural Circuits *9*.

Nazer, B., Hong, S., and Selkoe, D.J. (2008). LRP promotes endocytosis and degradation, but not transcytosis, of the amyloid-β peptide in a blood-brain barrier in vitro model. Neurobiol. Dis. *30*, 94–102.

Neumann, H., and Daly, M.J. (2013). Variant TREM2 as risk factor for Alzheimer's disease. N. Engl. J. Med. *368*, 182–184.

Newington, J.T., Rappon, T., Albers, S., Wong, D.Y., Rylett, R.J., and Cumming, R.C. (2012). Overexpression of Pyruvate Dehydrogenase Kinase 1 and Lactate Dehydrogenase A in Nerve Cells Confers Resistance to Amyloid β and Other Toxins by Decreasing Mitochondrial Respiration and Reactive Oxygen Species Production. J. Biol. Chem. *287*, 37245–37258.

Nicholson, A.M., Finch, N.A., Almeida, M., Perkerson, R.B., van Blitterswijk, M., Wojtas, A., Cenik, B., Rotondo, S., Inskeep, V., Almasy, L., et al. (2016). Prosaposin is a regulator of progranulin levels and oligomerization. Nat. Commun. *7*.

Nicoll, J.A.R., Yamada, M., Frackowiak, J., Mazur-Kolecka, B., and Weller, R.O. (2004). Cerebral amyloid angiopathy plays a direct role in the pathogenesis of Alzheimer's disease: Pro-CAA position statement. Neurobiol. Aging *25*, 589–597.

Norden, D.M., and Godbout, J.P. (2013). Review: Microglia of the aged brain: primed to be activated and resistant to regulation. Neuropathol. Appl. Neurobiol. *39*, 19–34.

Nuzzo, D., Inguglia, L., Walters, J., Picone, P., and Di Carlo, M. (2017). A Shotgun Proteomics Approach Reveals a New Toxic Role for Alzheimer's Disease Aβ Peptide: Spliceosome Impairment. J. Proteome Res.

Okada, H., Zhang, W., Peterhoff, C., Hwang, J.C., Nixon, R.A., Ryu, S.H., and Kim, T.-W. (2010). Proteomic identification of sorting nexin 6 as a negative regulator of BACE1-mediated APP processing. FASEB J. *24*, 2783–2794.

O'Keefe, J., and Nadel, L. (1978). The hippocampus as a cognitive map (Oxford : New York: Clarendon Press ; Oxford University Press).

Orre, M., Kamphuis, W., Osborn, L.M., Jansen, A.H.P., Kooijman, L., Bossers, K., and Hol, E.M. (2014). Isolation of glia from Alzheimer's mice reveals inflammation and dysfunction. Neurobiol. Aging *35*, 2746–2760.

Ortega-Cubero, S., Lorenzo-Betancor, O., Lorenzo, E., Agúndez, J.A.G., Jiménez-Jiménez, F.J., Ross, O.A., Wurster, I., Mielke, C., Lin, J.-J., Coria, F., et al. (2015). TREM2 R47H variant and risk of essential tremor: A cross-sectional international multicenter study. Parkinsonism Relat. Disord. *21*, 306–309.

Painter, M.M., Atagi, Y., Liu, C.-C., Rademakers, R., Xu, H., Fryer, J.D., and Bu, G. (2015). TREM2 in CNS homeostasis and neurodegenerative disease. Mol. Neurodegener. *10*, 43.

PAPEZ JW (1937). A proposed mechanism of emotion. Arch. Neurol. Psychiatry *38*, 725–743.

Pappolla, M.A., Omar, R.A., and Vinters, H.V. (1991). Image analysis microspectroscopy shows that neurons participate in the genesis of a subset of early primitive (diffuse) senile plaques. Am. J. Pathol. *139*, 599–607.

Paradowska-Gorycka, A., and Jurkowska, M. (2013). Structure, expression pattern and biological activity of molecular complex TREM-2/DAP12. Hum. Immunol. *74*, 730–737.

Paranjape, G.S., Gouwens, L.K., Osborn, D.C., and Nichols, M.R. (2012). Isolated Amyloid-β(1–42) Protofibrils, But Not Isolated Fibrils, Are Robust Stimulators of Microglia. ACS Chem. Neurosci. *3*, 302–311.

Paresce, D.M., Chung, H., and Maxfield, F.R. (1997). Slow Degradation of Aggregates of the Alzheimer's Disease Amyloid β-Protein by Microglial Cells. J. Biol. Chem. *272*, 29390–29397.

Park, J.-S., Ji, I.J., An, H.J., Kang, M.-J., Kang, S., Kim, D.-H., and Yoon, S.-Y. (2015a). Disease-associated mutations of TREM2 alter the processing of N-linked oligosaccharides in the Golgi apparatus. Traffic n/a-n/a.

Park, M., Yi, J.-W., Kim, E.-M., Yoon, I.-J., Lee, E.-H., Lee, H.-Y., Ji, K.-Y., Lee, K.-H., Jang, J.-H., Oh, S.-S., et al. (2015b). Triggering Receptor Expressed on Myeloid Cells 2 (TREM2) Promotes Adipogenesis and Diet-Induced Obesity. Diabetes *64*, 117–127.

Parra-Damas, A., Valero, J., Chen, M., España, J., Martín, E., Ferrer, I., Rodríguez-Alvarez, J., and Saura, C.A. (2014). Crtc1 Activates a Transcriptional Program Deregulated at Early Alzheimer's Disease-Related Stages. J. Neurosci. *34*, 5776–5787.

Pastoll, H., Solanka, L., van Rossum, M.C.W., and Nolan, M.F. (2013). Feedback Inhibition Enables Theta-Nested Gamma Oscillations and Grid Firing Fields. Neuron *77*, 141–154.

Peng, Y., Barreda Tomás, F.J., Klisch, C., Vida, I., and Geiger, J.R.P. (2017). Layer-Specific Organization of Local Excitatory and Inhibitory Synaptic Connectivity in the Rat Presubiculum. Cereb. Cortex N. Y. NY *27*, 2435–2452.

Perez, S.E., Nadeem, M., He, B., Miguel, J.C., Malek-Ahmadi, M.H., Chen, K., and Mufson, E.J. (2017). Neocortical and hippocampal TREM2 protein levels during the progression of Alzheimer's disease. Neurobiol. Aging *54*, 133–143.

Perry, V.H., and Holmes, C. (2014). Microglial priming in neurodegenerative disease. Nat. Rev. Neurol. *10*, 217–224.

Perry, R.T., Gearhart, D.A., Wiener, H.W., Harrell, L.E., Barton, J.C., Kutlar, A., Kutlar, F., Ozcan, O., Go, R.C.P., and Hill, W.D. (2008). Hemoglobin binding to Aβ and HBG2 SNP association suggest a role in Alzheimer's disease. Neurobiol. Aging *29*, 185–193.

Pfeifer, L.A., White, L.R., Ross, G.W., Petrovitch, H., and Launer, L.J. (2002). Cerebral amyloid angiopathy and cognitive function The HAAS autopsy study. Neurology *58*, 1629–1634.

Piccio, L., Buonsanti, C., Mariani, M., Cella, M., Gilfillan, S., Cross, A.H., Colonna, M., and Panina-Bordignon, P. (2007). Blockade of TREM-2 exacerbates experimental autoimmune encephalomyelitis. Eur. J. Immunol. *37*, 1290–1301.

Piccio, L., Deming, Y., Del-Águila, J.L., Ghezzi, L., Holtzman, D.M., Fagan, A.M., Fenoglio, C., Galimberti, D., Borroni, B., and Cruchaga, C. (2016). Cerebrospinal fluid soluble TREM2 is higher in Alzheimer disease and associated with mutation status. Acta Neuropathol. (Berl.).

Pietrzik, C.U., Busse, T., Merriam, D.E., Weggen, S., and Koo, E.H. (2002). The cytoplasmic domain of the LDL receptor-related protein regulates multiple steps in APP processing. EMBO J. *21*, 5691–5700.

Pike, C.J., Overman, M.J., and Cotman, C.W. (1995). Amino-terminal deletions enhance aggregation of beta-amyloid peptides in vitro. J. Biol. Chem. *270*, 23895–23898.

Pineda, D., AmpurdanÉS, C., Medina, M.G., Serratosa, J., Tusell, J.M., Saura, J., Planas, A.M., and Navarro, P. (2012). Tissue plasminogen activator induces microglial inflammation via a noncatalytic molecular mechanism involving activation of mitogen-activated protein kinases and Akt signaling pathways and AnnexinA2 and Galectin-1 receptors. Glia *60*, 526–540.

Poliani, P.L., Wang, Y., Fontana, E., Robinette, M.L., Yamanishi, Y., Gilfillan, S., and Colonna, M. (2015). TREM2 sustains microglial expansion during aging and response to demyelination. J. Clin. Invest.

Portelius, E., Bogdanovic, N., Gustavsson, M.K., Volkmann, I., Brinkmalm, G., Zetterberg, H., Winblad, B., and Blennow, K. (2010). Mass spectrometric characterization of brain amyloid beta isoform signatures in familial and sporadic Alzheimer's disease. Acta Neuropathol. (Berl.) *120*, 185–193.

Portelius, E., Lashley, T., Westerlund, A., Persson, R., Fox, N.C., Blennow, K., Revesz, T., and Zetterberg, H. (2015). Brain Amyloid-Beta Fragment Signatures in Pathological Ageing and Alzheimer's Disease by Hybrid Immunoprecipitation Mass Spectrometry. Neurodegener. Dis. *15*, 50–57.

Probst, A., Langui, D., and Ulrich, J. (1991a). Alzheimer's Disease: A Description of the Structural Lesions. Brain Pathol. *1*, 229–239.

Probst, A., Langui, D., Ipsen, S., Robakis, N., and Ulrich, J. (1991b). Deposition of beta/A4 protein along neuronal plasma membranes in diffuse senile plaques. Acta Neuropathol. (Berl.) *83*, 21–29.

Prokop, S., Miller, K.R., Drost, N., Handrick, S., Mathur, V., Luo, J., Wegner, A., Wyss-Coray, T., and Heppner, F.L. (2015). Impact of peripheral myeloid cells on amyloid-β pathology in Alzheimer's disease–like mice. J. Exp. Med. jem.20150479.

Puglielli, L., Tanzi, R.E., and Kovacs, D.M. (2003). Alzheimer's disease: the cholesterol connection. Nat. Neurosci. *6*, 345–351.

Qi, X., and Ma, J. (2017). The role of amyloid beta clearance in cerebral amyloid angiopathy: more potential therapeutic targets. Transl. Neurodegener. *6*.

Quan, X., Yue, W., Luo, Y., Cao, J., Wang, H., Wang, Y., and Lu, Z. (2015). The protein arginine methyltransferase PRMT5 regulates Aβ-induced toxicity in human cells and Caenorhabditis elegans models of Alzheimer's disease. J. Neurochem. *134*, 969–977.

Ramos, M.C., Tenorio, R., Martínez-García, A., Sastre, I., Vilella-Cuadrada, E., Frank, A., Rosich-Estragó, M., Valdivieso, F., and Bullido, M.J. (2006). Association of DSC1, a gene modulated by adrenergic stimulation, with Alzheimer's disease. Neurosci. Lett. *408*, 203–208.

Rayaprolu, S., Mullen, B., Baker, M., Lynch, T., Finger, E., Seeley, W.W., Hatanpaa, K.J., Lomen-Hoerth, C., Kertesz, A., Bigio, E.H., et al. (2013). TREM2 in neurodegeneration: evidence for association of the p.R47H variant with frontotemporal dementia and Parkinson's disease. Mol. Neurodegener. *8*, 19.

Rebeck, G.W., Harr, S.D., Strickland, D.K., and Hyman, B.T. (1995). Multiple, diverse senile plaque-associated proteins are ligands of an apolipoprotein E receptor, the alpha 2-macroglobulin receptor/low-density-lipoprotein receptor-related protein. Ann. Neurol. *37*, 211–217.

van Rheenen, W., Shatunov, A., Dekker, A.M., McLaughlin, R.L., Diekstra, F.P., Pulit, S.L., van der Spek, R.A.A., Võsa, U., de Jong, S., Robinson, M.R., et al. (2016). Genome-wide association analyses identify new risk variants and the genetic architecture of amyotrophic lateral sclerosis. Nat. Genet. *48*, 1043–1048.

Ries, M., Loiola, R., Shah, U.N., Gentleman, S.M., Solito, E., and Sastre, M. (2016). The anti-inflammatory Annexin A1 induces the clearance and degradation of the amyloid-β peptide. J. Neuroinflammation *13*.

Rogers, J., and Lue, L.-F. (2001). Microglial chemotaxis, activation, and phagocytosis of amyloid β-peptide as linked phenomena in Alzheimer's disease. Neurochem. Int. *39*, 333–340.

Rogers, J., Luber-Narod, J., Styren, S.D., and Civin, W.H. (1988). Expression of immune system-associated antigens by cells of the human central nervous system: relationship to the pathology of Alzheimer's disease. Neurobiol. Aging *9*, 339–349.

Rogers, J., Schultz, J., Brachova, L., Lue, L.F., Webster, S., Bradt, B., Cooper, N.R., and Moss, D.E. (1992a). Complement activation and beta-amyloid-mediated neurotoxicity in Alzheimer's disease. Res. Immunol. *143*, 624–630.

Rogers, J., Cooper, N.R., Webster, S., Schultz, J., McGeer, P.L., Styren, S.D., Civin, W.H., Brachova, L., Bradt, B., and Ward, P. (1992b). Complement activation by beta-amyloid in Alzheimer disease. Proc. Natl. Acad. Sci. U. S. A. *89*, 10016–10020.

Rogers, J., Strohmeyer, R., Kovelowski, C. j., and Li, R. (2002). Microglia and inflammatory mechanisms in the clearance of amyloid β peptide. Glia *40*, 260–269.

Roggendorf, W., Strupp, S., and Paulus, W. (1996). Distribution and characterization of microglia/macrophages in human brain tumors. Acta Neuropathol. (Berl.) *92*, 288–293.

Rohn, T.T. (2013). The Triggering Receptor Expressed on Myeloid Cells 2: "TREM-ming" the Inflammatory Component Associated with Alzheimer's Disease.

Rosenthal, S.L., and Kamboh, M.I. (2014). Late-Onset Alzheimer's Disease Genes and the Potentially Implicated Pathways. Curr. Genet. Med. Rep. *2*, 85–101.

Rosenthal, S.L., Wang, X., Demirci, F.Y., Barmada, M.M., Ganguli, M., Lopez, O.L., and Kamboh, M.I. (2012). Beta-amyloid toxicity modifier genes and the risk of Alzheimer's disease. Am. J. Neurodegener. Dis. *1*, 191–198.

Rosenthal, S.L., Bamne, M.N., Wang, X., Berman, S., Snitz, B.E., Klunk, W.E., Sweet, R.A., Demirci, F.Y., Lopez, O.L., and Kamboh, M.I. (2015). More evidence for association of a rare TREM2 mutation (R47H) with Alzheimer's disease risk. Neurobiol. Aging *36*, 2443.e21-26.

Roussos, P., Katsel, P., Fam, P., Tan, W., Purohit, D.P., and Haroutunian, V. (2015). The triggering receptor expressed on myeloid cells 2 (TREM2) is associated with enhanced inflammation, neuropathological lesions and increased risk for Alzheimer's dementia. Alzheimers Dement. *11*, 1163–1170.

Roy, J., Sarkar, A., Parida, S., Ghosh, Z., and Mallick, B. (2017). Small RNA sequencing revealed dysregulated piRNAs in Alzheimer's disease and their probable role in pathogenesis. Mol. Biosyst. *13*, 565–576.

Russo, C., Schettini, G., Saido, T.C., Hulette, C., Lippa, C., Lannfelt, L., Ghetti, B., Gambetti, P., Tabaton, M., and Teller, J.K. (2000). Neurobiology: Presenilin-1 mutations in Alzheimer's disease. Nature *405*, 531–532.

Russo, C., Violani, E., Salis, S., Venezia, V., Dolcini, V., Damonte, G., Benatti, U., D'Arrigo, C., Patrone, E., Carlo, P., et al. (2002). Pyroglutamate-modified amyloid β-peptides – AβN3(pE) – strongly affect cultured neuron and astrocyte survival. J. Neurochem. *82*, 1480–1489.

Sanchez-Mejias, E., Navarro, V., Jimenez, S., Sanchez-Mico, M., Sanchez-Varo, R., Nuñez-Diaz, C., Trujillo-Estrada, L., Davila, J.C., Vizuete, M., Gutierrez, A., et al. (2016). Soluble phospho-tau from Alzheimer's disease hippocampus drives microglial degeneration. Acta Neuropathol. (Berl.) *132*, 897–916.

Santiago, J.A., Bottero, V., and Potashkin, J.A. (2017). Dissecting the Molecular Mechanisms of Neurodegenerative Diseases through Network Biology. Front. Aging Neurosci. *9*.

Sasaki, A., and Nakazato, Y. (1992). The identity of cells expressing MHC class II antigens in normal and pathological human brain. Neuropathol. Appl. Neurobiol. *18*, 13–26.

Sasaki, A., Kakita, A., Yoshida, K., Konno, T., Ikeuchi, T., Hayashi, S., Matsuo, H., and Shioda, K. (2015). Variable expression of microglial DAP12 and TREM2 genes in Nasu-Hakola disease. Neurogenetics 1–12.

Sasaki, Y., Ohsawa, K., Kanazawa, H., Kohsaka, S., and Imai, Y. (2001). Iba1 Is an Actin-Cross-Linking Protein in Macrophages/Microglia. Biochem. Biophys. Res. Commun. *286*, 292–297.

Satoh, J., Tabunoki, H., Ishida, T., Yagishita, S., Jinnai, K., Futamura, N., Kobayashi, M., Toyoshima, I., Yoshioka, T., Enomoto, K., et al. (2011). Immunohistochemical characterization of microglia in Nasu-Hakola disease brains. Neuropathology *31*, 363–375.

Satoh, J., Kawana, N., Yamamoto, Y., Ishida, T., Saito, Y., and Arima, K. (2013). A survey of TREM2 antibodies reveals neuronal but not microglial staining in formalin-fixed paraffin-embedded postmortem Alzheimer's brain tissues. Alzheimers Res. Ther. *5*, 30.

Satoh, J., Motohashi, N., Kino, Y., Ishida, T., Yagishita, S., Jinnai, K., Arai, N., Nakamagoe, K., Tamaoka, A., Saito, Y., et al. (2014). LC3, an autophagosome marker, is expressed on oligodendrocytes in Nasu-Hakola disease brains. Orphanet J. Rare Dis. *9*, 68.

Satoh, J., Kino, Y., Motohashi, N., Ishida, T., Yagishita, S., Jinnai, K., Arai, N., Nakamagoe, K., Tamaoka, A., Saito, Y., et al. (2015). Immunohistochemical characterization of CD33 expression on microglia in Nasu-Hakola disease brains. Neuropathology n/a-n/a.

Saura, C.A. (2012). CREB-Regulated Transcription Coactivator 1-Dependent Transcription in Alzheimer's Disease Mice. Neurodegener. Dis. *10*, 250–252.

Schmid, C.D., Sautkulis, L.N., Danielson, P.E., Cooper, J., Hasel, K.W., Hilbush, B.S., Sutcliffe, J.G., and Carson, M.J. (2002). Heterogeneous expression of the triggering receptor expressed on myeloid cells-2 on adult murine microglia. J. Neurochem. *83*, 1309–1320.

Sekar, S., McDonald, J., Cuyugan, L., Aldrich, J., Kurdoglu, A., Adkins, J., Serrano, G., Beach, T.G., Craig, D.W., Valla, J., et al. (2015). Alzheimer's disease is associated with altered expression of genes involved in immune response and mitochondrial processes in astrocytes. Neurobiol. Aging *36*, 583–591.

Sengupta, U., Nilson, A.N., and Kayed, R. (2016). The Role of Amyloid-β Oligomers in Toxicity, Propagation, and Immunotherapy. EBioMedicine *6*, 42–49.

Serrano-Pozo, A., Frosch, M.P., Masliah, E., and Hyman, B.T. (2011). Neuropathological Alterations in Alzheimer Disease. Cold Spring Harb. Perspect. Med. *1*.

Shackleton, B., Crawford, F., and Bachmeier, C. (2016). Inhibition of ADAM10 promotes the clearance of Aβ across the BBB by reducing LRP1 ectodomain shedding. Fluids Barriers CNS *13*.

Shaffer, L.M., Dority, M.D., Gupta-Bansal, R., Frederickson, R.C.A., Younkin, S.G., and Brunden, K.R. (1995). Amyloid β protein (Aβ) removal by neuroglial cells in culture. Neurobiol. Aging *16*, 737–745.

Sheng, J.G., Mrak, R.E., and Griffin, W.S. (1998). Enlarged and phagocytic, but not primed, interleukin-1 alpha-immunoreactive microglia increase with age in normal human brain. Acta Neuropathol. (Berl.) *95*, 229–234.

Shi, Q., Chowdhury, S., Ma, R., Le, K.X., Hong, S., Caldarone, B.J., Stevens, B., and Lemere, C.A. (2017). Complement C3 deficiency protects against neurodegeneration in aged plaque-rich APP/PS1 mice. Sci. Transl. Med. *9*, eaaf6295.

Shibata, M., Yamada, S., Kumar, S.R., Calero, M., Bading, J., Frangione, B., Holtzman, D.M., Miller, C.A., Strickland, D.K., Ghiso, J., et al. (2000). Clearance of Alzheimer's amyloid-β1-40 peptide from brain by LDL receptor–related protein-1 at the blood-brain barrier. J. Clin. Invest. *106*, 1489–1499.

Shih, A.Y., Fernandes, H.B., Choi, F.Y., Kozoriz, M.G., Liu, Y., Li, P., Cowan, C.M., and Klegeris, A. (2006). Policing the Police: Astrocytes Modulate Microglial Activation. J. Neurosci. *26*, 3887–3888.

Shikuma, C.M., Gangcuangco, L.M.A., Killebrew, D.A., LiButti, D.E., Chow, D.C., Nakamoto, B.K., Liang, C.Y., Milne, C.I.P., Ndhlovu, L.C., Barbour, J.D., et al. (2014). The Role of HIV and Monocytes/Macrophages in Adipose Tissue Biology. J. Acquir. Immune Defic. Syndr. 1999 *65*, 151–159.

Shipley, M.T. (1974). Presubiculum afferents to the entorhinal area and the Papez circuit. Brain Res. *67*.

Sieber, M.W., Jaenisch, N., Brehm, M., Guenther, M., Linnartz-Gerlach, B., Neumann, H., Witte, O.W., and Frahm, C. (2013). Attenuated Inflammatory Response in Triggering Receptor Expressed on Myeloid Cells 2 (TREM2) Knock-Out Mice following Stroke. PLoS ONE *8*.

Silva, P.N., Furuya, T.K., Braga, I.L., Rasmussen, L.T., Labio, R.W., Bertolucci, P.H., Chen, E.S., Turecki, G., Mechawar, N., Payão, S.L., et al. (2014). Analysis of HSPA8 and HSPA9 mRNA Expression and Promoter Methylation in the Brain and Blood of Alzheimer's Disease Patients. J. Alzheimers Dis. *38*, 165–170.

Simonnet, J., Nassar, M., Stella, F., Cohen, I., Mathon, B., Boccara, C.N., Miles, R., and Fricker, D. (2017). Activity dependent feedback inhibition may maintain head direction signals in mouse presubiculum. Nat. Commun. *8*.

Sipe, G.O., Lowery, R.L., Tremblay, M.-È., Kelly, E.A., Lamantia, C.E., and Majewska, A.K. (2016). Microglial P2Y12 is necessary for synaptic plasticity in mouse visual cortex. Nat. Commun. *7*.

Slattery, C.F., Beck, J.A., Harper, L., Adamson, G., Abdi, Z., Uphill, J., Campbell, T., Druyeh, R., Mahoney, C.J., Rohrer, J.D., et al. (2014). R47H TREM2 variant increases risk of typical early-onset Alzheimer's disease but not of prion or frontotemporal dementia. Alzheimers Dement. J. Alzheimers Assoc.

Smith, C., Gentleman, S.M., Leclercq, P.D., Murray, L.S., Griffin, W.S.T., Graham, D.I., and Nicoll, J.A.R. (2013). The neuroinflammatory response in humans after traumatic brain injury. Neuropathol. Appl. Neurobiol. *39*.

Smith, P.Y., Hernandez-Rapp, J., Jolivette, F., Lecours, C., Bisht, K., Goupil, C., Dorval, V., Parsi, S., Morin, F., Planel, E., et al. (2015). miR-132/212 deficiency impairs tau metabolism and promotes pathological aggregation in vivo. Hum. Mol. Genet. *24*, 6721–6735.

Solje, E., Hartikainen, P., Valori, M., Vanninen, R., Tiihonen, J., Hakola, P., Tienari, P.J., and Remes, A.M. (2014). The C9ORF72 expansion does not affect the phenotype in Nasu-Hakola disease with the DAP12 mutation. Neurobiol. Aging *35*, 1780.e13-1780.e17.

Song, L., Lee, C., and Schindler, C. (2011). Deletion of the murine scavenger receptor CD68. J. Lipid Res. *52*, 1542–1550.

Spellman, D.S., Wildsmith, K.R., Honigberg, L.A., Tuefferd, M., Baker, D., Raghavan, N., Nairn, A.C., Croteau, P., Schirm, M., Allard, R., et al. (2015). Development and Evaluation of a Multiplexed Mass Spectrometry-Based Assay for Measuring Candidate Peptide Biomarkers in Alzheimer's Disease Neuroimaging Initiative (ADNI) CSF. Proteomics Clin. Appl. *9*, 715–731.

Spies, P.E., Slats, D., Sjogren, J.M.C., Kremer, B.P.H., Verhey, F.R.J., and Verbeek, M.G.M.O.R. and M.M. (2010). The Cerebrospinal Fluid Amyloid β42/40 Ratio in the Differentiation of Alzheimers Disease from Non-Alzheimers Dementia.

Storck, S.E., and Pietrzik, C.U. (2017). Endothelial LRP1 – A Potential Target for the Treatment of Alzheimer's Disease. Pharm. Res. 1–15.

Streit, W.J., Sammons, N.W., Kuhns, A.J., and Sparks, D.L. (2004). Dystrophic microglia in the aging human brain. Glia *45*, 208–212.

Streit, W.J., Braak, H., Xue, Q.-S., and Bechmann, I. (2009). Dystrophic (senescent) rather than activated microglial cells are associated with tau pathology and likely precede neurodegeneration in Alzheimer's disease. Acta Neuropathol. (Berl.) *118*, 475–485.

van Strien, N.M., Cappaert, N.L.M., and Witter, M.P. (2009). The anatomy of memory: an interactive overview of the parahippocampal–hippocampal network. Nat. Rev. Neurosci. *10*, 272–282.

Strittmatter, W.J., Saunders, A.M., Schmechel, D., Pericak-Vance, M., Enghild, J., Salvesen, G.S., and Roses, A.D. (1993a). Apolipoprotein E: high-avidity binding to beta-amyloid and increased frequency of type 4 allele in late-onset familial Alzheimer disease. Proc. Natl. Acad. Sci. U. S. A. *90*, 1977–1981.

Strittmatter, W.J., Weisgraber, K.H., Huang, D.Y., Dong, L.M., Salvesen, G.S., Pericak-Vance, M., Schmechel, D., Saunders, A.M., Goldgaber, D., and Roses, A.D. (1993b). Binding of human apolipoprotein E to synthetic amyloid beta peptide: isoform-specific effects and implications for late-onset Alzheimer disease. Proc. Natl. Acad. Sci. U. S. A. *90*, 8098–8102.

Styren, S.D., Civin, W.H., and Rogers, J. (1990). Molecular, cellular, and pathologic characterization of HLA-DR immunoreactivity in normal elderly and Alzheimer's disease brain. Exp. Neurol. *110*, 93–104.

Suarez-Calvet, M., Kleinberger, G., Araque Caballero, M.A., Brendel, M., Rominger, A., Alcolea, D., Fortea, J., Lleo, A., Blesa, R., Gispert, J.D., et al. (2016). sTREM2 cerebrospinal fluid levels are a potential biomarker for microglia activity in early-stage Alzheimer's disease and associate with neuronal injury markers. EMBO Mol. Med.

Sun, Z., Xie, Y., Chen, Y., Yang, Q., Quan, Z., Dai, R., and Qing, H. (2017). Rab21, a Novel PS1 Interactor, Regulates γ-Secretase Activity via PS1 Subcellular Distribution. Mol. Neurobiol. 1–15.

Suzuki, S.C., and Takeichi, M. (2008). Cadherins in neuronal morphogenesis and function. Dev. Growth Differ. *50*, S119–S130.

Swiatkowski, P., Murugan, M., Eyo, U.B., Wang, Y., Rangaraju, S., Oh, S.B., and Wu, L.-J. (2016). Activation of microglial P2Y12 receptor is required for outward potassium currents in response to neuronal injury. Neuroscience *318*, 22–33.

Szaruga, M., Veugelen, S., Benurwar, M., Lismont, S., Sepulveda-Falla, D., Lleo, A., Ryan, N.S., Lashley, T., Fox, N.C., Murayama, S., et al. (2015). Qualitative changes in human γ-secretase underlie familial Alzheimer's disease. J. Exp. Med. jem.20150892-.

Takahashi, K., Rochford, C.D.P., and Neumann, H. (2005). Clearance of apoptotic neurons without inflammation by microglial triggering receptor expressed on myeloid cells-2. J. Exp. Med. *201*, 647–657.

Tan, T., Song, Z., Yuan, L., Xiong, W., Deng, X., Ni, B., Chen, Y., and Deng, H. (2016). Genetic analysis of TREM2 variants in Chinese Han patients with sporadic Parkinson's disease. Neurosci. Lett. *612*, 189–192.

Tang, Y., and Le, W. (2015). Differential Roles of M1 and M2 Microglia in Neurodegenerative Diseases. Mol. Neurobiol. 1–14.

Tanzi, R.E., Moir, R.D., and Wagner, S.L. (2004). Clearance of Alzheimer's Aβ Peptide: The Many Roads to Perdition. Neuron *43*, 605–608.

Tennstaedt, A., Pöpsel, S., Truebestein, L., Hauske, P., Brockmann, A., Schmidt, N., Irle, I., Sacca, B., Niemeyer, C.M., Brandt, R., et al. (2012). Human High Temperature Requirement Serine Protease A1 (HTRA1) Degrades Tau Protein Aggregates. J. Biol. Chem. *287*, 20931–20941.

Thal, D.R., Arendt, T., Waldmann, G., Holzer, M., Zedlick, D., Rüb, U., and Schober, R. (1998). Progression of neurofibrillary changes and PHF-τ in end-stage Alzheimer's disease is different from plaque and cortical microglial pathology. Neurobiol. Aging *19*, 517–525.

Thal, D.R., Rüb, U., Schultz, C., Sassin, I., Ghebremedhin, E., Tredici, K.D., Braak, E., and Braak, H. (2000). Sequence of Aβ-Protein Deposition in the Human Medial Temporal Lobe. J. Neuropathol. Exp. Neurol. *59*, 733–748.

Thal, D.R., Rüb, U., Orantes, M., and Braak, H. (2002). Phases of A beta-deposition in the human brain and its relevance for the development of AD. Neurology *58*, 1791–1800.

Thameem Dheen, S., Kaur, C., and Ling, E.-A. (2007). Microglial Activation and its Implications in the Brain Diseases. Curr. Med. Chem. *14*, 1189–1197.

Thelen, M., Razquin, C., Hernández, I., Gorostidi, A., Sánchez-Valle, R., Ortega-Cubero, S., Wolfsgruber, S., Drichel, D., Fliessbach, K., Duenkel, T., et al. (2014). Investigation of the role of rare TREM2 variants in frontotemporal dementia subtypes. Neurobiol. Aging *35*, 2657.e13-2657.e19.

Thrash, J.C., Torbett, B.E., and Carson, M.J. (2009). Developmental Regulation of TREM2 and DAP12 Expression in the Murine CNS: Implications for Nasu-Hakola Disease. Neurochem. Res. *34*, 38–45.

Tian, H., Qian, J., Ai, L., Li, Y., Su, W., Kong, X., Xu, J., and Fang, J. (2017). Upregulation of ASAP3 contributes to colorectal carcinogenesis and indicates poor survival outcome. Cancer Sci. *108*, 1544–1555.

Tong, Y., Xu, Y., Scearce-Levie, K., Ptáček, L.J., and Fu, Y.-H. (2010). COL25A1 triggers and promotes Alzheimer's disease-like pathology in vivo. Neurogenetics *11*, 41–52.

Town, T., Nikolic, V., and Tan, J. (2005). The microglial. J. Neuroinflammation *2*, 24.

Tukker, J.J., Tang, Q., Burgalossi, A., and Brecht, M. (2015). Head-Directional Tuning and Theta Modulation of Anatomically Identified Neurons in the Presubiculum. J. Neurosci. *35*, 15391–15395.

Tuppo, E.E., and Arias, H.R. (2005). The role of inflammation in Alzheimer's disease. Int. J. Biochem. Cell Biol. *37*, 289–305.

Uhrig, M., Brechlin, P., Jahn, O., Knyazev, Y., Weninger, A., Busia, L., Honarnejad, K., Otto, M., and Hartmann, T. (2008). Upregulation of CRABP1 in human neuroblastoma cells overproducing the Alzheimer-typical Aβ42 reduces their differentiation potential. BMC Med. *6*, 38.

Ulrich, J.D., and Holtzman, D.M. (2016). TREM2 Function in Alzheimer's disease and neurodegeneration. ACS Chem. Neurosci.

Ulrich, J.D., Finn, M.B., Wang, Y., Shen, A., Mahan, T.E., Jiang, H., Stewart, F.R., Piccio, L., Colonna, M., and Holtzman, D.M. (2014). Altered microglial response to Aβ plaques in APPPS1-21 mice heterozygous for TREM2. Mol. Neurodegener. *9*, 20.

Ulvestad, E., Williams, K., Mørk, S., Antel, J., and Nyland, H. (1994). Phenotypic differences between human monocytes/macrophages and microglial cells studied in situ and in vitro. J. Neuropathol. Exp. Neurol. *53*, 492–501.

Van Gool, D., David, G., Lammens, M., Baro, F., and Dom, R. (1993). Heparan sulfate expression patterns in the amyloid deposits of patients with Alzheimer's and Lewy body type dementia. Dement. Basel Switz. *4*, 308–314.

Vandenabeele, P., and Fiers, W. (1991). Is amyloidogenesis during Alzheimer's disease due to an IL-1-/IL-6-mediated 'acute phase response' in the brain? Immunol. Today *12*, 217–219.

Varvel, N.H., Grathwohl, S.A., Degenhardt, K., Resch, C., Bosch, A., Jucker, M., and Neher, J.J. (2015). Replacement of brain-resident myeloid cells does not alter cerebral amyloid-β deposition in mouse models of Alzheimer's disease. J. Exp. Med. *212*, 1803–1809.

Vasconcelos, B., Stancu, I.-C., Buist, A., Bird, M., Wang, P., Vanoosthuyse, A., Van Kolen, K., Verheyen, A., Kienlen-Campard, P., Octave, J.-N., et al. (2016). Heterotypic seeding of Tau fibrillization by pre-aggregated Abeta provides potent seeds for prion-like seeding and propagation of Tau-pathology in vivo. Acta Neuropathol. (Berl.) *131*, 549–569.

Veerhuis, R., Janssen, I., Hack, C.E., and Eikelenboom, P. (1995). Early complement components in Alzheimer's disease brains. Acta Neuropathol. (Berl.) *91*, 53–60.

Verghese, P.B., Castellano, J.M., Garai, K., Wang, Y., Jiang, H., Shah, A., Bu, G., Frieden, C., and Holtzman, D.M. (2013). ApoE influences amyloid-β (Aβ) clearance despite minimal apoE/Aβ association in physiological conditions. Proc. Natl. Acad. Sci. U. S. A. *110*, E1807–E1816.

Wang, S.-P., and Wang, L.-H. (2016). Disease implication of hyper-Hippo signalling. Open Biol. *6*.

Wang, P., Joberty, G., Buist, A., Vanoosthuyse, A., Stancu, I.-C., Vasconcelos, B., Pierrot, N., Faelth-Savitski, M., Kienlen-Campard, P., Octave, J.-N., et al. (2017). Tau interactome mapping based identification of Otub1 as Tau deubiquitinase involved in accumulation of pathological Tau forms in vitro and in vivo. Acta Neuropathol. (Berl.) *133*, 731–749.

Wang, Y., Cella, M., Mallinson, K., Ulrich, J.D., Young, K.L., Robinette, M.L., Gilfillan, S., Krishnan, G.M., Sudhakar, S., Zinselmeyer, B.H., et al. (2015). TREM2 Lipid Sensing Sustains the Microglial Response in an Alzheimer's Disease Model. Cell *160*, 1061–1071.

Wang, Y., Ulland, T.K., Ulrich, J.D., Song, W., Tzaferis, J.A., Hole, J.T., Yuan, P., Mahan, T.E., Shi, Y., Gilfillan, S., et al. (2016). TREM2-mediated early microglial response limits diffusion and toxicity of amyloid plaques. J. Exp. Med. *213*, 667–675.

Webster, S., and Rogers, J. (1996). Relative efficacies of amyloid β peptide (Aβ) binding proteins in Aβ aggregation. J. Neurosci. Res. *46*, 58–66.

Webster, S., O'Barr, S., and Rogers, J. (1994). Enhanced aggregation and β structure of amyloid β peptide after coincubation with C1Q. J. Neurosci. Res. *39*, 448–456.

Webster, S., Glabe, C., and Rogers, J. (1995). Multivalent Binding of Complement Protein C1q to the Amyloid β-Peptide (Aβ) Promotes the Nucleation Phase of Aβ Aggregation. Biochem. Biophys. Res. Commun. *217*, 869–875.

Wegiel, J., and Wisniewski, H.M. (1990). The complex of microglial cells and amyloid star in three-dimensional reconstruction. Acta Neuropathol. (Berl.) *81*, 116–124.

Wegiel, J., Wang, K.-C., Tarnawski, M., and Lach, B. (2000). Microglial cells are the driving force in fibrillar plaque formation, whereas astrocytes are a leading factor in plaque degradation. Acta Neuropathol. (Berl.) *100*, 356–364.

Weisgraber, K.H., Roses, A.D., and Strittmatter, W.J. (1994). The role of apolipoprotein E in the nervous system. Curr. Opin. Lipidol. *5*, 110–116.

Weldon, D.T., Rogers, S.D., Ghilardi, J.R., Finke, M.P., Cleary, J.P., O'Hare, E., Esler, W.P., Maggio, J.E., and Mantyh, P.W. (1998). Fibrillar β-Amyloid Induces Microglial Phagocytosis, Expression of Inducible Nitric Oxide Synthase, and Loss of a Select Population of Neurons in the Rat CNS In Vivo. J. Neurosci. *18*, 2161–2173.

Wencel, P.L., Lukiw, W.J., Strosznajder, J.B., and Strosznajder, R.P. (2017). Inhibition of Poly(ADP-ribose) Polymerase-1 Enhances Gene Expression of Selected Sirtuins and APP Cleaving Enzymes in Amyloid Beta Cytotoxicity. Mol. Neurobiol. 1–12.

Wes, P.D., Easton, A., Corradi, J., Barten, D.M., Devidze, N., DeCarr, L.B., Truong, A., He, A., Barrezueta, N.X., Polson, C., et al. (2014). Tau Overexpression Impacts a Neuroinflammation Gene Expression Network Perturbed in Alzheimer's Disease. PLoS ONE *9*.

Whittaker, G.C., Orr, S.J., Quigley, L., Hughes, L., Francischetti, I.M.B., Zhang, W., and McVicar, D.W. (2010). The Linker for Activation of B Cells (LAB)/Non-T Cell Activation Linker (NTAL) Regulates Triggering Receptor Expressed on Myeloid Cells (TREM)-2 Signaling and Macrophage Inflammatory Responses Independently of the Linker for Activation of T Cells. J. Biol. Chem. *285*, 2976–2985.

Winkler, K., Scharnagl, H., Tisljar, U., Hoschützky, H., Friedrich, I., Hoffmann, M.M., Hüttinger, M., Wieland, H., and März, W. (1999). Competition of Aβ amyloid peptide and apolipoprotein E for receptor-mediated endocytosis. J. Lipid Res. *40*, 447–455.

Wisniewski, T., and Frangione, B. (1992). Apolipoprotein E: a pathological chaperone protein in patients with cerebral and systemic amyloid. Neurosci. Lett. *135*, 235–238.

Wisniewski, H.M., Wegiel, J., Wang, K.C., Kujawa, M., and Lach, B. (1989). Ultrastructural studies of the cells forming amyloid fibers in classical plaques. Can. J. Neurol. Sci. J. Can. Sci. Neurol. *16*, 535–542.

Wisniewski, H.M., Wegiel, J., and Kotula, L. (1996). Review: David Oppenheimer Memorial Lecture 1995: Some neuropathological aspects of Alzheimer's disease and its relevance to other disciplines*. Neuropathol. Appl. Neurobiol. *22*, 3–11.

Wisniewski, H.M., Sadowski, M., Jakubowska-Sadowswka, K., Tarnawski, M., and Wegiel, J.D. (1998). Diffuse, Lake-like Amyloid-[beta] Deposits in the Parvopyramidal Layer of the Presubiculum in Alzheimer Disease. J. Neuropathol. *57*, 674–683.

Wittnam, J.L., Portelius, E., Zetterberg, H., Gustavsson, M.K., Schilling, S., Koch, B., Demuth, H.-U., Blennow, K., Wirths, O., and Bayer, T.A. (2012). Pyroglutamate Amyloid β (Aβ) Aggravates Behavioral Deficits in Transgenic Amyloid Mouse Model for Alzheimer Disease. J. Biol. Chem. *287*, 8154–8162.

Wu, H.-M., Zhang, L.-F., Ding, P.-S., Liu, Y.-J., Wu, X., and Zhou, J.-N. (2014). Microglial activation mediates host neuronal survival induced by neural stem cells. J. Cell. Mol. Med. n/a-n/a.

Wu, Y., Zhang, S., Xu, Q., Zou, H., Zhou, W., Cai, F., Li, T., and Song, W. (2016). Regulation of global gene expression and cell proliferation by APP. Sci. Rep. *6*.

Wunderlich, P., Glebov, K., Kemmerling, N., Tien, N.T., Neumann, H., and Walter, J. (2013). Sequential Proteolytic Processing of the Triggering Receptor Expressed on Myeloid Cells-2 (TREM2) Protein by Ectodomain Shedding and γ-Secretase-dependent Intramembranous Cleavage. J. Biol. Chem. *288*, 33027–33036.

Xin, S.-H., Tan, L., Cao, X., Yu, J.-T., and Tan, L. (2018). Clearance of Amyloid Beta and Tau in Alzheimer's Disease: from Mechanisms to Therapy. Neurotox. Res. 1–16.

Xu, Z., Xiao, N., Chen, Y., Huang, H., Marshall, C., Gao, J., Cai, Z., Wu, T., Hu, G., and Xiao, M. (2015). Deletion of aquaporin-4 in APP/PS1 mice exacerbates brain Aβ accumulation and memory deficits. Mol. Neurodegener. *10*.

Yaghmoor, F., Noorsaeed, A., Alsaggaf, S., Aljohani, W., Scholtzova, H., Boutajangout, A., and Wisniewski, T. (2014). The Role of TREM2 in Alzheimer's Disease and Other Neurological Disorders. J. Alzheimers Dis. Park. *4*.

Yamada, M. (2000). Cerebral amyloid angiopathy: An overview. Neuropathology *20*, 8–22.

Yamada, M. (2002). Risk Factors for Cerebral Amyloid Angiopathy in the Elderly. Ann. N. Y. Acad. Sci. *977*, 37–44.

Yamada, M., Tsukagoshi, H., Otomo, E., and Hayakawa, M. (1987). Cerebral amyloid angiopathy in the aged. J. Neurol. *234*, 371–376.

Yamada, M., Ohsawa, K., Imai, Y., Kohsaka, S., and Kamitori, S. (2006). X-ray Structures of the Microglia/Macrophage-specific Protein Iba1 from Human and Mouse Demonstrate Novel Molecular Conformation Change Induced by Calcium binding. J. Mol. Biol. *364*, 449–457.

Yang, C., Huang, X., Huang, X., Mai, H., Li, J., Jiang, T., Wang, X., and Lü, T. (2016). Aquaporin-4 and Alzheimer's Disease. J. Alzheimers Dis. *52*, 391–402.

Yang, C.-N., Wu, M.-F., Liu, C.-C., Jung, W.-H., Chang, Y.-C., Lee, W.-P., Shiao, Y.-J., Wu, C.-L., Liou, H.-H., Lin, S.-K., et al. (2017a). Differential protective effects of connective tissue growth factor against Aβ neurotoxicity on neurons and glia. Hum. Mol. Genet. *26*, 3909–3921.

Yang, J., Zhang, R., Shi, C., Mao, C., Yang, Z., Suo, Z., Torp, R., and Xu, Y. (2017b). AQP4 Association with Amyloid Deposition and Astrocyte Pathology in the Tg-ArcSwe Mouse Model of Alzheimer's Disease. J. Alzheimers Dis. *57*, 157–169.

Yeh, F.L., Wang, Y., Tom, I., Gonzalez, L.C., and Sheng, M. (2016). TREM2 Binds to Apolipoproteins, Including APOE and CLU/APOJ, and Thereby Facilitates Uptake of Amyloid-Beta by Microglia. Neuron *91*, 328–340.

Yin, Z., Raj, D., Saiepour, N., Dam, D.V., Brouwer, N., Holtman, I.R., Eggen, B.J.L., Möller, T., Tamm, J.A., Abdourahman, A., et al. (2017). Immune hyperreactivity of Aβ plaque-associated microglia in Alzheimer's disease. Neurobiol. Aging *55*, 115–122.

Yoshino, Y., Yamazaki, K., Ozaki, Y., Sao, T., Yoshida, T., Mori, T., Mori, Y., Ochi, S., Iga, J.-I., and Ueno, S.-I. (2017). INPP5D mRNA Expression and Cognitive Decline in Japanese Alzheimer's Disease Subjects. J. Alzheimers Dis. *58*, 687–694.

Yu, L., Boyle, P.A., Nag, S., Leurgans, S., Buchman, A.S., Wilson, R.S., Arvanitakis, Z., Farfel, J.M., De Jager, P.L., Bennett, D.A., et al. (2015). APOE and Cerebral Amyloid Angiopathy in Community Dwelling Older Persons. Neurobiol. Aging *36*, 2946–2953.

Yuan, P., Condello, C., Keene, C.D., Wang, Y., Bird, T.D., Paul, S.M., Luo, W., Colonna, M., Baddeley, D., and Grutzendler, J. (2016). TREM2 Haplodeficiency in Mice and Humans Impairs the Microglia Barrier Function Leading to Decreased Amyloid Compaction and Severe Axonal Dystrophy. Neuron *90*, 724–739.

Zandl-Lang, M., Fanaee-Danesh, E., Sun, Y., Čančar, I., Gali, C.C., Kober, A., Albrecher, N.M., Tam-Amersdorfer, C., Stracke, A., Storck, S., et al. (2017). Regulatory effects of simvastatin and apoJ on APP processing and amyloid-β clearance in blood-brain barrier endothelial cells. Biochim. Biophys. Acta.

Zerbinatti, C.V., Wozniak, D.F., Cirrito, J., Cam, J.A., Osaka, H., Bales, K.R., Zhuo, M., Paul, S.M., Holtzman, D.M., and Bu, G. (2004). Increased soluble amyloid-β peptide and memory deficits in amyloid model mice overexpressing the low-density lipoprotein receptor-related protein. Proc. Natl. Acad. Sci. U. S. A. *101*, 1075–1080.

Zetterberg, H., and Mattsson, N. (2014). Understanding the cause of sporadic Alzheimer's disease. Expert Rev. Neurother. *14*, 621–630.

Zhang, B., Kirov, S., and Snoddy, J. (2005). WebGestalt: an integrated system for exploring gene sets in various biological contexts. Nucleic Acids Res. *33*, W741–W748.

Zhang, C., Wu, B., Beglopoulos, V., Wines-Samuelson, M., Zhang, D., Dragatsis, I., Südhof, T.C., and Shen, J. (2009). Presenilins are essential for regulating neurotransmitter release. Nature *460*, 632–636.

Zhang, G., Zhang, X., Wang, X., and Li, J.-P. (2014a). Towards Understanding the Roles of Heparan Sulfate Proteoglycans in Alzheimer's Disease. BioMed Res. Int. *2014*.

Zhang, X., Li, Y., Xu, H., and Zhang, Y. (2014b). The γ-secretase complex: from structure to function. Front. Cell. Neurosci. *8*.

Zhang, Z.-G., Li, Y., Ng, C.T., and Song, Y.-Q. (2015). Inflammation in Alzheimer's Disease and Molecular Genetics: Recent Update. Arch. Immunol. Ther. Exp. (Warsz.) *63*, 333–344.

Zhao, Y., and Lukiw, W.J. (2013). TREM2 signaling, miRNA-34a and the extinction of phagocytosis. Front. Cell. Neurosci. *7*.

Zhao, Y., and Lukiw, W.J. (2015). Microbiome-generated amyloid and potential impact on amyloidogenesis in Alzheimer's disease (AD). J. Nat. Sci. *1*.

Zhao, Y., Bhattacharjee, S., Jones, B.M., Dua, P., Alexandrov, P.N., Hill, J.M., and Lukiw, W.J. (2013). Regulation of TREM2 expression by an NF-κB-sensitive miRNA-34a. Neuroreport *24*, 318–323.

Zhao, Z., Ho, L., Wang, J., Qin, W., Festa, E.D., Mobbs, C., Hof, P., Rocher, A., Masur, S., Haroutunian, V., et al. (2005). Connective tissue growth factor (CTGF) expression in the brain is a downstream effector of insulin resistance- associated promotion of Alzheimer's disease β-amyloid neuropathology. FASEB J. *19*, 2081–2082.

Zheng, H., Liu, C.-C., Atagi, Y., Chen, X.-F., Jia, L., Yang, L., He, W., Zhang, X., Kang, S.S., Rosenberry, T.L., et al. (2016). Opposing roles of the triggering receptor expressed on myeloid cells 2 and triggering receptor expressed on myeloid cells-like transcript 2 in microglia activation. Neurobiol. Aging *42*, 132–141.

Zheng, H., Jia, L., Liu, C.-C., Rong, Z., Zhong, L., Yang, L., Chen, X.-F., Fryer, J.D., Wang, X., Zhang, Y., et al. (2017). TREM2 Promotes Microglial Survival by Activating Wnt/β-Catenin Pathway. J. Neurosci. *37*, 1772–1784.

Zhong, L., Chen, X.-F., Zhang, Z.-L., Wang, Z., Shi, X.-Z., Xu, K., Zhang, Y.-W., Xu, H., and Bu, G. (2015). DAP12 stabilizes the C-terminal fragment of the triggering receptor expressed on myeloid cells-2 (TREM2) and protects against LPS-induced pro-inflammatory response. J. Biol. Chem. jbc.M115.645986.

Zinser, E.G., Hartmann, T., and Grimm, M.O.W. (2007). Amyloid beta-protein and lipid metabolism. Biochim. Biophys. Acta BBA - Biomembr. *1768*, 1991–2001.

Zotova, E., Holmes, C., Johnston, D., Neal, J.W., Nicoll, J. a. R., and Boche, D. (2011). Microglial alterations in human Alzheimer's disease following Aβ42 immunization. Neuropathol. Appl. Neurobiol. *37*, 513–524.

WHO | Dementia.

Appendix

Appendix

a

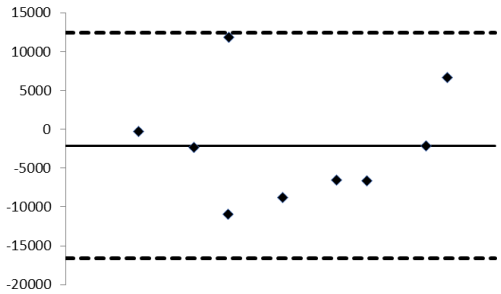

b

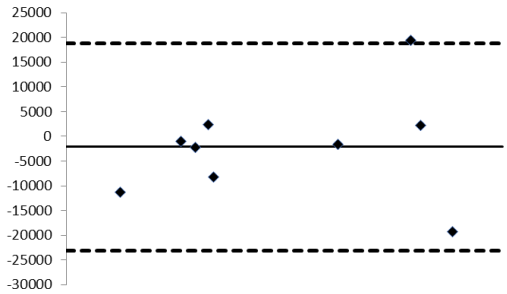

c

	10 squares	20 squares
R square	0.002	0.034
Regression significance (p value)	0.900	0.635

Appendix Table 1: Bland-altman plots to determine number of random squares to be analysed. (a) Plot for ten squares, (b) plot for twenty squares, (c) Statistics for both sets of results. A lower R square value and greater p value for regression signifies a more reliable method. Ten squares is a reliable method in this instance.

Case	Disease type	Code	Concentration (ng/µl)	A260/A280	A260/A230
1	TREM2 SAD	B11	102.4	1.99	2.10
2	TREM2 SAD	B7	36.3	2.00	1.93
3	TREM2 Control	B8	70.3	2.01	2.07
4	TREM2 Control	B10	65.0	2.02	2.07
5	TREM2 SAD	B9	87.0	2.28	2.10
6	TREM2 FAD	B12	89.3	1.97	1.60
7	SAD	C4	197.0	2.11	2.53
9	SAD	C5	91.8	1.99	1.91
10	SAD	C7	16.4	2.14	1.87
11	SAD	C9	114.5	1.98	1.85
12	SAD	C1	77.0	1.99	2.06
13	SAD	C6	91.0	2.01	2.17
14	SAD	C2	55.5	2.00	2.08
15	SAD	C8	46.9	2.07	2.17
17	SAD	C10	43.7	1.99	1.79
18	SAD	C3	48.5	2.00	1.92
26	FAD	D6	80.0	2.01	2.08
29	FAD	C11	173.0	2.13	2.67
30	FAD	D2	38.5	1.94	1.69
31	FAD	D1	15.1	2.15	1.89
32	FAD	C12	40.3	2.05	1.65
33	FAD	D5	66.0	2.00	1.68
34	FAD	D3	54.9	2.03	1.98
35	FAD	D4	46.5	1.97	1.60
37	Control	D7	85.0	2.03	2.26
38	Control	D9	74.0	2.01	1.85
39	Control	D8	71.9	2.03	2.23
40	Control	D12	52.3	2.04	0.57
41	Control	D10	51.5	1.99	2.17
42	Control	D11	75.6	1.99	1.37

Appendix Table 2: RNA concentration and spectrophotometer readings for Nanostring samples. Case number refers to the case in Table 2.3. Code refers to the well the sample was run on the Nanostring chip.

Official Symbol	Accession	Official Full Name
Human inflammation panel genes		
AGER	NM_001136.3	advanced glycosylation end product-specific receptor
ALOX12	NM_000697.1	arachidonate 12-lipoxygenase
ALOX15	NM_001140.3	arachidonate 15-lipoxygenase
ALOX5	NM_000698.2	arachidonate 5-lipoxygenase
AREG	NM_001657.2	amphiregulin
ARG1	NM_000045.2	arginase, liver
ATF2	NM_001880.2	activating transcription factor 2
BCL2L1	NM_138578.1	BCL2-like 1
BCL6	NM_001706.2	B-cell CLL/lymphoma 6
BIRC2	NM_001166.3	baculoviral IAP repeat containing 2
C1QA	NM_015991.2	complement component 1, q subcomponent, A chain
C1QB	NM_000491.3	complement component 1, q subcomponent, B chain
C1R	NM_001733.4	complement component 1, r subcomponent
C1S	NM_001734.2	complement component 1, s subcomponent
C2	NM_000063.3	complement component 2
C3	NM_000064.2	complement component 3
C3AR1	NM_004054.2	complement component 3a receptor 1
C4A	NM_007293.2	complement component 4A (Rodgers blood group)
C5	NM_001735.2	complement component 5
C6	NM_000065.2	complement component 6
C7	NM_000587.2	complement component 7
C8A	NM_000562.2	complement component 8, alpha polypeptide
C8B	NM_000066.2	complement component 8, beta polypeptide
C9	NM_001737.3	complement component 9
CCL11	NM_002986.2	chemokine (C-C motif) ligand 11
CCL13	NM_005408.2	chemokine (C-C motif) ligand 13
CCL16	NM_004590.2	chemokine (C-C motif) ligand 16
CCL17	NM_002987.2	chemokine (C-C motif) ligand 17
CCL19	NM_006274.2	chemokine (C-C motif) ligand 19
CCL2	NM_002982.3	chemokine (C-C motif) ligand 2
CCL20	NM_004591.1	chemokine (C-C motif) ligand 20
CCL21	NM_002989.2	chemokine (C-C motif) ligand 21
CCL22	NM_002990.3	chemokine (C-C motif) ligand 22
CCL23	NM_145898.1	chemokine (C-C motif) ligand 23
CCL24	NM_002991.2	chemokine (C-C motif) ligand 24
CCL3	NM_002983.2	chemokine (C-C motif) ligand 3
CCL4	NM_002984.2	chemokine (C-C motif) ligand 4
CCL5	NM_002985.2	chemokine (C-C motif) ligand 5
CCL7	NM_006273.2	chemokine (C-C motif) ligand 7
CCL8	NM_005623.2	chemokine (C-C motif) ligand 8
CCR1	NM_001295.2	chemokine (C-C motif) receptor 1
CCR2	NM_001123041.2	chemokine (C-C motif) receptor 2
CCR3	NM_001837.2	chemokine (C-C motif) receptor 3
CCR4	NM_005508.4	chemokine (C-C motif) receptor 4

Official Symbol	Accession	Official Full Name
CCR7	NM_001838.2	chemokine (C-C motif) receptor 7
CD163	NM_004244.4	CD163 molecule
CD4	NM_000616.3	CD4 molecule
CD40	NM_001250.4	CD40 molecule, TNF receptor superfamily member 5
CD40LG	NM_000074.2	CD40 ligand
CD55	NM_000574.3	CD55 molecule, decay accelerating factor for complement (Cromer blood group)
CD86	NM_175862.3	CD86 molecule
CDC42	NM_001039802.1	cell division cycle 42 (GTP binding protein, 25kDa)
CEBPB	NM_005194.2	CCAAT/enhancer binding protein (C/EBP), beta
CFB	NM_001710.5	complement factor B
CFD	NM_001928.2	complement factor D (adipsin)
CFL1	NM_005507.2	cofilin 1 (non-muscle)
CREB1	NM_134442.2	cAMP responsive element binding protein 1
CRP	NM_000567.2	C-reactive protein, pentraxin-related
CSF1	NM_000757.4	colony stimulating factor 1 (macrophage)
CSF2	NM_000758.2	colony stimulating factor 2 (granulocyte-macrophage)
CSF3	NM_000759.2	colony stimulating factor 3 (granulocyte)
CXCL1	NM_001511.1	chemokine (C-X-C motif) ligand 1 (melanoma growth stimulating activity, alpha)
CXCL10	NM_001565.1	chemokine (C-X-C motif) ligand 10
CXCL2	NM_002089.3	chemokine (C-X-C motif) ligand 2
CXCL3	NM_002090.2	chemokine (C-X-C motif) ligand 3
CXCL5	NM_002994.3	chemokine (C-X-C motif) ligand 5
CXCL6	NM_002993.3	chemokine (C-X-C motif) ligand 6 (granulocyte chemotactic protein 2)
CXCL9	NM_002416.1	chemokine (C-X-C motif) ligand 9
CXCR1	NM_000634.2	chemokine (C-X-C motif) receptor 1
CXCR2	NM_001557.2	chemokine (C-X-C motif) receptor 2
CXCR4	NM_003467.2	chemokine (C-X-C motif) receptor 4
CYSLTR1	NM_006639.2	cysteinyl leukotriene receptor 1
CYSLTR2	NM_020377.2	cysteinyl leukotriene receptor 2
DAXX	NM_001350.3	death-domain associated protein
DDIT3	NM_004083.4	DNA-damage-inducible transcript 3
DEFA1	NM_004084.2	defensin, alpha 1
ELK1	NM_005229.3	ELK1, member of ETS oncogene family
FASLG	NM_000639.1	Fas ligand (TNF superfamily, member 6)
FLT1	NM_002019.4	fms-related tyrosine kinase 1 (vascular endothelial growth factor/vascular permeability factor receptor)
FOS	NM_005252.2	FBJ murine osteosarcoma viral oncogene homolog
FXYD2	NM_021603.3	FXYD domain containing ion transport regulator 2
GNAQ	NM_002072.2	guanine nucleotide binding protein (G protein), q polypeptide
GNAS	NM_080425.1	GNAS complex locus

Official Symbol	Accession	Official Full Name
GNB1	NM_002074.3	guanine nucleotide binding protein (G protein), beta polypeptide 1
GNGT1	NM_021955.3	guanine nucleotide binding protein (G protein), gamma transducing activity polypeptide 1
GRB2	NM_203506.2	growth factor receptor-bound protein 2
HDAC4	NM_006037.3	histone deacetylase 4
HIF1A	NM_001530.2	hypoxia inducible factor 1, alpha subunit (basic helix-loop-helix transcription factor)
HLA-DRA	NM_019111.3	major histocompatibility complex, class II, DR alpha
HLA-DRB1	NM_002124.1	major histocompatibility complex, class II, DR beta 1
HMGB1	NM_002128.4	high mobility group box 1
HMGB2	NM_001130688.1	high mobility group box 2
HMGN1	NM_004965.6	high mobility group nucleosome binding domain 1
HRAS	NM_005343.2	v-Ha-ras Harvey rat sarcoma viral oncogene homolog
HSH2D	NM_032855.2	hematopoietic SH2 domain containing
HSPB1	NM_001540.3	heat shock 27kDa protein 1
HSPB2	NM_001541.3	heat shock 27kDa protein 2
IFI44	NM_006417.4	interferon-induced protein 44
IFIT1	NM_001548.3	interferon-induced protein with tetratricopeptide repeats 1
IFIT2	NM_001547.4	interferon-induced protein with tetratricopeptide repeats 2
IFIT3	NM_001031683.2	interferon-induced protein with tetratricopeptide repeats 3
IFNA1	NM_024013.1	interferon, alpha 1
IFNB1	NM_002176.2	interferon, beta 1, fibroblast
IFNG	NM_000619.2	interferon, gamma
IL10	NM_000572.2	interleukin 10
IL10RB	NM_000628.3	interleukin 10 receptor, beta
IL11	NM_000641.2	interleukin 11
IL12A	NM_000882.2	interleukin 12A (natural killer cell stimulatory factor 1, cytotoxic lymphocyte maturation factor 1, p35)
IL12B	NM_002187.2	interleukin 12B (natural killer cell stimulatory factor 2, cytotoxic lymphocyte maturation factor 2, p40)
IL13	NM_002188.2	interleukin 13
IL15	NM_000585.3	interleukin 15
IL17A	NM_002190.2	interleukin 17A
IL18	NM_001562.2	interleukin 18 (interferon-gamma-inducing factor)
IL18RAP	NM_003853.2	interleukin 18 receptor accessory protein
IL1A	NM_000575.3	interleukin 1, alpha
IL1B	NM_000576.2	interleukin 1, beta
IL1R1	NM_000877.2	interleukin 1 receptor, type I
IL1RAP	NM_002182.2	interleukin 1 receptor accessory protein
IL1RN	NM_173842.1	interleukin 1 receptor antagonist

Official Symbol	Accession	Official Full Name
IL2	NM_000586.2	interleukin 2
IL21	NM_021803.2	interleukin 21
IL22	NM_020525.4	interleukin 22
IL22RA2	NM_181309.1	interleukin 22 receptor, alpha 2
IL23A	NM_016584.2	interleukin 23, alpha subunit p19
IL23R	NM_144701.2	interleukin 23 receptor
IL3	NM_000588.3	interleukin 3 (colony-stimulating factor, multiple)
IL4	NM_000589.2	interleukin 4
IL5	NM_000879.2	interleukin 5 (colony-stimulating factor, eosinophil)
IL6	NM_000600.1	interleukin 6 (interferon, beta 2)
IL6R	NM_000565.2	interleukin 6 receptor
IL7	NM_000880.2	interleukin 7
IL8	NM_000584.2	interleukin 8
IL9	NM_000590.1	interleukin 9
IRF1	NM_002198.1	interferon regulatory factor 1
IRF3	NM_001571.5	interferon regulatory factor 3
IRF5	NM_002200.3	interferon regulatory factor 5
IRF7	NM_001572.3	interferon regulatory factor 7
ITGB2	NM_000211.2	integrin, beta 2 (complement component 3 receptor 3 and 4 subunit)
JUN	NM_002228.3	jun proto-oncogene
KEAP1	NM_012289.3	kelch-like ECH-associated protein 1
KNG1	NM_000893.2	kininogen 1
LIMK1	NM_002314.3	LIM domain kinase 1
LTA	NM_000595.2	lymphotoxin alpha (TNF superfamily, member 1)
LTB	NM_002341.1	lymphotoxin beta (TNF superfamily, member 3)
LTB4R	NM_181657.3	leukotriene B4 receptor
LTB4R2	NM_019839.4	leukotriene B4 receptor 2
LY96	NM_015364.2	lymphocyte antigen 96
MAFF	NM_001161572.1	v-maf musculoaponeurotic fibrosarcoma oncogene homolog F (avian)
MAFG	NM_002359.2	v-maf musculoaponeurotic fibrosarcoma oncogene homolog G (avian)
MAFK	NM_002360.3	v-maf musculoaponeurotic fibrosarcoma oncogene homolog K (avian)
MAP2K1	NM_002755.2	mitogen-activated protein kinase kinase 1
MAP2K4	NM_003010.2	mitogen-activated protein kinase kinase 4
MAP2K6	NM_002758.3	mitogen-activated protein kinase kinase 6
MAP3K1	NM_005921.1	mitogen-activated protein kinase kinase kinase 1, E3 ubiquitin protein ligase
MAP3K5	NM_005923.3	mitogen-activated protein kinase kinase kinase 5
MAP3K7	NM_145333.1	mitogen-activated protein kinase kinase kinase 7
MAP3K9	NM_033141.2	mitogen-activated protein kinase kinase kinase 9
MAPK1	NM_138957.2	mitogen-activated protein kinase 1
MAPK14	NM_001315.1	mitogen-activated protein kinase 14

Official Symbol	Accession	Official Full Name
MAPK3	NM_001040056.1	mitogen-activated protein kinase 3
MAPK8	NM_002750.2	mitogen-activated protein kinase 8
MAPKAPK2	NM_004759.3	mitogen-activated protein kinase-activated protein kinase 2
MAPKAPK5	NM_003668.2	mitogen-activated protein kinase-activated protein kinase 5
MASP1	NM_139125.3	mannan-binding lectin serine peptidase 1 (C4/C2 activating component of Ra-reactive factor)
MASP2	NM_139208.1	mannan-binding lectin serine peptidase 2
MAX	NM_002382.3	MYC associated factor X
MBL2	NM_000242.2	mannose-binding lectin (protein C) 2, soluble
MEF2A	NM_005587.2	myocyte enhancer factor 2A
MEF2BNB-MEF2B	NM_005919.2	MEF2BNB-MEF2B readthrough
MEF2C	NM_002397.3	myocyte enhancer factor 2C
MEF2D	NM_005920.2	myocyte enhancer factor 2D
MKNK1	NM_003684.3	MAP kinase interacting serine/threonine kinase 1
MMP3	NM_002422.3	matrix metallopeptidase 3 (stromelysin 1, progelatinase)
MMP9	NM_004994.2	matrix metallopeptidase 9 (gelatinase B, 92kDa gelatinase, 92kDa type IV collagenase)
MRC1	NM_002438.2	mannose receptor, C type 1
MX1	NM_002462.2	myxovirus (influenza virus) resistance 1, interferon-inducible protein p78 (mouse)
MX2	NM_002463.1	myxovirus (influenza virus) resistance 2 (mouse)
MYC	NM_002467.3	v-myc myelocytomatosis viral oncogene homolog (avian)
MYD88	NM_002468.3	myeloid differentiation primary response gene (88)
MYL2	NM_000432.3	myosin, light chain 2, regulatory, cardiac, slow
NFATC3	NM_004555.2	nuclear factor of activated T-cells, cytoplasmic, calcineurin-dependent 3
NFE2L2	NM_006164.3	nuclear factor (erythroid-derived 2)-like 2
NFKB1	NM_003998.2	nuclear factor of kappa light polypeptide gene enhancer in B-cells 1
NLRP3	NM_001079821.2	NLR family, pyrin domain containing 3
NOD1	NM_006092.1	nucleotide-binding oligomerization domain containing 1
NOD2	NM_022162.1	nucleotide-binding oligomerization domain containing 2
NOS2	NM_000625.4	nitric oxide synthase 2, inducible
NOX1	NM_007052.4	NADPH oxidase 1
NR3C1	NM_001018074.1	nuclear receptor subfamily 3, group C, member 1 (glucocorticoid receptor)
OAS2	NM_016817.2	2'-5'-oligoadenylate synthetase 2, 69/71kDa
OASL	NM_198213.1	2'-5'-oligoadenylate synthetase-like

Official Symbol	Accession	Official Full Name
OXER1	NM_148962.3	oxoeicosanoid (OXE) receptor 1
PDGFA	NM_002607.5	platelet-derived growth factor alpha polypeptide
PIK3C2G	NM_004570.4	phosphatidylinositol-4-phosphate 3-kinase, catalytic subunit type 2 gamma
PLA2G4A	NM_024420.2	phospholipase A2, group IVA (cytosolic, calcium-dependent)
PLCB1	NM_182734.1	phospholipase C, beta 1 (phosphoinositide-specific)
PPP1R12B	NM_002481.3	protein phosphatase 1, regulatory subunit 12B
PRKCA	NM_002737.2	protein kinase C, alpha
PRKCB	NM_212535.1	protein kinase C, beta
PTGDR2	NM_004778.1	prostaglandin D2 receptor 2
PTGER1	NM_000955.2	prostaglandin E receptor 1 (subtype EP1), 42kDa
PTGER2	NM_000956.2	prostaglandin E receptor 2 (subtype EP2), 53kDa
PTGER3	NM_000957.2	prostaglandin E receptor 3 (subtype EP3)
PTGER4	NM_000958.2	prostaglandin E receptor 4 (subtype EP4)
PTGFR	NM_000959.3	prostaglandin F receptor (FP)
PTGIR	NM_000960.3	prostaglandin I2 (prostacyclin) receptor (IP)
PTGS1	NM_000962.2	prostaglandin-endoperoxide synthase 1 (prostaglandin G/H synthase and cyclooxygenase)
PTGS2	NM_000963.1	prostaglandin-endoperoxide synthase 2 (prostaglandin G/H synthase and cyclooxygenase)
PTK2	NM_005607.3	PTK2 protein tyrosine kinase 2
RAC1	NM_198829.1	ras-related C3 botulinum toxin substrate 1 (rho family, small GTP binding protein Rac1)
RAF1	NM_002880.2	v-raf-1 murine leukemia viral oncogene homolog 1
RAPGEF2	NM_014247.2	Rap guanine nucleotide exchange factor (GEF) 2
RELA	NM_021975.2	v-rel reticuloendotheliosis viral oncogene homolog A (avian)
RELB	NM_006509.2	v-rel reticuloendotheliosis viral oncogene homolog B
RHOA	NM_001664.2	ras homolog family member A
RIPK1	NM_003804.3	receptor (TNFRSF)-interacting serine-threonine kinase 1
RIPK2	NM_003821.5	receptor-interacting serine-threonine kinase 2
ROCK2	NM_004850.3	Rho-associated, coiled-coil containing protein kinase 2
RPS6KA5	NM_004755.2	ribosomal protein S6 kinase, 90kDa, polypeptide 5
SHC1	NM_001130040.1	SHC (Src homology 2 domain containing) transforming protein 1
SMAD7	NM_005904.2	SMAD family member 7
STAT1	NM_007315.2	signal transducer and activator of transcription 1, 91kDa
STAT2	NM_005419.2	signal transducer and activator of transcription 2, 113kDa
STAT3	NM_139276.2	signal transducer and activator of transcription 3 (acute-phase response factor)

Official Symbol	Accession	Official Full Name
TBXA2R	NM_001060.3	thromboxane A2 receptor
TCF4	NM_003199.1	transcription factor 4
TGFB1	NM_000660.3	transforming growth factor, beta 1
TGFB2	NM_003238.2	transforming growth factor, beta 2
TGFB3	NM_003239.2	transforming growth factor, beta 3
TGFBR1	NM_004612.2	transforming growth factor, beta receptor 1
TLR1	NM_003263.3	toll-like receptor 1
TLR2	NM_003264.3	toll-like receptor 2
TLR3	NM_003265.2	toll-like receptor 3
TLR4	NM_138554.2	toll-like receptor 4
TLR5	NM_003268.3	toll-like receptor 5
TLR6	NM_006068.2	toll-like receptor 6
TLR7	NM_016562.3	toll-like receptor 7
TLR8	NM_016610.2	toll-like receptor 8
TLR9	NM_017442.2	toll-like receptor 9
TNF	NM_000594.2	tumor necrosis factor
TNFAIP3	NM_006290.2	tumor necrosis factor, alpha-induced protein 3
TNFSF14	NM_003807.2	tumor necrosis factor (ligand) superfamily, member 14
TOLLIP	NM_019009.2	toll interacting protein
TRADD	NM_003789.2	TNFRSF1A-associated via death domain
TRAF2	NM_021138.3	TNF receptor-associated factor 2
TREM2	NM_018965.3	triggering receptor expressed on myeloid cells 2
TSLP	NM_033035.4	thymic stromal lymphopoietin
TWIST2	NM_057179.2	twist homolog 2 (Drosophila)
TYROBP	NM_003332.3	TYRO protein tyrosine kinase binding protein
Genes added to panel - neurodegeneration related		
ABCA7	NM_033308.1	ATP-binding cassette sub-family A member 7
ADAM10	NM_001110.2	Disintegrin and metalloprotease domain-containing protein 10
AIF1 (Iba1)	NM_032955.1	Allograft inflammatory factor 1
APH1A	NM_001077628.1	Gamma-secretase subunit APH1A
APH1B	NM_001145646.1	Gamma-secretase subunit APH1B
APOE	NM_000041.2	apolipoprotein e
APP	NM_000484.3	Amyloid beta A4 protein
BACE1	NM_012104.3	Beta-secretase 1
CD33	NM_001177608.1	Myeloid cell surface antigen CD33
CD68	NM_001251.2	Macrosialin
CLU	NM_203339.2	Clusterin
CoQ10A	NM_001099337.1	Coenzyme Q-binding protein COQ10 homolog A, mitochondrial
CoQ2	NM_015697.7	4-hydroxybenzoate polyprenyltransferase, mitochondrial
CR1	XM_006711166.2	Complement receptor type 1
CTSD	NM_001909.3	Cathepsin D

Official Symbol	Accession	Official Full Name
FCGR1A (CD64)	NM_000566.3	High affinity immunoglobulin gamma Fc receptor 1
GFAP	NM_002055.4	Glial fibrillary acidic protein
IL4RA	NM_000418.3	Interleukin-4 receptor subunit alpha
KLK6	NM_002774.3	Kallikrein 6
MAPT	NM_016834.3	Microtubule-associated protein tau
MRC1	NM_002438.2	Macrophage mannose receptor 1
NeuN	NM_001082575.1	Neuronal nuclei
P2RX7	NR_033948.1	P2X purinoreceptor 7
PEN2	NM_172341.1	Gamma-secretase subunit PEN2
PSEN1	NM_000021.2	Presenilin 1
PSEN2	NM_000447.2	Presenilin 2
SNCA	NM_000345.2	Alpha-synuclein
SOCS3	NM_003955.3	Suppressor of cytokine signalling 3
TREM1	NM_001242589.1	Triggering receptor expressed on myeloid cells 1
TSPO	NM_000714.4	Translocator protein
Housekeeping genes		
CLTC	NM_004859.2	clathrin, heavy chain (Hc)
GAPDH	NM_002046.3	glyceraldehyde-3-phosphate dehydrogenase
GUSB	NM_000181.1	glucuronidase, beta
HPRT1	NM_000194.1	hypoxanthine phosphoribosyltransferase 1
PGK1	NM_000291.2	phosphoglycerate kinase 1
TUBB	NM_178014.2	tubulin, beta class I

Appendix Table 3: List of genes used for nanostring analysis. Genes included those from the Human Inflammation Panel designed by Nanostring, thirty custom added genes related to neurodegeneration and housekeeping genes.

Gene Name	Control	SAD	FAD	TREM2 SAD	TREM2 FAD	TREM2 Control	Control vs. SAD	P value of: Control vs. SAD	Control vs. FAD	P value of: Control vs. FAD	Control vs. TREM2 SAD	P value of: Control vs. TREM2 SAD	Control vs. TREM2 FAD	P value of: Control vs. TREM2 FAD	Control vs. TREM2 Control	P value of: Control vs. TREM2 Control
ABCA7	189.93	339	295.49	514.01	544.82	185.53	1.78	0.0192	1.56	0.1027	2.13	0.0025	2.26	0.0445	1.3	0.1294
ADAM10	542.12	771.98	716.58	1202.38	1024.62	868.18	1.42	0.0005	1.32	0.0056	1.75	0.1099	1.49	0.1435	1.26	0.6066
AGER	32.33	55.04	48.03	59.43	61.85	36.98	1.7	0.0069	1.49	0.1083	1.45	0.5129	1.51	0.0921	1.11	0.5086
AIF1	348.37	348.14	336.66	626.95	346.67	227.97	1	0.998	1.03	0.9263	1.42	0.6199	1.27	0.5759	1.94	0.2813
ALOX12	1.92	1.87	2.23	5.12	2.17	1.02	1.03	0.9416	1.16	0.7664	2.32	0.1278	1.02	0.9661	2.16	0.0736
ALOX15	10.95	18.72	12.58	14.28	60.18	11.46	1.71	0.1023	1.15	0.8244	1.03	0.9732	4.33	0.0164	1.21	0.3934
ALOX5	236.47	276.99	318.59	600.57	415.34	181.05	1.17	0.5549	1.35	0.5011	2	0.3104	1.39	0.4007	1.66	0.1127
APH1A	596.43	835.95	799.1	1413.32	1025.48	920.34	1.4	0.01	1.34	0.066	1.87	0.1142	1.36	0.2915	1.22	0.4322
APH1B	266.5	305.36	246.13	433.39	345.91	425.32	1.15	0.1935	1.08	0.5177	1.28	0.2774	1.02	0.7793	1.26	0.3929
APOE	4204.16	7235.88	6240.44	13205.84	8258.37	3936.9	1.72	0.005	1.48	0.0782	2.48	0.1485	1.55	0.4009	1.35	0.474
APP	19720.44	21666.61	19213.21	24370.35	28842.07	30319.48	1.1	0.3207	1.03	0.8085	1.03	0.7956	1.15	0.2358	1.21	0.0902
AREG	4.1	2.35	7.88	4.63	2.71	2.36	1.75	0.4678	1.92	0.5373	1.04	0.9646	1.78	0.6559	2.05	0.5572
ARG1	9.65	4.4	13.82	6.58	34.44	8.62	2.19	0.1824	1.43	0.6891	1.86	0.4512	2.82	0.1183	1.42	0.4718
ATF2	1116.59	1153.73	1099.9	1125.54	1520.18	1614.9	1.03	0.7718	1.02	0.8978	1.26	0.4113	1.07	0.7192	1.14	0.2828
BACE1	1099.77	1174.42	983.79	1331.6	1455.45	2598.8	1.07	0.6464	1.12	0.4465	1.05	0.7287	1.04	0.721	1.86	0.3069
BCL2L1	1658.7	2676.48	2296.48	5015.73	4073.34	1783.33	1.61	0.0056	1.38	0.1581	2.38	0.0571	1.94	0.241	1.18	0.1249
BCL6	1353.36	2509.78	3416.49	5203.26	4839.84	1383.9	1.85	0.0226	2.52	0.0096	3.03	0.0586	2.82	0.1636	1.24	0.2306
BIRC2	789.2	945.78	1005.13	1425.74	1351.84	1168.33	1.2	0.0201	1.27	0.0046	1.42	0.0893	1.35	0.0893	1.17	0.4984
C1QA	105.59	106.43	145.68	310.15	167.96	50.2	1.01	0.983	1.38	0.4419	2.32	0.3636	1.25	0.7495	2.67	0.0205
C1QB	748.58	789.38	1172.66	2062.52	1034.21	371.18	1.05	0.906	1.57	0.3376	2.17	0.4104	1.09	0.9041	2.56	0.0512
C1R	406.1	511.04	1138.83	1023.44	1190	293.19	1.26	0.5056	2.8	0.0562	1.99	0.5245	2.31	0.1562	1.76	0.14
C1S	413.57	444.09	794.42	760.66	839.81	367.84	1.07	0.7885	1.92	0.1592	1.45	0.5981	1.6	0.271	1.43	0.1552
C2	63.45	77.28	125.6	77.62	130.36	50.82	1.22	0.3381	1.98	0.1153	1.04	0.9682	1.62	0.1317	1.58	0.4989
C3	716.86	972.89	1014.54	1799	1070.01	558.18	1.36	0.3783	1.42	0.2854	1.98	0.3013	1.18	0.7915	1.63	0.5514

Gene Name	Control	SAD	FAD	TREM2 SAD	TREM2 FAD	TREM2 Control	Control vs. SAD	P value of: Control vs. SAD	Control vs. FAD	P value of: Control vs. FAD	Control vs. TREM2 SAD	P value of: Control vs. TREM2 SAD	Control vs. TREM2 FAD	P value of: Control vs. TREM2 FAD	Control vs. TREM2 Control	P value of: Control vs. TREM2 Control
C3AR1	153.39	266.66	259.66	607.88	343.02	116.95	1.74	0.0472	1.69	0.1762	3.13	0.1546	1.76	0.5333	1.66	0.2103
C4A	712.84	1757.19	1654.96	2412.3	2113.42	1166.48	2.47	0.0358	2.32	0.0477	2.67	0.3483	2.34	0.0427	1.29	0.7702
C5	54.58	90.38	86.29	86.63	96.43	134.17	1.66	0.0127	1.58	0.0185	1.25	0.2648	1.39	0.0381	1.94	0.2034
C6	1.05	1.45	1.89	2.87	2.17	2.3	1.38	0.0172	1.81	0.0275	2.46	0.1134	1.86	0.1589	1.97	0.5642
C7	52.27	39.96	116.81	97.51	182.51	41.45	1.31	0.6253	2.23	0.3264	1.47	0.6	2.75	0.0579	1.6	0.382
C8A	1.05	1.68	1.45	2.87	2.17	1.03	1.6	0.0008	1.38	0.1317	2.46	0.1134	1.86	0.1589	1.13	0.1838
C8B	1.05	1.84	1.67	2.87	2.17	1.05	1.76	0.0042	1.6	0.0508	2.46	0.1134	1.86	0.1589	1.11	0.2419
C9	1.28	1.63	1.61	2.87	2.17	1.03	1.28	0.2987	1.26	0.4321	1.98	0.1751	1.5	0.2516	1.4	0.1975
CCL11	1.05	1.49	1.67	2.87	2.17	1.03	1.42	0.0128	1.6	0.0508	2.46	0.1134	1.86	0.1589	1.13	0.1838
CCL13	1.05	1.58	1.67	2.87	2.17	1.03	1.51	0.0046	1.6	0.0508	2.46	0.1134	1.86	0.1589	1.13	0.1838
CCL16	1.34	1.97	2.43	2.87	2.17	1.05	1.48	0.2153	1.82	0.1812	1.97	0.1905	1.49	0.2991	1.39	0.2997
CCL17	1.05	1.58	1.4	2.87	2.17	1.03	1.51	0.0033	1.34	0.0802	2.46	0.1134	1.86	0.1589	1.13	0.1838
CCL19	15.74	19.71	41.72	6.81	38.07	14.26	1.25	0.7079	2.65	0.1484	2.93	0.0915	1.91	0.3792	1.4	0.5034
CCL2	58.82	207.92	283.3	551.32	495.88	73.22	3.53	0.0478	4.82	0.0288	7.39	0.139	6.65	0.294	1.02	0.9866
CCL20	1.05	1.87	3.98	2.87	2.17	1.42	1.79	0.004	3.81	0.0556	2.46	0.1134	1.86	0.1589	1.21	0.6188
CCL21	1.05	1.48	1.9	2.87	2.17	1.03	1.42	0.0166	1.82	0.0373	2.46	0.1134	1.86	0.1589	1.13	0.1838
CCL22	1.05	1.97	1.88	2.02	2.17	2.72	1.89	0.0121	1.8	0.069	1.74	0.3767	1.87	0.1557	2.35	0.5505
CCL23	1.05	1.69	1.99	2.87	2.17	1	1.61	0.0008	1.9	0.0399	2.52	0.1077	1.91	0.1486	1.14	0.1764
CCL24	2.96	2.69	1.86	5.48	2.32	3.4	1.1	0.8118	1.59	0.3212	1.52	0.696	1.56	0.6581	1.06	0.8974
CCL3	7.68	12.17	23.39	9.02	7.95	12.5	1.59	0.5134	3.05	0.1404	1.08	0.9547	1.22	0.9161	1.28	0.8978
CCL4	35.08	26.76	42.25	18.42	27.29	34.92	1.31	0.4945	1.2	0.6867	2.41	0.2782	1.63	0.2279	1.27	0.8676
CCL5	4.09	13.38	15.13	15.58	13.15	3.7	3.27	0.0839	3.7	0.1087	3.12	0.3542	2.64	0.1405	1.35	0.8535
CCL7	1.05	1.68	1.15	2.87	2.17	1.03	1.6	0.0008	1.1	0.2407	2.52	0.1077	1.91	0.1486	1.1	0.3044
CCL8	1.05	1.48	2.19	2.87	2.17	1.02	1.41	0.0133	2.09	0.0474	2.46	0.1134	1.86	0.1589	1.14	0.158

Gene Name	Control	SAD	FAD	TREM2 SAD	TREM2 FAD	TREM2 Control	Control vs. SAD	P value of: Control vs. SAD	Control vs. FAD	P value of: Control vs. FAD	Control vs. TREM2 SAD	P value of: Control vs. TREM2 SAD	Control vs. TREM2 FAD	P value of: Control vs. TREM2 FAD	Control vs. TREM2 Control	P value of: Control vs. TREM2 Control
CCR1	43.13	46.37	48.69	51.65	57.27	32.65	1.08	0.8657	1.13	0.7964	1.06	0.9722	1.05	0.9028	1.68	0.2035
CCR2	1.76	3.44	7.1	9.32	3.36	1.05	1.95	0.1848	4.03	0.0775	4.7	0.334	1.7	0.7181	1.89	0.1783
CCR3	1.04	1.78	1.67	2.87	2.17	1.03	1.7	0.0006	1.6	0.0495	2.57	0.1042	1.94	0.1462	1.09	0.3632
CCR4	1.8	2.44	2.19	3.04	1.41	1.49	1.35	0.3743	1.22	0.6009	1.39	0.4833	1.56	0.2657	1.47	0.4586
CCR7	1.1	1.87	2.08	2.87	2.17	1.03	1.7	0.0075	1.89	0.0495	2.34	0.1214	1.77	0.157	1.19	0.1568
CD163	74.64	78.36	218.76	439.06	223.43	37.01	1.05	0.9361	2.93	0.2305	4.64	0.2064	2.36	0.1774	2.56	0.1935
CD33	11.76	8.82	14.44	36.69	23.76	9.52	1.33	0.5264	1.23	0.7445	2.46	0.2659	1.59	0.2405	1.57	0.4956
CD4	33.49	39.95	56.24	91.07	73.61	35.11	1.19	0.4322	1.68	0.0815	2.14	0.3103	1.73	0.2748	1.21	0.354
CD40	49.57	76.48	100.55	117.85	139.93	61.01	1.54	0.0874	2.03	0.0194	1.87	0.0967	2.23	0.1185	1.03	0.9039
CD40LG	1.05	1.86	1.67	2.87	2.17	1.03	1.78	0.0015	1.6	0.0508	2.46	0.1134	1.86	0.1589	1.13	0.1838
CD55	126.25	202.5	160.57	312.41	246.62	216.33	1.6	0.0069	1.27	0.0797	1.95	0.0425	1.54	0.3662	1.35	0.5244
CD68	136.77	186.57	260.15	359.63	235.09	141.99	1.36	0.1972	1.9	0.0182	2.07	0.2528	1.36	0.4495	1.22	0.6176
CD86	13.58	17.67	17.77	40.19	15.33	16.14	1.3	0.5631	1.31	0.6308	2.33	0.2501	1.12	0.7903	1.07	0.9038
CDC42	4203.45	4127.74	3787.4	5975.39	5251.03	5143.92	1.02	0.6867	1.11	0.1824	1.12	0.4594	1.02	0.8875	1.04	0.8088
CEBPB	854.34	1030.38	1938.02	2382.35	2426.32	787.34	1.21	0.4064	2.27	0.0122	2.2	0.063	2.24	0.2165	1.38	0.1329
CFB	87.38	102.3	246.31	244.4	224.68	57.25	1.17	0.577	2.82	0.0593	2.21	0.425	2.03	0.2867	1.94	0.1524
CFD	28.41	34.63	26.94	53.79	37.03	12.44	1.22	0.5726	1.05	0.9237	1.49	0.2623	1.03	0.9384	2.9	0.2759
CFL1	13002.54	13345.57	11922.26	16790.01	17202.29	15854.6	1.03	0.6196	1.09	0.1983	1.02	0.801	1.04	0.4943	1.04	0.3303
CLU	53696.47	75322.2	93128.3	92165.85	115303.41	62745.54	1.4	0.005	1.73	0.0108	1.35	0.4592	1.69	0.0773	1.09	0.481
CR1	48.96	59.96	59.56	41.53	75.77	72.72	1.22	0.5747	1.22	0.7626	1.49	0.6892	1.22	0.7176	1.17	0.9214
CREB1	704.62	975.75	973.98	1400.21	1407.96	925.92	1.38	0.0072	1.38	0.0236	1.57	0.0283	1.58	0.1129	1.04	0.8296
CRP	1.1	1.72	1.67	2.87	4.38	1.03	1.57	0.0298	1.53	0.0732	2.31	0.1244	3.53	0.5261	1.21	0.1382
CSF1	113.66	267.15	326.38	532.54	538.01	182.88	2.35	0.0053	2.87	0.0123	3.69	0.0986	3.73	0.2682	1.27	0.7553
CSF2	3.29	3.42	2.86	10.21	5.05	2.1	1.04	0.9059	1.15	0.7467	2.45	0.3212	1.21	0.8841	1.98	0.5016

Gene Name	Control	SAD	FAD	TREM2 SAD	TREM2 FAD	TREM2 Control	Control vs. SAD	P value of: Control vs. SAD	Control vs. FAD	P value of: Control vs. FAD	Control vs. TREM2 SAD	P value of: Control vs. TREM2 SAD	Control vs. TREM2 FAD	P value of: Control vs. TREM2 FAD	Control vs. TREM2 Control	P value of: Control vs. TREM2 Control
CSF3	8.89	3.98	6.12	5.63	6.7	2.87	2.24	0.3354	1.45	0.6834	1.86	0.5241	1.56	0.6643	3.64	0.3984
CTSD	3343.76	5158.64	4878.47	9326.44	7262.01	4896.18	1.54	0.0005	1.46	0.0662	2.2	0.1044	1.71	0.2071	1.15	0.4393
CXCL1	81.55	68.15	128.66	339.35	286.72	42.59	1.2	0.7542	1.58	0.4398	3.28	0.1991	2.77	0.4375	2.43	0.6162
CXCL10	6.05	8.32	6.8	25.32	2.17	3.81	1.37	0.5767	1.12	0.8779	3.43	0.6633	3.4	0.0564	1.94	0.3056
CXCL2	107.7	94.39	214.46	188.37	217.71	112.9	1.14	0.7287	1.99	0.2412	1.38	0.6195	1.59	0.5189	1.21	0.5589
CXCL3	16.16	13.1	39.01	22.86	29.46	16.07	1.23	0.5468	2.41	0.1751	1.12	0.8746	1.44	0.3303	1.28	0.6118
CXCL5	29.06	32.03	36.33	29.94	42.23	46.45	1.1	0.6561	1.25	0.4118	1.23	0.7725	1.15	0.5214	1.26	0.3159
CXCL6	3.27	8.75	13.81	4.08	22.8	10.52	2.68	0.0957	4.23	0.0607	1.06	0.9469	5.92	0.1435	2.73	0.0863
CXCL9	1.64	2.65	1.87	8.84	1.84	1.03	1.61	0.1819	1.14	0.6906	4.59	0.3236	1.05	0.9277	1.87	0.0618
CXCR1	18.63	35.58	44.28	35.58	31.05	27.24	1.91	0.0839	2.38	0.0714	1.51	0.5845	1.31	0.4756	1.15	0.8192
CXCR2	5.62	26.4	51.8	42.82	62.79	9.77	4.7	0.0692	9.22	0.015	6.11	0.0345	8.96	0.0178	1.39	0.6469
CXCR4	164.43	376.94	431.2	614.82	609.55	253.33	2.29	0.0307	2.62	0.0442	2.95	0.1929	2.92	0.1021	1.21	0.6167
CYSLTR1	24.2	21.6	31.26	32.06	24.8	20.74	1.12	0.6836	1.29	0.4895	1.04	0.8895	1.24	0.821	1.48	0.3277
CYSLTR2	85.33	137.58	140.73	168.81	194.41	102.66	1.61	0.0021	1.65	0.0269	1.56	0.1683	1.8	0.0252	1.05	0.4956
CoQ10A	315.26	443.62	405.09	571.8	554.24	419.13	1.41	0.0001	1.28	0.1518	1.43	0.2045	1.39	0.0945	1.05	0.6106
CoQ2	69.25	89.13	95.22	151.99	113.75	92.27	1.29	0.0434	1.37	0.0078	1.73	0.1125	1.3	0.0103	1.05	0.7976
DAXX	487.43	789.39	784.93	1313.04	1162.47	643.93	1.62	0.0008	1.61	0.0205	2.12	0.0659	1.88	0.1113	1.04	0.6765
DDIT3	624.74	827.21	1286.11	1400.05	1340.22	925.31	1.32	0.017	2.06	0.0085	1.77	0.1445	1.69	0.1984	1.17	0.4491
DEFA1	31	20.16	25.64	19.22	31.02	4.76	1.54	0.7245	1.21	0.8982	2.05	0.58	1.27	0.8928	8.25	0.3619
ELK1	520.65	1030.47	924.02	1437.08	1931.48	401.3	1.98	0.0128	1.77	0.11	2.18	0.1581	2.93	0.046	1.65	0.1541
FASLG	1.05	1.78	2.11	2.87	2.17	1.03	1.7	0.0012	2.01	0.0582	2.46	0.1134	1.86	0.1589	1.13	0.1838
FCGR1A	181.16	142.44	168.42	185.96	163.49	100.07	1.27	0.5295	1.08	0.8407	1.24	0.8533	1.41	0.539	2.3	0.0282
FLT1	1108.17	1523.2	2276.55	3217.89	4069.62	698.84	1.37	0.3004	2.05	0.0555	2.29	0.3306	2.9	0.0276	2.01	0.3637
FOS	657.25	800.52	2080.39	1721.16	1568.64	1134.3	1.22	0.4949	3.17	0.0536	2.07	0.4656	1.88	0.1112	1.36	0.6754

Gene Name	Control	SAD	FAD	TREM2 SAD	TREM2 FAD	TREM2 Control	Control vs. SAD	P value of: Control vs. SAD	Control vs. FAD	P value of: Control vs. FAD	Control vs. TREM2 SAD	P value of: Control vs. TREM2 SAD	Control vs. TREM2 FAD	P value of: Control vs. TREM2 FAD	Control vs. TREM2 Control	P value of: Control vs. TREM2 Control
FXYD2	38.62	63.43	54.88	78.88	97.84	43.87	1.64	0.0056	1.42	0.3406	1.61	0.0235	2	0.127	1.12	0.7472
GFAP	30455.98	60563.46	71161.77	90586.38	76572.51	50251.64	1.99	0.0132	2.34	0.0119	2.35	0.278	1.98	0.0137	1.3	0.7109
GNAQ	3078.45	3992.3	3835.19	5342.89	5985.81	3545.13	1.3	0.0008	1.25	0.1858	1.37	0.3304	1.53	0.0824	1.1	0.2984
GNAS	3912.56	4359.78	4583.61	5864.88	6337.23	6329.91	1.11	0.3164	1.17	0.2251	1.18	0.5337	1.28	0.0391	1.28	0.3393
GNB1	8717.4	9280.99	9169.2	12328.92	12906.74	11887.72	1.06	0.4605	1.05	0.6722	1.12	0.6436	1.17	0.0777	1.08	0.4608
GNGT1	1.05	1.69	1.68	2.87	2.17	1.03	1.61	0.0008	1.6	0.0509	2.46	0.1134	1.86	0.1589	1.13	0.1838
GRB2	40.53	39.53	37.37	74.26	65.37	66.03	1.03	0.8939	1.08	0.6831	1.44	0.0104	1.27	0.0667	1.28	0.048
HDAC4	673.22	1050.65	1080.62	1721.3	1929.93	807.77	1.56	0.0095	1.61	0.0541	2.02	0.0904	2.26	0.0009	1.06	0.6122
HIF1A	2411.9	3204.34	3168.81	4454.22	5439.5	2875.07	1.33	0.0421	1.31	0.0927	1.46	0.2662	1.78	0.294	1.06	0.5323
HLA-DRA	1195.25	1360.24	1520	3029.41	1087.53	967.91	1.14	0.6709	1.27	0.4921	2	0.4402	1.39	0.6306	1.57	0.5227
HLA-DRB1	795.06	879.45	1124.32	2034.53	1315.1	689.59	1.11	0.8442	1.41	0.5341	2.02	0.5471	1.3	0.767	1.46	0.6674
HMGB1	1630.3	1972.64	1884.15	2981.86	2244.16	2659.49	1.21	0.0131	1.16	0.0429	1.44	0.0755	1.09	0.6604	1.29	0.2377
HMGB2	252.9	303.95	366.11	497.3	454.36	235.6	1.2	0.2272	1.45	0.1448	1.55	0.1808	1.42	0.3751	1.36	0.1357
HMGN1	1287.33	1785.18	1817.02	2875.47	2036.18	1538.52	1.39	0.0165	1.41	0.0558	1.76	0.1071	1.25	0.4149	1.06	0.8835
HRAS	342.09	357.9	391.14	456.44	552.07	354.54	1.05	0.6525	1.14	0.4441	1.05	0.8465	1.27	0.5016	1.22	0.1562
HSH2D	2.1	1.88	1.39	4.97	2.17	1.03	1.12	0.8698	1.51	0.5606	2.02	0.476	1.13	0.8628	2.39	0.2431
HSPB1	505.19	1351.6	2898.42	2748.11	3749.8	429.84	2.68	0.0044	5.74	0.0041	4.29	0.0657	5.85	0.1633	1.49	0.323
HSPB2	279.12	700.42	751.62	1208.11	1322.87	396.28	2.51	0.0008	2.69	0.009	3.41	0.0618	3.74	0.211	1.12	0.5513
IFI44	83.11	125.73	144.56	315.65	170.15	127.24	1.51	0.0365	1.74	0.0537	3	0.3398	1.61	0.5148	1.21	0.6913
IFIT1	779.35	1000.62	793.78	2492.58	1465.2	1210.94	1.28	0.1135	1.02	0.9052	2.52	0.2199	1.48	0.0159	1.23	0.4101
IFIT2	162.14	217.21	153.53	632.42	378.38	172.06	1.34	0.1888	1.06	0.8226	3.08	0.3362	1.84	0.1835	1.2	0.8237
IFIT3	84.22	114.83	77.56	388.03	131.45	125.82	1.36	0.022	1.09	0.6058	3.63	0.3115	1.23	0.0197	1.18	0.567
IFNA1	2.2	2.57	2.36	2.87	1.84	11.32	1.16	0.7217	1.07	0.8923	1.08	0.879	1.44	0.5127	4.26	0.0243
IFNB1	1.05	1.68	1.67	2.87	2.17	1.03	1.6	0.0008	1.6	0.0508	2.46	0.1134	1.86	0.1589	1.13	0.1838

Gene Name	Control	SAD	FAD	TREM2 SAD	TREM2 FAD	TREM2 Control	Control vs. SAD	P value of: Control vs. SAD	Control vs. FAD	P value of: Control vs. FAD	Control vs. TREM2 SAD	P value of: Control vs. TREM2 SAD	Control vs. TREM2 FAD	P value of: Control vs. TREM2 FAD	Control vs. TREM2 Control	P value of: Control vs. TREM2 Control
IFNG	1.05	1.68	1.8	2.87	2.17	1.03	1.6	0.0008	1.72	0.0289	2.46	0.1134	1.86	0.1589	1.13	0.1838
IL10	1.29	2.36	3.93	3.41	2.17	1.03	1.83	0.0225	3.05	0.0387	2.26	0.0355	1.44	0.2666	1.47	0.0393
IL10RB	218.44	262.08	296.53	463.5	334.33	249.32	1.2	0.3631	1.36	0.1931	1.67	0.088	1.21	0.4788	1.11	0.7903
IL11	4.83	4.81	3.69	2.87	8.8	3.4	1	0.9926	1.31	0.6342	2.13	0.1487	1.44	0.4195	1.8	0.159
IL12A	10.78	12.72	29.3	10.37	18.6	32.13	1.18	0.6408	2.72	0.0176	1.32	0.803	1.36	0.3856	2.35	0.1911
IL12B	1.04	1.61	1.61	2.02	2.17	2.16	1.55	0.0065	1.54	0.0784	1.81	0.3515	1.94	0.1462	1.94	0.5242
IL13	1.05	1.58	1.67	2.87	2.17	1.03	1.51	0.0046	1.6	0.0508	2.46	0.1134	1.86	0.1589	1.13	0.1838
IL15	10.64	17.97	17.82	44.08	27.43	14.56	1.69	0.0373	1.67	0.0892	3.27	0.2802	2.03	0.3459	1.08	0.6808
IL17A	1.1	1.77	1.67	2.87	2.17	3.03	1.61	0.0007	1.52	0.0748	2.4	0.1147	1.81	0.1448	2.53	0.5389
IL18	133.78	225.98	293.5	535.67	354.49	146.54	1.69	0.1121	2.19	0.0629	3.16	0.039	2.09	0.2779	1.16	0.6789
IL18RAP	2.17	2.91	4.17	2.02	5.19	1.03	1.34	0.6421	1.92	0.4715	1.24	0.7837	2.07	0.4799	2.44	0.1876
IL1A	2.07	3.28	2.02	3.04	1.41	7.5	1.58	0.2547	1.03	0.9469	1.18	0.7351	1.84	0.1698	2.9	0.2444
IL1B	22.66	16.95	15.68	6.42	20.69	31.7	1.34	0.5566	1.44	0.4554	4.48	0.2215	1.39	0.5004	1.1	0.7847
IL1R1	34.89	49.5	106.88	94.12	117.38	17.92	1.42	0.2877	3.06	0.026	2.13	0.2334	2.65	0.0282	2.47	0.4853
IL1RAP	401.69	406.61	467.6	633.91	530.26	415.11	1.01	0.8963	1.16	0.1881	1.24	0.0019	1.04	0.3726	1.23	0.2658
IL1RN	7.21	6.19	26.87	14.45	8.72	2.76	1.16	0.7181	3.73	0.1074	1.58	0.7729	1.05	0.8743	3.32	0.0398
IL2	1.53	2.28	1.33	7.14	2.19	1.05	1.49	0.3128	1.15	0.7095	3.9	0.0165	1.2	0.8057	1.74	0.1621
IL21	1.05	1.68	1.68	2.87	2.17	1.03	1.6	0.0008	1.6	0.0509	2.46	0.1134	1.86	0.1589	1.13	0.1838
IL22	1.05	1.68	1.67	2.87	2.17	1.03	1.6	0.0008	1.6	0.0508	2.46	0.1134	1.86	0.1589	1.13	0.1838
IL22RA2	1.05	1.68	1.67	2.87	2.17	1.03	1.6	0.0008	1.6	0.0508	2.46	0.1134	1.86	0.1589	1.13	0.1838
IL23A	1.29	1.8	1.63	2.87	2.17	2.76	1.4	0.2424	1.26	0.4641	1.92	0.1917	1.45	0.2845	1.84	0.1836
IL23R	1.47	2.88	2.11	2.4	1.84	4.33	1.96	0.0395	1.43	0.3524	1.4	0.5723	1.08	0.8795	2.54	0.0135
IL3	1.05	1.68	1.67	2.87	2.17	1.03	1.6	0.0008	1.6	0.0508	2.46	0.1134	1.86	0.1589	1.13	0.1838
IL4	1.23	1.95	1.68	2.87	2.17	1.7	1.59	0.0747	1.36	0.2405	2.02	0.1627	1.53	0.2155	1.2	0.7704

Gene Name	Control	SAD	FAD	TREM2 SAD	TREM2 FAD	TREM2 Control	Control vs. SAD	P value of: Control vs. SAD	Control vs. FAD	P value of: Control vs. FAD	Control vs. TREM2 SAD	P value of: Control vs. TREM2 SAD	Control vs. TREM2 FAD	P value of: Control vs. TREM2 FAD	Control vs. TREM2 Control	P value of: Control vs. TREM2 Control
IL4RA	90.55	102.74	188.26	301.58	208.42	74.06	1.13	0.642	2.08	0.1042	2.63	0.2252	1.82	0.2934	1.55	0.5873
IL5	2.07	4	3.11	6.12	3.4	10.36	1.94	0.1127	1.51	0.4124	2.43	0.2062	1.35	0.8111	4.12	0.031
IL6	11.23	6.61	17.68	24.5	18.72	9.69	1.7	0.422	1.57	0.5794	1.79	0.5771	1.37	0.649	1.41	0.7653
IL6R	88.87	122.14	157.68	293.92	224.03	81.68	1.37	0.1229	1.77	0.0465	2.61	0.1933	1.99	0.1976	1.38	0.0833
IL7	1.25	1.7	1.61	2.52	2.17	1.03	1.36	0.2324	1.29	0.3921	1.79	0.3419	1.54	0.2263	1.37	0.2312
IL8	46.2	61.65	132	173.14	185.43	12.22	1.33	0.5011	2.86	0.1111	2.96	0.1596	3.17	0.4433	4.79	0.5333
IL9	1.04	1.36	2.05	2.87	2.17	1.03	1.3	0.0474	1.96	0.063	2.57	0.1042	1.94	0.1462	1.09	0.3632
IRF1	21.33	59.21	73.2	259.86	96.59	28.85	2.78	0.0292	3.43	0.018	9.61	0.209	3.57	0.1174	1.07	0.8511
IRF3	64.07	100.43	117.78	168.1	142.09	98.95	1.57	0.0093	1.84	0.0092	2.07	0.1548	1.75	0.0025	1.22	0.1139
IRF5	54.65	88.96	75.38	191.72	110.1	54.19	1.63	0.04	1.38	0.3572	2.77	0.1079	1.59	0.4953	1.28	0.5877
IRF7	11.05	36.03	33.7	44.77	52.83	10.76	3.26	0.0141	3.05	0.0578	3.2	0.5291	3.77	0.2046	1.3	0.5962
ITGB2	186.35	328.5	416.07	766.34	418.55	129.32	1.76	0.1145	2.23	0.0675	3.24	0.1727	1.77	0.207	1.83	0.3024
JUN	604.6	524.71	1103.28	713.6	964.05	710.97	1.15	0.1362	1.82	0.0389	1.07	0.6978	1.26	0.0337	1.08	0.8008
KEAP1	213.51	372.72	301.8	648.47	609.01	276.7	1.75	0.0003	1.41	0.1537	2.4	0.079	2.25	0.1122	1.02	0.8663
KLK6	96.4	203.82	87.95	332.28	260.01	799.55	2.11	0.1216	1.1	0.8257	2.72	0.3143	2.13	0.2344	6.54	0.2703
KNG1	4.16	3.2	3.91	6.86	9.91	6.19	1.3	0.602	1.06	0.9088	1.3	0.7239	1.88	0.1446	1.17	0.8545
LIMK1	1861.21	1838.25	1658.52	2263.42	2983.26	2251.27	1.01	0.894	1.12	0.5991	1.04	0.9068	1.26	0.019	1.05	0.8333
LTA	5.03	9.39	13.8	12.96	39.55	8.81	1.87	0.2842	2.75	0.1544	2.03	0.3701	6.21	0.0044	1.38	0.5714
LTB	9.25	17.18	13.01	7.87	6.22	9.73	1.86	0.0925	1.41	0.4702	1.49	0.3392	1.89	0.7575	1.2	0.5264
LTB4R	45.05	57.85	61.61	109.19	96.76	29.24	1.28	0.3582	1.37	0.3696	1.91	0.274	1.69	0.1485	1.95	0.0301
LTB4R2	42.46	55.94	50.22	90.59	64.12	48.68	1.32	0.0912	1.18	0.3878	1.68	0.1416	1.19	0.2197	1.11	0.6293
LY96	168.69	161.36	262.55	307.12	286.15	111.23	1.05	0.8141	1.56	0.1447	1.44	0.4066	1.34	0.4521	1.92	0.0117
MAFF	41.27	110.06	180.8	405.38	303.67	33.55	2.67	0.0611	4.38	0.0059	7.75	0.1274	5.8	0.2198	1.56	0.5395
MAFG	618.75	777.93	776.6	1194.04	1254.25	594.87	1.26	0.0248	1.26	0.3563	1.52	0.2685	1.6	0.3239	1.32	0.1576

Gene Name	Control	SAD	FAD	TREM2 SAD	TREM2 FAD	TREM2 Control	Control vs. SAD	P value of: Control vs. SAD	Control vs. FAD	P value of: Control vs. FAD	Control vs. TREM2 SAD	P value of: Control vs. TREM2 SAD	Control vs. TREM2 FAD	P value of: Control vs. TREM2 FAD	Control vs. TREM2 Control	P value of: Control vs. TREM2 Control
MAFK	763.61	1239.47	1119.04	2383.66	1738.43	972.32	1.62	0.0095	1.47	0.071	2.46	0.1281	1.8	0.4009	1	0.979
MAP2K1	3524.14	3296.22	3058.5	3289.39	4919.48	4328.11	1.07	0.6035	1.15	0.3406	1.36	0.2167	1.1	0.6543	1.03	0.8593
MAP2K4	1768.6	1757.89	1818.74	2199.13	3076.82	2318.78	1.01	0.9677	1.03	0.8844	1.02	0.9469	1.37	0.0657	1.03	0.8746
MAP2K6	187.11	231.73	239.47	211.67	298.94	281.53	1.24	0.0086	1.28	0.2141	1.12	0.7833	1.26	0.2861	1.19	0.0244
MAP3K1	217.55	303.89	370.52	536.83	460.2	277.51	1.4	0.0025	1.7	0.0162	1.95	0.0899	1.67	0.3082	1.01	0.9746
MAP3K5	624.92	835.55	898.03	978.26	1214.79	693.6	1.34	0.0041	1.44	0.0096	1.23	0.4505	1.53	0.0653	1.14	0.1516
MAP3K7	968.19	1151.03	1172.16	1589.16	1624.3	1371.33	1.19	0.0033	1.21	0.026	1.29	0	1.32	0.166	1.12	0.0239
MAP3K9	590.1	611.49	599.91	639.17	1026.45	717.29	1.04	0.808	1.02	0.9519	1.17	0.7863	1.37	0.0432	1.04	0.8868
MAPK1	5144.49	5389.07	5030.87	6418.12	6834.98	6064.7	1.05	0.521	1.02	0.7622	1.02	0.7849	1.05	0.7025	1.08	0.1941
MAPK14	1138.48	1377.92	1535.53	1846.48	2003.1	1308.73	1.21	0.0078	1.35	0.0054	1.28	0.1718	1.39	0.0004	1.1	0.1597
MAPK3	5693.47	6831.73	5784.22	8405.47	8393.47	5478.84	1.2	0.0396	1.02	0.8937	1.16	0.5968	1.16	0.23	1.32	0.0237
MAPK8	1074.68	1091.52	995.38	1249.32	1578.62	1302.22	1.02	0.8465	1.08	0.6143	1.09	0.7089	1.16	0.0501	1.05	0.6443
MAPKAPK2	266.06	520	646.99	1190.52	952.12	355.96	1.95	0.0019	2.43	0.0054	3.53	0.0728	2.82	0.2272	1.06	0.8784
MAPKAPK5	951.85	1427.34	1328.04	2212.9	1804.52	1194.29	1.5	0.0006	1.4	0.0375	1.83	0.0614	1.5	0.3241	1.01	0.8816
MAPT	4349.65	4748.61	3870.27	6423.27	6737.65	4140.08	1.09	0.2477	1.12	0.5238	1.16	0.5937	1.22	0.0434	1.33	0.0326
MASP1	11.98	17.49	33.71	19.25	25.17	43.87	1.46	0.2704	2.81	0.0363	1.27	0.7572	1.66	0.4734	2.89	0.3412
MASP2	1.63	2.46	3.9	6.31	7.53	5.09	1.5	0.3558	2.38	0.1803	3.22	0.2784	3.84	0.1438	2.6	0.0274
MAX	1318.72	1850.31	1971.45	3273.27	2950.67	1613.99	1.4	0.0035	1.49	0.0172	1.96	0.0591	1.76	0.2707	1.04	0.582
MBL2	1.05	1.68	1.67	2.87	2.17	1.03	1.6	0.0008	1.6	0.0508	2.46	0.1134	1.86	0.1589	1.13	0.1838
MEF2A	3115.33	4145.18	4102.06	5673.51	5710.97	3789.33	1.33	0.0002	1.32	0.0105	1.44	0.0151	1.45	0.0732	1.04	0.7125
MEF2BNB-MEF2B	5.05	10.61	7.44	7.51	8.75	9.57	2.1	0.0563	1.47	0.4815	1.17	0.8362	1.37	0.513	1.49	0.2315
MEF2C	4806.42	4283.04	4700.78	4633.48	6496.44	6739.17	1.12	0.4352	1.02	0.9201	1.32	0.5604	1.07	0.7406	1.11	0.7429
MEF2D	1552.91	1543.79	1375.72	1589.94	2003.64	1758.31	1.01	0.9055	1.13	0.4411	1.24	0.6071	1.02	0.931	1.12	0.4738

Gene Name	Control	SAD	FAD	TREM2 SAD	TREM2 FAD	TREM2 Control	Control vs. SAD	P value of: Control vs. SAD	Control vs. FAD	P value of: Control vs. FAD	Control vs. TREM2 SAD	P value of: Control vs. TREM2 SAD	Control vs. TREM2 FAD	P value of: Control vs. TREM2 FAD	Control vs. TREM2 Control	P value of: Control vs. TREM2 Control
MKNK1	787.58	1055.1	1095.52	1431.5	1311.21	816.59	1.34	0.007	1.39	0.044	1.43	0.0878	1.31	0.0627	1.22	0.3353
MMP3	1.34	2.52	3.62	4.22	5.05	2.3	1.89	0.0704	2.71	0.088	2.83	0.1681	3.39	0.442	1.54	0.6947
MMP9	9.69	14.12	63.87	24.11	31.94	1.37	1.46	0.7282	6.59	0.1341	2.12	0.5462	2.81	0.4033	8.26	0.0808
MRC1	44.22	14.38	33.4	55	64.19	26.26	3.08	0.0197	1.32	0.7575	1.02	0.9782	1.14	0.6579	2.14	0.479
MX1	984.84	1214.08	1084.74	3448.56	1440.19	1252.41	1.23	0.0473	1.1	0.2968	2.76	0.3109	1.15	0.2522	1	0.9754
MX2	43.66	60.09	50.57	190.92	63.1	53.5	1.38	0.1851	1.16	0.5993	3.45	0.2764	1.14	0.6656	1.03	0.9199
MYC	151.64	201.75	303.86	394.65	342.74	134.93	1.33	0.2718	2	0.0414	2.05	0.0773	1.78	0.2395	1.43	0.4619
MYD88	99.86	138.67	228.9	303.03	235.6	101.52	1.39	0.2199	2.29	0.021	2.39	0.2351	1.86	0.082	1.25	0.3724
MYL2	1.23	3.54	1.98	2.87	2.17	1	2.88	0.0051	1.61	0.2339	2.02	0.1627	1.53	0.2155	1.42	0.1204
NFATC3	214.09	346.66	394.29	487.74	512.8	280.49	1.62	0.0005	1.84	0.0018	1.8	0.0572	1.89	0.0855	1.03	0.8838
NFE2L2	725.19	1045.34	1470.84	1849.19	1726.46	1096.19	1.44	0.0257	2.03	0.0014	2.01	0.0495	1.88	0.1731	1.19	0.656
NFKB1	66.11	110.24	121.61	203.05	176.81	124.01	1.67	0.006	1.84	0.0004	2.42	0.1855	2.11	0.3065	1.48	0.2775
NLRP3	61.42	83.38	53.46	83.32	58.97	86.26	1.36	0.081	1.15	0.7758	1.07	0.8908	1.32	0.7117	1.11	0.4271
NOD1	47	58.62	77.22	122.13	90.16	52.6	1.25	0.2595	1.64	0.1298	2.05	0.1417	1.51	0.2926	1.13	0.5176
NOD2	8.03	9.56	13.03	44.79	15.33	6.77	1.19	0.7578	1.62	0.5314	4.4	0.3766	1.51	0.4869	1.5	0.4872
NOS2	106.13	151.76	85.13	154.17	157.5	93.05	1.43	0.0656	1.25	0.2841	1.15	0.6782	1.17	0.2985	1.45	0.4424
NOX1	6.42	11.41	4.54	10.18	15.06	12.41	1.78	0.1702	1.41	0.4966	1.25	0.8097	1.85	0.3307	1.52	0.296
NOX4	2.11	5.45	7.28	7.27	4.19	5.48	2.58	0.0223	3.44	0.0269	2.82	0.1511	1.63	0.4674	2.13	0.6056
NR3C1	1670.21	2303.49	2200.37	3005.22	2944.63	2785.3	1.38	0.0351	1.32	0.059	1.42	0.0244	1.39	0.1101	1.32	0.0949
NeuN	1029.8	1165.51	901.21	986.44	1543.22	1208.03	1.13	0.3194	1.14	0.5039	1.32	0.5856	1.18	0.4494	1.08	0.8088
OAS2	61.1	119.55	100.96	363.77	162.63	103.72	1.96	0.0079	1.65	0.0907	4.7	0.2756	2.1	0.3077	1.34	0.4696
OASL	2.99	4.46	3.03	13.01	4.19	5.1	1.49	0.2637	1.01	0.9736	3.58	0.4991	1.15	0.8212	1.4	0.7929
OXER1	10.22	11.61	14.66	21.01	18.51	16.35	1.14	0.7456	1.43	0.2552	1.62	0.5454	1.43	0.4236	1.26	0.5884
P2RX7	343.62	517.46	416.56	773.37	709.23	646.32	1.51	0.0095	1.21	0.2117	1.77	0.0023	1.63	0.0261	1.48	0.5611

Gene Name	Control	SAD	FAD	TREM2 SAD	TREM2 FAD	TREM2 Control	Control vs. SAD	P value of: Control vs. SAD	Control vs. FAD	P value of: Control vs. FAD	Control vs. TREM2 SAD	P value of: Control vs. TREM2 SAD	Control vs. TREM2 FAD	P value of: Control vs. TREM2 FAD	Control vs. TREM2 Control	P value of: Control vs. TREM2 Control
PDGFA	178.71	247.67	288.05	356.17	405.32	266.78	1.39	0.0103	1.61	0.0057	1.57	0.1407	1.79	0.0009	1.18	0.585
PEN2	545.94	709.58	654.52	1166.65	934.76	595.37	1.3	0.0537	1.2	0.2949	1.69	0.1216	1.35	0.3458	1.16	0.6036
PIK3C2G	14.87	17.61	8.45	15.91	3.38	13.79	1.18	0.394	1.76	0.0371	1.19	0.5893	5.58	0.2126	1.37	0.426
PLA2G4A	67.66	68.91	93.87	147.55	105.22	62.71	1.02	0.9072	1.39	0.0803	1.72	0.1993	1.23	0.3332	1.37	0.5007
PLCB1	2767.57	3145.69	2949.28	2924.32	4644.68	3207.87	1.14	0.3093	1.07	0.7692	1.2	0.7392	1.32	0.1887	1.09	0.7169
PPP1R12B	475.45	593.58	559.94	600.58	807.54	939.52	1.25	0.0582	1.18	0.2153	1	0.9719	1.34	0.1832	1.56	0.1438
PRKCA	1535.17	2141.49	2566.38	2907.12	3235.97	1707.37	1.39	0.0066	1.67	0.01	1.49	0.3866	1.66	0.1763	1.14	0.0304
PRKCB	4450.21	5335.96	4535.07	5998.35	8347.35	4433.44	1.2	0.0929	1.02	0.9305	1.06	0.8919	1.48	0.0158	1.27	0.2788
PSEN1	633.19	802.73	721.42	1331.95	1034.26	1458.24	1.27	0.0348	1.14	0.1032	1.66	0.233	1.29	0.0995	1.82	0.389
PSEN2	291.48	310.86	314.98	428.85	389.75	317.71	1.07	0.414	1.08	0.4306	1.16	0.4171	1.05	0.4682	1.16	0.0937
PTGDR2	42.67	87.02	47.19	102.36	96.74	46.05	2.04	0.053	1.11	0.853	1.89	0.4081	1.79	0.1607	1.18	0.7457
PTGER1	1.05	1.8	1.67	2.87	2.17	1.03	1.72	0.0023	1.6	0.0508	2.46	0.1134	1.86	0.1589	1.13	0.1838
PTGER2	6.06	15.87	12.87	8.3	5.65	4.14	2.62	0.0588	2.12	0.2874	1.08	0.9528	1.36	0.871	1.86	0.7387
PTGER3	87.58	78.28	86.39	81.33	85.78	67.54	1.12	0.6848	1.01	0.9723	1.37	0.2293	1.29	0.3621	1.64	0.1545
PTGER4	8.15	10.08	26.29	14.39	10.39	10.78	1.24	0.5609	3.23	0.0313	1.39	0.7147	1.01	0.9956	1.04	0.9138
PTGFR	10.95	13.55	23.29	8.5	60.05	15.21	1.24	0.7063	2.13	0.3728	1.63	0.5605	4.32	0.0145	1.1	0.8309
PTGIR	1.16	1.8	1.69	2.87	2.17	1.03	1.55	0.0493	1.45	0.1705	2.21	0.1287	1.68	0.1532	1.26	0.2573
PTGS1	23.64	37.55	41.14	58.53	41.38	29.79	1.59	0.0411	1.74	0.107	1.95	0.0493	1.38	0.2448	1.01	0.9872
PTGS2	109.3	88.13	151.96	120.94	161.93	89.86	1.24	0.2234	1.39	0.1348	1.15	0.6402	1.17	0.1688	1.54	0.6075
PTK2	5485.04	7227.5	6038.03	10211.49	9340.37	5792.11	1.32	0.0027	1.1	0.3948	1.47	0.1449	1.34	0.0048	1.2	0.0068
RAC1	3264	3815.16	4029.66	5612.78	5216.37	5202.95	1.17	0.0239	1.23	0.0235	1.36	0.1421	1.26	0.0741	1.26	0.0713
RAF1	616.39	877.49	985.99	1455.53	1447.13	922.48	1.42	0.0046	1.6	0.0027	1.86	0.041	1.85	0.1404	1.18	0.2078
RAPGEF2	1417.18	1705.76	1604.4	2089.04	2586.04	1657.88	1.2	0.06	1.13	0.3334	1.16	0.5537	1.44	0.0853	1.08	0.7356
RELA	89.43	174.77	189.17	354.36	327.93	149.42	1.95	0.0024	2.12	0.0023	3.12	0.052	2.89	0.2144	1.32	0.4289

Gene Name	Control	SAD	FAD	TREM2 SAD	TREM2 FAD	TREM2 Control	Control vs. SAD	P value of: Control vs. SAD	Control vs. FAD	P value of: Control vs. FAD	Control vs. TREM2 SAD	P value of: Control vs. TREM2 SAD	Control vs. TREM2 FAD	P value of: Control vs. TREM2 FAD	Control vs. TREM2 Control	P value of: Control vs. TREM2 Control
RELB	35.36	36.94	49.65	79.29	62.03	37.09	1.04	0.7872	1.4	0.0984	1.77	0.3526	1.38	0.5501	1.21	0.158
RHOA	682.94	871	1221.45	1770.81	1393.76	1371.86	1.28	0.0695	1.79	0.0076	2.04	0.0971	1.61	0.087	1.58	0.3039
RIPK1	316.13	462.85	482.31	802.69	650.3	419.43	1.46	0.0164	1.53	0.0402	2	0.1023	1.62	0.1745	1.05	0.6818
RIPK2	298.89	327.23	414.56	535.54	464.96	409.74	1.09	0.3313	1.39	0.0242	1.41	0.0683	1.23	0.0581	1.08	0.821
ROCK2	2980.88	3737.17	3908.35	5127.17	5515.33	3706.11	1.25	0.0328	1.31	0.0231	1.36	0.2764	1.46	0.1428	1.02	0.9084
RPS6KA5	921.95	1470.97	1109.71	2129.67	1731.11	1480.62	1.6	0.0004	1.2	0.0902	1.82	0.0004	1.48	0.0823	1.27	0.0218
SHC1	310.21	408.86	689.41	655.62	782.79	307.53	1.32	0.1059	2.22	0.0073	1.67	0.1911	1.99	0.1052	1.28	0.0984
SMAD7	412.81	655.94	829.49	977.51	962.58	654.23	1.59	0.002	2.01	0.0036	1.87	0.2092	1.84	0.1962	1.25	0.3281
SNCA	5496.88	4673.89	3376.47	4549.4	5305.78	4902.24	1.18	0.0309	1.63	0.0262	1.53	0.1314	1.31	0.3044	1.42	0.0249
SOCS3	118.59	143.54	357.6	508.6	358.51	78.49	1.21	0.7387	3.02	0.1143	3.38	0.2894	2.38	0.2372	1.92	0.5071
STAT1	406.49	392.47	435.79	1068.55	477.7	854.76	1.04	0.8183	1.07	0.6908	2.07	0.4565	1.08	0.5882	1.66	0.0109
STAT2	1431.87	2154.76	1910.69	3903.2	2496.73	2037.23	1.5	0.001	1.33	0.0234	2.15	0.219	1.38	0.1421	1.12	0.7225
STAT3	1748.55	2697.34	3527.85	5383.82	4578.06	2182.83	1.54	0.0289	2.02	0.0177	2.43	0.1289	2.06	0.2296	1.02	0.9333
TBXA2R	4.19	5.78	6.93	10.91	23.85	3.79	1.38	0.4802	1.65	0.3727	2.05	0.5553	4.49	0.0386	1.4	0.8375
TCF4	3251.19	4394.53	4352.03	6233.65	6514.26	3651.28	1.35	0.0053	1.34	0.0996	1.51	0.1566	1.58	0.1256	1.13	0.1678
TGFB1	141.96	348.55	409.2	850.22	607.02	160.76	2.46	0.0024	2.88	0.0141	4.72	0.0813	3.37	0.2421	1.12	0.6498
TGFB2	577.63	867.97	1269.86	1125.8	1866.28	706.91	1.5	0.0237	2.2	0.0004	1.54	0.2055	2.55	0.0004	1.04	0.824
TGFB3	213.7	591.89	403.18	741.42	661.33	346.68	2.77	0.0014	1.89	0.0411	2.74	0.1421	2.44	0.316	1.28	0.5244
TGFBR1	318.98	515.85	510.06	900.67	696.33	365.14	1.62	0.0144	1.6	0.0792	2.23	0.2114	1.72	0.3647	1.11	0.7636
TLR1	180.57	224.38	216.35	421.45	267.65	161.88	1.24	0.2423	1.2	0.5811	1.84	0.2721	1.17	0.7303	1.41	0.3891
TLR2	112.24	177.47	230.95	508.01	280.96	96.07	1.58	0.2538	2.06	0.1571	3.57	0.0819	1.97	0.2955	1.48	0.2984
TLR3	48.11	60.76	52.04	111.52	68.42	52.55	1.26	0.3514	1.08	0.7507	1.83	0.3413	1.12	0.7522	1.16	0.6794
TLR4	388.04	651.59	768.6	945.32	1015.86	440.29	1.68	0.0011	1.98	0.0461	1.92	0.2088	2.06	0.2442	1.12	0.6997
TLR5	67.64	87.9	93.17	164.18	124.42	51.18	1.3	0.223	1.38	0.4383	1.91	0.0886	1.45	0.4786	1.68	0.2248

Gene Name	Control	SAD	FAD	TREM2 SAD	TREM2 FAD	TREM2 Control	Control vs. SAD	P value of: Control vs. SAD	Control vs. FAD	P value of: Control vs. FAD	Control vs. TREM2 SAD	P value of: Control vs. TREM2 SAD	Control vs. TREM2 FAD	P value of: Control vs. TREM2 FAD	Control vs. TREM2 Control	P value of: Control vs. TREM2 Control
TLR6	60.78	69.29	84.84	111.72	101.47	61.55	1.14	0.5537	1.4	0.2698	1.45	0.4245	1.32	0.6047	1.25	0.513
TLR7	24.99	28.25	30.23	62.07	28.56	15.1	1.13	0.7386	1.21	0.5353	1.96	0.2127	1.11	0.9108	2.1	0.0505
TLR8	7.78	12.23	33.62	39.55	40.63	3.6	1.57	0.4334	4.32	0.0403	4.17	0.1076	4.29	0.0402	2.63	0.2783
TLR9	14.16	20.89	35.33	40.47	73.38	9.96	1.48	0.3396	2.5	0.0879	2.25	0.1828	4.09	0.1548	1.8	0.1736
TNF	1.11	2.85	1.45	6.01	1.41	1.03	2.57	0.004	1.3	0.212	4.7	0.1966	1.1	0.7612	1.24	0.0905
TNFAIP3	84.63	107.64	223.49	254.26	251.36	59.62	1.27	0.3881	2.64	0.0951	2.37	0.2897	2.34	0.276	1.8	0.0348
TNFSF14	1.23	2.8	2.14	2.87	4.56	6.25	2.27	0.0117	1.74	0.1658	2.02	0.1627	3.22	0.4264	4.41	0.0051
TOLLIP	5696.49	6637.88	6004.14	8432.85	10346.95	4408.31	1.17	0.1946	1.05	0.8009	1.17	0.6838	1.43	0.0054	1.64	0.0874
TRADD	27.82	50.2	49.11	71.06	78.95	41.25	1.8	0.0376	1.77	0.0582	2.01	0.0359	2.24	0.1609	1.17	0.5017
TRAF2	160.32	232	304.51	351.57	396.38	213.84	1.45	0.0146	1.9	0.0197	1.73	0.1486	1.95	0.2322	1.05	0.7534
TREM1	2.86	3.71	5.8	2.52	4.99	9.57	1.3	0.482	2.03	0.2394	1.39	0.5975	1.43	0.4573	2.75	0.0292
TREM2	70.04	142.45	151.39	215.35	193.66	81.45	2.03	0.0139	2.16	0.0081	2.42	0.0405	2.18	0.2702	1.09	0.9114
TSLP	4.47	6.86	12.62	5.17	14.14	9.17	1.53	0.3136	2.82	0.0579	1.1	0.817	2.49	0.1404	1.62	0.4262
TSPO	23.19	50.9	54.86	113.9	79.53	31.63	-2.2	0.0465	2.37	0.0929	3.87	0.0361	2.71	0.2279	1.08	0.8496
TWIST2	16.51	12.24	21.2	9.14	27.97	8.78	1.35	0.3181	1.28	0.5193	2.29	0.1676	1.34	0.3975	2.38	0.3198
TYROBP	448.45	630.26	839.27	1473.77	850.64	351.05	1.41	0.2067	1.87	0.0371	2.59	0.1688	1.5	0.4505	1.62	0.3504
CLTC	3948.01	3612.09	3719.84	4345.29	5183.08	5046.3	1.09	0.3433	1.06	0.5814	1.15	0.2288	1.04	0.6801	1.01	0.9435
GAPDH	28768.73	28176.37	29936.19	30678.52	41197.88	36030.03	1.02	0.7624	1.04	0.563	1.19	0.4511	1.13	0.0571	1.01	0.8077
GUSB	128.53	160.81	120.85	242.18	134.04	173.21	1.25	0.3442	1.06	0.7933	1.49	0.3632	1.22	0.2657	1.06	0.838
HPRT1	2916.06	2317.79	2080.72	2234.1	2513.32	4395.75	1.26	0.214	1.4	0.1128	1.66	0.2059	1.47	0.1668	1.19	0.5074
PGK1	7778.7	7925.97	8587.72	9220.33	11858.94	9205.08	1.02	0.8252	1.1	0.1863	1.07	0.6389	1.2	0.0219	1.07	0.7234
TUBB	1611.36	1410.59	1583.3	2015.67	1767.74	2069.75	1.14	0.1122	1.02	0.83	1.01	0.8793	1.16	0.0659	1.01	0.8393

Appendix Table 4: Nanostring results. Average counts for each disease group are listed followed by the fold change of each group compared to control with the significance of this fold change. Red highlights upregulation and green highlights downregulation compared to controls.

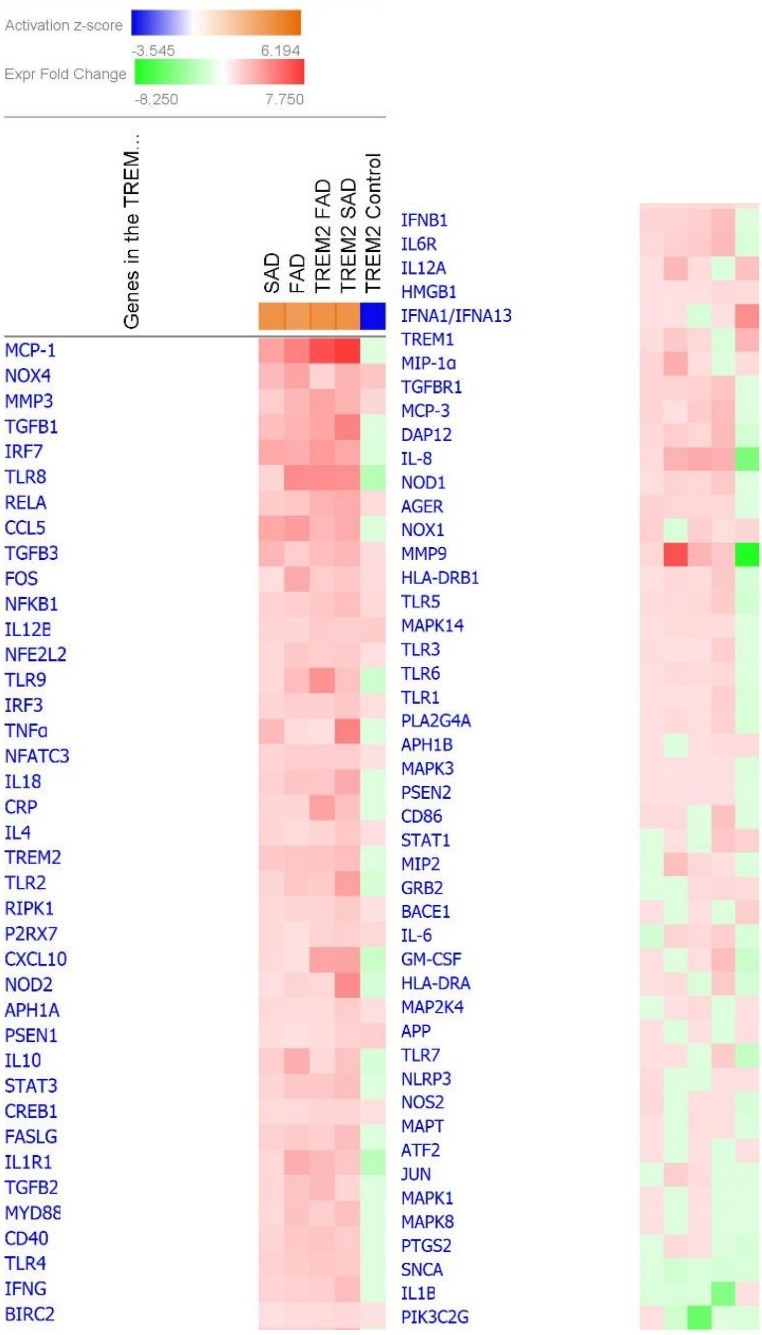

Appendix Table 5: Gene heatmap for TREM1 signalling pathway. All genes shown are associated with the pathway. Red shows upregulated genes and green shows downregulated genes compared to controls.

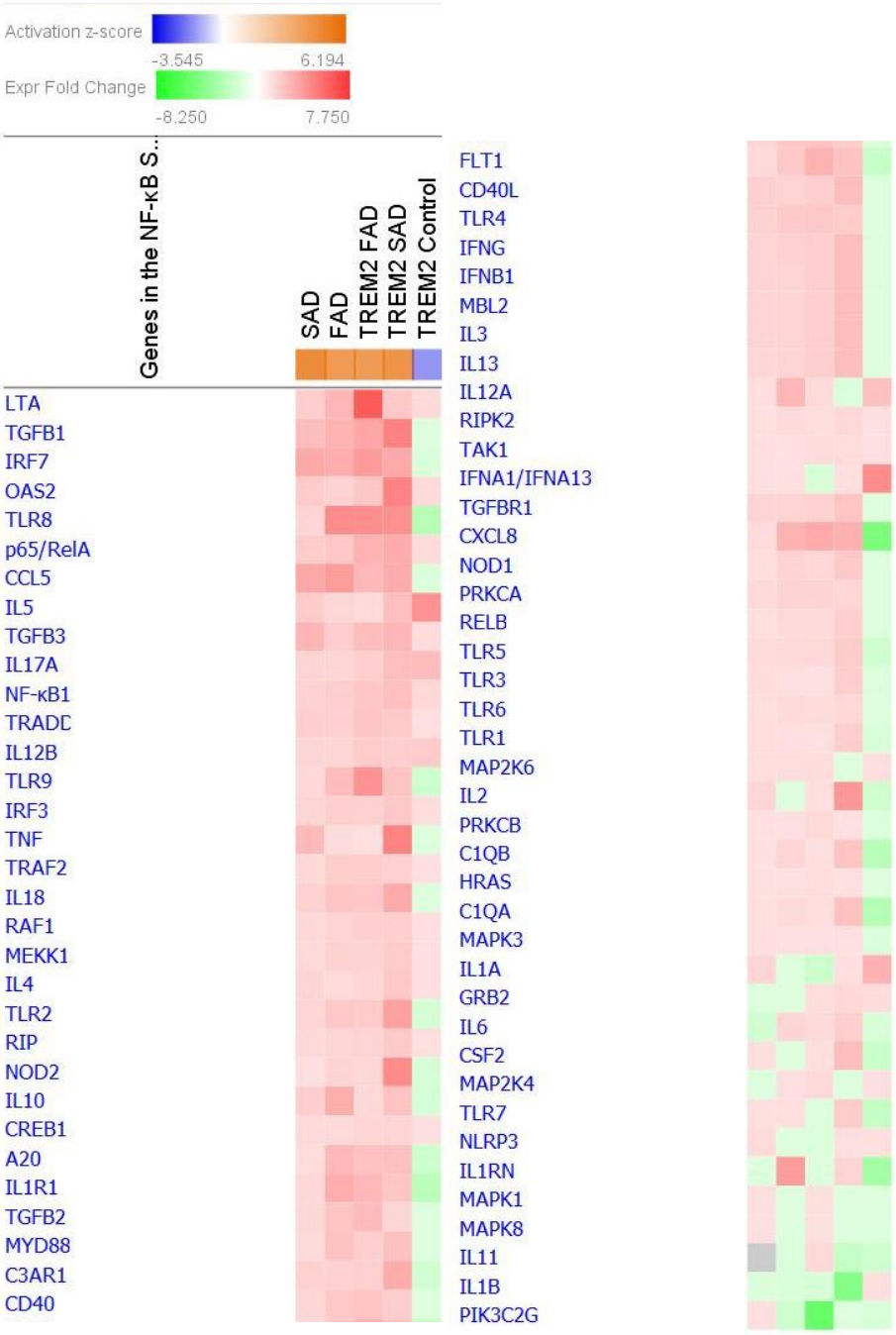

Appendix Table 6: Gene heatmap for NF-κB signalling pathway. All genes shown are associated with the pathway. Red shows upregulated genes and green shows downregulated genes compared to controls.

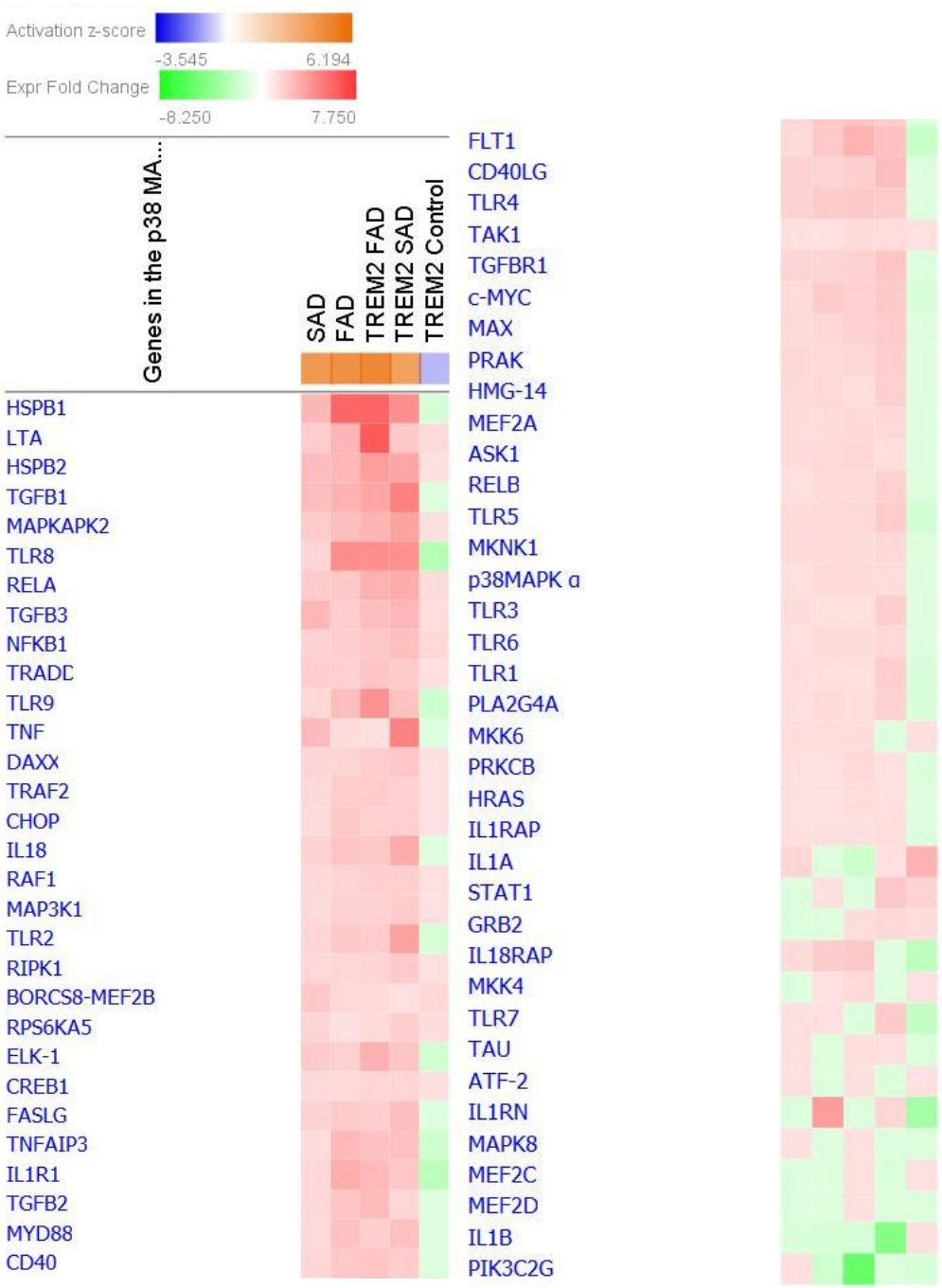

Appendix Table 7: Gene heatmap for p38 MAPK signalling pathway. All genes shown are associated with the pathway. Red shows upregulated genes and green shows downregulated genes compared to controls.

SAD		FAD PSEN1		FAD APP		TREM2 FAD		TREM2 SAD		TREM2 Control	
Up-regulated	**Down-regulated**	**Up-regulated**	**Down-regulated**	**Up-regulated**	**Down-regulated**	**Up-regulated**	**Down-regulated**	**Up-regulated**	**Down-regulated**	**Up-regulated**	**Down-regulated**
ACE	*ABCD3*	*SEPT8*	*ABCA7*	*SEPT2*	*ABI2*	SEPT2	SEPT3	*SEPT6*	*ABCA7*	*MARC2*	*A2M*
ACSS1	*ABCG8*	*ACAA1*	*ACAP2*	*SEPT3*	*ACACB*	AAK1	ABI2	*SEPT7*	*ACBD6*	*SEPT2*	A2M
ACSS3	*ACAA1*	*ACAA2*	ACAP2	*SEPT6*	*ACAT2*	*ABI2*	ACACB	*ABAT*	*ACOT7*	A1BG	*AAK1*
ADPRHL2	*ACOT8*	ACAN	*ACSF3*	*SEPT7*	*ACBD6*	*ABI3BP*	*ACBD6*	*ACAA1*	*ACOT8*	*ABCF2*	ABR
AKR1A1	ADAM11	*ACTR3B*	*ACSL6*	*SEPT8*	ACE	ABLIM2	ACBD7	*ACAA2*	*ACSBG1*	ACOT13	*ACSL3*
ALDH4A1	*AFG3L2*	ACVR1B	ADAMTS2	*SEPT9*	ACSM2B	ACADVL	ADAM11	*ACAT2*	ADAM11	*ACTB*	ACSS1
ALDH6A1	*ALDH3A2*	*ADAR*	*ADGRB2*	*ABLIM2*	*ACTL6B*	*ACLY*	*ADGRB2*	*ACO2*	*ADSS*	*ACTN1*	*ACSS3*
ALDH9A1	ALYREF	*ADRM1*	*AGAP2*	*ACAA2*	*AFG3L2*	ACOT2	ADNP	*ACSS1*	*AFG3L2*	*ACTN2*	*ADGRB2*
ALMS1	*AP2S1*	*AHCY*	*AIP*	*ACLY*	*AGAP2*	ACSL3	*AGAP2*	*ACSS3*	*AK5*	*ACTN3*	*ADSS*
ANXA2	*APOO*	*AHCYL1*	*AK5*	*ACOT1*	AGL	ACSL6	*AGFG1*	*ADAR*	*AKAP5*	*ADAM22*	*AFG3L2*
APBA1	*ARFGEF1*	*AKR1A1*	*ANKMY2*	*ACOT9*	AHCYL1	*ACSS1*	*AGK*	ADCY3	*ANK1*	*ADAMTS20*	*AGFG1*
APOE	*ARFGEF3*	*AKR1B1*	ANKRD18B	*ACSS1*	AHSG	*ACSS3*	AGK	ADD2	AP3B2	*ADD2*	AGL
APP	*ASAP3*	*ALDH2*	*ANKS1B*	*ACSS3*	*ALB*	*ACTN2*	AGL	ADGB	*AP3D1*	*AHCYL1*	*AHSA1*
ARF6	*ASNS*	*AMPD2*	*APBA1*	*ACTBL2*	*ALDOA*	ACTN2	*AK5*	*ADGRL1*	*ARFGEF3*	*AHNAK*	*AK4*
ARFGEF1	ATG7	*ANXA11*	APC2	ACTBL2	*ANKRD12*	ACTR10	*AK9*	*ADH5*	*ARHGAP26*	AIP	AK5
ARFIP2	AZI2	*ANXA2*	*APCS*	*ACTN4*	*APBA1*	ACY1	ANKFY1	ADPRHL1	ARHGAP26	*AK9*	*AKAP10*
ARHGEF4	*B2M*	*ANXA4*	*ARF6*	*ACTR1A*	ARFGEF2	ADAM10	ANKRD36	*AGFG1*	ARHGEF12	AK9	AKAP12
ASAH1	*C2CD2L*	*ANXA5*	*ARFGAP1*	*ADH5*	*ARFGEF3*	ADAM22	AP2A1	*AGL*	*ARMC10*	*AKAP6*	*AKAP5*
ASAP2	*CA1*	*AP2S1*	*ARFGEF3*	AGAP3	*ASAP1*	ADAM23	AP2A2	*AGRN*	*ASAP3*	*AKAP9*	ALB
BAIAP3	CA1	AP3D1	ARFGEF3	AGRN	ASAP1	ADD2	AP2M1	*AHCYL1*	*ASNS*	ALDH3A2	ALYREF
BBS1	*CA2*	*APBA2*	*ARHGAP21*	*AHSA1*	*ASAP3*	ADD3	AP2S1	AHCYL1	*ATG2A*	*ALDH9A1*	ANKFY1
C14orf159	*CADM2*	*APBB1IP*	*ARHGAP26*	*AK1*	*ASNS*	ADSS	*AP3D1*	*AHNAK*	ATP2A3	*ALDOC*	*ANKIB1*
C4A	*CADM3*	*APOB*	*ARHGAP35*	*AK3*	*ATP1A4*	*AFG3L2*	AP3S1	AHSG	*ATPAF1*	*ALMS1*	ANXA2
CABP1	*CAMK4*	*APOE*	*ARHGEF9*	*AKR1A1*	*ATP1B1*	AHCYL1	*APBA1*	*AKAP12*	ATXN10	*ANK3*	*AP1B1*

SAD		FAD PSEN1		FAD APP		TREM2 FAD		TREM2 SAD		TREM2 Control	
Up-regulated	**Down-regulated**	**Up-regulated**	**Down-regulated**	**Up-regulated**	**Down-regulated**	**Up-regulated**	**Down-regulated**	**Up-regulated**	**Down-regulated**	**Up-regulated**	**Down-regulated**
CALD1	*CAMSAP2*	*APOL2*	*ARID4A*	*AKR1B1*	ATP2C1	*AHSA1*	*APOA1*	*AKR1A1*	*BCR*	*ANKRD36*	AP1B1
CCDC88A	*CAPZA2*	*APP*	*ARMC9*	*ALDH1L1*	*ATP6V0D1*	AHSG	*ARFGEF3*	*AKR1C2*	*C2CD3*	*ANXA1*	APOH
CCNB3	*CARF*	*APPL1*	*ASNS*	*ALDH6A1*	*ATP6V1F*	AK5	ARFGEF3	AKR1C2	*CA1*	*AP2B1*	*ARFGAP1*
CCT2	*CAST*	*AQP4*	*ASPM*	*ALDH9A1*	*ATP6V1G2*	*AKAP12*	ARHGAP44	*ALB*	CA1	*AP2M1*	ARFGEF2
CKB	CCAR2	*ARFGEF2*	*ATAT1*	*ALS2CR12*	*AVPR1B*	AKAP12	ARHGEF12	ALDH3A2	*CA2*	*APEX1*	*ARHGAP26*
CLASP2	CD44	*ARHGAP23*	ATG7	*ANKRD28*	*BASP1*	*AKAP5*	ARHGEF6	*ALDH6A1*	*CADM2*	*AQP4*	*ARHGEF11*
CLIC4	CDC42	*ASPH*	*ATP6V0D1*	*ANLN*	*C16orf70*	*AKR1B1*	ASAP1	ALDH9A1	*CAMK2A*	*ARF3*	ARID3B
CNN3	*CDON*	*ATAD3C*	*ATP8B4*	*ANXA11*	C1orf95	*AKR1C1*	*ASAP3*	*ALMS1*	*CAMK2D*	ARHGAP35	*ARID4A*
CNOT1	CDR2	*ATP6V1D*	*BAG6*	*ANXA5*	*C9orf172*	*ALB*	ASMTL	*ANKRD36*	*CAMK4*	ARMC9	*ARL3*
CNP	CEND1	*AZGP1*	*BAI1*	*ANXA6*	*CA1*	ALB	*ASNS*	*ANXA1*	*CAMKK1*	*ARPC3*	*ARMC10*
COL25A1	*CFH*	*BAG3*	*BCKDK*	APC	CA4	*ALDH1L1*	ATAD1	*ANXA2*	CAMKK1	*ASAH1*	*ARMC9*
COL6A2	*CNOT1*	BAG6	BGN	*APOE*	*CABP1*	*ALDH3A2*	ATIC	ANXA5	*CAMSAP1*	ASAH1	*ASAP3*
COL7A1	CORO1A	*BCAS1*	*BRK1*	*APP*	*CADM2*	ALDH3A2	ATP5C1	AP3D1	*CAND1*	*ASAP1*	*ASS1*
COL9A2	*COX5A*	*BCL2L13*	*BRSK1*	*ARHGDIA*	*CADM3*	*ALDH4A1*	*ATP5J2-PTCD1*	*APBB1*	*CBWD2*	*ASH2L*	*ATG2A*
COMMD3	CPNE4	*BICD1*	C1orf95	ARHGEF6	*CADM4*	ALDH4A1	ATP6V0D1	*APEX1*	CCAR2	*ASRGL1*	*ATIC*
CORO1C	*CRIP2*	*BRAF*	*C9orf172*	*ARL3*	*CAMK2A*	*ALDH6A1*	*ATP6V1B1*	APOB	CCBL2	*ASXL2*	ATP2A3
CRAT	*CTNND2*	*BROX*	*CACNG3*	*ARRB1*	CAMK2A	ALDH7A1	ATP8A2	*APOE*	CCDC183	ATG7	ATP2B2
CROCC2	*CXXC1*	*BSN*	CADPS2	*ASAH1*	*CAMKK1*	*ALDOC*	*BANF1*	APOL2	*CCDC43*	*ATM*	BAG3
CRTC1	DDX3X	BZRAP1	*CALM1*	*ATAD1*	*CAMSAP1*	ALDOC	*BASP1*	*APP*	CCDC51	*ATP1A1*	*BBS1*
DBNL	*DEPDC5*	*BZW2*	*CAMK2A*	*ATP2A2*	CAPN8	*ALMS1*	BCL2L13	ARFGEF3	CCNG1	*ATP1A3*	BCAS3
DCLK2	*DHTKD1*	*C4A*	*CAMK2B*	ATP2A3	*CASK*	*ANK3*	*BCLAF1*	ARFIP2	CDC42BPA	*ATP5F1*	BGN
DCTN2	*DMTN*	*CALB2*	*CAMK4*	*ATP2B1*	*CD59*	*ANKIB1*	BPHL	*ARMC9*	*CDH6*	*ATP5H*	*BPHL*
DDX23	*DMWD*	*CALML4*	*CAMKK1*	*ATP8A1*	*CD81*	*ANKRD35*	BSDC1	*ASAH1*	CDH8	*ATP5J*	BZW2
DES	*DNAAF5*	*CALR*	*CAMKK2*	*ATRNL1*	*CD9*	ANKS1B	BSN	ASCL4	*CEP170*	BAG5	*C14orf159*

SAD		FAD PSEN1		FAD APP		TREM2 FAD		TREM2 SAD		TREM2 Control	
Up-regulated	**Down-regulated**	**Up-regulated**	**Down-regulated**	**Up-regulated**	**Down-regulated**	**Up-regulated**	**Down-regulated**	**Up-regulated**	**Down-regulated**	**Up-regulated**	**Down-regulated**
DGKI	DYNLRB1	*CALU*	*CAMKV*	*BCKDHA*	*CDH13*	*ANLN*	*C1orf94*	ATG4B	*CFAP69*	*BANF1*	*C2CD3*
DLAT	*EIF4A3*	*CAST*	*CAMSAP1*	BCLAF1	*CDH23*	*ANXA1*	*C1RL*	*ATP1A3*	*CFH*	BASP1	*C3*
DLG1	*EIF4G2*	CCDC6	*CAND1*	*BIN1*	CDH8	*ANXA2*	*C2CD3*	*ATP2A2*	*CHD5*	*BGN*	C4A
DNM3	*EMC8*	*CCHCR1*	*CAP2*	*BLVRB*	*CDK18*	ANXA2	C5orf42	BCLAF1	*CIAPIN1*	*BSN*	CA1
DRC3	*EPB42*	*CD81*	*CAPN1*	*C1orf123*	*CDON*	ANXA3	CADM2	*BPHL*	CIRBP	C2CD3	CALCOCO1
DSC1	*EPHA4*	CD9	*CASKIN1*	*C4B*	*CDS2*	*ANXA4*	*CADM3*	*C14orf159*	*CMAS*	*CALD1*	CAMK2A
EHBP1	EPHB2	*CDC42EP4*	*CBWD2*	*CACNA2D2*	CENPE	*ANXA5*	CADPS	*C1orf229*	CNN1	*CALM1*	*CAMK4*
EIF3E	*ERP29*	*CDH23*	*CCDC88A*	CAPNS1	*CEP290*	ANXA5	CAMK1	*C1QB*	*COASY*	*CAMK2A*	*CAMSAP2*
EPPK1	*FARSA*	CENPK	*CCDC88C*	*CCDC171*	*CFAP57*	*ANXA6*	*CAMK2A*	*C2CD5*	*COBL*	*CAMK2G*	CASP5
ERCC6L2	*GAP43*	*CEP350*	*CCT8*	*CCDC22*	*CHD5*	APC	CAMK2A	*C3*	COL4A1	*CAPZB*	*CCBL2*
EZR	GAP43	CFAP45	CDC42BPA	*CCDC87*	*CIRBP*	APOA1	*CAMK2B*	*C4A*	*CTTNBP2NL*	*CASK*	CCBL2
FBN1	GNA11	*CHGB*	CDH15	*CCDC93*	*CKAP5*	APOA2	CAMK2B	*CABP1*	*CUBN*	CASK	CCDC136
FBXO2	*GNL1*	*CLIC4*	*CDK5*	CCNG1	*CLCC1*	APOB	*CAMK2D*	*CACYBP*	CUX2	*CC2D1A*	*CCDC43*
FGA	GPR158	*CLSTN1*	*CELSR1*	*CDC37*	*CMAS*	*APOE*	CAMK2D	CADM3	CYP20A1	*CCDC144A*	CCDC43
FGB	*H2AFY2*	*CLU*	*CEP152*	CEP152	*COASY*	APOE	*CAMK2G*	CALD1	DCTN4	CCDC30	CCDC6
FGFR2	*HBA1*	*CNDP2*	*CEP170B*	*CEP192*	*COL22A1*	*APP*	*CAMKK1*	CAMK2A	*DENND4A*	*CCT5*	CCDC73
FGG	HECTD4	CNNM4	*CGN*	*CFL2*	*COL6A5*	APP	CAMKK1	CAMK2B	*DGKZ*	CD9	*CCDC88A*
FGG	*HIST1H1E*	*CNTNAP1*	CHL1	*CGNL1*	COPS3	*APPL1*	CAMKK2	CAPG	*DHTKD1*	CEP152	CCHCR1
FLNB	*HMGB1P1*	*COL18A1*	*CIRBP*	CHCHD2	CORO1A	ARFGEF1	*CAMKV*	*CAPS*	*DHX34*	*CEP170*	CDH8
FSCN1	*HPCAL1*	COMMD6	*CKM*	*CHCHD3*	*CPLX2*	ARFIP1	*CAMSAP2*	CAPS	DHX9	*CEP170B*	*CHGB*
GALK1	IFT172	*CORO2B*	*CLASP2*	CHST2	*CPNE7*	ARFIP2	*CAPS*	CASC5	DLAT	*CHCHD6*	CHGB
GCLC	IRF2BP2	*CPLX2*	*CLIP1*	CLASP1	*CPNE8*	*ARHGAP32*	CASKIN1	*CBR1*	*DLGAP4*	*CHMP4B*	*CIAPIN1*
GFAP	ITSN2	*CPNE2*	*CLPB*	*CLIC4*	CPSF7	ARHGAP35	CCDC51	CBR3	*DMWD*	CIAPIN1	*CKB*
GFAP	KAT6A	CPOX	*CMAS*	*CLTCL1*	CRYM	*ARHGDIA*	CCHCR1	CBX1	*DNAAF3*	*CKMT1A*	*CKM*

SAD		FAD PSEN1		FAD APP		TREM2 FAD		TREM2 SAD		TREM2 Control	
Up-regulated	**Down-regulated**	**Up-regulated**	**Down-regulated**	**Up-regulated**	**Down-regulated**	**Up-regulated**	**Down-regulated**	**Up-regulated**	**Down-regulated**	**Up-regulated**	**Down-regulated**
GLRX3	KCNH1	CPSF7	*CNKSR2*	*CNDP2*	*CRYZ*	ARRB1	CD59	CCDC144B	*DNAAF5*	CKMT2	*CLIC5*
GOLGA4	*KPNA6*	*CPT1A*	CNN1	*COL25A1*	CSTB	*ASRGL1*	CDC42BPA	*CCDC88A*	*DNAJB11*	*CLIP1*	CLIP2
GRPEL1	*KSR1*	*CSRP1*	*CNTNAP2*	COPB2	*CTNND2*	ATP1B3	*CDH13*	*CCT8*	*DNM1L*	CLTCL1	CNNM4
GSTK1	*KTN1*	*CTGF*	*COASY*	*COPE*	CUL1	*ATP5D*	*CDK18*	CD44	*DOC2A*	*CMAS*	CNTN2
GSTM3	*LMO7*	*CUL3*	*CPNE4*	*COPS2*	*CXXC1*	*ATP6V1A*	*CDS2*	CDH23	EHHADH	*CNP*	COG1
H3F3A	*MARCKS*	*DCDC2*	*CPNE5*	*COPS4*	*CYC1*	ATP6V1C1	CEND1	*CGNL1*	EIF3B	*CNTN1*	COL6A1
HADHA	*MBP*	*DCT*	*CRIP2*	*CORO1B*	DDX19A	ATP6V1G1	CETN2	*CKB*	*EMC8*	*COL1A2*	*COPB1*
HADHB	*MKRN1*	DDX18	*CSNK2B*	CORO1C	DDX59	ATPAF2	CFB	*CLIC1*	EML1	*COL6A1*	COPS7A
HAPLN4	*MTCH2*	*DDX46*	CTBP1	*CPT1A*	DECR1	*ATRNL1*	*CHGA*	CLIC1	*EPB42*	*COL6A2*	*CORO1A*
HIST1H2BK	*MTMR2*	DDX53	CTTNBP2	*CRABP1*	*DENND4A*	*ATXN2*	CHGB	*CLIC4*	EPC2	CORO1C	COX6A1
HNRNPA2B1	MUT	DGAT1	*CUL1*	*CRK*	DEPDC4	BAG3	CHL1	*CLIP1*	*EPPK1*	*COX5B*	CPLX2
HOMER2	*MYH11*	*DICER1*	*DCLK1*	*CROCC*	*DIAPH1*	BCAM	*CHMP4B*	*CLTCL1*	ERVK-24	CPNE4	*CRIP2*
HSP90AA1	NASP	*DKK3*	*DDB1*	*CST3*	*DKFZp566H1924*	BCAS1	*CIRBP*	CMPK1	ESYT2	CST3	*CRKL*
HSP90AB1	NBPF15	*DMWD*	*DDN*	*CTNND1*	*DKFZp686J1372*	BDP1	CIRBP	*CMPK2*	*ETFA*	*CTPS1*	*CROCC*
HSPB1	*NCAM1*	*DNAJB6*	*DGKZ*	CYFIP1	DLG3	*BGN*	CKB	*CNTNAP1*	FAAP100	*CTSB*	CRYL1
IDH3B	NCKAP5	DNM3	*DHX57*	*CYLD*	DNPH1	BGN	*CNKSR2*	*COL1A2*	*FAHD2A*	*CTSD*	*CTNNA1*
IMPDH2	NDUFA9	*DNPEP*	DHX9	DBN1	*DPP6*	*BLVRB*	CNRIP1	*COL6A3*	*FAM179B*	CUL2	CTNNB1
IRF2BP1	*NUCKS1*	DOCK10	*DNAH2*	*DCLK2*	*ECT2*	BLVRB	*COA6*	COL6A5	*FBF1*	*CUL3*	CTPS2
KIF15	*OPCML*	DPP7	*DNAJA3*	*DCTN1*	EHBP1	*C14orf159*	*COASY*	COPS4	FDXR	*CYFIP2*	*CTTN*
KMT2C	*PAICS*	*DRG1*	*DNAJB2*	*DCTN2*	Em:AP000351.3	C1orf167	COL5A1	*CORO1B*	*FSD1*	*DCTN2*	*CTTNBP2NL*
KRT1	*PALM*	*DYNC1I2*	*DNAJB4*	*DDX23*	ENAH	*C1QTNF6*	*COPS4*	*CORO1C*	FTCD	*DDN*	CUTA
KRT14	PALM	*DYNC1LI1*	DNAJC5	DDX4	*EPB42*	*C21orf62*	CORO1A	*CORO2B*	*FUBP1*	*DDX49*	CUX2
KRT16	PCP4	*ECHDC1*	*DNAJC6*	DGKZ	EPC2	*C4A*	CORO1B	CPSF7	FXYD6	DFFA	*CXXC1*

SAD		FAD PSEN1		FAD APP		TREM2 FAD		TREM2 SAD		TREM2 Control	
Up-regulated	**Down-regulated**	**Up-regulated**	**Down-regulated**	**Up-regulated**	**Down-regulated**	**Up-regulated**	**Down-regulated**	**Up-regulated**	**Down-regulated**	**Up-regulated**	**Down-regulated**
KRT17	PDAP1	*EFHD2*	*DNM3*	*DLAT*	EPHA5	C4A	CORO1C	*CRABP1*	*GAD2*	*DGKZ*	DCAF11
KRT38	*PDIA4*	*EHBP1*	*DOCK6*	DLGAP3	EPHB3	*CA1*	COX6A1	CRABP1	GLS	DHRS7C	DCDC1
KRT5	PDK2	EHBP1	*DTX3*	*DMXL2*	EPN3	CA1	*COX6B1*	*CRAT*	*GNB2L1*	*DIAPH1*	*DDAH2*
KRT6A	*PDZRN4*	*EHD2*	*EBF1*	*DNAH10*	ETFDH	*CA2*	COX7A2	*CSDE1*	GNL1	*DLG3*	*DDX19A*
KRT6B	*PEBP1*	ELAVL1	*EFR3A*	*DSCR3*	*EVI5L*	CA2	COX7C	*CTNND1*	*GOLGB1*	*DLG4*	DENND2D
KRT6C	*PITPNM3*	*ENDOD1*	*EIF2AK2*	*DUT*	F3	CACNA1A	*CPNE3*	CTR9	*GPATCH2*	*DLGAP1*	DES
KRT9	*PJA2*	*ENPP6*	*EIF3G*	*DVL1*	*FAM131B*	CADM4	*CPNE7*	CUL5	*GPR98*	*DLGAP2*	*DGKI*
LETM1	*PPFIA1*	ENPP6	EIF3G	*DYNC1LI1*	FAM71D	*CALB2*	CRIP2	CYP11B1	GPR98	*DLGAP3*	DHX9
LONP1	*PRIM1*	*EPHX1*	*ENO1*	*ECHS1*	*FAM71F1*	CALCOCO1	CRKL	CYP2C8	GPRIN1	*DMD*	DIP2B
LRPAP1	*PRNP*	*EPS8*	*EPB41L1*	*EEF1D*	*FARSA*	CALD1	CRMP1	*DBI*	GRIA2	*DNAJA3*	*DIRAS2*
LTF	*PRODH*	*ERMN*	ERC1	*EEF1G*	FDXR	*CAMK4*	CRYM	*DBN1*	*GTPBP1*	*DNAJC11*	*DLAT*
LZTS3	*PRRT2*	*ERO1A*	*ESYT1*	*EHD1*	*FER1L5*	*CAND1*	CRYZ	DCAF11	*HBS1L*	*DOCK6*	DLG4
MAPT	*PSMD1*	*ERP44*	ETFDH	*EHD2*	FGG	CAPN2	CSE1L	*DCDC2*	*HECW1*	*DSP*	DLG5
MCCC1	*PTK2B*	*EXOC8*	*EVI5L*	*EIF2AK2*	*FLRT2*	CARS	*CSNK2B*	*DCTN1*	*HIST1H1E*	*DYNC1I1*	*DLST*
MRPL47	*PTPRF*	*FAF2*	FAAP100	*EIF3D*	*FN1*	CARS2	CTH	*DCTN2*	*HIVEP3*	*DYNC1LI2*	*DMTN*
MUT	RAB3GAP1	*FAM114A2*	*FAM131B*	*ENOPH1*	*GAP43*	CAT	*CTIF*	*DHX9*	*HMGB1*	*EIF2S3*	*DMXL2*
MYEF2	RAB4B	*FAM118B*	*FAM81A*	*EPN3*	*GAPDH*	*CBR1*	*CTTN*	DKFZp434B2017	*HNRNPA0*	ELAVL4	DMXL2
MYH6	*RAB5A*	FAM149B1	FAM83F	*ERCC5*	GFAP	CBR3	CUL1	*DLAT*	*HNRNPL*	EMC1	*DNAAF5*
MYH9	*RAPGEF4*	*FAM169A*	*FAM98C*	*ERP44*	*GFM1*	CC2D1A	*CXXC1*	*DLD*	HNRNPUL1	*ENO1*	DNAJA1
MYO9A	*RHOBTB1*	FARP1	*FARSA*	EVL	*GJA1*	CCAR2	*CYC1*	*DLG1*	HSPA4L	*ENO2*	DNAJC9-AS1
NACA	*SCG2*	*FARP2*	*FAT1*	*FABP7*	GNA11	CCBL2	*CYCS*	DLG3	IFT81	*ENO3*	DNMT1
NAE1	SDR39U1	*FBLN1*	*FBXO44*	FABP7	GNAL	CCDC136	DBN1	DNPH1	IMPDH2	ERC2	DOCK2
NANS	SDSL	FGG	*FBXO8*	FAM131B	*GNB2L1*	CCDC6	DBNL	*DOCK3*	*INA*	*ESYT1*	DST
NCK1	SENP6	*FHAD1*	*FGD6*	FAM20C	*GNG3*	*CCDC87*	DCAF11	*DSCAML1*	IQSEC1	*FABP3*	*EEA1*

SAD		FAD PSEN1		FAD APP		TREM2 FAD		TREM2 SAD		TREM2 Control	
Up-regulated	**Down-regulated**	**Up-regulated**	**Down-regulated**	**Up-regulated**	**Down-regulated**	**Up-regulated**	**Down-regulated**	**Up-regulated**	**Down-regulated**	**Up-regulated**	**Down-regulated**
NFS1	*SIRPA*	*FMNL1*	*FKBP15*	*FBN1*	GOLGA4	CCT4	DCDC1	*DSG2*	*ITPR1*	FBLN1	EFR3B
NISCH	*SLC12A7*	FMNL1	*FLNA*	*FGA*	*GOT1*	CD44	DCLK1	*ECT2*	KDM5A	*FBXO44*	*EHD3*
NLRP4	*SLC4A1*	*FSCN1*	*FLNB*	FGA	*GOT2*	CD9	DCTN1	EEF1E1	KRT15	*FBXO8*	EIF3B
NRCAM	*SNAP91*	*FTH1*	*FN1*	*FGB*	GPR98	CDKN1B	*DDN*	EMC1	*KSR1*	*FGA*	*EIF3K*
OBSCN	*SON*	FTH1	FTCD	FGB	*GRID2IP*	CDS2	DDX1	EMC2	KYNU	*FGB*	*EIF3L*
OGDHL	SPTA1	*FTL*	*FXR1*	FGD4	GRM2	CELSR1	DDX17	ENAH	*LARP1*	*FGG*	*EIF4G2*
OLFML1	*SRR*	*FTSJ3*	*GAD2*	*FILIP1*	*GRSF1*	CFAP54	*DGKB*	*ENO1*	LIX1L	*FNDC1*	EMC2
OLFML2B	STRAP	*FYCO1*	*GAK*	*FKBP4*	*GSR*	CFH	*DGKI*	ENTPD2	LMO7	*FOCAD*	EPB41
OSBPL8	SV2B	*GANAB*	*GART*	*FMNL1*	*GTPBP1*	CHORDC1	*DIAPH1*	*EPHX1*	LYNX1	FSCN1	*EPN1*
PAFAH1B3	*SYNPO*	*GARS*	GAS7	*FMNL2*	*GYS1*	*CLASP1*	*DLG4*	*EWSR1*	LZTS3	FTO	EPRS
PARD3	TAGLN	*GFAP*	*GDA*	FTL	*HADHA*	*CLCC1*	DLG4	EXOC2	*MAP2K4*	*FXR1*	EPS8
PC	*TAGLN3*	GFAP	GFM2	*GALK1*	*HBA1*	*CLIC4*	*DLGAP2*	*EZR*	*MAP4*	GAN	*ERO1A*
PCDH17	*TAX1BP1*	*GIMAP1*	*GNA15*	*GAS7*	*HEPACAM*	CLIP2	*DLGAP3*	FABP5	MDN1	GAP43	ERO1A
PCYT2	*TBC1D10B*	*GLUD1*	*GOLGA4*	GAS7	*HIST1H1E*	CLTCL1	DLGAP3	*FABP7*	*MIPOL1*	*GAPDH*	ERVK-24
PDE4B	*TBC1D8B*	*GLUD2*	*GOLGB1*	*GDI1*	HIST1H2BK	*CLU*	*DLST*	*FAM98B*	*MKRN1*	*GCC2*	EZR
PDHX	*TCEAL3*	GMPR	GRIA2	GFAP	HNRNPDL	CLU	DNAJA2	*FBN1*	*MYH1*	*GFAP*	F13A1
PDP1	*TECPR1*	*GMPR2*	*GRIA3*	*GIGYF2*	*HNRNPL*	*CMAS*	DNAJC5	*FGG*	*MYH11*	*GJA1*	FAAP100
PGAM1	THOP1	*GNA14*	GRIA3	GJA1	*HP*	CNDP1	DNM1L	*FH*	*MYL9*	*GLIPR2*	*FAM171B*
PHB	*THY1*	*GNB2L1*	*GRID2IP*	*GNAI2*	*HP1BP3*	CNN1	*DOCK4*	*FHAD1*	*MYRIP*	GLIPR2	FAM171B
PHB2	*TIAM1*	*GNB5*	*GRIN2B*	*GNAL*	*HSP90AB2P*	CNTN2	*DPYSL4*	*FHL1*	MYT1L	*GLRX3*	*FARP1*
PI4KA	TLN2	*GPATCH8*	*GRSF1*	*GNB1*	HSP90AB3P	CNTNAP2	DRG1	FHL1	*NBPF8*	GLS	*FARSA*
PLCB1	TMEM44	*GRIA2*	*GUCY1B3*	*GOLGA2*	HSPA1L	CNTRL	DSTN	FKBP5	NCL	*GNA13*	*FARSB*
PLCD3	TNKS1BP1	*GRIK1*	*H2AFY*	*GPI*	HSPB1	COBLL1	*DYNC1I1*	*FLOT1*	*NCOR2*	*GNAO1*	*FASN*
PLCG1	*TNRC18*	GRM3	*HBS1L*	*GPR158*	IFFO2	COG1	DYNLRB1	*FTH1*	NEDD4	*GNAS*	FASN

SAD		FAD PSEN1		FAD APP		TREM2 FAD		TREM2 SAD		TREM2 Control	
Up-regulated	**Down-regulated**	**Up-regulated**	**Down-regulated**	**Up-regulated**	**Down-regulated**	**Up-regulated**	**Down-regulated**	**Up-regulated**	**Down-regulated**	**Up-regulated**	**Down-regulated**
PNN	*TPM2*	*GSS*	*HECW1*	*GPSM2*	*IGHG1*	COL12A1	EHHADH	FTH1	NIT2	*GNB1*	FBF1
PNPLA6	TPM2	*GSTP1*	HERC3	*GRIA2*	*IGKC*	COL4A1	EIF3B	*FTL*	NOC3L	*GNG7*	*FDFT1*
PPIA	TRIP11	*HAPLN1*	*HINT2*	*GRM3*	IGLL5	*COL6A1*	*EIF3K*	FTL	*NSF*	*GOLGA3*	FDXR
PPIF	*TRPV4*	*HAPLN2*	HK2	*GSTM2*	*ITGAV*	COL6A1	EIF4A1	GALNT7	*NUCKS1*	GOLGB1	FGFR1
PPT1	*TSPAN32*	HAPLN2	*HLA-A*	*GSTM3*	*KHSRP*	*COL6A2*	EIF4B	*GAPDH*	OGDHL	GPD1	*FHAD1*
PRDX5	*UBE2K*	*HAPLN4*	HNRNPUL2-BSCL2	*GSTP1*	*KIAA1468*	*COL9A2*	EIF4G2	GC	OGT	*GPM6A*	*FLNB*
PRPF6	*UNC13B*	HAPLN4	*HSD17B4*	*HADHB*	*KSR1*	*COMT*	EIF5	*GFAP*	*OSBPL7*	*GRID2IP*	*FLNC*
PRPF8	*UQCRC1*	*HIBADH*	*HSP90AA5P*	*HAPLN4*	KYNU	*COPS2*	*ELAVL2*	GFAP	*PAICS*	*GRIPAP1*	FLNC
PSMB2	UQCRFS1	*HIP1*	*HSPA12A*	*HARS*	*LARP1*	*COTL1*	EML1	*GLUD1*	PARP1	GRM7	FRYL
PSMC4	*USP11*	*HIST1H1E*	*HSPG2*	*HDAC5*	LRRC42	CP	EPB41L1	GMCL1	PARP14	*GSK3B*	*FSD1*
PTPRN	*USP34*	*HOOK3*	*IARS*	HDLBP	LRRC53	CPNE7	*EPHA4*	GMPR2	*PCDHGA3*	*GSN*	GABBR1
PYGM	*USP4*	*HSD17B10*	*IDH2*	*HERC5*	*LSAMP*	CPSF7	EPS15L1	*GNA13*	*PCLO*	GSTK1	GAD1
QARS	*VCPIP1*	*HSPB1*	*IGHG2*	HRG	*MDH1*	*CPT1A*	ERC1	*GNB1*	*PDIA6*	*GTPBP1*	*GAD2*
RAB3C	VGF	HSPB1	*IGSF9B*	*HSD17B10*	MEIOB	*CRABP1*	*ERC2*	GNG12	*PFKL*	*H1F0*	*GAK*
RIC8A	VPS51	*HUWE1*	*INTS3*	*HSP90AA1*	MGST3	CRABP1	ERVK-24	*GOLGA3*	PGM5	*H2AFV*	GBAS
RPL22	*WDFY1*	*HYOU1*	*IQSEC1*	*HSP90AB1*	MICU2	*CRYAB*	FAF2	*GOLGA8R*	PHLDB3	*H2AFY*	GC
RPS3	*WDR64*	HYOU1	*IQUB*	*HSP90AB3P*	MLLT4	CRYZL1	FAM169A	*GPI*	*PIP5K1C*	*H3F3A*	GLMN
RTCB	ZBED4	HYPK	*ITGB1*	*HSPA1A*	*MMS19*	CSNK2B	FAM171A2	*GPNMB*	*PITPNM2*	*HADHB*	*GLS*
S100A13	*ZC3H14*	*ILF2*	*ITPKA*	*HSPA6*	*MORN1*	*CSRP1*	FAM171B	*GRIA2*	*PITPNM3*	HAPLN4	*GNL1*
SAMD9L		*ISOC2*	*JUP*	*HSPA8*	*MPDZ*	CSRP1	*FAM81A*	*GSTM3*	PLCL1	HAUS3	GPD1L
SARAF		*ITPR1*	*KIF3B*	*HSPA9*	*MTOR*	CTAGE4	FARSB	GSTM3	*PPM1E*	*HDGF*	*GPR98*
SCG2		*JAKMIP3*	*KRT1*	*HSPB1*	MYH10	CTBP1	*FBL*	GSTT1	PPP1R11	*HEPACAM*	GRIA2
SFXN2		*KCNIP4*	*KRT2*	*HTRA1*	*MYH6*	CTNNA3	FBXO2	*GTF3C1*	*PPP6R2*	*HIST1H2AA*	*GRPEL1*

SAD		FAD PSEN1		FAD APP		TREM2 FAD		TREM2 SAD		TREM2 Control	
Up-regulated	**Down-regulated**	**Up-regulated**	**Down-regulated**	**Up-regulated**	**Down-regulated**	**Up-regulated**	**Down-regulated**	**Up-regulated**	**Down-regulated**	**Up-regulated**	**Down-regulated**
SH3KBP1		*KIAA1468*	*KRT7*	*HTT*	MYH7B	CTNNB1	FECH	H2AFZ	*PRPF40A*	*HIST1H2AH*	GSTM1
SHANK1		KIAA2026	*KRT9*	*IARS*	*MYO9A*	CTNND1	*FGD6*	*HADHA*	*PRUNE2*	*HIST1H2BC*	GUCY1B3
SLC25A22		*KIF27*	*LARP1*	*IDH3A*	NAE1	CTNND2	FKBP8	*HADHB*	PSG5	*HIST1H4A*	H2AFY
SLC9A3R2		KLC3	*LARS*	*IDH3B*	NCL	*CUL3*	*FLNB*	*HAPLN4*	PSMD4	HIST1H4A	H3F3A
SNCA		*KPNA1*	*LONRF3*	IDH3G	*NEB*	CUL3	FLOT1	HGH1	*PTPRC*	*HK1*	HBA1
SNRNP200		*KREMEN2*	LPP	*ISOC2*	*NGEF*	CUL5	FNBP1	*HINT2*	*PTPRK*	HNRNPD	HBB
SNRPE		KRT2	LRRC53	ITGB8	*NIPSNAP3A*	*CUL9*	FREM1	*HIST1H2BH*	*PTPRN*	HNRNPDL	HBD
SQSTM1		KRT4	*LSM14B*	ITSN2	NKTR	CUX1	*FSD1*	HIST1H2BH	*PXN*	HNRNPU	*HEBP1*
SSBP1		*LETM1*	*MAP1B*	KDM5A	NLGN2	CUX2	FTO	*HIST1H4A*	RAB17	*HNRNPUL1*	HEBP2
STK10		*LIMCH1*	*MAPK8IP3*	*KIF5B*	NNT	*DAAM2*	*GABBR1*	HIST1H4A	RAB2B	HNRNPUL2	HECTD1
SUB1		*LMAN1*	*MARK1*	KIRREL	*NRCAM*	DAB2	GABBR1	*HNRNPA2B1*	RAB4B	*HOMER1*	HERC2
SUCLA2		*LMBRD2*	MBOAT7	KTN1	*NTM*	DARS	GABRB1	*HNRNPK*	*RANBP3L*	*HOMER2*	HGS
SUCLG2		LMX1B	*MBP*	*LAMC1*	NUCB2	*DBI*	GAD2	*HNRNPR*	*RAPGEF4*	*HP1BP3*	*HIST1H1E*
SYNM		LPIN1	*MPO*	*LNP*	*NUCKS1*	DBI	*GAP43*	HP	RASSF2	*HSPA8*	*HMOX2*
THNSL1		LRPPRC	MPP1	*LPP*	*OMG*	*DCTN1*	GAP43	*HSD17B10*	RB1CC1	*HSPD1*	*HNRNPA1*
TIMM44		LTF	*MPP2*	*LTA4H*	*OPCML*	*DCTN2*	GDAP1	*HSP90AA1*	*RBM4*	*HSPH1*	HNRNPUL1
TJP2		*LTN1*	*MPRIP*	*LTF*	*PAICS*	DDAH2	GDAP1L1	*HSPA1A*	*RECQL5*	*IFT122*	HSD11B1
TLDC1		*MAG*	*MRPL11*	*LTN1*	*PARK7*	DDX21	*GIT1*	*HSPB1*	*RFTN1*	*IGHA2*	HSPA12B
TNKS1BP1		MAP3K3	MST1R	*LYN*	*PCDHGA8*	DDX3Y	*GLDC*	HSPB1	RGPD8	*IGHG1*	HSPA4L
TRA2B		*MAPT*	*MTIF2*	LYNX1	*PCLO*	DDX59	GLS	*HSPG2*	ROCK1	*IGKC*	HSPA6
TSC2		MAPT	*MTMR7*	MAN2A2	PCP4	DEF6	GNAZ	*HTRA1*	*RPL10A*	IL1B	HUWE1
TXNRD2		*MCU*	*MYH13*	*MAPRE1*	*PEBP1*	DES	GNB5	*IARS2*	*RUNDC3A*	*IMMT*	*IDH2*
UBA2		*MFN2*	MYH2	*MAPT*	*PFKL*	DHRS7	GNG10	*IDH3A*	*SAMD11*	*INF2*	*IFI16*

SAD		FAD PSEN1		FAD APP		TREM2 FAD		TREM2 SAD		TREM2 Control	
Up-regulated	**Down-regulated**	**Up-regulated**	**Down-regulated**	**Up-regulated**	**Down-regulated**	**Up-regulated**	**Down-regulated**	**Up-regulated**	**Down-regulated**	**Up-regulated**	**Down-regulated**
UBC		*MGAM*	*MYH6*	*MCU*	*PFKP*	DHX9	GNPDA2	*IDH3B*	*SCRIB*	*IQSEC2*	IGBP1
UBL4A		*MGLL*	*MYL9*	*MPI*	*PHF24*	DISC1	GPI	*IDH3G*	SEC16A	*IRAK1*	IGLON5
UBN1		*MPI*	MYL9	*MSN*	PHYHIPL	DLAT	*GRID2IP*	IFIT1	SEMA4D	ITGB8	ILVBL
USP7		*MPP5*	*NBAS*	MTCH1	*PI4KA*	DLC1	*GRM5*	IFIT3	SENP6	*JUP*	IMPA2
VPS26B		MPRIP	*NCOA7*	*MTCL1*	PIK3C2A	DMXL2	GRM8	IGHG4	*SFXN3*	*KALRN*	INADL
VPS33A		*MRPL46*	*NCOR1*	MYO1D	*PJA2*	*DNAJA2*	*GRSF1*	*IQGAP1*	*SGSM1*	*KANK3*	*INPP4A*
VPS35		MYOM2	NDC80	*MYO5C*	PLCD3	DNAJC2	GSK3A	ITGB1	SI	KDM2B	INTS3
ZNF618		*MYRIP*	*NDUFA2*	*NAGK*	*PLXNC1*	DOC2A	*GSTM3*	ITGB4	SIRT2	KIAA0513	*IQSEC3*
		NDUFB6		POTEKP		*GYS1*		*SLC12A5*		*ISCA1*	*KIF27*
		NDUFS2		*PPP1R9A*		*H1F0*		SLC27A6		ITPR1	*KRT1*
		NEDD4L		*PPP2R5E*		*H2AFJ*		*SMG1*		KCNIP4	*KRT10*
		NGEF		*PPP3R1*		*H2AFV*		*SON*		KDM5D	KRT10
		NSF		PPP5C		*H2AFY*		*SOWAHC*		KHSRP	*KRT2*
		NUAK1		*PRDX6*		*H3F3B*		*SPG11*		KIAA1467	*KRT4*
		NUBPL		*PRNP*		*HBS1L*		SPOCK2		KIF13A	*KRT9*
		OAS1		*PRPF40A*		*HDGFRP3*		*SPTBN2*		KIF3A	*LAMA2*
		OGDHL		*PRPH*		HGS		SQRDL		KIF3B	*LAMA5*
		OGT		*PRR14L*		*HIST1H1E*		*SRP14*		KLC3	*LARS*
		PA2G4		*PRRT2*		*HIST1H2AA*		*SRRM2*		KNG1	*LDHB*
		PACS1		*PSMD10*		*HIST1H4A*		*SYN3*		*KPNA6*	*LIMCH1*
		PACSIN1		*R3HDM1*		*HIVEP3*		*SYNE1*		KRT9	LLGL1
		PALM3		*RAPGEF4*		*HMGB1P1*		*TAGLN*		*KSR1*	*LMNB2*
		PARP14		*RBM4*		HMOX2		TAGLN		*KTN1*	LPP
		PCCA		*RDX*		HNRNPA2B1		*TAX1BP1*		KTN1	*LRRC59*

SAD		FAD PSEN1		FAD APP		TREM2 FAD		TREM2 SAD		TREM2 Control	
Up-regulated	**Down-regulated**	**Up-regulated**	**Down-regulated**	**Up-regulated**	**Down-regulated**	**Up-regulated**	**Down-regulated**	**Up-regulated**	**Down-regulated**	**Up-regulated**	**Down-regulated**
		PDAP1		REEP5		HNRNPAB		*TBC1D8B*		*LAP3*	*LRRFIP2*
		PDK2		*RHOB*		HNRNPDL		*TBL3*		LATS1	*LSAMP*
		PDZRN3		*RHOT1*		HNRNPH1		*TECPR1*		LINGO1	*LTN1*
		PEX5		*RPL10A*		*HNRNPH2*		TERF2		LMO7	*LVRN*
		PFKL		*RPL14*		*HNRNPLL*		THOP1		LNP	LYRM4
		PFKP		*RPL21*		*HNRNPM*		TM9SF4		*LONP1*	MACF1
		PHACTR1		*RPL7A*		HNRNPM		TNS3		*LRP1*	MALT1
		PIK3C2A		*RPLP2*		*HOMER1*		*TPM2*		LRRC32	*MAP1A*
		PIKFYVE		*RPS3A*		*HP1BP3*		TPM4		*LRRC45*	*MAP1B*
		PIN1		*RPS8*		HPCA		*TRAPPC10*		*LRSAM1*	MAP2K1
		PIP5K1C		*RPSA*		HPCAL1		*TRPV4*		*LSM2*	*MAP4*
		PITPNM3		RTN4RL2		HPCAL4		*TSC1*		LSP1	*MCF2L*
		PKHD1L1		SAFB2		HSDL2		UBE2D2		*MADD*	*MCM5*
		PKP4		*SCML2*		HSPA4L		UBE2N		MAGED1	MCU
		PLCB1		*SEC16A*		HTRA1		*UBL4A*		*MAP2K4*	*MECP2*
		PLCL2		*SEC23A*		*ICAM5*		*UTP15*		*MAP2K6*	*MMRN1*
		PLEKHA1		*SEMA3D*		*IDH2*		*VCL*		MAP2K6	*MPDZ*
		POTEE		SENP6		IDH2		VGF		*MAP3K11*	MPP7
		POTEF		*SFXN1*		IDH3A		*VTI1B*		MAP6	*MRAS*
		PPID		*SFXN3*		IGLC2		*WDR19*		*MAPK3*	*MRPS22*
		PPM1E		SFXN3		*IGSF9B*		*WNK2*		MEIOB	*MSN*
		PPP1R12B		*SGSM1*		*IQSEC1*		*ZC3H14*		MEST	*MUC16*
		PPP1R21		*SIRPA*		*ITPKA*		*ZEB2*		METAP2	*MYH10*
		PPP1R9A		*SLC12A5*		ITSN2		ZMYM1		*MKRN1*	*MYH16*

SAD		FAD PSEN1		FAD APP		TREM2 FAD		TREM2 SAD		TREM2 Control	
Up-regulated	**Down-regulated**	**Up-regulated**	**Down-regulated**	**Up-regulated**	**Down-regulated**	**Up-regulated**	**Down-regulated**	**Up-regulated**	**Down-regulated**	**Up-regulated**	**Down-regulated**
		PRKAA2		*SLC17A7*		*JAK2*		ZMYND8		MRVI1	*MYH9*
		PRKCA		SLC17A7		*KALRN*		*ZNF287*		*MSRA*	*MYL12A*
		PRKCB		*SLC25A22*		KCTD12		ZNF852		MST1R	*MYL6*
		PRKCG		SMARCC2		KIAA0513				MTFR1L	*MYL6B*
		PRKRA		*SNAP91*		KIAA1211L				*MTMR2*	*MYO1C*
		PRPF8		*SNCA*		KIF20B				MTURN	*NACA*
		PSAP		*SNCG*		KIF3B				*MUT*	NCAPD3
		PTGES3		*SOD1*		KIF5C				*MYH1*	*NCL*
		PTPN23		*SOD2*		KLC3				*MYH4*	*NCOR2*
		PTPRF		*SON*		*KNG1*				*MYO18B*	*NDRG1*
		PTPRN		SPOCK2		KRT15				MYO1D	NDUFA6
		PTPRN2		SQSTM1		*KSR1*				MYO6	*NDUFS4*
		PTRF		SRL		LARP1				NAALADL2	NDUFS4
		PVRL1		*SRRM2*		LASP1				NCEH1	*NEB*
		QSOX1		*SRSF5*		LCP1				*NCK2*	NECAB1
		RAB3B		STARD9		LGALSL				*NDUFS2*	NEDD8
		RAB3C		*STMN1*		LMNB1				NEDD4L	*NEFH*
		RAB3GAP1		STXBP4		LMO7				*NES*	*NEFL*
		RAB4B		*SYNPO*		LOC102724023				NF1	*NEFM*
		RAD54L		SYP		LONP1				NFASC	*NFASC*
		RALBP1		SYT1		LRRC32				*NFS1*	*NIT2*
		RAN		*TAOK1*		LRRC47				NIN	*NME2*
		RANBP3L		*TBC1D10B*		*LRRC7*				*NNT*	NUAK1
		RAPGEF4		*TBC1D8B*		LRRC8A				NPTX1	*NUCKS1*

SAD		FAD PSEN1		FAD APP		TREM2 FAD		TREM2 SAD		TREM2 Control	
Up-regulated	**Down-regulated**	**Up-regulated**	**Down-regulated**	**Up-regulated**	**Down-regulated**	**Up-regulated**	**Down-regulated**	**Up-regulated**	**Down-regulated**	**Up-regulated**	**Down-regulated**
		RASA3		*TBL3*		*LZTS3*				*NRXN1*	*NUDC*
		RASGRP1		*TCEAL3*		MADD				*NUMA1*	OSBPL2
		RB1CC1		*TF*		MAP1S				*OGDHL*	*PACSIN1*
		RECQL5		THAP4		MAP2				OGDHL	PAK3
		REPS2		THUMPD3		*MAP3K11*				*OGN*	*PARK7*
		RPH3A		*THY1*		MAPK10				*OTUB1*	*PARP1*
		RPL10A		*TNR*		MAPK8IP3				*OXCT2*	PC
		RPL13AP3		TRIM24		MAPRE3				*PAFAH1B3*	*PCSK1N*
		RPL17		*TRIM32*		*MARCKS*				PAICS	PCYT2
		RPL27		*TSFM*		*MATR3*				PALMD	PDCD5
		RPL36		*TSNAXIP1*		MBOAT7				PANK4	*PDZRN3*
		RPL4		*TTC23*		*MBP*				PAPOLA	*PEBP1*
		RPS13		*TTR*		*MECP2*				*PCCA*	PEX19
		RPS8		TUBB1		MECR				*PCK2*	*PGBD5*
		RPS9		*TXN*		MFN2				*PDE1B*	*PGK2*
		RPTOR		TXN2		MGEA5				*PDE4B*	*PGM1*
		SAFB		TXNRD2		*MGST3*				*PDIA4*	*PHB2*
		SAFB2		*UBL4A*		MGST3				*PDIA6*	*PHGDH*
		SAMM50		*UBR1*		*MKRN1*				PDK2	*PHYHIPL*
		SARS2		*UBXN6*		*MOB2*				PDPK1	*PLCD1*
		SBF2		*UQCRC1*		MORC3				*PDXK*	*PLEC*
		SCFD1		*UQCRFS1*		MRI1				*PDZRN4*	*PLEKHB1*
		SCN2A		*USP34*		*MRTO4*				PEPD	*PLP1*
		SCP2		VARS		MTCH1				*PFKL*	*PLPP3*

SAD		FAD PSEN1		FAD APP		TREM2 FAD		TREM2 SAD		TREM2 Control	
Up-regulated	**Down-regulated**	**Up-regulated**	**Down-regulated**	**Up-regulated**	**Down-regulated**	**Up-regulated**	**Down-regulated**	**Up-regulated**	**Down-regulated**	**Up-regulated**	**Down-regulated**
		SDK2		*VCAN*		MT-CO2				PFKP	*PNN*
		SDR39U1		*VCL*		MTFR1L				PGM2	PPP1R12B
		SEC63		*VDAC2*		*MTIF2*				*PGRMC1*	PPP1R3A
		SEL1L		*VPS13A*		*MTMR2*				*PHPT1*	PPP3CA
		SHANK3		VPS26B		*MTMR7*				PIK3R1	*PPP3R1*
		SIRT5		*VPS45*		*MTOR*				*PIP4K2A*	*PPT1*
		SLC12A7		WASF1		MTX2				*PIP4K2C*	*PRDX1*
		SLC39A12		*ZNF365*		MYLK				*PLAA*	*PRDX2*
		SLC6A12				*MYRIP*				PLCB1	*PRDX6*
		SLFN11				NAPG				*PLCL2*	*PSAP*
		SLIRP				NCALD				*PLXNA1*	*PSD*
		SNRPE				NCAM1				PLXNA1	*PSIP1*
		SNW1				NCAPD3				*PMFBP1*	PSMB2
		SNX3				NCEH1				*POLR1C*	*PSMD2*
		SPATA1				NCKAP1				*PPM1E*	PTCH1
		SPG20				NCKIPSD				*PPME1*	*PTEN*
		SPIRE1				NCL				*PPP1CA*	*PTK2B*
		SPOCK2				*NDUFA12*				PPP1R21	PTPRT
		SRC				*NDUFA2*				*PPP2R4*	*RAB11FIP1*
		SRSF1				NDUFA7				PRELP	RAB39B
		SRSF10				NDUFAB1				PREP	*RAB7A*
		SRSF6				*NDUFB4*				PRKDC	*RABGAP1*
		SSB				NDUFB4				*PRPF8*	*RASGRF2*
		STK38L				*NDUFS3*				*PRUNE*	RBM41

SAD		FAD PSEN1		FAD APP		TREM2 FAD		TREM2 SAD		TREM2 Control	
Up-regulated	**Down-regulated**	**Up-regulated**	**Down-regulated**	**Up-regulated**	**Down-regulated**	**Up-regulated**	**Down-regulated**	**Up-regulated**	**Down-regulated**	**Up-regulated**	**Down-regulated**
		STOX2				NECAB1				PSD3	RHPN2P1
		SYNCRIP				NECAB2				PSMA1	RNF141
		SYNPO				NEDD4				*PSMC3*	RNH1
		SYP				NEDD4L				*PSMC4*	*ROCK2*
		TAGLN				NFS1				*PSMD10*	ROGDI
		TAGLN				*NID2*				PSMD13	*RPL10*
		TANC2				NOC3L				*PTPN23*	*RPL11*
		TFRC				*NOP56*				*PTPRE*	*RPL12*
		THNSL1				*NOP58*				*PTPRN*	*RPL13*
		THRAP3				*NOVA2*				*PTPRN2*	*RPL17*
		TLN1				*NPM1*				*PTRF*	*RPL18*
		TMEM44				*NPTN*				PTRF	*RPL21*
		TNIK TNKS1BP 1				NPTN				PUDP	*RPL22*
						NPTX1				*PUF60*	*RPL24*
		TNRC18				NRN1				*PXN*	*RPL27*
		TNXB				*NRXN1*				PYGM	*RPL27A*
		TOP2B				*NUBPL*				*RAB24*	*RPL3*
		TPM2				NUCB2				*RAB3B*	*RPL4*
		TSC1				NUCKS1				RANBP6	*RPL5*
		TSFM				NUMA1				RANGAP1	*RPL6*
		TTC21B				*NUMBL*				RASSF2	*RPL7*
		TTC25				NUMBL				*RBSN*	*RPL7A*
		TTYH2				NUP214				RDH13	*RPL8*
		TUBB4A				OLA1				RFXANK	*RPLP0*

SAD		FAD PSEN1		FAD APP		TREM2 FAD		TREM2 SAD		TREM2 Control	
Up-regulated	**Down-regulated**	**Up-regulated**	**Down-regulated**	**Up-regulated**	**Down-regulated**	**Up-regulated**	**Down-regulated**	**Up-regulated**	**Down-regulated**	**Up-regulated**	**Down-regulated**
		TUFM				OLR1				RGS3	RPS10
		TXNRD1				OPA1				*RILPL1*	*RPS13*
		UACA				*OPCML*				*RMDN3*	*RPS14*
		UBXN6				*OPHN1*				*RMND1*	*RPS23*
		UFL1				*OPTN*				*RNF20*	*RPS24*
		UGT1A6				OSBPL2				*RNF40*	*RPS3*
		UROS				OXCT1				RPL7A	*RPS4X*
		USP11				PACSIN1				RPN2	*RPS8*
		USP5				PAK1				*RPSA*	*RPS9*
		UTY				PALM2				*RRP1B*	RSF1
		VAT1				PAM				*RTN4*	*RTN1*
		VCL				*PARD3*				RUVBL1	*S100A13*
		VCPIP1				PCBP1				*SAMM50*	*SARS*
		VGF				PCLO				SAMM50	SART3
		VPS41				PCSK1N				SBF1	SASH1
		WDR1				PDE1B				*SCAI*	*SBF1*
		WDR37				PDE2A				*SEC16A*	*SCFD1*
		WDR7				*PHB*				SEC22B	*SCN8A*
		WNK2				*PHF24*				*SEC23A*	*SCYL1*
		XIRP2				PHF24				SERPINB6	SEC23A
		XRCC6				PHYHIP				SH3KBP1	*SET*
		ZNF470				PHYHIPL				SIX6OS1	*SETX*
						PIN1				*SLC12A7*	*SHTN1*
						PIP4K2C				SLC17A7	SI

SAD		FAD PSEN1		FAD APP		TREM2 FAD		TREM2 SAD		TREM2 Control	
Up-regulated	**Down-regulated**	**Up-regulated**	**Down-regulated**	**Up-regulated**	**Down-regulated**	**Up-regulated**	**Down-regulated**	**Up-regulated**	**Down-regulated**	**Up-regulated**	**Down-regulated**
						PIR				SLC35A2	*SKP1*
						PITPNM2				*SLC4A1*	SLC14A1
						PITPNM3				SLC4A1	*SLC1A2*
						PJA2				SLC6A17	*SLC25A5*
						PLCL1				*SLC8A2*	*SLC25A6*
						POLDIP2				*SNPH*	*SLC44A1*
						PPFIA4				*SNX2*	SLC4A10
						PPIL1				*SOGA3*	*SLK*
						PPP1R1B				SPARCL1	*SLMAP*
						PPP1R9A				SPTA1	SLU7
						PPP2R5E				*SPTB*	*SMARCA5*
						PRKCE				*SQSTM1*	SMS
						PRKCG				SRGAP1	*SNCA*
						PRKRA				*SRR*	*SNRNP200*
						PRNP				*SRRM2*	*SNRPD3*
						PRPS2				*STK38L*	*SNRPE*
						PRUNE2				STOM	*SOD1*
						PSAP				STRAP	*SPAG9*
						PSAP				*STXBP1*	*SPG11*
						PSD3				*STXBP5*	*SRI*
						PSMD4				*SUCLG1*	*SRSF1*
						PTEN				*SYNJ2BP*	*SRSF10*
						PTGES2				TAGLN	*SRSF2*
						PTPRF				*TBC1D10B*	*SRSF4*

SAD		FAD PSEN1		FAD APP		TREM2 FAD		TREM2 SAD		TREM2 Control	
Up-regulated	**Down-regulated**	**Up-regulated**	**Down-regulated**	**Up-regulated**	**Down-regulated**	**Up-regulated**	**Down-regulated**	**Up-regulated**	**Down-regulated**	**Up-regulated**	**Down-regulated**
						PVRL1				TBC1D23	*SRSF5*
						RAB11FIP5				*TBCB*	*SRSF6*
						RAB15				TBCC	ST3GAL1
						RAB1A				*TCF25*	STAT1
						RAB3B				*TECPR1*	STXBP1
						RAB5A				*TGM2*	SUCLG1
						RABGAP1L				*TIAM1*	*SYNE2*
						RABGGTB				*TIGD4*	*SYNGAP1*
						RALGAPB				*TJP2*	*SYNJ1*
						RALY				TJP3	*SYNM*
						RANBP3L				TLN2	*SYNPO*
						RANBP6				*TMPO*	SYP
						RAP1GAP				*TNKS1BP1*	*TCP1*
						RAP1GAP2				*TNPO2*	TECPR1
						RAPGEF2				TNS3	*TFAM*
						RAPGEF4				*TOM1*	TIGAR
						RASGRF2				TPM2	*TJP1*
						RB1CC1				*TRIM28*	*TKT*
						RBM14				TRIM32	TLDC1
						RBSN				*TRPV4*	*TLN2*
						RCN2				*TSC1*	TNC
						REPS2				*TSC2*	*TOP1*
						REXO2				TSR2	*TOP2B*
						RGS7				*TTC25*	TPPP3

SAD		FAD PSEN1		FAD APP		TREM2 FAD		TREM2 SAD		TREM2 Control	
Up-regulated	**Down-regulated**	**Up-regulated**	**Down-regulated**	**Up-regulated**	**Down-regulated**	**Up-regulated**	**Down-regulated**	**Up-regulated**	**Down-regulated**	**Up-regulated**	**Down-regulated**
						RHOT1				TTC25	*TRANK1*
						RMDN3				TTR	TRAP1
						ROCK1				TTYH2	*TRIP11*
						RPA3				*TUBB2A*	*TUBA4A*
						RPGRIP1L				*TWF2*	*TUFM*
						RPH3A				*UBA1*	TXNRD2
						RPL10				*UBA2*	*UACA*
						RPL10A				*UCHL3*	*UBC*
						RPL12				*UHRF1BP 1L*	*UBE2N*
						RPL14				UNC13B	UBR5
						RPL17				*UNK*	*UCHL1*
						RPL17				*USO1*	UGP2
						RPL18				*USP11*	*UQCRC1*
						RPL22				*USP4*	UQCRQ
						RPL35A				USP47	USO1
						RPL4				*USP7*	*USP44*
						RPL7A				VARS	*USP9X*
						RPLP2				*VCL*	*UTY*
						RPS16				VIM	*VDAC1*
						RPS17				*VPS35*	*VDAC2*
						RPS5				VPS35	*VIM*
						RPS6KC1				VPS50	*VPS13D*
						RPS7				*WDFY1*	VPS51
						RPS7				WDFY4	*VSNL1*

SAD		FAD PSEN1		FAD APP		TREM2 FAD		TREM2 SAD		TREM2 Control	
Up-regulated	**Down-regulated**	**Up-regulated**	**Down-regulated**	**Up-regulated**	**Down-regulated**	**Up-regulated**	**Down-regulated**	**Up-regulated**	**Down-regulated**	**Up-regulated**	**Down-regulated**
						RPS8				*WDR1*	*WASL*
						RTN4RL2				*WDR61*	*WDR19*
						RUFY3				*WIPI2*	WDR47
						SAFB				XPNPEP1	*WNK2*
						SAMD9				*ZADH2*	*XRCC5*
						SAMM50				ZBED8	*XRCC6*
						SARS2				ZMYM1	*ZCCHC17*
						SCFD1				ZMYND8	ZNF518B
						SCG2				*ZNF638*	
						SCN3A					
						SDE2					
						SDR39U1					
						SDSL					
						SEC63					
						SEL1L					
						SEMA4D					
						SENP6					
						SET					
						SGSM1					
						SGTA					
						SH3GL2					
						SH3GL3					
						SH3KBP1					
						SHC1					

SAD		FAD PSEN1		FAD APP		TREM2 FAD		TREM2 SAD		TREM2 Control	
Up-regulated	**Down-regulated**	**Up-regulated**	**Down-regulated**	**Up-regulated**	**Down-regulated**	**Up-regulated**	**Down-regulated**	**Up-regulated**	**Down-regulated**	**Up-regulated**	**Down-regulated**
						SHTN1					
						SIRPA					
						SIRPA					
						SLC12A5					
						SLC12A7					
						SLC17A7					
						SLC25A22					
						SLC25A22					
						SLC25A27					
						SLC27A6					
						SLC2A3					
						SLC4A10					
						SLC6A17					
						SLC6A7					
						SLK					
						SMARCA5					
						SNAP25					
						SNAP91					
						SNAP91					
						SNCA					
						SNCAIP					
						SNRNP70					
						SNW1					
						SNX3					

SAD		FAD PSEN1		FAD APP		TREM2 FAD		TREM2 SAD		TREM2 Control	
Up-regulated	**Down-regulated**	**Up-regulated**	**Down-regulated**	**Up-regulated**	**Down-regulated**	**Up-regulated**	**Down-regulated**	**Up-regulated**	**Down-regulated**	**Up-regulated**	**Down-regulated**
						SON					
						SPAG7					
						SPAG9					
						SPATA2					
						SPECC1L-ADORA2A					
						SPG11					
						SPG20					
						SPIRE1					
						SRSF1					
						SRSF10					
						SRSF2					
						SRSF5					
						SRSF7					
						STIL					
						STK39					
						STRN3					
						STX1A					
						STX1B					
						STX6					
						STXBP1					
						SUCLA2					
						SULT4A1					
						SV2A					
						SV2B					

SAD		FAD PSEN1		FAD APP		TREM2 FAD		TREM2 SAD		TREM2 Control	
Up-regulated	**Down-regulated**	**Up-regulated**	**Down-regulated**	**Up-regulated**	**Down-regulated**	**Up-regulated**	**Down-regulated**	**Up-regulated**	**Down-regulated**	**Up-regulated**	**Down-regulated**
						SVIP					
						SYN1					
						SYNGAP1					
						SYNGR3					
						SYNPO					
						SYNPO					
						SYP					
						SYT1					
						SYT5					
						TAX1BP1					
						TBC1D10B					
						TBC1D15					
						TBC1D8B					
						TBCA					
						TBCB					
						TBL3					
						TBRG4					
						TCF20					
						TERF2					
						TFRC					
						TGFBI					
						THY1					
						TIGAR					
						TJP1					

SAD		FAD PSEN1		FAD APP		TREM2 FAD		TREM2 SAD		TREM2 Control	
Up-regulated	**Down-regulated**	**Up-regulated**	**Down-regulated**	**Up-regulated**	**Down-regulated**	**Up-regulated**	**Down-regulated**	**Up-regulated**	**Down-regulated**	**Up-regulated**	**Down-regulated**
						TMEM43					
						TMEM94					
						TMX4					
						TNKS1BP1					
						TOMM70A					
						TP53BP1					
						TPPP					
						TRIB2					
						TRIM24					
						TRIM67					
						TRIO					
						TSC1					
						TSC22D2					
						TSFM					
						TSPAN7					
						TTC21B					
						TUBA4A					
						TUBA8					
						TUBB					
						TUBB2A					
						TUBB4A					
						TXN2					
						TYRO3					
						UACA					

SAD		FAD PSEN1		FAD APP		TREM2 FAD		TREM2 SAD		TREM2 Control	
Up-regulated	**Down-regulated**	**Up-regulated**	**Down-regulated**	**Up-regulated**	**Down-regulated**	**Up-regulated**	**Down-regulated**	**Up-regulated**	**Down-regulated**	**Up-regulated**	**Down-regulated**
						UBA2					
						UBAP2L					
						UBE2D2					
						UBE2N					
						UBE3C					
						UBXN6					
						UCHL1					
						USP11					
						USP47					
						UTP15					
						VAMP2					
						VAPB					
						VAT1L					
						VCAN					
						VDAC3					
						VGF					
						VPS29					
						WASF1					
						WDFY1					
						WDFY4					
						WIPI2					
						WNK2					
						XRCC5					
						XRCC5					

SAD		FAD PSEN1		FAD APP		TREM2 FAD		TREM2 SAD		TREM2 Control	
Up-regulated	**Down-regulated**	**Up-regulated**	**Down-regulated**	**Up-regulated**	**Down-regulated**	**Up-regulated**	**Down-regulated**	**Up-regulated**	**Down-regulated**	**Up-regulated**	**Down-regulated**
						XRCC6					
						YWHAB					
						YWHAE					
						YWHAG					
						YWHAH					
						ZBTB22					
						ZNF511					
						ZNF852					

Appendix Table 4: Proteins greater than 1.5 fold change compared to control in each disease group